Julia Armbruster, BSc

Biochemical characterization and immobilization of a new peroxygenase P450Jα from Jeotgalicoccus sp. ATCC 8456 for selective α-hydroxylation of fatty acids

MASTERARBEIT

zur Erlangung des akademischen Grades

Diplom-Ingenieurin

Masterstudium Biotechnologie

eingereicht an der

Technischen Universität Graz

Betreuer

Univ.-Prof. Dipl.-Ing. Dr. techn. Bernd Nidetzky

Institut für Biotechnologie und Bioprozesstechnik

Dipl.-Biol. Dr.rer.nat. Alexander Dennig

Graz, Juli 2019

Eidesstattliche Erklärung

Ich erkläre an Eides statt, dass ich die vorliegende Arbeit selbstständig verfasst, andere als die angegebenen Quellen/Hilfsmittel nicht benutzt, und die den benutzten Quellen wörtlich und inhaltlich entnommenen Stellen als solche kenntlich gemacht habe.

Graz, am ....
(Unterschrift)

Statutory Declaration

I declare that I have authored this thesis independently, that I have not used other than the declared sources / resources, and that I have explicitly marked all material which has been quoted either literally or by content from the used sources.

Graz, ...
date (signature)

Kurzfassung

Fettsäuren sind wichtige Bestandteile von Lebensmittelabfällen und deshalb sind sie auch interessante Substrate für die Abfallaufwertung. Neben der Energie konsumierenden chemischen Aufwertung könnte auch die Anwendung von effizienten und selektiven Biokatalysatoren eine wichtige Rolle spielen. Die Cytochrome P450 Enzyme haben sich als vielversprechende Katalysatoren für die Umwandlung von Fettsäuren herausgestellt, wobei speziell die Peroxygenasen der CYP152 Familie mit Umwandlungszahlen von bis zu 3000 min^{-1} herausstechen. OleT ist das außergewöhnlichste Mitglied der CYP152 Familie, da es bevorzugt die Decarboxylierung und nicht die Hydroxylierung von Fettsäuren katalysiert. Dieser Katalysator wurde aus *Jeotgalicoccus sp.* ATCC 8456 isoliert, in welchem auch die neue α-Hydroxylase $P450_{J\alpha}$ entdeckt wurde. Diese Arbeit handelt von der biochemischen und katalytischen Charakterisierung von $P450_{J\alpha}$ um das Potential des Katalysators für die Anwendung in industriellen Prozessen zu untersuchen. Zuerst wurde $P450_{J\alpha}$ basierend auf Übereinstimmungen der DNA-Sequenzen und strukturellen Ähnlichkeiten der CYP152 Familie zugeordnet. Nach der erfolgreichen Proteinexpression wurde die Dissoziationskonstante von $P450_{J\alpha}$ für Fettsäuren mit mittlerer Kettenlänge untersucht. Überraschend dabei war, dass die erhaltenen k_D-Werte mehr als zehnmal so hoch waren als bereits veröffentlichte Daten von anderen CYP152 Mitgliedern. Trotzdem ist $P450_{J\alpha}$ ein sehr effizienter Katalysator für die Umwandlung von Fettsäuren. Die katalytische Charakterisierung zeigte die höchsten Umwandlungszahlen von $P450_{J\alpha}$ für Ölsäure mit 731 min^{-1}. $P450_{J\alpha}$ hydroxyliert selektiv die α-Position der Fettsäure, wobei nur Spuren der β-Hydroxyfettsäure detektiert wurden (<5%). Außerdem zeigt das gebildete Produkt eine Selektivität von >95% für das *S*-Enantiomer. Neben der Hydroxylierung katalysiert $P450_{J\alpha}$ auch die oxidative Decarboxylierung von kurzkettigen Fettsäuren (<C10:0), welche zur Bildung von 1-Alkenen führt. Umwandlungen von Fettsäuren mit $P450_{J\alpha}$ im präparativen Maßstab zeigten, dass eines der größten Probleme die Stabilität des Katalysators ist, welche noch zusätzlich durch die Anwendung von Peroxid als Oxidationsmittel reduziert wird. Eine geschicktere H_2O_2 Versorgung durch die Kopplung der Umwandlung der Fettsäuren mit einer Peroxid freisetzenden Reaktion (GOX) führte zu einer verbesserten Stabilität von $P450_{J\alpha}$ und machte eine komplette Umwandlung des Substrates möglich. Eine andere Option um die Robustheit des Katalysators zu erhöhen ist die Immobilisierung auf festem Trägermaterial. Neben der Stabilitätserhöhung erleichtert die Immobilisierung des Enzyms auch die Anwendung in kontinuierlichen Systemen und das Downstream Processing. Der Vergleich von zwei Immobilisierungsstrategien sowie ein Screening von verschiedenen Trägermaterialien führten zu einem aktiven heterogenen Katalysator basierend auf $P450_{J\alpha}$.

Abstract

Fatty acids are major components of food waste which turns them into interesting substrates for waste-to-value approaches. Next to the energy consuming chemical valorization also efficient and selective biocatalysts could be applied. Cytochrome P450s proved to be promising candidates in fatty acid conversion whereas especially the peroxygenases from the CYP152 family stand out with turnover numbers of up to 3000 min^{-1}. OleT is the most extraordinary member as it preferably catalyzes the decarboxylation over the hydroxylation of fatty acid. Said catalyst was isolated from *Jeotgalicoccus sp.* ATCC 8456, which is also the organism where the newly discovered α-hydroxylase $P450_{J\alpha}$ is derived from. This work deals with the biochemical and catalytical characterization of the OleT paralog $P450_{J\alpha}$ to determine its potential for applications in industrial scales. First, $P450_{J\alpha}$ was annotated to the CYP152 family based on sequence similarities and structural resemblances. After successful protein expression, the dissociation constant of $P450_{J\alpha}$ for medium chain fatty acids was determined. Surprisingly, the obtained k_D-values were tenfold compared to already reported data from CYP152 family members. Still, $P450_{J\alpha}$ efficiently catalyzes the conversion of fatty acids. The catalytic characterization revealed highest turnover numbers of $P450_{J\alpha}$ for oleic acid with 731 min^{-1}. $P450_{J\alpha}$ selectively hydroxylates the α-carbon of the fatty acids, whereas only traces of the β-hydroxyfatty acid (<5%) could be detected. Furthermore, the formed product displayed high selectivity for the *S*-enantiomer (e.e. value >95%). Besides hydroxylation, $P450_{J\alpha}$ also catalyzes the oxidative decarboxylation of short chain fatty acids (<C10:0) which leads to the formation of 1-alkenes. Conversions of fatty acids with $P450_{J\alpha}$ in preparative scale revealed one major problem namely catalyst stability, which is additionally decreased by the use of peroxide as oxidant. The application of a smarter peroxide supply by coupling the fatty acid conversion to a peroxide releasing reaction (GOX) led to an increase in robustness of $P450_{J\alpha}$ whereas full substrate conversion could be reached. Another possibility to enhance the catalyst stability is the immobilization of the catalyst on solid carrier material. Besides stability improvement, the immobilization of enzymes also facilitates the application in continuous systems and downstream processing. The comparison of two different immobilization strategies as well as a screening of different carrier materials led to an active heterogeneous catalyst based on $P450_{J\alpha}$.

Acknowledgements

First of all, I would like to express my gratitude to Prof. Dr. Bernd Nidetzky for giving me the opportunity to work on such an interesting project and to be part of the institute. Additional, I dearly value your thoughtful comments during the meetings and institute seminars which greatly contributed to the success of the project.

In the following, I would like to thank Dr. Alexander Dennig for his caring supervision throughout the whole project. Numerous long lasting scientific and inspiring discussions as well as your time and effort play a big role in the success of my thesis. I really appreciate your trust in me as a student and furthermore how you challenged me to become a better scientist.

Further, I want to thank Dr. Juan Bolivar for providing the carrier materials used for the immobilization. Additional, I am very grateful that you shared your expert knowledge in immobilization and carrier materials with me.

Furthermore, I would also like to thank my colleagues Martin Pfeiffer for the generation of the homology model and Mathilde Steinmassl for the preparation of the expression strain. I am very grateful for the great working environment which owes to all of the colleagues from the institute. Thank you for inspirational talks and for helping me out in any possible situation.

Finally, I would like to thank everyone who supported me on my way including my family and friends. Thank you for every motivational quote, all the laughs we shared, your trust in me and all the unforgettable memories we created. Each and every one of you has his part in my technical and personal development.

Contents

List of Figures

List of Tables

Abbreviations

Abs	Absorption
BSTFA	N,O-Bis(trimethylsilyl)trifluoroacetamide
CPG	Controlled porosity glass
DMAP	4-Dimethylaminopyridine
DMSO	Dimethyl sulfoxide
DTT	Dithiothreitol
D/L-HIC-DH	D/L-isocaproate dehydrogenase from *Lactobacillus confuses*
EtOH	Ethanol
EziG^{TM}	Carrier from EnginZyme
E_{bound}	Bound enzyme
2-OH FA	α-hydroxyfatty acid
3-OH FA	β-hydroxyfatty acid
GC-FID	Gas chromatographer coupled to flame ionzation detector
GOX	Glucose oxidase
^{1}H-NMR	Proton nuclear magnetic resonance
IPTG	Isopropyl β-D-1-thiogalactopyranoside
KPi	Phosphate buffer
k_{cat}	Catalytic constant [min^{-1}]
k_D	Dissociation constant [µM]
L-LOX	L-Lactate oxygenase
MeOH	Methanol
NAD(P)	Nicotinamide adenine dinucleotide (phosphate)
OleT	Cytochrome P450 fatty acid decarboxylase from *Jeotgalicoccus sp.* ATCC 8456
$P450_{J\alpha}$	Cytochrome P450 fatty acid α-hydroxylase from *Jeotgalicoccus sp.* ATCC 8456 (His-tagged)
$P450_{CLA}$	Cytochrome P450 fatty acid α-hydroxylase from *Clostridium acetobutylicum* (His-tagged)
$P450_{BS\beta}$	Cytochrome P450 fatty acid β-hydroxylase from *Bacillus subtilis* (His-tagged)
$P450_{BS\beta\_z}$	Z_{basic2}-tagged $P450_{BS\beta}$

$P450_{BM3}$	Cytochrome P450 fatty acid α-hydroxylase from *Bacillus megaterium* (His-tagged)
$P450_{BM3\_Z}$	Z_{basic2}-tagged $P450_{BM3}$
SDS-PAGE	Sodium dodecyl sulfate polyacrylamide gel electrophoresis
TB	Terrific broth
TTN	Total turnover number [-]
TON	Turnover number [min^{-1}]
Z_{basic2}	Protein tag Z_{basic2}

1. Introduction

1.1. Fatty acid valorization as waste-to-value approach

Fatty acids are classified as lipids and are mainly distinguished by the saturation of the aliphatic chain. Unsaturated fatty acids like oleic acid (C18:1) have at least one C=C double bond in contrast to saturated fatty acids such as dodecanoic acid (C12:0). Especially straight chain fatty acids appear in nature in a large variety of vegetable oils [1, 2]. This is why lipids and therefore also fatty acids are major components of food waste (Figure 1) [3]. As the increase in food „waste“ generation is an emerging problem for our society, there is an urgent need for the removal and the valorization of waste compounds [4–7]. This turns fatty acids into an interesting substrate for waste-to-value approaches.

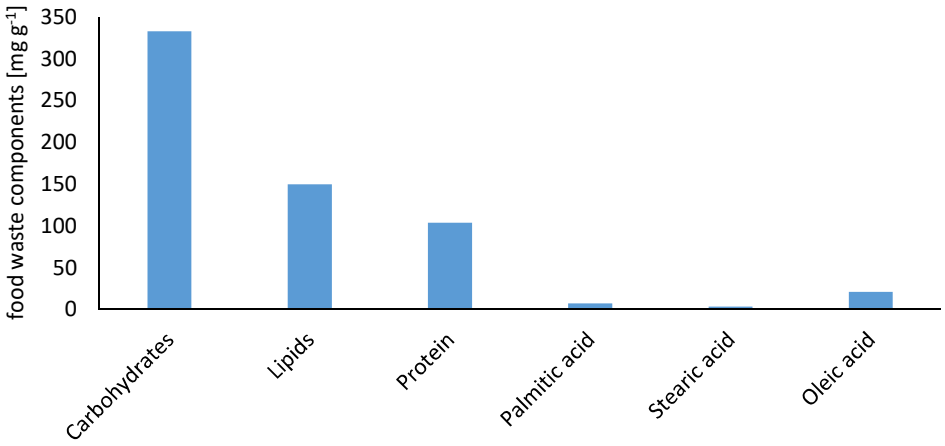

Figure 1 Main components of food waste. Data taken from Pleissner et al 2013 [3].

Fatty acids are already used as cheap starting points for the chemical synthesis of various valuable compounds. Disadvantages are the requirement of great thermal efforts as well as high pressures (up to 200 °C and 200 bar). Chemical conversion is mainly focused on the carboxy-group (>90%) as the selectivity for ω-functionalization or other carbon atoms within the aliphatic chain is low due to unfavorable thermodynamics. The reasons why chemical synthesis is still state of the art in industry are mostly economic [8–10]. An alternative is the application of biocatalysts which display high regio- and stereoselectivities and which catalyze reactions under mild conditions [11]. Cytochrome P450s turned out to be a promising enzymatic class in fatty acid conversion based on their broad spectrum of C-H activations. This also includes hydroxylations at various carbon positions [12–14]. Formed hydroxy fatty acids are valuable compounds as their field of application is broad ranging from polymer chemistry over pharmaceuticals to cosmetics [15]. In particular α-hydroxy fatty acids are interesting as they can be further converted into α-ketoacids, which permit access to a great variety of synthetic/chemical building blocks [16–18].

1.2. Cytochrome P450s as key player in fatty acid conversion

Cytochrome P450s (CYPs, P450s) contain a heme b group and owe their name to the shift in absorption maximum from 420 to 450 nm if the reduced Fe^{2+} binds to carbon monoxide (CO) [19]. P450s are able to perform a variety of reactions including hydroxylations, decarboxylations and epoxidations [20–22]. Based on their large spectrum of C-H activations, P450s are also promising candidates in fatty acid conversion [12–14]. Hydroxylation for instance can appear at various carbon positions ranging from α- and β- to various ω-carbons [23–25]. Cytochrome P450s are divided into several subclasses according to sequence similarities and based on different electron transport systems [26, 27]. Electron supply is either guaranteed by external enzymatic partners or by an integrated reductase domain (self-sufficient systems), which binds the nicotine amide cofactor and electron donor for O_2 activation [27]. Figure 2 shows the catalytic cycle of P450s, starting with the shift from low to high spin heme by replacement of the bound water initiated by substrate binding close to the heme iron [28]. The reactive oxygen species "compound 1" is formed via sequential supply of two electrons and homolytic O_2 cleavage or via the peroxide shunt pathway which is fueled directly by H_2O_2. Due to uncoupling of the iron heme complex (no product formed during electron transfer/compound 2 is not reached) a loss of redox-equivalents can occur [29–32].

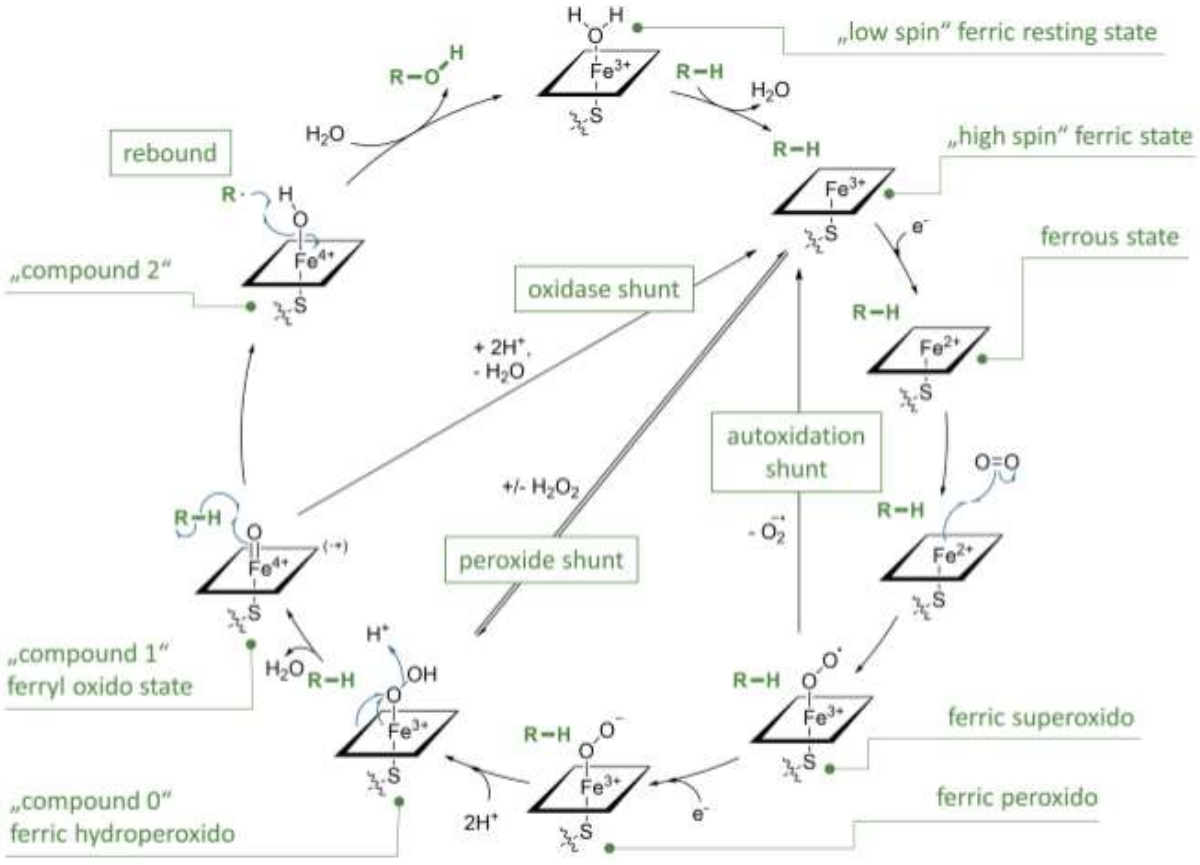

Figure 2 Catalytic cycle of cytochrome P450s including shunt pathways. Figure taken from Hammerer et al 2018 [33].

1.3. P450s peroxygenases

A small subclass of P450s is able to utilize H_2O_2 as oxidant via the peroxide shunt pathway (Figure 2). Advantages are the circumvention of cofactors like NAD(P)H or additional enzymes and also the uncoupling is potentially reduced. Since the peroxide shunt pathway is a shortcut, one of the three possibilities of uncoupling is eliminated. Most P450s peroxygenases are members of the CYP152 subclass, all having a conserved arginine in the active site essential for substrate binding and potentially also for H_2O_2 activation . An extraordinary example of the CYP152 family is OleT, which mainly performs decarboxylation over hydroxylation . Hsieh et al (2017) proposed a reaction mechanism for the oxidative decarboxylation of fatty acids. After formation of active compound 1, a substrate radical is formed by an attack at the β-carbon atom leading to the iron(IV)-hydroxide. Subsequent formation of a potential substrate carbocation allows subtraction of CO_2 and double bond formation (Figure 3) .

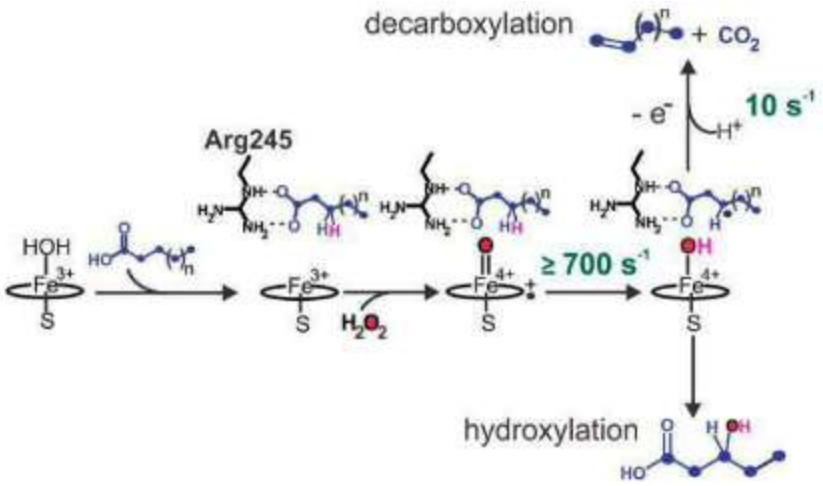

Figure 3 Proposed reaction mechanism of OleT for fatty acid conversion including the pathways for decarboxylation (top) and hydroxylation (bottom). Interaction between the carboxyl-group of the substrate and arginine residue in the active site is depictured whereas an attack at the β-carbon atom is necessary for the decarboxylation route. Figure taken from Hsieh et al. 2017 [34].

Several members of the CYP152 subfamily are already characterized from a biochemical and catalytical point of view. A further outstanding candidate is the α-hydroxylase $P450_{SP\alpha}$ derived from *Sphingomonas paucimobilis*. High turnover numbers (3000 min^{-1}) as well as high regio- and stereoselectivity are displayed by this exceptional catalyst. The major drawback is the extremely low expression yield of the wild-type enzyme in *E. coli* [16, 35] . Another CYP152 classified as α-hydroxylase is the robust peroxygenase $P450_{CLA}$ isolated from *Clostridium acetobutylicum*. Turnover rates as well as the enantiomeric excess could not reach the values of $P450_{SP\alpha}$. However, Girhard et al 2007 reported a regioselectivity towards the α-position of C12:0 with >99% and protein expression yielded 20 to 50 mg per liter culture. $P450_{CLA}$ also proved to be suitable for preparative synthesis [36, 37]. The CYP152 subfamily also includes the β-hydroxylase $P450_{BS\beta}$ derived from *Bacillus subtilis*. Said catalyst has high

turnover numbers (1400 min^{-1}), but drawbacks are the low regio- and enantioselectivities for the α- and β-carbons [36, 38]. OleT is the most extraordinary member of the CYP152 class and was isolated from *Jeotgalicoccus sp*. ATCC 8456. It is classified as decarboxylase and displays a comparably low turnover rate (1.1 min^{-1}) for conversion of fatty acids [39]. Another disadvantage is the low regioselectivity caused by the formation of various by-products [21, 40–42]. To get a closer insight into biochemical and catalytical properties of the CYP152 members the key catalytic parameters are summarized in

Table 1. Selected criteria for characterization were expression yield [mg L^{-1} culture], substrate conversion [%], regio- and stereoselectivity towards the α-position [%], catalytical constant k_{cat} [min^{-1}], dissociation constant [µM] as well as 1-alkene formation (as measure for chemoselectivity).

	Expression yield [mg L^{-1}]	Regio-selectivity α [%]	Enantio-selectivity α (*R*:*S*)	k_{cat} [min^{-1}]	Dissociation constant k_D [µM]	1-alkene formation
$P450_{CLA}$	>25 [36]	>99[a] [36]	32:68[d] [16]	266[c] [37]	221[a] [36]	no [36]
$P450_{SPα}$	Poor [Ref]	>99[b] [38]	3:97[b] [38]	3000[a] [35]	140[a] [35]	no [38]
$P450_{BSβ}$	>25 [36]	12.4[a] [36]	76:24[b] [38]	1400[b] [38]	88[a] [36]	yes [40]
OleT	20 [41]	7.0[a] [34]	-	1.1[b] [39]	2.8[a][34]	yes [40]

Table 1 Biochemical and catalytical characterization of selected P450s classified as CYP152. Reaction set-up with C12:0 (a), C14:0 (b), C10:0 (c) and C8:0 (d).

	Expression yield [mg L^{-1}]	Regio-selectivity α [%]	Enantio-selectivity α (*R*:*S*)	k_{cat} [min^{-1}]	Dissociation constant k_D [µM]	1-alkene formation
$P450_{CLA}$	>25 [36]	>99[a] [36]	32:68[d] [16]	266[c] [37]	221[a] [36]	no [36]
$P450_{SPα}$	Poor [Ref]	>99[b] [38]	3:97[b] [38]	3000[a] [35]	140[a] [35]	no [38]
$P450_{BSβ}$	>25 [36]	12.4[a] [36]	76:24[b] [38]	1400[b] [38]	88[a] [36]	yes [40]
OleT	20 [41]	7.0[a] [34]	-	1.1[b] [39]	2.8[a][34]	yes [40]

To summarize most characterized CYP152s do not combine all desired features for application as industrial catalyst for fatty acid activation (α/β-carbons). While $P450_{SPα}$ displays outstandingly high turnover numbers the very low (soluble) protein expression limit application in larger scales. Especially for CYP152, a high yielding enzyme production is essential as the application of whole-cell systems is not possible. The main reason therefore are the present catalases (high turnover numbers) degrading the peroxide which is on the other hand required for efficient fatty acid conversion with peroxygenases from the CYP152 family [12, 43].

1.4. Current limitations in fatty acid conversion with P450s

Cytochrome P450s have a huge potential for industrial applications based on the great variety in C-H activations catalyzed. This is underlined by high regio- and stereoselectivities as well as high turnover numbers compared to chemical catalysts [33]. Table 2 gives an overview of current limitations for the conversion of fatty acids with P450s. The main focus was on the two key players namely the catalyst and the substrate. A major drawback of P450s is often low activity in comparison to many implemented industrial enzymes. For instance, the cytochrome $P450_{BM3}$ reaches a k_{cat} value of 84.1 s^{-1} whereas already implemented amylases from *Bacillus amyloliquefaciens* reach 2260 s^{-1} [44, 45].This problem can be addressed by protein engineering [46]. Another point to consider is the necessity of co-factors and electron supply to the heme iron. This requires smart cofactor regeneration systems (NAD(P)H) or further catalyst stability improvement (H_2O_2) [36, 47, 48]. The usage of H_2O_2 bears the additional advantage of a potentially reduced uncoupling of the heme iron complex based on the peroxide shunt pathway [33, 49].Concerning the substrate, the major problem is often the limited solubility. Medium and long-chain fatty acids are only soluble to a certain extend (2 mM C12:0 [50]) in aqueous solutions due to their hydrophobicity [51]. A possible solution could be a system consisting of two phases, where the substrate is dissolved in a high concentration in the organic phase [52]. Further additional solvents could enhance the solubility of fatty acids as well as the supplementation of cyclodextrins [53, 54].

Table 2 Overview of the limitations for prep-scale application of P450s converting fatty acids [51].

	Limitations
Catalyst	Enzyme expression
	Catalyst activity
	Cofactor regeneration
	Coupling efficiency
	Operational Stability
Substrate	Solubility

Operational catalyst stability turned out to be one of the major problems to address. Only moderate turnover numbers of the P450s require a robust catalyst to reach acceptable product yields [12]. Next to electron donors like NAD(P)H also peroxide is used for fatty acid conversion with P450s, whereas the H_2O_2 decreases the operational catalyst stability [36]. Therefore stability improvement of the catalyst needed to be taken into account. A promising approach especially for preparative scale productions could be the immobilization of P450s on solid carrier material. The binding of a catalyst on the carrier enhances the robustness by establishing a microenvironment in the particle that shields the catalyst from external influences [55–58].

1.5. Production of heterogeneous catalyst via immobilization

The production of heterogeneous biocatalysts is typically carried out by immobilization on solid carrier material. Next to an enhanced stability due to the protected microenvironment of the particle, immobilization also improves the reusability of the "expensive" catalyst. Further advantages are the enlarged variety in reactor design, the advanced implementation in continuous systems and a facilitated recovery of formed products and applied enzymes [55–57, 59]. Particularly for P450 monooxygenases, an immobilization could also improve the recovery of the required and expensive cofactor [60]. Immobilization of P450s was already reported before addressing the cofactor recycling by co-immobilization [50]. A major drawback during the immobilization process is often the loss in activity compared to the free enzyme. This decrease in activity was also reported for the immobilization of cytochrome P450s. Reasons therefore are enzyme inactivation due to changes in pH and salt concentration required for a successful immobilization, conformational changes caused by the binding to the carrier as well as inaccessibility of the active site. More frequently, mass transfer limitations can occur especially in case of nanoporous structures [58, 61–64]. For industrial purpose, a complete purification of the catalyst before immobilization is not always feasible depending on the formed product. Therefore, not only purified catalyst but also crude lysate containing the target protein is used for immobilization (Figure 4). Occurring problems with this direct approach include contaminations with other proteins which could have an impact on the catalyzed reaction (by-product formation, more catalyst needed). Furthermore, the immobilization efficiency based on the amount of catalyst bound per loading could be decreased due to blockage of binding sites [55].

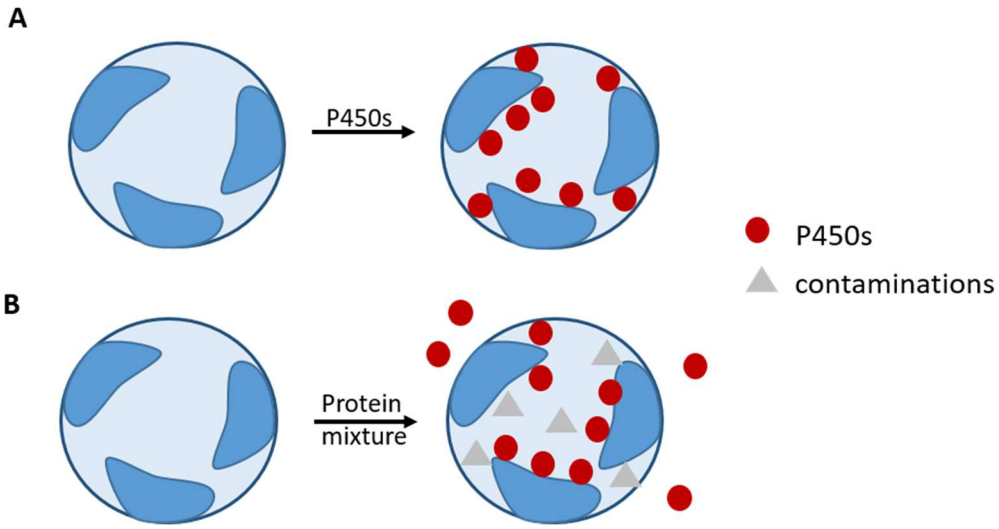

Figure 4 Graphic representation of the immobilization process of P450s in porous carriers. Immobilization of purified catalyst (A) in comparison to immobilization of crude lysates containing the target protein (here P450s) (B). Figure adapted from Garcia-Galan et al 2011 [55].

The immobilization efficiency is not only influenced by the catalyst but also by the carrier material. Said solid compound is designed to enhance in the ideal and best case the catalyst stability and to enable the reusability of the enzyme. Furthermore, the carrier is constructed to facilitate the control of the whole biocatalytical process. Therefore the choice should be done in respect to the later applied reactor set-up as well as downstream processing. For instance, the right carrier material could facilitate the removal of the heterogeneous catalyst (filtration). Those requirements already point out why the selection of a suitable carrier material is one of the key parameters on the way to the successful generation of a functional heterogeneous catalyst. Concerning the carrier itself, several parameters like pore size, hydrophobicity and particle shape affect the immobilization [65]. rier materials.

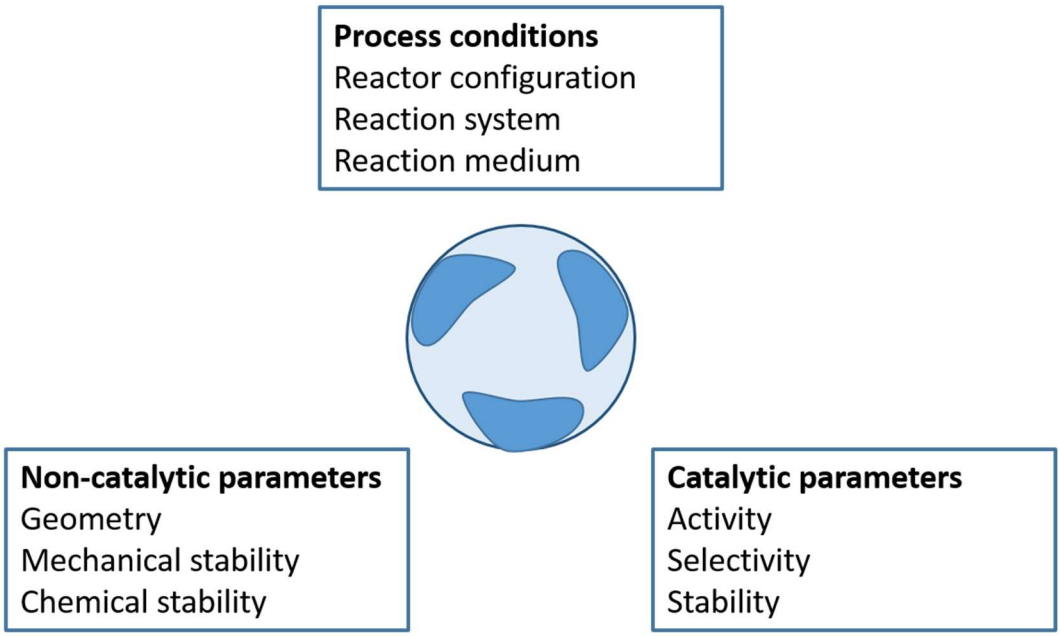

Figure 5 gives a summary of the most important parameters influencing the immobilization process and the choice of suitable carrier materials.

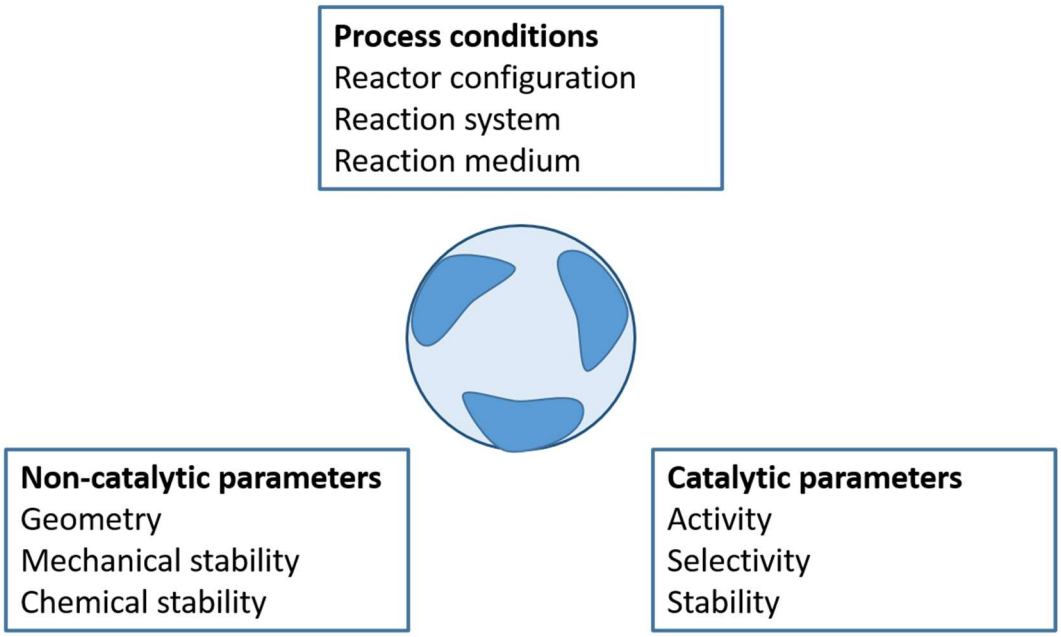

Figure 5 Parameters influencing the immobilization process and the particle selection. Figure adapted from Cao et al (2003) [65].

1.6. Immobilization strategies

Immobilization could be carried out according to four main principles namely adsorption, entrapment, covalent binding and membrane entrapment [58]. Adsorption of the protein to a carrier is the simplest way of immobilization. Therefore most important are the conditions to guarantee a strong, fast and efficient fixation of the catalyst on a solid carrier. Additionally this strategy is also strongly affected by the structure/nature of the catalyst. Successful irreversible immobilization could also be accomplished by covalent coupling of the protein to a carrier. This approach is more complicated as most of the carriers need specific treatment beforehand excluding epoxyacrylic materials [58, 61, 64]. Next to already mentioned immobilization strategies, Ducharme and Auclaire (2018) proposed several possibilities for the immobilization of P450s including a non-covalent approach and the application of a peptide linker [66]. One of the major drawbacks for all reported strategies are the lower activities of immobilized enzymes compared to free catalysts. Concerning P450s, reported recovered activities after immobilization range from 33% (P450 from rat liver microsomes) to 81% for CYP102A2 [67, 68]. The following section gives a deeper insight into two immobilization strategies selected for the production of a heterogeneous catalyst of members from the CYP152 family in this thesis.

Bolivar and Nidetzky (2012) proposed a new strategy to immobilize proteins on silica and negatively charged surfaces applying a cationic protein tag [69]. The small tag Z_{basic2} (7 kDa) is therefore cloned either at the C- or N-terminus of the target protein. [70–72]. Z_{basic2} is strongly positively charged caused by the high number of arginines and for this reason shows high affinity towards negatively charged surfaces [73, 74] (Figure 6A). For the attachment of the Z_{basic2}-tag at the N-terminus, no affection of the protein expression yield as well as the activity and selectivity of the catalyst were reported so far [73]. Bolivar and Nidetzky (2012) state that Z_{basic2} is a promising alternative for protein immobilization as the interaction is highly stable due to ionic binding. Additional, only the Z_{basic2} tag interacts with the negatively charged surface pointing out that the catalytic part of the enzyme is not directly or to a certain extend less involved in binding to the carrier. Therefore, an activity loss due to structural changes during the immobilization should be reduced [69]. A successful application of this immobilization strategy for P450s was reported by Valikhani et al (2018). The immobilization was carried out directly from the cell extract containing the enzyme, whereas no purification step is required [74]. For single enzyme immobilization of $P450_{BM3\_Z}$ a total activity of 21.6 $U/g_{carrier}$ for the hydroxylation of anisol was reached [50]. In comparison, Dennig et al (2013) reported a specific activity of the native $P450_{BM3}$ for anisol with 0.65 U/mg [50, 75]. Furthermore, already reported immobilizations of $P450_{BM3}$ could not reach similar activities. For instance, Solé et al (2018) reported an activity of 1.8 $U/g_{carrier}$ for sodium laureate applying an entrapment approach for immobilization [76].

A second and non-covalent immobilization strategy is based on a widely applied method for affinity chromatography, where a polyhistidine tag forms a metal chelate complex with a potential carrier material activated with metals like Ni^{2+} (Figure 6B) [77–79]. Therefore the production of a heterogeneous catalyst via His-tag affinity binding could couple the purification and immobilization of a target protein in one step [80]. This is underlined by the strong affinity between the carrier and the protein tag, which leads to highly selective interactions [81, 82]. Advantages thereof are the avoidance of the expensive and time-consuming chromatography step and the immobilization directly from the cell extract containing the desired enzyme [55, 74]. Piesecki et al (1993) reported the successful coupling of purification and immobilization using a His-tagged β-galactosidase. Up to 64% of the activity could be determined for the immobilized catalyst in respect to the activity of the soluble His-tagged β-galactosidase. Beneficial was the reusability of the immobilized enzyme as the soluble β-galactosidase is completely inactive after one round of production of the allyl-β-D-galactopyranosid. Noteworthy, the activity of the immobilized catalyst was reduced after every batch reaction [78].

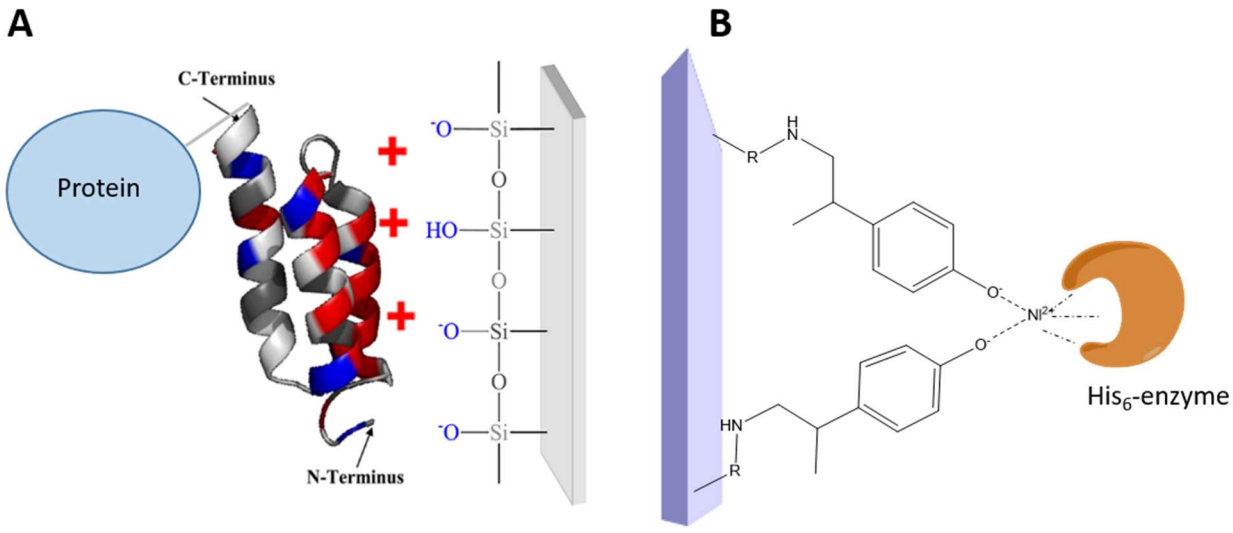

Figure 6 Comparison of two protein immobilization approaches namely via ionic binding (A) and affinity binding (B). For ionic binding on silica the positively charged Z_{basic2} protein tag is required. Affinity binding is given by the interaction of the polyhistidine tag and the activated carrier material. Figure adapted from Bolivar and Nidetzky 2012 (A) [69] and from Engelmark et al 2014 (B) [80].

Comparing both immobilization strategies, the greatest difference lies in the binding of the enzyme to the carrier material. An ionic bond is formed between the Z_{basic2}-tag from the target protein and the negatively charged carrier. In contrast, affinity between the histidine residues and the metal ion leads to a chelate complex and successful immobilization of the target protein via His-tag. High selectivities for the target protein is given for both approaches under the right conditions. Overall the ionic bond is very strong, which could especially enhance the reusability of the immobilized enzyme. However, the Z_{basic2} protein tag (7 kDa) is fairly large compared to the His-tag (<1 kDa). Still possible negative

effects on the recombinant protein expression in *E. coli* were not reported yet [69, 77]. Although, Valikhani et al (2018) could reach a concentration of 4 µmol L^{-1} of the Z_{basis2} tagged $P450_{BM3}$ in the cell free extract [50]. In contrast, Solé et al (2018) reported a concentration of 45 µmol L^{-1} for the His-tagged version of the protein [76]. Concluded, both immobilization strategies have the potential to be the key to a successful immobilization of the CYP152s.

1.7. Aim of this thesis

The aim of this project is to characterize and determine the synthetic potential of the newly discovered fatty acid hydroxylase $P450_{J\alpha}$ that was identified and isolated from *Jeotgalicoccus sp.* ATCC 8456 a Gram positive bacteria. Being a paralog of the decarboxylase OleT the biochemical characterization of $P450_{J\alpha}$ is of significant relevance in terms of evolutionary, mechanistic and biocatalytical point of view. The biochemical characterization should allow to annotate $P450_{J\alpha}$ to a CYP subclass (CYP152 family) based on sequence, structure and function of the protein. The catalytic characterization of the enzyme covers specific activity (turnover numbers), substrate affinity (dissociation constants) coupling efficiency as well as regio- and stereoselectivity for hydroxylation of selected fatty acids. Beyond this, the protein expression and the storage stability of the catalyst are investigated, which is in particular important for further synthetic applications. A significant challenge in peroxygenase catalysis remains the controlled supplementation of H_2O_2 to avoid rapid catalyst inactivation. To improve the catalyst lifetime two approaches are evaluated a) direct supplementation of H_2O_2 under controlled conditions and b) slow release via enzymatic generation or alternative slow release systems. In a further approach the biochemically characterized enzyme should be tested in form of a heterogeneous catalyst. Heterogeneous catalysts offer several advantageous features including high catalyst density, re-usability and catalyst stabilization. Two different oriented and mild immobilization strategies should be applied a) via ionic with Z_{basic2} protein tag and b) affinity binding via His-tag. Both strategies would allow a simultaneous and partial purification which is required for peroxygenases. In order to identify a suitable carrier screening of different metal-activated carriers will be carried out. To this end, this thesis aims to facilitate the use of P450 peroxygenase in fatty acid conversion to evaluate its potential for industrial application. Fatty acid conversions in particular with P450 peroxygenases require more selective, robust and stable catalysts for application in industrial processes.

2. Material and Methods

2.1. Materials

2.1.1. Chemicals

All chemicals used were purchased from Roth, Sigma Aldrich or Tokyo Chemical Industry if not indicated differently.

Table 3 List of applied chemicals

Hydrogen peroxide	Roth (Karlsruhe, Germany)
Urea-Hydrogen peroxide	Sigma Aldrich (St. Louis, Missouri, United States)
1-octanol	Sigma Aldrich (St. Louis, Missouri, United States)
Sodium dodecyl sulfate	New England Biolabs (Ipswich, Massachusetts, United States)
(Trimehtlysilyl)diazomethane	Sigma Aldrich (St. Louis, Missouri, United States)
N,O-Bis(trimethylsilyl)trifluoroacetamide	Sigma Aldrich (St. Louis, Missouri, United States)
Ethylchloroformate	Sigma Aldrich (St. Louis, Missouri, United States)
4-Dimethylaminopyridine	Sigma Aldrich (St. Louis, Missouri, United States)
Deutereate Methanol	Sigma Aldrich (St. Louis, Missouri, United States)
Iminodiacetic acid	Sigma Aldrich (St. Louis, Missouri, United States)
(Z)-9-Octadecenoic Acid	AppliChem (Darmstadt, Germany)
B-Per® Bacterial Protein Extraction Reagent	Thermo Fisher Scientific Inc. (Waltham, Massachusetts, USA)

2.1.2. Carrier

Materials (agarose, sepharose and controlled porosity glass) and metals ($NiSO_4$, $CuSO_4$) used for carrier production were either purchased from Roth (Karlsruhe, Germany) or from Sigma Aldrich (St. Louis, Missouri, United States).

Table 4 Overview of purchased carrier material for immobilization

	Company	properties	Functional groups/ chelated metal ions	Pore size [nm]
EziG Fe1™	EnginZyme AB (Stockholm, Sweden)	hydrophilic	Fe^{3+}	50 ± 5
EziG Fe2™	EnginZyme AB (Stockholm, Sweden)	hydrophobic	Fe^{3+}	30 ± 5
EziG Fe3™	EnginZyme AB (Stockholm, Sweden)	semi-hydrophilic	Fe^{3+}	30 ± 5
ReliSorb™ SP400	Residion S.r.l. (Milan, Italy)	Strong cation exchanger	sulphonic	40-50
ReliZyme™	Residion S.r.l. (Milan, Italy)	hydrophilic	epoxy?	40-60

EziG™ carriers are based on controlled porosity glass. ReliSorb™ SP400 and ReliZyme™ are made of a polymetacrylate polymer and a methacrylic polymer matrix, respectively.

2.1.3. Growth media and supplements

All media components and supplements were purchased from Roth (Karlsruhe, Germany). Except for the δ -aminolevulinic acid, which was obtained from Sigma Aldrich (St. Louis, Missouri, United States). Media components were dissolved in water and autoclaved at 121 °C for 20 min. Supplements prepared as were added after autoclaving.

Table 5 List of used media including compound concentrations and supplements

	Component	Concentration
LB-Media	Tryptone	10 g L^{-1}
	Yeast extract	5 g L^{-1}
	NaCl	10 g L^{-1}
TB-Media	KH_2PO_4	2.31 g L^{-1}
	K_2HPO_4	12.54 g L^{-1}
	Tryptone	20 g L^{-1}
	Yeast extract	24 g L^{-1}
	Glycerol	4 mL L^{-1}
Supplements	δ -aminolevulinic acid	0.5 mM
	IPTG	0.2 mM

	Kanamycin	50 µg mL^{-1}
	Trace element solution	0.5 mg L^{-1} $CaCl_2 \cdot 2H_2O$, 0.18 mg L^{-1} $ZnSO_4 \cdot 7H_2O$, 0.1 mg L^{-1} $MnSO_4 \cdot H_2O$, 20.1 mg L^{-1} Na_2-EDTA, 16.7 mg L^{-1} $FeCl_3 \cdot 6H_2O$, 0.16 mg L^{-1} $CuSO_4 \cdot 5H_2O$

2.1.4. Enzymes

Table 6 List of applied enzymes

	Activity	Source	Company
Lysozyme	≥35000 U mg^{-1}	Chicken egg white	Roth (Karlsruhe, Germany)
Glucose oxidase	150-200 U mg^{-1}	*Aspergillus niger*	Sigma Aldrich (St. Louis, Missouri, United states)
Catalase	2000-5000 U mg^{-1}	Bovine liver	Sigma Aldrich (St. Louis, Missouri, United states)
D/L-HIC	10 U mg^{1}	*Lactobacillus confuses*	-
L-LOX	?	*Aerococcus viridans*	-

2.1.5. Bacterial strain

Table 7 Bacterial strain used for protein expression

Strain	Properties
Escherichia coli BL21(DE3)	str. B F^- ompT gal dcm lon $hsdS_B(r_B^- m_B^-)$ λ(DE3 [lacI lacUV5-T7p07 ind1 sam7 nin5]) $[malB^+]_{K-12}(\lambda^S)$

2.1.6. Laboratory devices

Table 8 List of laboratory devices

Analytical Balance ENTRIS® 224I-1S	Sartorius AG (Goettingen, Germany)
Balance LE224S	Sartorius AG (Goettingen, Germany)
WPA CO8000 Cell Density Meter	Biochrom WPA (Cambridge, UK)

Sterile workbench Bioair Auro 2000 Laminar Flow	EuroClone S.p.A. (Milan, Italy)
Rotary shaker CERTOMAT® BS-1	Sartorius AG (Goettingen, Germany)
Ultracentrifuge Sorvall® Evolution RC	Thermo Fisher Scientific (Waltham, Massachusetts, USA)
Vortex Reax 2000	Heidolph Instruments GmbH &Co.KG, (Schwabach, Germany)
Fisher Scientific* Model 705 Sonic Dismembrator	Thermo Fisher Scientific (Waltham, Massachusetts, USA)
Eppendorf Centrifuge 5415 R	Eppendorf AG (Hamburg, Germany)
Minisart® Single use filter unit 0.45 µm	Sartorius AG (Goettingen, Germany)
ÄKTAprime plus	Amershan BioSciences, GE Healthcare (Chicago, IL, USA)
HiTrap SP FF column, 5 mL	GE Healthcare Life Sciences (Chicago, Illinois, USA)
HisTrap HP protein purification column	GE Healthcare Life Sciences (Chicago, Illinois, USA)
Centrifugal concentrator Vivaspin®	Sartorius AG (Goettingen, Germany)
Varian Cary® 50 UV-Vis spectrophotometer	Varian Medical Systems Inc (Palo Alto, California)
Infinite M200	Tecan Group AG (Männedorf, Switzerland)
DeNovix DS-11 Spectrophotometer	DeNovix Inc. (Wilmington, North Carolina, USA)
GC-MS: 7890B GC – 5977A MSD	Agilent Technologies (Santa Clara, California, USA)
GC-FID: Hewlett Packard Series II	(Hewlett-Packard, Palo Alto, California, United States)
CP Chirasil-DEX CB	Agilent Technologies (Santa Clara, California, USA)
OXR430-HS	Pyroscience GmbH (Aachen, Germany)
NuPAGE™ 4-12% Bis-Tris Gel	Invitrogen Thermo Fisher Scientific (Carlsbad, California, United States)
LDS Sample Buffer (4x)	Invitrogen Thermo Fisher Scientific (Carlsbad, California, United States)

Rotator SB3	Stuart equipment (Staffordshire, United Kingdom)
Alitea-XV	Bioengineering AG (Zurich, Switzerland)
MCP-CPF Process IP65	IsmaTec (Wertheim, Germany)
Laborota 4000	Heidolph Instruments GmbH &Co.KG (Schwabach, Germany)
Christ ALPHA 1-4	B. Braun Biotech GmbH (Berlin, Germany)
Bruker Magnetic Resonance Spectroscopy	Bruker (Billerica, Massachusetts, United States)

2.2. Protein expression and purification of CYP152

2.2.1. Cultivation in shaking flasks

E. coli BL21 (DE3) cells carrying the plasmid coding for the respective CYP152 genes [21, 36, 83], were grown in 50 mL lysogeny broth (LB) media supplemented with 50 µg mL^{-1} kanamycin for plasmid maintenance. From this pre-culture 2.5 mL were taken to inoculate 250 mL terrific broth (TB) media. 50 µg mL^{-1} of kanamycin and 250 µL of a sterile filtrated trace element solution were added. Cultivation took place at 37 °C and 100 rpm until an OD_{600} of 0.8 was reached. Subsequently, cultures were induced with IPTG (0.2 M) and supplemented with the heme precursor δ-aminolevulinic acid (0.5 M) followed by incubation at 20 °C and 100 rpm for 20 h. The cells were harvested and separated from the cultivation broth by centrifugation (8850 x g, 15 min and 4 °C). Subsequently, produced cell pellets were frozen at -30 °C to enhance cell disruption. According to this protocol the His-tagged $P450_{J\alpha}$ (Figure 13), $P450_{CLA}$ and $P450_{BS\beta}$ (Figure 59) as well as the $P450_{BS\beta\_Z}$ (Figure 46) were expressed successfully.

2.2.2. Affinity chromatography

For cell disruption, frozen cell pellets (<5 g) were resuspended in 20 mL buffer A (0.1 M KPi buffer, pH 7.5, 300 mM KCl, 25 mM imidazole) containing 1 mg mL^{-1} lysozyme. The cell suspension was incubated at least for one hour at 37 °C (Figure 7A). Subsequently, the digested cells were disrupted with a sonic dismembrator for 6 min with 60% amplitude (pulse for 2 sec; pause for 4 sec). The cell suspension was centrifuged (16110 x g, 15 min, 4 °C) to remove cell debris followed by filtration of the supernatant (1.2 µm cellulose-acetate filter).

For His-Tag purification buffer B (elution buffer 0.1 M KPi, pH 7.5, 300 mM KCl and 400 mM imidazole) and buffer C (dialysis buffer 0.1 mM KPi, pH 7.5, 300 mM KCl) were prepared. The His-Trap™ column was stripped and recharged with a fresh $NiSO_4$ solution according to the protocol of GE Healthcare. As P450s appear as red colored proteins caused by the functional heme group, the purification could be done simply with a peristaltic pump connected to the purification column. Equilibration of the purification column was done with buffer A followed by loading of the protein suspension (Figure 7B). Unbound proteins were eluted by washing the column with 10 column volumes of buffer A. Buffer B was used for elution of the target protein. Subsequently, the column was extensively washed with buffer B (10 column volumes) followed by ddH_2O (10 column volumes). For long term storage at 4 °C the His-Trap™ column was kept in EtOH (>20%). First the enzyme solution was concentrated to 2 mL by centrifugation at 3200 x g, 15 min and 4 °C with a centrifugal concentrator (30 kDa). Subsequently, buffer C (10 mL) was added followed by centrifugation (3200 x g, 15 min, 4 °C).These steps were

repeated at least three times to completely remove the imidazole from the purification process. Finally, the active protein concentration was determined by carbon monoxide titration [84].

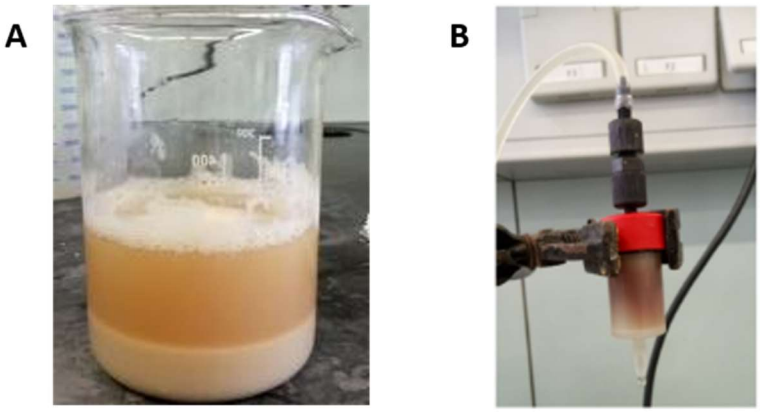

Figure 7 Cell disruption (A) and protein affinity chromatography column (B) representing the protein purification process. Resuspended cell pellets after incubation with lysozyme for 1h at 37 °C with lysozyme (A). Slightly red supernatant due to the red P450s and on bottom the cell debris. His-Trap™ column during affinity chromatography (B). Red color indicates the bound P450 protein.

2.2.3. Ion exchange chromatography

The frozen cell pellets were resuspended in 50 mM KPi buffer with pH 7.5 containing 1 mg mL^{-1} lysozyme. After incubation at 37°C for at least 1 h, the cell disruption, centrifugation and filtration were carried out as described in the section above (2.2.2). For the purification of $P450_{BS\beta\_Z}$ via cation exchange chromatography the Aekta system was used to monitor the elution of target proteins. The HiTrap™ cation exchange column was equilibrated with 10 column volumes of the resuspension buffer (50 mM KPi, pH 7.5), followed by loading of the filtrated protein solution. Subsequently, 10 column volumes of the resuspension buffer were used to remove unbound proteins. Elution of bound proteins was done using a NaCl gradient. For this, the resuspension buffer was gradually mixed with an elution buffer solution (50 mM KPi, pH 7.5, 2 M NaCl) from 0 to 100% with a final volume of 100 mL. Elution of proteins was recorded by the installed UV-detector (280 nm wavelength). After the purification, the column was extensively washed with 10 column volumes of elution buffer (50 mM KPi, pH 7.5, 2 M NaCl) followed by ddH_2O (10 column volumes) and finally kept in 20% EtOH for long term storage at 4 °C. The collected fractions were pooled and concentrated to 2 mL by centrifugation (3200 x g, 15 min, 4 °C) with a centrifugal concentrator (30 kDa cut off). Subsequently, the active protein concentration was determined with carbon monoxide titration [84].

2.2.4. Protein size and purity determination (SDS-PAGE) of $P450_{J\alpha}$

The protein size of $P450_{J\alpha}$ was calculated using the Expasy online tool. Beforehand the DNA sequence of $P450_{J\alpha}$ was translated into the corresponding protein sequence (Expasy translate tool). The theoretically calculated molecular mass of $P450_{J\alpha}$ (monomer) is 48.2 kDa. To verify the formation and

purity of $P450_{J\alpha}$ during the cultivation and purification of the enzyme a SDS-PAGE was carried out. The following samples were loaded onto a 4 to 12% SDS-gel: a) before induction, b) after 20 h of protein expression, c) after cell disruption and d) the purified $P450_{J\alpha}$. For this cells were treated with B-Per reagent (cell lysis reagent) according to the supplier's protocol of Thermo Fisher Scientific. In order to estimate the protein concentration in a sample a spectro-photometrical measurement was performed, where the absorption at 260 nm and 280 nm was measured. Before loading the samples onto the SDS-gel they are diluted with ddH_2O to a final concentration of 1 mg mL^{-1} per lane. 14 µL of the protein sample were mixed with 5 µL of SDS and 1 µL of DTT. Proteins were denaturated by heating the samples to 95 °C for at least 10 min followed centrifugation (16110 x g, 2 min, room temperature) and loading of the gel (15 µL per sample). As reference size standard the unstained page ruler (5 µL) from Thermo Fisher Scientific was used. The SDS-gel was run with 200 V for 60 min. Subsequently, the gel is stained with a Coomassie Blue solution (1 g dissolved in MeOH 50% (v/v) and acetic acid 10% (v/v)). Stained gels were destained in a solution containing ddH_2O, MeOH and acetic acid in a ratio of 50/40/10 (v/v).

2.3. Biochemical characterization of $P450_{J\alpha}$

2.3.1. Sequence alignment of CYP152s

A BLAST search with the sequence of $P450_{J\alpha}$ was carried out using the online tool from the National Center for Biotechnology Information. Highest sequence similarities were reached for enzymes from the CYP152 family. This led to the selection of already characterized CYP152s for the generation of a sequence alignment with Clustal Omega from the European Molecular Biology Laboratory. Based on the obtained result from the sequence alignment a phylogenetic tree was generated using Jalview [85]. Numbers flanking the branches are indicating the similarity of the sequences.

2.3.2. Generation of a homology model of $P450_{J\alpha}$

To determine the structural features of $P450_{J\alpha}$ a homology model was generated based on already existing crystal structures of $P450_{BS\beta}$ [86] and $P450_{SP\alpha}$ [38]. The pdb files ($P450_{BS\beta}$: 1izo [86] and $P450_{SP\alpha}$: 3awm [38]) of the template crystal structures were obtained from UniProt. First the protein sequence of $P450_{J\alpha}$ was entered into the SwissModel [87] online tool to generate the homology model. Subsequently, the pdb files from $P450_{BS\beta}$ and $P450_{SP\alpha}$ were added as template files. The resulting protein structures for $P450_{J\alpha}$ only depictured the holoenzyme without any ligands (heme b, fatty acid). Therefore the heme group and the fatty acid (C16:0) were modeled into the active site of $P450_{J\alpha}$ using YASARA. As the interaction of the active site with the substrate is of great interest, LigPlots were generated by applying LigPlus [88]. Therefore the pdb files were loaded into the program and the corresponding ligand (fatty acid) was chosen. Resulting LigPlot depictures the interactions between

the active site of the target protein and the respective ligand/substrate. LigPlots were also prepared for $P450_{SP\alpha}$, $P450_{BS\beta}$ and OleT (pdb: 4l40 [41]) based on their readily available crystal structure models. Concerning $P450_{CLA}$, the LigPlot was based on a beforehand prepared homology model. This homology model was generated based on the crystal structure of $P450_{SP\alpha}$ applying the same programs as already mentioned above.

2.3.3. Quantification of active P450 concentration by CO-titration

Carbon monoxide titration is used to determine the active protein concentration of P450s [84]. Therefore, Fe^{3+} of the heme needs to be reduced to Fe^{2+}, whereas the reducing agent is dithionite. For reduction of P450s, a spatula tip (2 mg) of sodium dithionite was mixed with a 1 to 20 dilution of the enzyme solution in buffer C. The first photometric measurement was done with the ungassed protein over a wavelength course of 300 to 600 nm. Subsequently, the samples was gassed with carbon monoxide (1 min), which binds to Fe^{2+} and shifts the absorption maximum from 420 nm to 450 nm. The sample is measured again over 300 to 600 nm. Differences between aerated and non-aerated samples are used to calculate the active protein concentration based on the Lambert-Beer law, whereas the extinction coefficient was 91 L $mmol^{-1}$ cm^{-1} and the layer thickness was 1 cm [84].

$$\Delta E = \varepsilon * c * d$$

ΔE	change of absorption
ε	extinction coefficient [L $mmol^{-1}$ cm^{-1}]
c	concentration [mM]
d	layer thickness [cm]

2.3.4. Dissociation constants of $P450_{J\alpha}$ for binding of fatty acids

Dissociation constants of fatty acids were determined photometrically by changes in the spin-shift states triggered by the substrate binding close to the heme iron. First, a 1.5 µM enzyme solution in buffer C was prepared. A baseline scan of the enzyme solution without substrate was done and used as reference. The fatty acid stock was prepared in DMSO. Afterwards <5 µL of the substrate stock (50 mM) were added to the enzyme solution, mixed and incubated for 30 s. Measurements took place over a wavelength course of 300 to 500 nm. Spin-state shifts appear at 388 to 395 nm for low spin and 417 nm to 422 nm for high spin [15, 34, 36, 38, 89–91]. Throughout the determination, the amount of substrate added per step was increased to 500 µM (= 100 µL). Further substrate addition was stopped when no further increase/decrease for high and low spin state shift was detectable. Subsequently, the absorption of the low spin state was subtracted from the corresponding value of the high spin state. Obtained values were curve fitted using Origin 9.0 software and Hill functions. Subsequently,

respective dissociation constants (k_D-values) could be calculated based on the obtained equations. The dissociation constant is a measure of the affinity from the enzyme to the substrate. Furthermore, the higher the k_D-value the lower is the affinity for the substrate [92] (Figure 8).

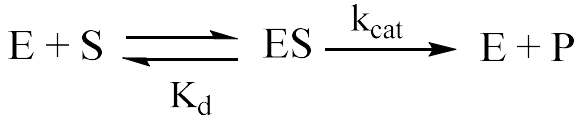

Figure 8 Scheme of enzymatic substrate conversion/product formation [92].

2.4. Reaction set-up for fatty acid conversion with $P450_{J\alpha}$

2.4.1. Optimization of the reaction set-up for fatty acid conversion with $P450_{J\alpha}$

An optimized reaction set-up was determined based on previous works using $P450_{CLA}$ [16, 21, 36] by investigating the influence of the buffer system, H_2O_2 pulsing rate/concentration and substrate to enzyme ratio. Concerning the buffer system varying KCl concentrations were examined ranging from 0 to 1000 mM. Dodecanoic acid (2 mM) was converted with 3 µM $P450_{J\alpha}$ and 0.5 mM H_2O_2 per 30 min in buffers with varying salt concentrations. The fatty acids were pre-dissolved in ethanol (2.5% of final volume) and added first followed by the buffer. Peroxide was applied in equimolar concentration related to the substrate. Reactions were carried out at 100 rpm and at room temperature.

2.4.1.1. H_2O_2 concentration optimization

The supplementation of the oxidant H_2O_2 was optimized in respect to the peroxide concentration per pulse. Applied reaction set-up was 5 mM dodecanoic acid, 6 µM $P450_{J\alpha}$ and differently concentrated peroxide pulses added every 30 min in buffer C. Supplemented peroxide concentrations ranged from 0 to 2000 mM per pulse (Table 9). The final peroxide concentration was equimolar in respect to the used substrate.

2.4.1.2. H_2O_2 pulsing optimization

Next to the concentration of peroxide per pulse, also the interval time between every pulse was investigated. Applied reaction set-up was again 5 mM dodecanoic acid and 6 µM $P450_{J\alpha}$.The interval times were varied from 5 min to 45 min and per pulse 0.25 mM H_2O_2 were added. In total 2.5 mM of peroxide was supplemented. An overview of the optimization concerning the peroxide supplementation for fatty acid conversion with $P450_{J\alpha}$ is given in Table 9.

Table 9 Optimization of H_2O_2 pulsing including the change in interval time [min] between the pulses and amount of H_2O_2 [mM] per pulse

Interval time per pulse [min]	H_2O_2 per pulse [µM]
5	50
10	250
15	500
30	666
45	1000
-	2000

2.4.2. Extended substrate screening

The substrate scope was extended to fatty acids with chain lengths from C6:0 to C16:0. Beyond saturated fatty acids also oleic acid, adipic acid and 10-undecene acid were used for further conversions. Applied reaction set-up was 2 mM fatty acid substrate, 3 µM $P450_{J\alpha}$ and 0.5 mM H_2O_2 per 30 min in buffer C. Peroxide concentration was equimolar to the substrate. Reactions were carried out under shaking (100 rpm) and at room temperature.

2.4.3. Determination of key catalytic parameters of $P450_{J\alpha}$ in fatty acid conversion

The characterization of $P450_{J\alpha}$ included the determination of the key catalytic parameters specific activity, (total) turnover number and coupling efficiency (Table 10). Each parameter required a specific reaction set-up, whereas an overview is given in Table 11. All reactions took place in buffer C. Oxidant supply either was done continuously with 0.5 mM H_2O_2 per 30 min (conversion) or added at once (specific activity and coupling). The final peroxide concentration was kept equimolar in relation to the substrate. Concerning the specific activity, the amount of enzyme was reduced to 1 µM for dodecanoic acid, decanoic acid and oleic acid due to high turnover rates and fast substrate conversion.

Table 10 Overview of the key catalytic parameters determined for fatty acid conversion with $P450_{J\alpha}$. The coupling efficiency describes the percentage of NAPDH/H_2O_2 utilized for hydroxylation of the fatty acid [93].

Catalytic parameter	Unit	Definition
Specific activity	U mg^{-1}	µmol substrate converted per min and mg catalyst applied
Total turnover number (TTN)	-	µM substrate converted per µM catalyst applied
Turnover number (TON)	min^{-1}	µM substrate converted per µM catalyst per min

Coupling efficiency	%	Substrate conversion in a fixed reaction set-up

Table 11 Reaction set-up for determination of catalytic numbers. 0.5 mM H_2O_2 per 30 min (a) and 1 mM H_2O_2 at once (b) until equimolar to the substrate concentration.

	Unit	Fatty acid [mM]	$P450_{J\alpha}$ [µM]	H_2O_2 [mM]	Time [min]
Conversion	%	2	3	2[a]	120
Specific activity	U mg^{-1}	1	3	1[b]	2, 5, 10
Coupling efficiency	%	1	1	1[b]	60

2.5. Product analysis using gas chromatography

2.5.1. Extraction and derivatization of substrates and products

For the extraction of fatty acids and the formed hydroxy fatty acids the reaction mixture (2 mL) was acidified by the addition of 200 µL HCl (37%). The extraction solvent was ethyl acetate containing 0.1 % (v/v) 1-octanol as internal standard. After extensive mixing to enhance the extraction yield, the samples were centrifuged at 3200 x g and room temperature for 2 min. The organic phase was separated and dried over Na_2SO_4 to remove residual water. Subsequently, derivatization is required for GC measurements of hydroxy fatty acids to facilitate the vaporization into the gas phase for GC-analysis. Therefore, samples were either methylated or silylated. The methylation of the fatty acid substrate and the 2-/3-hydroxy fatty acids led to the corresponding methyl esters. In contrast, the silylation resulted in silylated fatty acid substrates and hydroxy fatty acids [16]. For the methylation 60 µL of MeOH were mixed with 120 µL of the sample and 5 to 10 µL of diazomethane (applied in excess). For silylation, 100 µL of the reaction sample were mixed with 100 µL BSTFA and 100 µL of pyridine, followed by incubation at room temperature for 2h. Afterwards the samples were analyzed by gas chromatography (GC-MS/GC-FID). To quantify substrate depletion and product formation calibration curves were prepared accordingly. Both gas chromatographs were calibrated for the quantification of the substrates. Only the GC-FID was calibrated for the α-hydroxy dodecanoic acid as detection problems with the GC-MS for this compound appeared. Defined concentrations of fatty acids (0 to 5 mM) were prepared in buffer C and injected after extraction and derivatization. Results were plotted after dividing the obtained areas of the fatty acids by the area of the internal standard (1-octanol). Equations obtained from linear regression were used for quantification of the reaction outcome (e.g. Figure 76).

2.5.2. Gas chromatography coupled to flame ionization (GC-FID)

Two different GC methods were applied to analyze fatty acids and produced hydroxy fatty acid products. For quantification, a GC coupled to a flame ionization detector (GC-FID) from HP Series II was used. The carrier gas was hydrogen and the solvents to wash the syringe were toluene and methyl acetate. This device was equipped with an Agilent HP-5 column (30 m x 320 µm, 0.25 µm film) and only liquid samples could be analyzed. The applied method was "ACHRIAL" and the temperature program is shown in Table 12. For shorter chain fatty acids (<C10:0), the initial oven temperature was reduced to 60 °C. Furthermore, the inlet was heated up to 275 °C and the detector to 300 °C. Results were integrated manually and obtained peak areas were used for further calculations, whereas the internal standard 1-octanol was used for quantification. Authentic analytical standards were applied to determine the specific retention time of each compound.

Table 12 Temperature program method "ACHRIAL" for GC-FID measurement of liquid samples. For medium and long chain fatty acids (>C10:0) (a). For short chain fatty acids (<C10:0) (b).

Start	100 °C[a]/ 60 °C[b]
Hold	100 °C[a]/ 60 °C[b] for 5 min
Rise	20 °C per min
End	320 °C

2.5.3. Gas chromatography coupled to mass spectrometry (GC-MS)

To identify structures of formed reaction products a chromatographer equipped with a mass selective detector was applied. Compounds were identified based on mass fragmentation and in comparison to the NIST library as well as known fragmentation spectra of previous reported compounds [37], [94]. Helium was used as carrier gas and the GC-MS was equipped with an Agilent HP-5MS column (30 m x 320 µm, 0.25 µm film). The Agilent Technologies 7890B GC 5977A MSD was used to analyze liquid samples and to perform headspace measurements. Analysis of liquid samples was carried out by applying the identical heating programs as for the GC-FID (Table 12). For longer chain fatty acids like oleic acid the starting temperature was increased to 120 °C. Headspace analysis was carried out according to the temperature program in Table 13. This also included the pre-heating of the samples (80 °C) and the syringe (90 °C). For shorter chain fatty acids and their corresponding 1-alkenes the oven starting temperature was reduced to 50 °C (C6:0) or 60 °C (>C6:0). No internal standard was used for headspace analysis. Evaluation of the results was done with the corresponding ChemStation software. Quantification of 1-alkenes was given by beforehand prepared calibrations ranging from 0-250 µM of 1-alkenes in buffer C. The high volatility of 1-alkenes required a specific preparation. GC-MS headspace vials and the buffer C were frozen in liquid nitrogen before adding the 1-alkenes to reduce unwanted

evaporation. In particular the filled 20 mL GC-MS headspace vials were closed tightly to minimize any evaporation. Analysis of defined 1-alkene concentrations in the headspace vials was done with GC-MS and the applied concentrations were plotted against the obtained areas. Resulting equations from linear regression were used for further calculations.

Table 13 Temperature program for headspace analysis with GC-MS. For medium chain fatty acid substrates C10:0 to C16:0 (a), for short chain fatty acids >C6:0 (b) and C6:0 (c).

Start	70 °C[a]/60 °C[b]/50 °C[c]
Hold	70 °C[a]/60 °C[b]/50 °C[c] for 0.5 min
Rise	50 °C per min
End	320 °C

2.5.4. ^{1}H-NMR analysis of isolated α-hydroxy fatty acids

Structures and purity of isolated α-hydroxy fatty acids from conversions of dodecanoic acid, oleic acid and decanoic acid with $P450_{J\alpha}$ were determined by ^{1}H-NMR. First the reaction mixture from the preparative scale set-up (Section 2.5.6) was acidified with HCl (37%) to pH 1.0 until a white precipitate is formed. Subsequently, the volume was split on two conical falcons and 25 mL of the extraction agent ethyl acetate were added. After extensive mixing the samples were centrifuged at 3200 x g and at room temperature for 2 min followed by drying of the organic phase over Na_2SO_4. Extraction was repeated additional two times whereas also the reaction vessel was extensively washed with ethyl acetate. The solvent was removed under reduced pressure followed by freeze-drying overnight. For NMR analysis 20 to 30 mg of the isolated material were resuspended in 700 µL DMSO-d6. Additionally, also MeOH-d4 was applied since it allows simple removal from the isolated product. The ^{1}H-NMR spectra were recorded on a Bruker spectrometer (1H, 300.13 MHz). Chemical shifts are given in delta (δ) and the coupling constants in Hertz (Hz). Obtained shifts were integrated manually and conversion was calculated in respect to the amount of hydrogen atoms from α-carbons of fatty acids and α-hydroxy fatty acids. For instance the shift of DMSO-d6 is based on 6 hydrogen atoms whereas the α-position of the substrate corresponds to 2 H-atoms.

2.5.5. Determination of stereoselective formation of α-hydroxy acids

The determination of the stereoselectivity of $P450_{J\alpha}$ for the formation of α-hydroxy acids was carried out according to the protocol of Dennig et al (2019) [37]. Isolated α-hydroxy acids from enzymatic conversions of decanoic acid with $P450_{J\alpha}$ and $P450_{CLA}$ were used for the following reactions. Two milligrams of isolated product were converted with and 2 mg mL^{-1} L-LOX [16] in the presence of 2 mg mL^{-1} catalase overnight at 100 rpm and 25 °C. The reaction mixture containing the respective pro-

chiral-α-keto acid was split and two approaches were followed, one with L-HIC-dehydrogenase and the other with D-HIC dehydrogenase, each with approximately 10 U mg^{-1} [95]. Reaction set-up was 2 mg HIC-dehydrogenase, 2 mg mL^{-1} formate-dehydrogenase, and 400 µM NAD and 100 mM sodium formate, which were added to the reaction mixture from the L-LOX conversion. Reactions took place over night, at room temperature and under shaking (100 rpm).

Afterwards the reaction mixtures were freeze-dried in the reaction vessels (glass vial). The dried samples were dissolved in 700 µL MeOH, 2% (w/v) DMAP and 150 µL ethyl chloroformate, followed by incubation for 1 h at 50 °C. Afterwards MeOH was removed under pressurized air flow. Next step was the addition of 700 µL 2% (v/v) HCl and 700 µL ethyl acetate. After mixing and centrifugation (16110 x g, 2 min, room temperature) the organic phase was dried over Na_2SO_4. The extraction step was repeated three times and samples were analyzed with GC-FID equipped with a CP-Chirasil-DEX CB column (25 m x 320 µm, 0.25 µm film). The following temperature program was applied for baseline separation of analytes: 100 °C on hold for 1 min followed by a rise of 10 °C min^{-1} till 130 °C was reached, on hold for 5 min. Subsequently, temperature increased by 10 °C min^{-1} until 180 °C was reached on hold for 1 min (Figure 9). The method was verified by baseline separation of the *S*- and the *R*-enantiomer of the α-hyxdroxy decanoic acid (Figure 91).

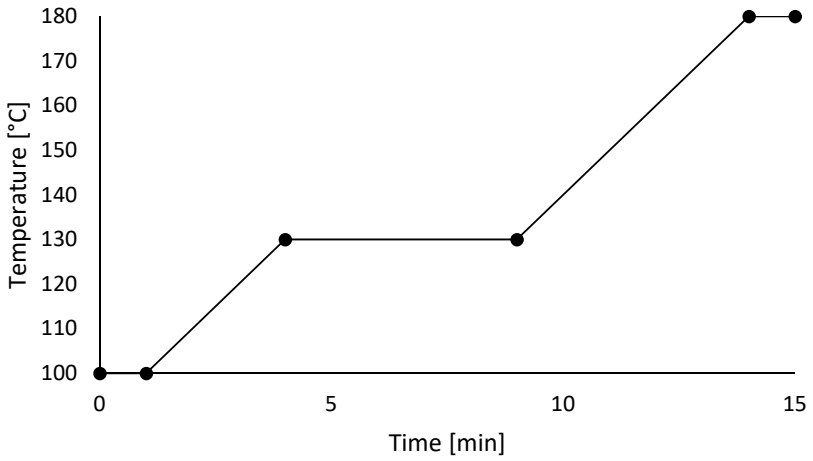

Figure 9 Temperature profile to determine the stereoselectivity of $P450_{J\alpha}$ for GC-FID analysis.

2.5.6. Preparative scale reactions with $P450_{J\alpha}$

For product isolation (several mg) and unambiguous structure identification, the reaction volume was scaled up from 2 mL to 50 and 100 mL, respectively. The reaction contained 6 µM $P450_{J\alpha}$ and 5 mM substrate in buffer C. Depending on the chain length of the fatty acid substrate, the order of component addition differed: a) dissolved C18:1 was supplemented with buffer C and b) the dissolved C12:0 and C10:0 were added to buffer C. H_2O_2 pulsing was supplemented automatically using a pump system for adding 0.8 mM H_2O_2 per 30 min from a 200 mM H_2O_2 stock (Figure 10) [37]. This corresponds

to 20 peroxide pulses with 200 µL volume every 30 min and in total 16 mM H_2O_2 were added. For preparation, the pump and its tubes were washed with ddH_2O followed by short washing with the H_2O_2 substrate solution (200 mM stock). Reactions were carried out under stirring (<100 rpm) and at room temperature. The pH-value was monitored throughout the whole reaction. Samples of 250 µL were taken at various time points and 25 µL of 37% HCl were added to stop the reaction. Samples were extracted, derivatized and analyzed with GC-MS and GC-FID.

Figure 10 Reaction set-up for prep-scale conversion of fatty acids with $P450_{J\alpha}$ utilizing a pump for automated H_2O_2 pulsing. A = reaction vessel with $P450_{J\alpha}$ and substrate. B = H_2O_2 stock solution (200 mM). C = Pump system.

2.6. Alternative H_2O_2 supplementation for P450 peroxygenases

2.6.1. In-situ generation of H_2O_2 with glucose oxidase (GOX)

Coupling the conversion of fatty acids with CYP152 to glucose oxidase could represent a slower H_2O_2 release system to extend the catalyst lifetime by circumventing high peroxide concentrations (>2 mM). The specific activity of the commercial GOX was determined using an O_2 -sensor. Calibration of the sensor was done by choosing two set-points. For this 100% oxygen saturation was defined using normal air (20% oxygen) and 0% oxygen when GOX converted 1 M glucose (1 mg GOX, buffer C). For the activity measurement a 1 M glucose and 1 mg mL^{-1} GOX in buffer C were required. The time-dependent depletion of O_2 after addition of GOX was utilized to calculate the specific activity.

Due to the very high turnover number (500 s^{-1} [96]) of the commercial GOX compared to the catalytic numbers of $P450_{J\alpha}$ four different dilutions (Table 14) of a 1 mg mL^{-1} GOX solution were investigated. A combined reaction set-up contained 2 mM C12:0, 3 µM $P450_{J\alpha}$ varying amount of GOX and 2 mM glucose in reaction buffer C. After extraction and derivatization, samples were analyzed with GC-MS.

Table 14 Dilutions of 1 mg mL^{-1} GOX solution for slower H_2O_2 release during fatty acid conversion with CYP152.

Dilutions of 1 mg mL^{-1} GOX
1:100
1:200
1:400
1:800

The investigation of amount of glucose in respect to the substrate was carried out with 2 mM C12:0, 3 µM $P450_{J\alpha}$ and 0.005 mg GOX. For this, glucose concentrations were varied from 2, 5 and 10 mM, whereas the substrate concentration was kept constant. Reactions took place over night at 100 rpm and 25 °C. Subsequently, the substrate concentration was increased to determine the effect of the GOX peroxide supply on the fatty acid conversion. The reaction set-up was based on equimolar glucose to substrate concentrations. Amounts of substrate/glucose and $P450_{J\alpha}$ used for these experiments are listed in Table 15. Reactions were carried out at 100 rpm, at room temperature and overnight. Samples were extracted, derivatized and analyzed by GC-MS.

Table 15 Reaction conditions for the conversion of varying C12:0 concentrations with $P450_{J\alpha}$ applying the slower peroxide release system with GOX.

C12:0/Glucose [mM]	$P450_{J\alpha}$ [µM]
2	3
5	3
10	3
10	6

2.6.2. Coupling fatty acid conversion with P450s to GOX and L-LOX

Next to the glucose oxidase, also a lipoxygenase was coupled to the fatty acid conversion with P450s.Tne L-LOX should drive the reaction further by removing the formed α-hydroxy acids. $P450_{BS\beta}$, which forms α- and β-hydroxy acids, was selected as model catalyst for the combined coupling with GOX and L-LOX in reactions to enhance substrate conversion. Initial reactions contained 5 mM C14:0 (2.5 % EtOH), 3 µM $P450_{BS\beta}$, 10 mM glucose, 0.005 mg GOX and 2 mg L-LOX. The reaction volume was reduced to 500 µL. Used volumes for extraction were adjusted accordingly: 100 µL 37% HCl and 500 µL ethyl acetate were used for organic extraction. After derivatization samples were analyzed with GC-MS.

2.6.3. Slow-release oxidant: Urea-H_2O_2

Urea-H_2O_2 was thought to slower release peroxide based on the higher molecular weight in comparison to H_2O_2. A catalase was applied as model to determine the accessibility of peroxide from Urea-H_2O_2. The formation of O_2 was used to determine the enzyme activity and measure the difference between H_2O_2 and Urea-H_2O_2. The O_2-sensor was calibrated as mentioned in section 2.6.1. A catalase stock solution containing 1 mg mL^{-1} catalase (2000-5000 U mg^{-1}, Sigma Aldrich) was prepared and diluted 1:1000 in buffer C. After addition of 250 µM H_2O_2 or Urea-H_2O_2 the formed O_2 was measured. The resulting slope was used to calculate the concentration of formed O_2 per minute. This directly correlates with the peroxide accessible as substrate for the catalase. The reactions to determine the effect of Urea-H_2O_2 in comparison to normal H_2O_2 contained 1 to 10 mM C10:0 and 3 µM $P450_{BS\beta}$. The H_2O_2 supply was varied starting with 0.5 mM per 30 min for 1, 2 and 3 mM C10:0. For 5 mM and 10 mM decanoic acid the amount per pulse was increased to 1 mM and 2 mM peroxide per 30 min, respectively. Final peroxide concentrations were equimolar to the corresponding substrate concentration. Reactions lasted for 6 h under shaking (100 rpm) and at room temperature before samples were analyzed by GC.

2.7. Production of a heterogeneous catalyst from P450s

2.7.1. Carrier selection for immobilization

For immobilization of P450s two commercially available carriers were used namely EziG™ from EnginZyme and ReliSorb™ from Residion. EziG™ is a ready-made carrier activated with Fe^{3+} and consisting of a controlled porosity glass with a pore diameter between 30 to 50 nm. As reported by Engelmark et al 2014, EziG™ could be applied to immobilize tagged proteins over affinity between the metal ion and the tagged protein [80]. EnginZyme reports that these particles could be used to link purification and immobilization in a single step. A selection of EziG™ carries with different properties is shown in (Table 16).EnginZyme carriers were used for the immobilization of His-tagged P450s ($P450_{J\alpha}$, $P450_{BS\beta}$, $P450_{CLA}$) via affinity binding.

Table 16 Summary of the selected carriers EziG™ from EnginZyme

	Carrier material	Coating	Properties	Pore diameter [nm]
EziG™ Fe1	CPG	-	hydrophilic	50 ± 5
EziG™ Fe2	CPG	Polyvinyl benzyl chloride	hydrophobic	30 ± 5
EziG™ Fe3	CPG	Blended co-polymers	semi-hydrophilic	30 ± 5

In contrast the ReliSorb™ carrier from Residion consists of highly porous polymethacrylate with a sulphonic group. Residion reports that ReliSorb™ could be applied to capture and purify proteins based on the cation exchange principle. Therefore, the immobilization would be based mainly on ionic interactions. The applied carrier was ReliSorb™ SP400 with a particle size of 75 to 200 µm and an average pore size of 40 to 60 nm. ReliSorb™ was used for the immobilization of P450s via binding with the strongly positive charged Z_{basic2}-tag [73, 74].

2.7.2. Activation of ReliZyme™, Agarose and CPG for immobilization of $P450_{J\alpha}$

Next to the ready-made commercial carriers, also a screening of different carrier materials was done to enhance the immobilization yield and the activity of the immobilized enzymes. The activation of the selected particles was done according to the protocol of Armisén et al (1999) [82]. A 10 mL solution containing 0.9 g of iminodiacetic acid (IDA) was prepared and the pH was set to 11.0 by supplementing concentrated NaOH. The particles were incubated in the IDA solution overnight, at room temperature and at 20 rpm in an end-to-end rotator. After three extensive washing steps with ddH_2O, the particles were incubated in 5 mg mL^{-1} $NiSO_4$ or $CuSO_4$ solution, respectively, for 1 h at room temperature and gentle mixing (20 rpm). Afterwards particles were washed again and stored in ddH_2O. The selected particle and metal combinations for the immobilization of the P450s are depicted in Table 17.

Table 17 Selection of materials and metals for preparation of activated particles

Particles	Metals
ReliZyme™	Ni^{2+}
Agarose	Ni^{2+}
Agarose	Cu^{2+}
CPG	Ni^{2+}
CPG	Cu^{2+}

2.7.3. Immobilization of P450s

The immobilization of the P450s was carried out as beforehand described by Valikhani et al (2018) [50]. Immobilization was done either directly from cell extract containing the enzyme [74] or using purified P450s. For both approaches the active enzyme concentration was determined via CO-titration [84]. The purified enzyme was diluted with buffer C to achieve an active enzyme concentration of 20 µM. For the freeze dried cell-free extract a maximum concentration of 20 mg mL^{-1} were applied based on beforehand determined activities. Then, 100 mg of carrier were washed with the immobilization buffer (50 mM KPi, 250 mM NaCl, pH 7.5) for the approach with Z_{basic2}-tag and with buffer C for the approach with the His-Tag. Subsequently, the enzyme solutions were added and all components were

incubated on the end-to-end rotator at 20 rpm and room temperature for 1 h. Afterwards the supernatant was collected to determine the remaining active enzyme concentration in the liquid phase with CO-titration and the protein concentration with photometrical measurement. The carrier was washed three times either with the immobilization buffer (Z_{basic2}-tag) or with buffer C (His-tag) followed by the next immobilization step. In total four immobilization steps were carried out for the binding approach with the Z_{basic2}-tag and 1 to 2 steps for the affinity binding approach with the His-tag. Immobilization efficiency was calculated based on the obtained active enzyme concentrations remaining in the supernatant (c) after the immobilization step in respect to the active P450 concentration of the starting solution (c0). The corresponding formula is given below [50].

$$\text{Immobilization yield} = \frac{(c0 - c)}{c0} \text{ x } 100$$

2.7.4. In-particle quantification of immobilized P450s

Immobilization efficiency calculations based on measuring the supernatant activity/protein concentration after immobilization is an indirect method to determine the amount of bound protein on a carrier. In contrast, in-particle measurement was thought to be a promising approach for direct determination of the immobilization success. For proof of principle, $P450_{BM3\_Z}$ was immobilized on sepharose activated with ? according to the description in 2.7.3. Sepharose was the particle of choice as it shows a transparent color, which would minimize the background absorption by other carrier materials during the photometrical measurement. A small spatula tip (<1 mg) of carrier was added to 200 µL of immobilization buffer in a 96-well of a microtiter plate. Subsequently, the reducing agent sodium dithionite was added followed by extensive mixing. The sample was analyzed spectro-photometrically with the plate reader according to the protocol of the CO-titration (section 2.3.3), whereas the gassing was carried out in the microtiter plate. Next to the active enzyme concentration, also the dissociation constants as well as the activity of the immobilized $P450_{BM3\_Z}$ (NADPH consumption) could be determined by photometrical in-particle measurement.

3. Results and discussion

3.1. Biochemical characterization of $P450_{J\alpha}$

3.1.1. Classification of $P450_{J\alpha}$ as CYP152 member by sequence similarities

To assign the newly discovered peroxygenase $P450_{J\alpha}$ derived from *Jeotgalicoccus sp.* ATCC 8456 to a CYP subclass a sequence alignment as well as a phylogenetic tree (Table 18,Figure 11) were generated using the online tools Clustal Omega and Jalview. Therefore, several already characterized CYP152 members were selected. Having a closer look into the phylogenetic tree, CYP152L2 marked the guide value (1491.72) with the lowest sequence similarities to the selected CYP152 members. This guide value equals the sum of all branches directing towards one sequence. Concluded, the lower the numbers flanking the branches the higher is the similarity between two sequences. Highest sequence identities in respect to $P450_{J\alpha}$ could be determined for CYP152N1, also known as $P450_{Ex\alpha}$. Said catalyst is derived from *Exiguobacterium sp*. AT1b and classified as α-hydroxylase. $P450_{Ex\alpha}$ utilizes H_2O_2 to efficiently convert medium chain fatty acids like C14:0 acid (k_{cat} 1900 min^{-1}). Interestingly conversions with $P450_{Ex\alpha}$ revealed the formation of shorter chain fatty acids next to the corresponding α-hydroxy acid if higher peroxide concentrations were applied [97]. Summarized, $P450_{J\alpha}$ could be annotated to the CYP152 family based on sequence identities of up to 50%. Additional the conserved arginine at position 241/242 and the nearby proline at position 243 could be found in the sequence of $P450_{J\alpha}$. This conserved residues in the active site are specific for CYP152 members (Figure 11B) [38, 86].

Table 18 Selection and overview of catalytically characterized members of the CYP152 family. There is no sequence identity of CYP152P1 and $P450_{J\alpha}$ (a), but CYP152P1 shows sequence identities for the other selected CYP152.

Nomenclature		Host organism	Enzymatic class	Sequence identity $P450_{J\alpha}$ [%]	Reference
CYP152	$P450_{J\alpha}$	*Jeotgalicoccus sp.* ATCC 8465	α-hydroxlase	-	This study
CYP152A1	$P450_{BS\beta}$	*Bacillus subtilis*	β-hydroxylase	48	Matsunaga et al (1999) [83]
CYP152A2	$P450_{CLA}$	*Clostridium acetobutylicum*	α-hydroxlase	44	Girhard et al (2007) [36]
CYP152A8	CYP-Aa162	*Alicyclobacillus acidocaldarius* LAA1	β-hydroxylase	46	Xu et al (2017) [98]
CYP152B1	$P450_{SP\alpha}$	*Sphingomonas paucimobilis*	α-hydroxlase	42	Matsunaga et al (1997) [99]
CYP152K6	-	*Bacillus methanolicus* MGA3	α-hydroxlase	48	Girvan et al (2018) [100]
CYP152L1	OleT	*Jeotgalicoccus sp.* ATCC 8456	decarboxylase	40	Rude et al (2011) [40]
CYP152L2	CYP-Sm46	*Staphylococcus massiliensis* S46	decarboxylase	36	Xu et al (2017) [98]
CYP152N1	$P450_{Ex\alpha}$	*Exiguobacterium sp.*	α-hydroxlase	50	Onoda et al (2018) [97]
CYP152P1	CYP-MP	*Methylbacterium popouli sp. nov.*	β-hydroxylase	0[a]	Amaya et al (2016) [101]

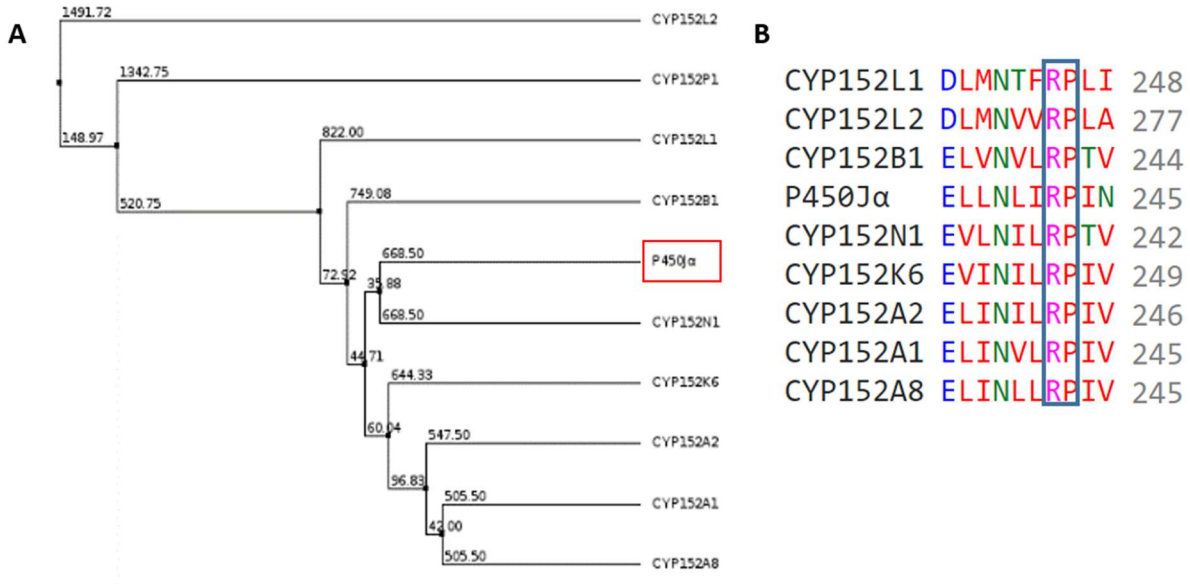

Figure 11 Phylogenetic tree based on sequences identity of characterized P450s from the CYP152 family (A). FASTA files were obtained from NCBI. Phylogenetic tree was visualized with Jalview and alignments were done with Clustal Omega. Sequence alignment revealed a conserved arginine residue (R) around position 241/242 and a proline at 243 [38] (B).

3.1.2. Structural relation between $P450_{J\alpha}$ and other CYP152s

Homology models of $P450_{J\alpha}$ and $P450_{CLA}$ were generated based on the crystal structures of the α-hydroxylase $P450_{SP\alpha}$ (pdb: 3awm) and the β-hydroxylase $P450_{BS\beta}$ (pdB: 1izo) both members of the CYP152 family. The obtained holoenzyme was as template for modeling the heme group and a fatty acid as substrate (C16:0) into the active site. In principal P450s consist of similar structural elements independent from their origin [102]. The heme ligand is embedded into the active site of the protein between the closer L helix and the farer I helix bound to a cysteine containing loop which includes a P450 specific sequence [103]. Concerning the active site, the arginine at position 241/242 turned out to be a key residue for interaction with fatty acids especially as shown for comparable enzymes like $P450_{BS\beta}$ and $P450_{SP\alpha}$. Formation of compound 1 using H_2O_2 as oxidant is based on the interaction of the carboxylate group of the substrate with the conserved arginine in the active site [38]. Comparing the homology model of $P450_{J\alpha}$ with already existing crystal structures of CYP152 family members certain differences in the binding pocket could be found (Figure 12A).

To depicture the interaction between substrate and active site a LigPlot was generated using LigPlus [88]. Based on the interactions (Van-der-Waals forces) of amino acid residues with the fatty acid substrate, the favor for certain chain lengths could be explained (Figure 12B). LigPlots were also generated for $P450_{CLA}$, $P450_{SP\alpha}$, $P450_{BS\beta}$ as well as OleT, which can be found in the appendix section (Figure 60). Comparing the LigPlots of the CYP152 members, it seemed that more interactions per CH_2-group between the amino acid residues and the fatty acid substrate are occurring for α-hydroxylases ($P450_{J\alpha}$, $P450_{CLA}$, $P450_{SP\alpha}$). This would for instance explain the low regioselectivity of the β-hydroxylase

$P450_{BS\beta}$ with a ratio for α:β of 43:57 and furthermore the formation of the volatile by-product 1-alkene [38]. However, LigPlots are only two dimensional and abstract representations of the active site indicating that several interactions could be missing.

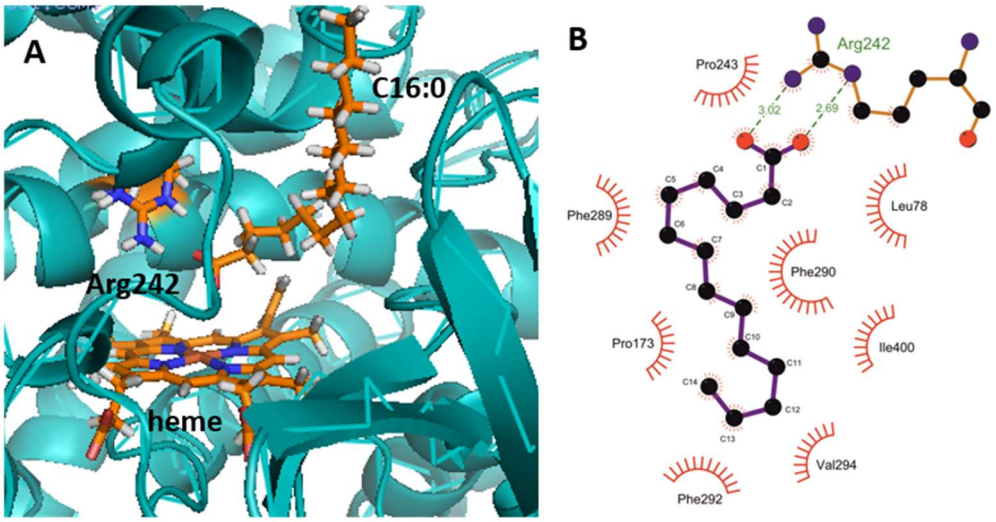

Figure 12 Homology model of $P450_{J\alpha}$ generated based on already existing crystal structures from CYP152 family members $P450_{BS\beta}$ and $P450_{SP\alpha}$ (A). Arg^{242} interacts with the carboxylate group of the substrate. The structure model was generated with Swissmodel whereas the heme group and the fatty acid (C16:0) were added with YASARA. Interactions between substrate and active site are presented by a LigPlot (LigPlus) (**B**).

3.1.3. Expression yield of $P450_{J\alpha}$ from shaking flask cultivation

The production of $P450_{J\alpha}$ included protein expression in shaking flasks followed by cell disruption and protein purification via affinity chromatography. The soluble protein distribution throughout the whole production process of $P450_{J\alpha}$ is depictured in Figure 13. Starting with lane 1 which shows the protein distribution of *E. coli* BL21 DE3 before induction with IPTG. The following lanes cover the whole purification process ranging from a sample after protein expression of 20 h (2), over cell disruption (3) to the purified and concentrated $P450_{J\alpha}$ (4). The clear band around 50 kDa can be used as reference point for the molecular mass of $P450_{J\alpha}$. The protein was obtained in a purity of >95%. This is especially important for peroxygenases (e.g. CYP152s) as traces of catalases would degrade the required oxidant H_2O_2. The calculated molecular weight of $P450_{J\alpha}$ was 48.2 kDa which corresponds to the determined size on the SDS-PAGE. Protein expression of $P450_{J\alpha}$ yielded 49 mg L^{-1} culture. Additional also $P450_{CLA}$ and $P450_{BS\beta}$ were produced successfully with an expression yield of 40 mg L^{-1} and 72.5 mg L^{-1} culture, respectively.

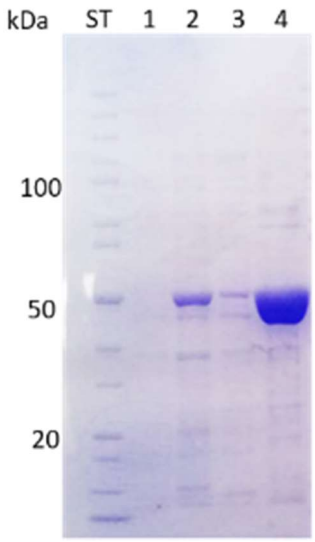

Figure 13 Protein distribution and purity as determined by SDS-PAGE. ST = unstained protein ladder (page-ruler Thermo Fisher Scientific). Lane 1: Protein distribution of *E. coli* BL21 DE3 before induction. Lane 2: After induction and 20 h of target protein expression. Lane 3: After cell disruption and lane 4 purified $P450_{J\alpha}$ (48.2 kDa).

Subsequently, the active protein concentration of the P450s was measured with CO-Titration [84]. The resulting curves after the photometrical measurement are shown in Figure 14A**Fehler! Verweisquelle konnte nicht gefunden werden.**. After reduction with dithionite and CO gassing (orange lane) the absorption maximum is shifted to 450 nm. Therefore the active protein concentration corresponds to the peak at 450 nm, whereas a peak at 420 nm indicates denatured enzyme. Figure 14A depictures the difference spectrum of gassed and not gassed sample, whereas a small peak at 420 nm could be detected. Therefore also inactive protein is present (<5%). Active enzyme concentration was calculated based on Lambert Beer-law with an extinction coefficient of 91 L $mmol^{-1}$ cm^{-1} [84].The highest active concentration reached for $P450_{J\alpha}$ was 403 µM directly after concentrating the purified protein. Production of $P450_{CLA}$ and $P450_{BS\beta}$ yielded 335 µM and 302 µM, respectively.

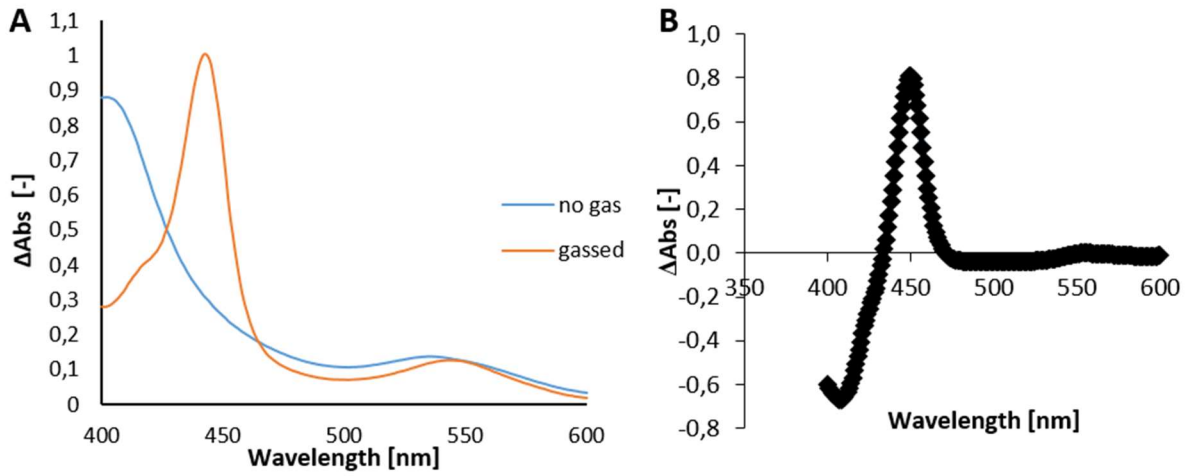

Figure 14 Absorbance spectra of $P450_{J\alpha}$ before and after CO gassing is shown A. In B CO-difference spectra obtained during CO-Titration with purified $P450_{J\alpha}$ is shown in. Measured and calculated active $P450_{J\alpha}$ concentration was 403 µM.

3.1.4. Storage stability of $P450_{J\alpha}$ in liquid

Problems in long term storage of biocatalysts are a drawback in implementation of enzymes in industrial processes. Low storage stabilities of the enzyme lead to more frequent as well as costly protein production and purification. This is why high storage stability is a desired property of biocatalysts [58]. During the storage of $P450_{J\alpha}$ for several weeks in liquid (buffer C without imidazole) at 4 °C no visible precipitation of the purified protein occurred. Therefore, the storage stability of the protein was further investigated. As the storage stability especially for α- and β- hydroxylases from CYP152 has not been reported before $P450_{CLA}$ and $P450_{BS\beta}$ were also included into the study. Active protein concentrations were monitored over 150 days applying CO-titration. Surprisingly $P450_{J\alpha}$ showed very high storage stability in liquid form at 4 °C. Even after more than 150 days only a minimal loss in active enzyme concentration of around 10% could be determined (Figure 15). This also indicates that $P450_{J\alpha}$ could be stored at high concentrations (15 mg mL^{-1}). In comparison, $P450_{CLA}$ showed similar storage stability whereas a loss of 15% in active protein concentration after 150 days was determined. Concerning the β-hydroxylase $P450_{BS\beta}$, the loss in active protein concentration already reached more than 40% after 70 days. A SDS-PAGE was carried out and revealed the formation of several smaller bands (<50 kDa) (Figure 59).

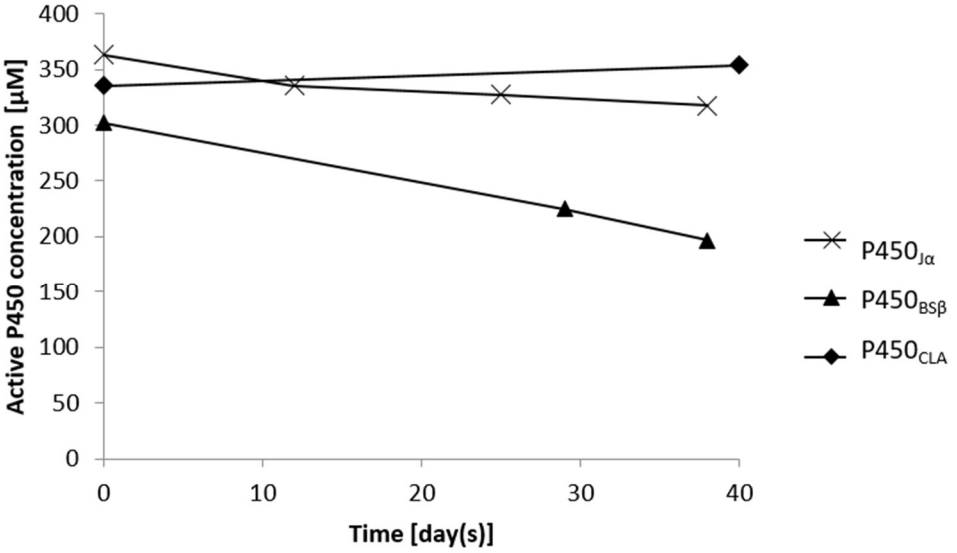

Figure 15 Storage stability of $P450_{J\alpha}$ $P450_{CLA}$ and $P450_{BS\beta}$ in buffer C (0.1 M KPi, 300 mM KCl, pH 7.5). Enzymes were stored in buffer C (without imidazole) and at 4 °C. Active protein concentration was determined by CO-titration.

3.1.5. Dissociation constants of $P450_{J\alpha}$ for fatty acid substrates

The dissociation constant (k_D) is a measure to describe the affinity of the protein to its substrate, whereas for P450s a low k_D-value corresponds to high affinity between the enzyme and the fatty acid. Therefore, a low dissociation constant is thought to be required for efficient substrate conversion. Concerning P450s, the k_D-value could be determined photometrically by shifts in spin states. The shift from low spin iron to high spin iron is triggered by substrate entering the active site [28]. Dissociation constants were determined by substrate titration (<5 µL; 50 mM Stock) to a 1.5 µM enzyme solution of $P450_{J\alpha}$ followed by photometrical measurement (300 to 500 nm) [36]. Obtained results showed typical spin state shifts at 420 nm to 430 nm (low spin iron) and 395 nm (high spin iron) (Figure 16). Determined k_D-value was 184 µM for dodecanoic acid (curve fitting with origin) (Figure 17). For OleT a k_D-value of 2.8 µM [34] and for $P450_{CLA}$ a k_D-value of 221 µM [36] for dodecanoic acid were reported. Next to C12:0, also the k_D-value of $P450_{J\alpha}$ for C10:0 was determined. The dissociation constant of $P450_{J\alpha}$ for C10:0 with 104 µM was even lower in respect to C12:0. This also fits the obtained conversions of C10:0 and C12:0 with $P450_{J\alpha}$ and H_2O_2 reaching more than 75%. Furthermore, the effect of DMSO on the shifts in spin states was investigated as the fatty acid substrate was dissolved in this solvent. Interestingly, DMSO triggers shifts especially for the low spin iron (Figure 61). Still, the influence on the determination of k_D-values was minor as the DMSO concentration in the set-up did not exceed 2%.

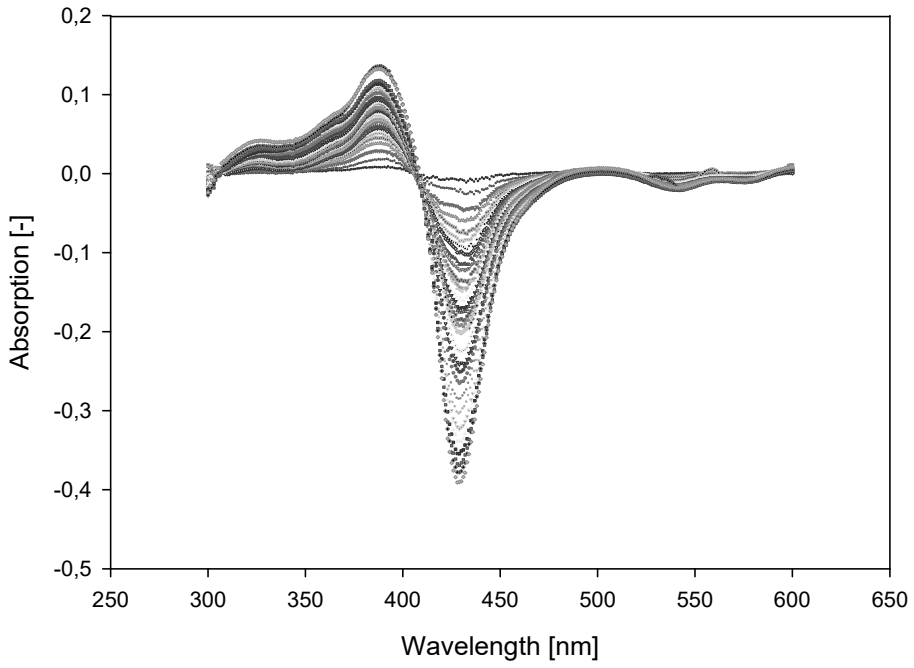

Figure 16 Spectral changes measured during substrate titration (C12:0) into a solution containing buffer C and purified $P450_{J\alpha}$. Change in absorption at 430 nm (low spin) and 395 nm (high spin) was determined spectrophotometrically upon substrate titration (5 µL per step from a 50 mM Stock) to an enzyme solution containing 1.5 µM $P450_{J\alpha}$.

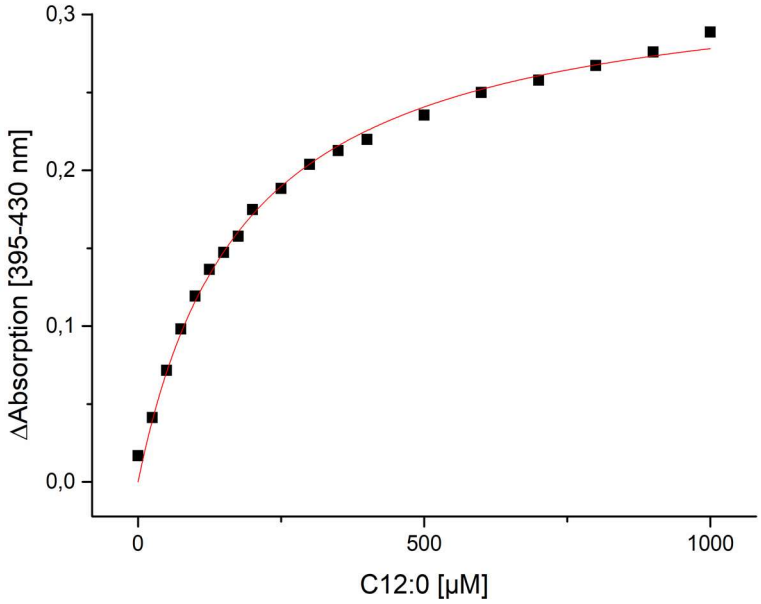

Figure 17 Peak-to-through difference obtained from k_D-value determination of $P450_{J\alpha}$ for C12:0. Calculation was based on subtraction of absorption of the low spin from the corresponding high spin iron. Data was fitted with Origin 9.0 software to Hill functions.

Table 19 compares the determined dissociation constants for $P450_{J\alpha}$ to reported data for $P450_{CLA}$ and $P450_{BS\beta}$ from Girhard et al (2007) [36]. Overall, the obtained k_D-values of $P450_{J\alpha}$ were in the same range and especially for C10:0 even lower. This indicates high affinity of $P450_{J\alpha}$ for medium chain fatty acids. Additionally, possible preparation errors were eliminated by determination of already published data (Figure 63), whereas the results for $P450_{CLA}$ and $P450_{BS\beta}$ were similar to reported k_D-values [36].

Table 19 Summary of dissociation constants of $P450_{J\alpha}$ for decanoic and dodecanoic acid. Also includes already reported data from Girhard et al 2007 [36] (a).

k_D-values [µM]	C10:0	C12:0
$P450_{J\alpha}$	104	184
$P450_{CLA}$	>1000[a]	221[a]
$P450_{BS\beta}$	414[a]	88[a]

3.2. Optimization of the reaction conditions for fatty acid conversion with $P450_{J\alpha}$

An optimized reaction set-up was required to complete the biochemical characterization of $P450_{J\alpha}$. Therefore different buffer conditions were applied, variations in substrate and enzyme concentrations were investigated and the peroxide supply was optimized.

3.2.1. Influence of salt concentration on catalytic activity of $P450_{J\alpha}$

The host organism of $P450_{J\alpha}$ *Jeotgalicoccus* was discovered in slightly salty habitats (2 to 3 % NaCl) [104–106]. Therefore the influence of varying salt (KCl) concentrations on the catalyst activity was investigated. Salt concentrations were varied from 0 to 1000 mM KCl and 2 mM C12:0 were converted with 3 µM $P450_{J\alpha}$ and equimolar peroxide to substrate concentrations. Figure 18 shows the obtained result of the screening. Highest substrate conversion of 65% was reached for 750 mM and 1000 mM KCl, but the difference between salt concentrations was minor and only around 10 to 15%. Obtained results indicate an enhanced catalyst stability in the presence of higher salt concentrations. The selected reaction buffer was 0.1 M KPi, 300 mM KCl and a pH of 7.5. Main reasons therefore are the small difference in conversion rates and the substrate solubility. The solubility limit for fatty acids with medium chain lengths (>C10:0) is around 2 mM in aqueous solutions and higher salt concentrations might enforce the substrate precipitation, which is detrimental for the biocatalytic conversion as less substrate is accessible to the enzyme.

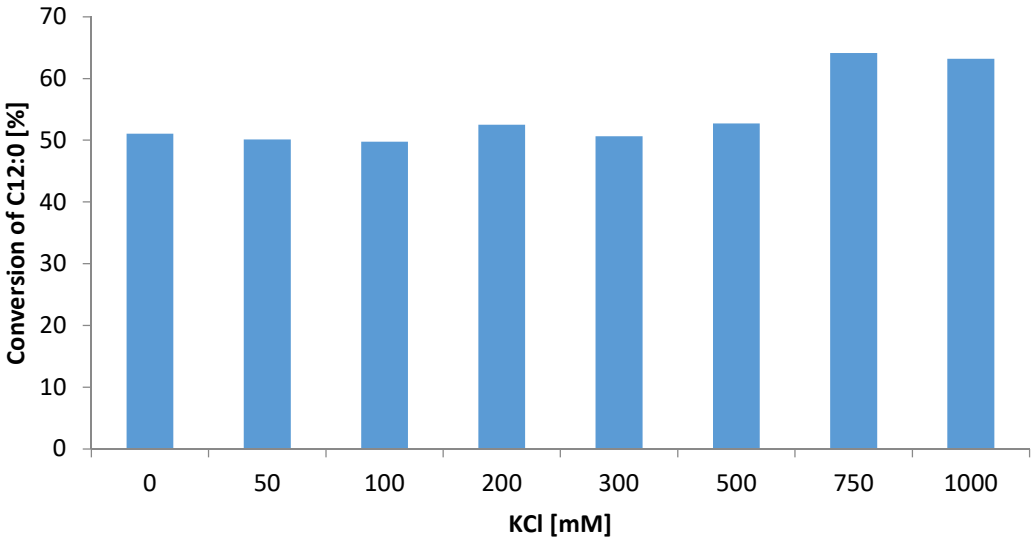

Figure 18 Conversion of C12:0 with $P450_{J\alpha}$ in buffer C with different KCl concentrations ranging from 0 to 1000 mM.

3.2.2. Influence of catalyst loading on conversion of dodecanoic acid

To achieve higher substrate conversion the catalyst concentration was increased while the substrate and therefore also the peroxide concentration remained constant. The amount of $P450_{J\alpha}$ was increased up to 6 µM (0.12 mol%) for the conversion of 2 mM C12:0. Obtained results are depicted in Figure 19. Conversion rates increased from 35% to around 55% for 2 µM to 4 and 6 µM of catalyst, respectively. Interestingly no significant difference could be detected between 4 µM and 6 µM of catalyst. Therefore, higher concentrations of $P450_{J\alpha}$ only have a limited effect on the conversion rates if the amount of substrate (2 mM) and peroxide (2 mM) stay constant/limiting. Based on this result the applied catalyst loading ranged from 0.06 mol% to 0.15 mol%.

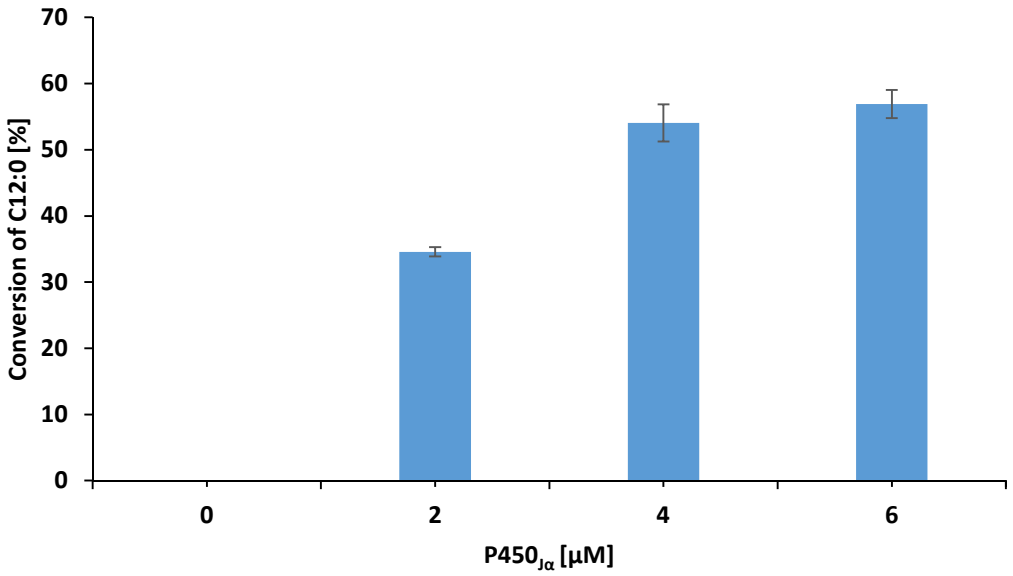

Figure 19 Investigation of different catalyst concentrations with constant substrate and H_2O_2 concentrations.

3.2.3. Supplementation strategies for H_2O_2

Another point to consider in the reaction set-up of P450s is the supply of the oxidant in the case of the peroxygenase $P450_{J\alpha}$ the H_2O_2. First the interval time between the peroxide pulses was taken into account varied followed by the amount of H_2O_2 added per pulse. The basic set-up contained 5 mM C12:0 and 6 µM of catalyst in buffer C. H_2O_2 pulsing interval were varied from 5 to 45 min while the amount of added peroxide was set to 250 µM per pulse (in total 2.5 mM H_2O_2). The influence of the interval time on the substrate conversion was not significant for 5 to 15 min (Figure 20). Longer interval times led to a decrease in conversion of around 10%. This indicates that the oxidant is already taken up after 15 min. Furthermore longer interval times (>15 min) could decrease the operational catalyst stability.

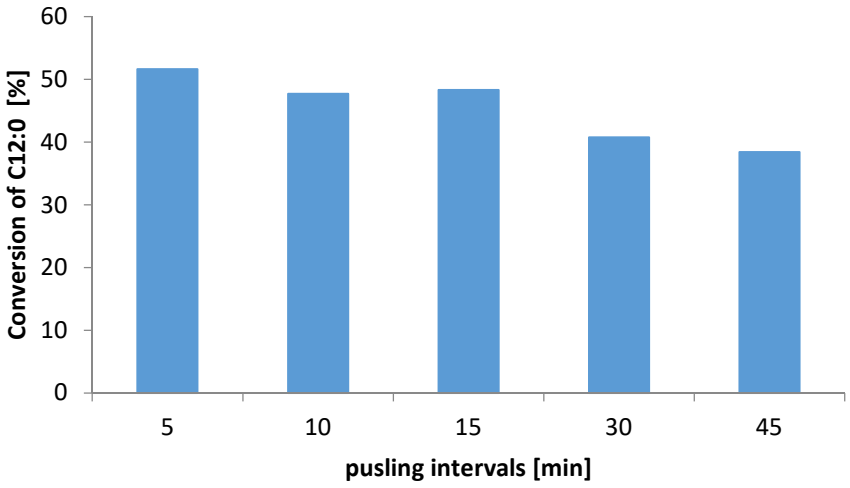

Figure 20 Optimization of the conversion of dodecanoic acid with $P450_{J\alpha}$ by varying the peroxide pulsing intervals. Interval time ranged from 5 to 45 min per pulse (250 µM H_2O_2) and in total 2.5 mM H_2O_2 were used.

Concerning the peroxide concentrations per pulse the range was set to 50 to 2000 µM per pulse (added every 30 min) and in total 5 mM of H_2O_2 were supplemented. Obtained results showed a clear preference towards 500 to 666 µM H_2O_2 (Figure 21). With this set-up a substrate conversion of 86% was reached. Concluded the optimized conversion of fatty acids with $P450_{J\alpha}$ is carried out in reaction buffer C with 300 mM KCl and 0.5 mM H_2O_2 per 30 min. In order to adapt the catalyst to a robust and automatized H_2O_2 feeding system the time between the pulses was expanded to 30 min. This modification had no or only minor detrimental effect on the substrate conversion.

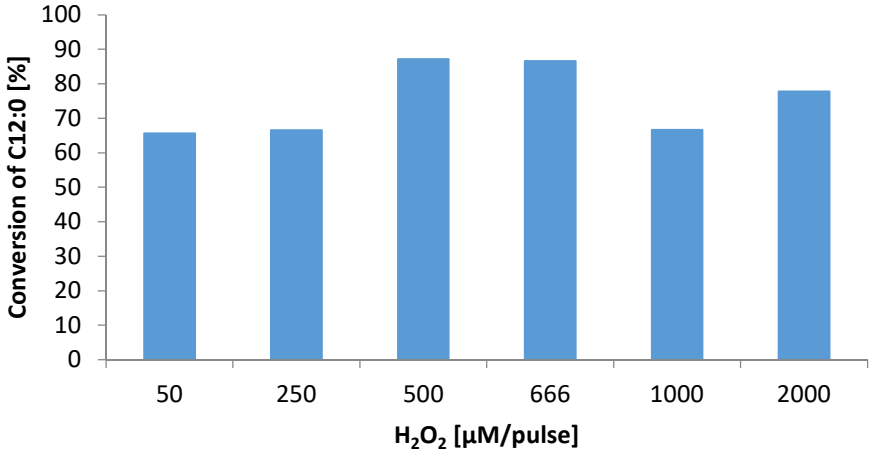

Figure 21 Screening for optimal H_2O_2 concentration per pulse for the conversion of 5 mM dodecanoic acid with $P450_{J\alpha}$. Peroxide concentrations ranged from 50 to 2000 µM and in total 5 mM oxidant was supplemented.

3.3. Catalytical characterization of $P450_{J\alpha}$

After finding a suitable reaction set-up for fatty acid conversion with $P450_{J\alpha}$ the key kinetic parameters including the specific activity, turnover numbers and coupling efficiency were determined. Additionally, the substrate scope was extended from C6:0 to C16:0. To complete the catalytic characterization of $P450_{J\alpha}$ also the stereo- and regioselectivity of $P450_{J\alpha}$ was investigated for the conversion of dodecanoic acid and decanoic acid, respectively.

3.3.1. Determination of the specific activity and turnover numbers of $P450_{J\alpha}$ for the conversion of selected fatty acids

The specific activity of $P450_{J\alpha}$ for fatty acid substrates was investigated in reaction samples from 2 to 10 min. Substrate depletion over time was used as measure for enzyme activity. Highest TON for C10:0 could be determined after 2 min with 98 min^{-1} (Table 20).Reasons therefore could be on one hand the availability of H_2O_2, which has been consumed rapidly. This represents the main challenge of conversions with peroxygenases like $P450_{J\alpha}$. The oxidant H_2O_2 is often the limiting factor in substrate conversion as already low peroxide concentrations lead to inactivation of the catalyst [16, 21]. On the other hand also the high dissociation constant of $P450_{J\alpha}$ with 1500 µM for C10:0 could have an impact. After two minutes only around 400 µM of substrate are left, which could be insufficient for effective substrate conversion due to the high k_D-value. As after 2 min the reaction seemed to be nearly finished the ratio of substrate to enzyme was changed. To improve activity measurements, lower enzyme concentrations were applied to reduce the velocity of the substrate conversion in the first 2 min of the reaction. This set-up was applied for C10:0 to C14:0 resulting in highest turnover numbers and specific activities of $P450_{J\alpha}$ for said substrates. Concerning C12:0, a specific activity of 8.2 U mg^{-1} and turnover numbers of 387 min^{-1} could be detected for $P450_{J\alpha}$.

Table 20 Determination of the specific activity of $P450_{J\alpha}$ for the conversion of C10:0. Reaction was stopped after 2, 5 and 10 min and samples were analyzed with GC-FID.

Time [min]	Conversion [%]	[µmol min^{-1}]	Specific activity [U mg^{-1}]	TON [min^{-1}]
2	59	23.5	2	98
5	56	9.1	0.8	38
10	56	4.5	0.4	19

Specific activities [U mg^{-1}] were calculated based on converted substrate in respect to reaction volume (2 mL) and amount of catalyst applied (3 µM).Turnover numbers equal the amount of substrate converted (µM) divided by the reaction time (min) and the amount of enzyme (µM) applied.

Coupling efficiencies were determined by applying equimolar concentrations of substrate as well as peroxide whereas the amount of catalyst was set to 1 µM. Obtained results are shown in Figure 22, where the conversion of decanoic acid with $P450_{J\alpha}$ and the formation of the corresponding α-hydroxy

fatty acid is shown. Formation of the α-hydroxy fatty acid was confirmed by mass fragmentation pattern analysis of reaction products and by comparison to the reported analytical data of the α-hydroxylase $P450_{CLA}$ [36]. Quantification was given by beforehand prepared calibrations. Determined coupling efficiencies equal the conversion rates after one hour of reaction time determined with a fixed reaction set-up.

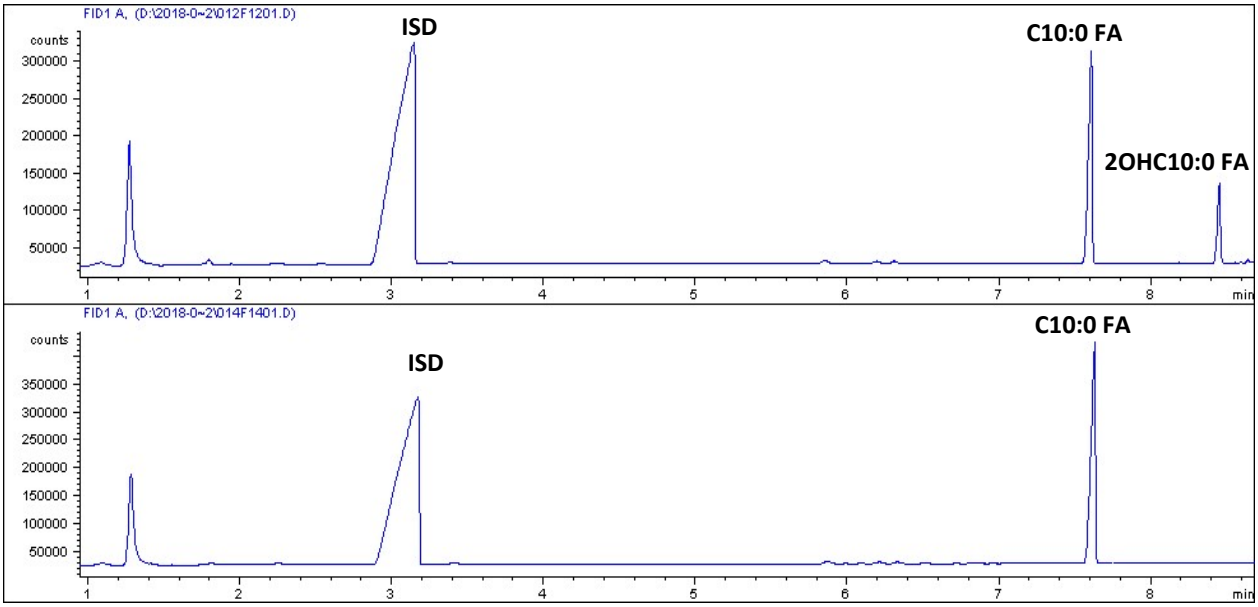

Figure 22 Determination of the coupling efficiency for conversions of C10:0 with $P450_{Jα}$. Samples were analyzed with GC-FID. Formation of α-hydroxy acids was beforehand confirmed by mass fragmentation (GC-MS) and comparison to analytical data of the α-hydroxylase $P450_{CLA}$ [36]. Chromatogram (bottom) is the control without catalyst. ISD = internal standard 0.1% (v/v) 1-octanol.

The substrate scope was further extended from C6:0 to C16:0 and the key kinetic numbers were determined as demonstrated beforehand for decanoic acid. Highest specific activity and therefore also turnover numbers were reached for dodecanoic acid with 8.2 U mg^{-1} and 387 min^{-1}, respectively. Also tetradecanoic acid as well as decanoic acid turned out to be suitable substrates with conversion rates around 78% and turnover numbers of 28 min^{-1} and 195 min^{-1}, respectively. Mainly even chain fatty acids were investigated as they are more common in nature and are therefore thought to be more suitable substrates. But $P450_{Jα}$ was also able to convert the odd chain fatty acid C15:0 with a conversion rate of 61%. Furthermore, the formation of volatile 1-alkenes was investigated due as gasoline smell evolved throughout the reactions. The 1-alkene formation was determined utilizing GC-MS headspace analysis. 1-alkenes were detected for conversions of octanoic and hexanoic acid. For substrates with longer chain lengths mainly α-hydroxy acids (>95%) were formed and only traces of the β-hydroxy product (<5%) could be detected for C10:0 to C16:0 indicating excellent regioselectivity for the formation of α-hydroxy fatty acids by $P450_{Jα}$ (Table 21).

Table 21 Summary of the kinetic characterization of $P450_{J\alpha}$ for fatty acid substrates (C6:0 to C16:0).

	conversion [%]	α-OH [%]	β-OH [%]	1-alkene	specific activity [U mg^{-1}]	TON [min^{-1}]	coupling [%]
C16:0	10	>98	<2	no	1	49	19
C15:0	61	>98	<2	no	0.2	8	29
C14:0	77	>98	<2	no	1	28	61
C12:0	86	>96	<4	no	8.2	387	85
C10:0	78	>95	<5	no	4	195	29
C8:0	15	>99	<1	yes	0.2	7	4
C6:0	63	>99	<1	yes	0.3	12	24

The conversion [%] was determined with the optimized reaction system. Specific activity [U mg^{-1}] corresponds to the µmol substrate converted per min and mg catalyst. Turnover number TON [min^{-1}] represents the µmol converted substrate per time and µmol catalyst.

The catalytic constant k_{cat} [min^{-1}] describes the substrate depletion or product formation rate in respect to amount of catalyst applied in respect to the reaction time [92]. Said characteristic parameter was also taken into account for evaluation of the catalytic performance of $P450_{J\alpha}$. From all members of the CYP152 family, $P450_{SP\alpha}$ shows the highest k_{cat} value with 3000 min^{-1} [35] for dodecanoic acid followed by $P450_{BS\beta}$ with a k_{cat} of 1400 min^{-1} [38] for tetradecanoic acid. $P450_{J\alpha}$ reaches a value of 387 min^{-1} for C12:0 which still outplays $P450_{CLA}$ and OleT (Table 22) [36, 39].

Table 22 Comparison of the catalytic constant k_{cat} [min^{-1}] of CYP152 members for fatty acid substrates from C10:0 to C14:0.

CYP152	k_{cat} [min^{-1}]	P450 [µM]	Substrate (Cx:0)	Substrate [µM]	Reference
$P450_{J\alpha}$	387	1	C12:0	1000	This study
$P450_{CLA}$	226	0.5	C10:0	10000	[37]
$P450_{SP\alpha}$	3000	0.05	C12:0	120	[35]
$P450_{BS\beta}$	1400	0.05	C14:0	120	[38]
OleT	1.1	1	C14:0	200	[39]

3.3.2. Regioselectivity of $P450_{J\alpha}$ towards α-carbon atom

Another key criteria to classify oxygenases and in particular CYP152s is the regioselectivity of the enzymes. For conversions of dodecanoic acid with $P450_{J\alpha}$ a regioselectivity of 95% for the α-carbon could be determined. $P450_{CLA}$ and $P450_{BS\beta}$ were selected for comparison as they are classified as α- and β-hydroxylase, respectively. Dennig et al (2018) reported a regioselectivity of $P450_{CLA}$ with >90% for the formation of α-hydroxy fatty acids [37]. In contrast, $P450_{BS\beta}$ displays a rather low regioselectivity for the α-position with 43% [38]. For visualization, the corresponding chromatograms are shown in Figure 23. As already mentioned in section 3.3.1, shorter chain fatty acids (<C8:0) yield 1-alkenes. The proposed reaction mechanism of fatty acid decarboxylation from Hsieh et al 2017 [34] states a necessary attack at the β-carbon atom, however no β-hydroxy acid formation could be detected for the shorter chain fatty acids (<C10:0). Regioselectivity of $P450_{J\alpha}$ for the α-position of short chain fatty acids is not decreased, but traces (<1%) of 1-alkenes could be detected. Concluded, $P450_{J\alpha}$ is a selective α-hydroxylase due to high regioselectivity (95%) for the hydroxylation at the α-carbon atom of fatty acids.

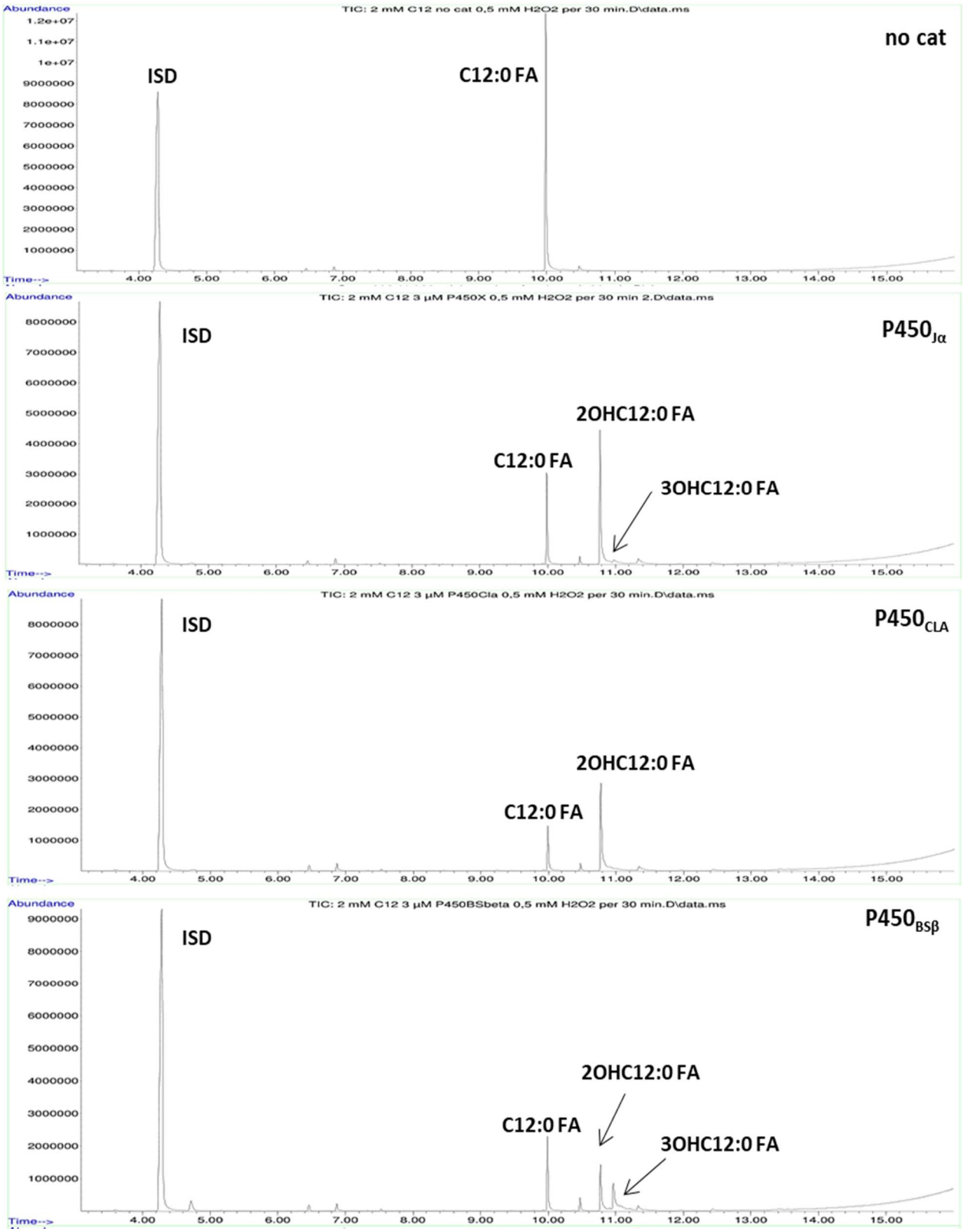

Figure 23 Regioselectivity of $P450_{Jα}$, $P450_{CLA}$ and $P450_{BSβ}$ for conversions of C12:0. Formation of α-hydroxy acids was confirmed by mass fragmentation and comparison with analytical data of $P450_{CLA}$ [36]. Formed β-hydroxy acids were identified by comparison to analytical data from $P450_{BSβ}$ [38]. Chromatogram on top is the control without catalyst. Samples were analyzed by GC-MS. ISD = internal standard 0.1% (v/v) 1-octanol.

3.3.3. Determination of stereoselective conversion of C10:0 by $P450_{J\alpha}$

The strategy to determine the stereoselectivity of $P450_{J\alpha}$ for conversions of fatty acids is depictured in Figure 24. Starting point is the conversion of the fatty acid (C10:0) with the $P450_{J\alpha}$ resulting in a potential mixture of *R*- and *S*-alcohol. A mixture containing both enantiomers could be expected as the α-hydroxylase $P450_{CLA}$ displays a rather low stereoselectivity for the *S*-enantiomer with 36% [37]. This mixture of 2-hydroxy acids functions as substrate for the L-LOX 2-hydroxy acid oxidase, which selectively converts the *S*-enantiomer of the α-hydroxy fatty acid into the corresponding α-ketoacid [107]. Additionally, $P450_{CLA}$ and $P450_{BS\beta}$ were applied as reference enzymes. Therefore, *R*-enantiomer of the α-hydroxy fatty acid will remain in the solution and can be used to assign stereoselectivity. To achieve proper separation of the enantiomers, products were derivatized (DMAP in MeOH, ethyl chloroformate) and subsequently analyzed by chrial GC-FID.

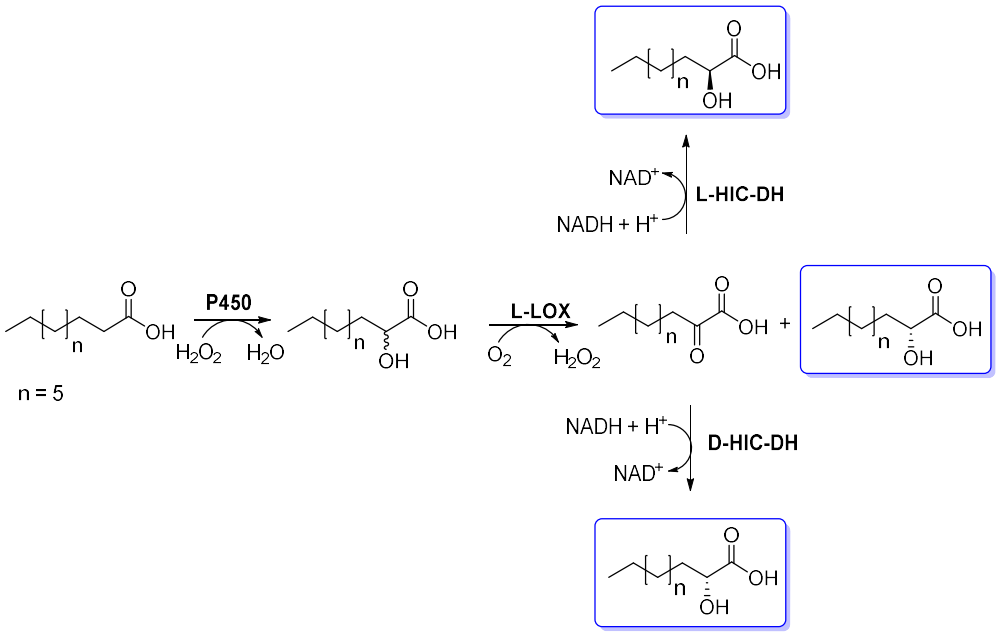

Figure 24 Strategy to determine the stereoselectivity of $P450_{J\alpha}$ for C10:0. C10:0 is converted by the CYP152 enzyme (P450) into a mixture of *S*-/*R*- alcohols. L-LOX only converts the *S*-enantiomer to α-ketoacid. Standards for *S*- and *R*-enantiomer are finally produced with L-/D-HIC-DH [37].

To ensure the identification of the peaks from the enantiomers over specific retention times, standards of the enantiomers were generated applying L/D-HIC-DH after the conversion with L-LOX. Said dehydrogenases reduce the α-ketoacid to the corresponding 2-hydroxy fatty acid in a stereoselective manner. Therefore the *R*-enantiomer could be produced by applying the D-HIC and on the other hand the *S*-enantiomer by using the L-HIC-DH. Only the production of the *R*-enantiomer of the α-hydrofatty acid with D-HIC-DH was successful. To verify the applied method, a reference of the racemate was produced. Therefore, the *R*-enantiomer from the D-HIC DH conversion was mixed with the isolated 2-hydroxy fatty acids from C10:0 conversion with $P450_{J\alpha}$. Subsequent chiral GC-FID analysis revealed a

baseline separation of the *S*- and the *R*-enantiomer (Figure 91 in appendix section). Figure 25 shows the obtained chromatograms from the GC-FID measurement. On top the produced standard for the *R*-enantiomer and on bottom the reaction outcome from the conversion of C10:0 with $P450_{J\alpha}$. A clear preference for the *S*-enantiomer (2:98) was detected and based on the peak areas the enantiomeric excess was calculated (equation below) to be >95% for the *S*-enantiomer of the α-hydroxy acid.

$$\text{e.e value} = \frac{\text{Area } (S) - \text{Area } (R)}{\text{Area } (S)} \text{ x } 100$$

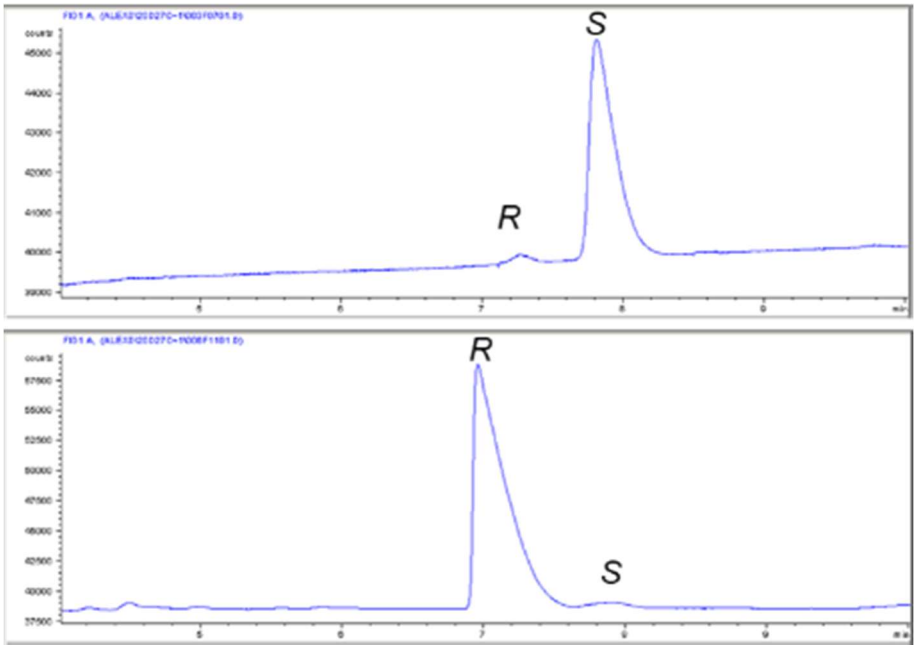

Figure 25 Determination of the stereoselectivity of $P450_{J\alpha}$ for conversions of decanoic acid. Top chromatogram shows the chiral analysis of *S*- and *R*-enantiomer of C10:0 produced with $P450_{J\alpha}$ and below the standard for the *R*-enantiomer produced with D-HIC-DH from an L-LOX oxidized S- and R-enantiomeric mixture from C10:0 conversion with $P450_{J\alpha}$.

Further, the e.e. values for $P450_{CLA}$ and $P450_{BS\beta}$ for the hydroxylation of C10:0 were determined, (chromatograms can be found in the appendix section). Determined e.e. values for hydroxylation of C10:0 at the α-position for $P450_{CLA}$ and $P450_{BS\beta}$ were 71% (*S*) and 26% (*R*), respectively. As reference from literature the e.e. value of $P450_{SP\alpha}$ is given with 98% (*S*) for tetradecanoic acid [35] (Table 23). In comparison to CYP152s, P450Jα forms α-hydroxy decanoic acids in acceptable enantiomeric purity.

Table 23 Comparison of e.e. values for CYP152s used in this work ($P450_{J\alpha}$, $P450_{CLA}$ and $P450_{BS\beta}$).

α- carbon	*S* [%]	*R* [%]	e.e. value [%]
$P450_{J\alpha}$	98	2	95
$P450_{CLA}$	85	15	71
$P450_{BS\beta}$	37	63	26
$P450_{SP\alpha}$	Matsunaga 2000[a] [35]		98

3.3.4. Formation of volatile by-product 1-alkene

Based on the proposed reaction mechanism for OleT [34] an attack at the carbon in β-position is necessary to form 1-alkenes. Therefore β-hydroxylases like $P450_{BS\beta}$ are also able to produce olefins via decarboxylation [40]. Contrary, α-hydroxylases are thought to exclusively catalyze hydroxylations [36]. GC-MS headspace analysis was used to determine 1-alkene formation by $P450_{BS\beta}$, $P450_{CLA}$ and $P450_{J\alpha}$. Due to the high volatility of the 1-alkenes, the optimized reaction set-up was adapted to one highly concentrated peroxide pulse into the reaction mixture. 1-Alkene detection (Figure 26) was possible for all of the three applied catalysts for conversions with hexanoic and octanoic acid. 1-nonene formation could be detected for conversions with $P450_{CLA}$ and $P450_{BS\beta}$.

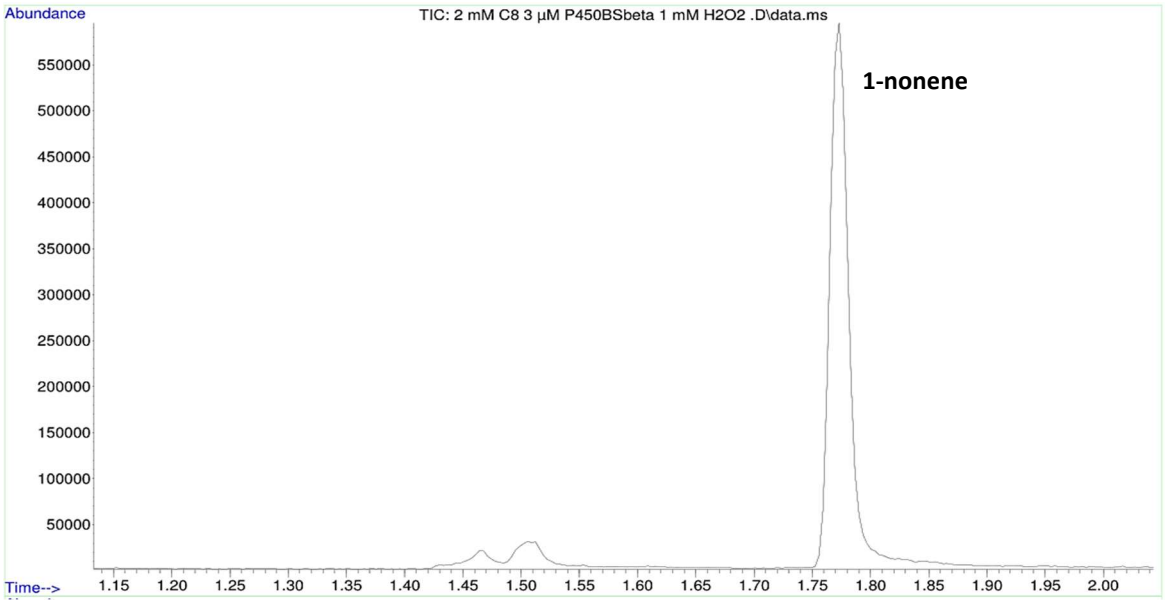

Figure 26 GC-MS trace of 1-nonene formation during conversion of C10:0 with $P450_{BS\beta}$. 1-nonene was detected with GC-MS headspace analysis. A GC-MS spectrum proving the 1-nonene formation can be found in the appendix section (Figure 117).

The efficiency of 1-alkene production was highest for $P450_{BS\beta}$ with 199 µM 1-nonene formed from C10:0. In regard to substrate conversion, 23% of the converted C10:0 results in 1-nonene (Table 24). For comparison, Liu et al (2014) indicated a 1-alkene production of 194 µM for conversion of tetradecanoic acid with OleT (TOF 1.1 min^{-1}) [39]. For $P450_{CLA}$ and $P450_{J\alpha}$ only traces of 1-alkenes could be detected (<1 %). Exclusively short chain fatty acids (<C10:0) were converted to 1-alkenes by the α-hydroxylases. Concluded, this is the first report on 1-alkene formation by the α-selective fatty acid hydroxylases from the CYP152 family.

Table 24 1-alkene formation during conversion of short chain fatty acids (≤ C10:0) with $P450_{J\alpha}$, $P450_{CLA}$ and $P450_{BS\beta}$. Selected substrates were C10:0, C8:0 and C6:0. 1-Alkenes were detected and quantified with GC-MS headspace analysis. Conversions were obtained from GC-FID analysis after extraction of residual fatty acids. n.d. = not detected

	Conversion [%]			1-alkene [µM]		
Substrate	$P450_{J\alpha}$	$P450_{CLA}$	$P450_{BS\beta}$	$P450_{J\alpha}$	$P450_{CLA}$	$P450_{BS\beta}$
C10:0	60	67	43	n.d.	8.4	199
C8:0	20	91	23	4	6.4	146
C6:0	6	11	40	1.6	4.6	53

3.3.5. Fatty acid conversion with $P450_{J\alpha}$ on preparative scale

To evaluate the synthetic potential of $P50_{J\alpha}$ for preparative scale applications, the reaction volume was increased from 2 mL to 50 mL. The constant H_2O_2 supply was ensured with a pump adding 0.8 mM peroxide per 30 min for 10 h (in total 20 times) [37]. Substrate C10:0, C12:0 and C18:1 were converted at 5 mM (0.86 to 1.41 g L^{-1}) into α-hydroxy fatty acids. Due to poor solubility of the substrates in water the formation of a white flocculent suspension occurred after addition of fatty acids. The reaction was monitored by taking samples at certain points which were analyzed by GC-MS. Highest conversion of 83% was reached for dodecanoic acid. Analysis revealed that there was no further conversion after 4 h and addition of 6.4 mM H_2O_2 (Figure 27).

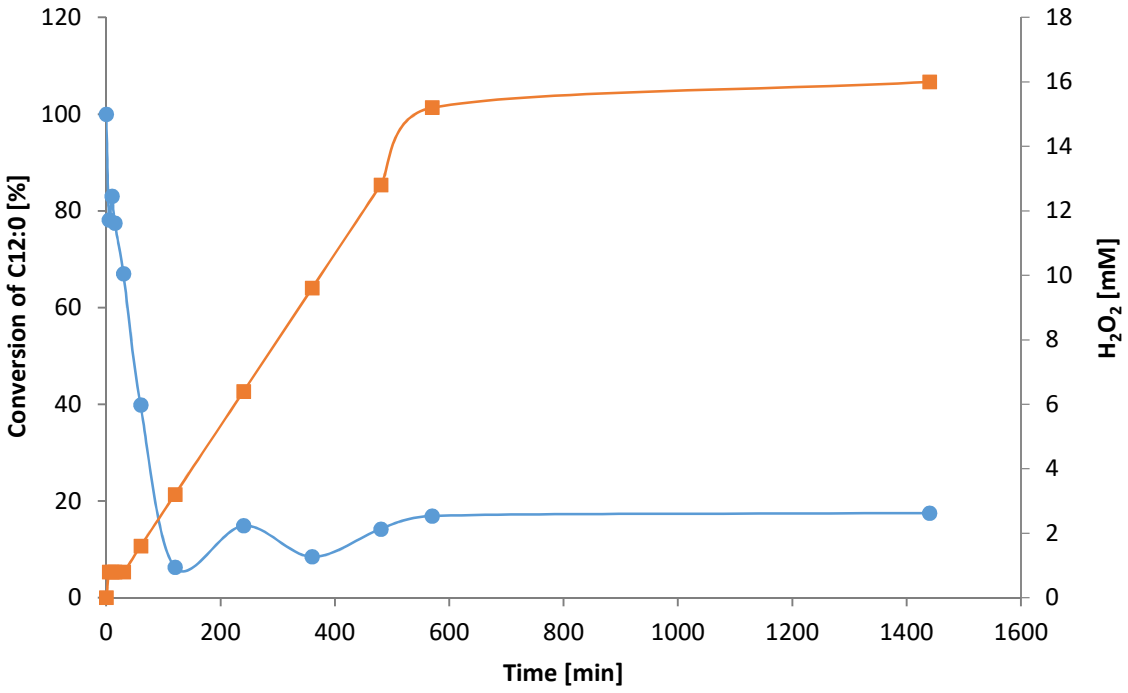

Figure 27 Time-dependent conversion of 5 mM C12:0 (blue) on 50 mL scale with $P450_{J\alpha}$. H_2O_2 (orange) was supplemented in pulsed-feed mode (20 times 0.8 mM H2O2 in 30 min intervals).

To monitor the operational stability of the enzyme, the color change throughout the reaction was followed as shown in Figure 28 [37]. Starting with a slightly red solution (functional heme cluster), the color faded over time and increasing amount of H_2O_2 .The color change also matches the results from the substrate conversion since after 4 h no further substrate conversion could be detected and the typically red color disappeared. This could be explained by the high peroxide concentrations which lead to inactivation of the catalyst [16, 21].

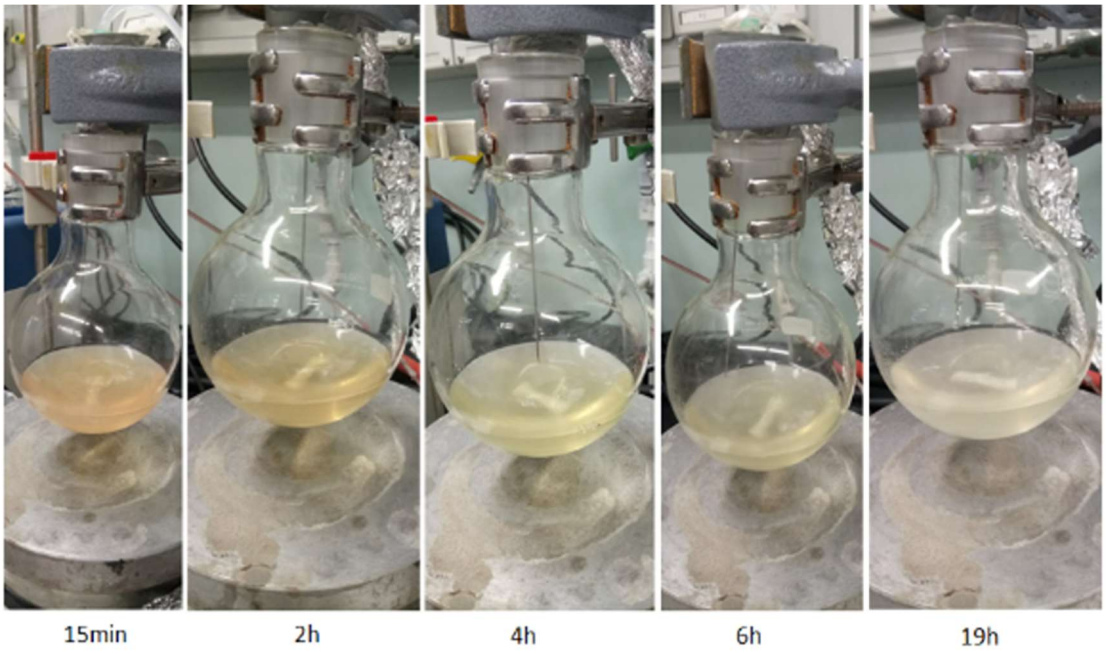

Figure 28 Decolorization of the reaction solution during conversion of dodecanoic acid with $P450_{J\alpha}$ and automated H_2O_2 supply. Red color indicates a fully functional heme cluster of $P450_{J\alpha}$.

Subsequently, a prep-scale conversion of decanoic acid with $P450_{J\alpha}$ was carried out. The reaction set-up was identical to the approach with dodecanoic acid. The low solubility of decanoic acid in water led to a white to transparent flocculent solution after addition of the fatty acid. Similar to the prep-scale of dodecanoic acid after 4 h no further conversion of C10:0 could be detected most likely due to the high peroxide concentration (Figure 29). The conversion of C10:0 reached 70% after 23 h and addition of 16 mM H_2O_2. (Figure 30). Subsequently, reaction mixtures were extracted with ethyl acetate and isolated solid materials were further analyzed by NMR to confirm the formation and purity of the reaction products.

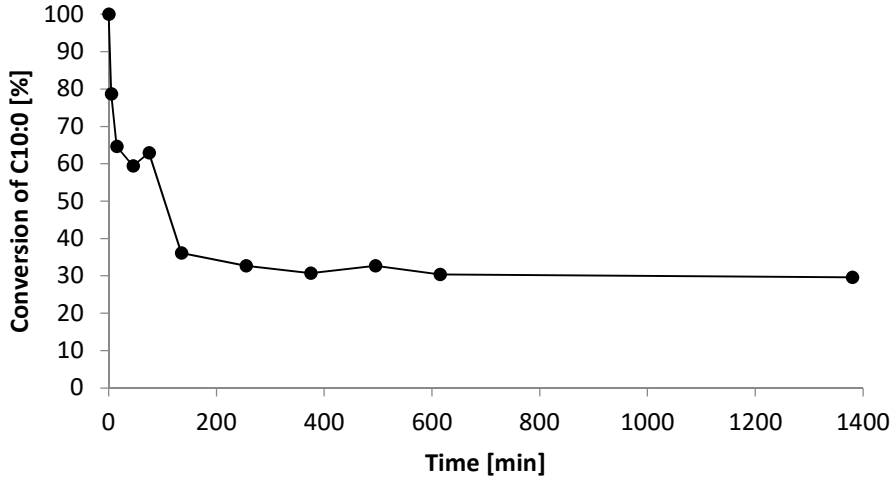

Figure 29 Prep-scale conversion of decanoic acid with $P450_{J\alpha}$ in 50 mL with automated peroxide supply. Substrate depletion was analyzed by GC-MS.

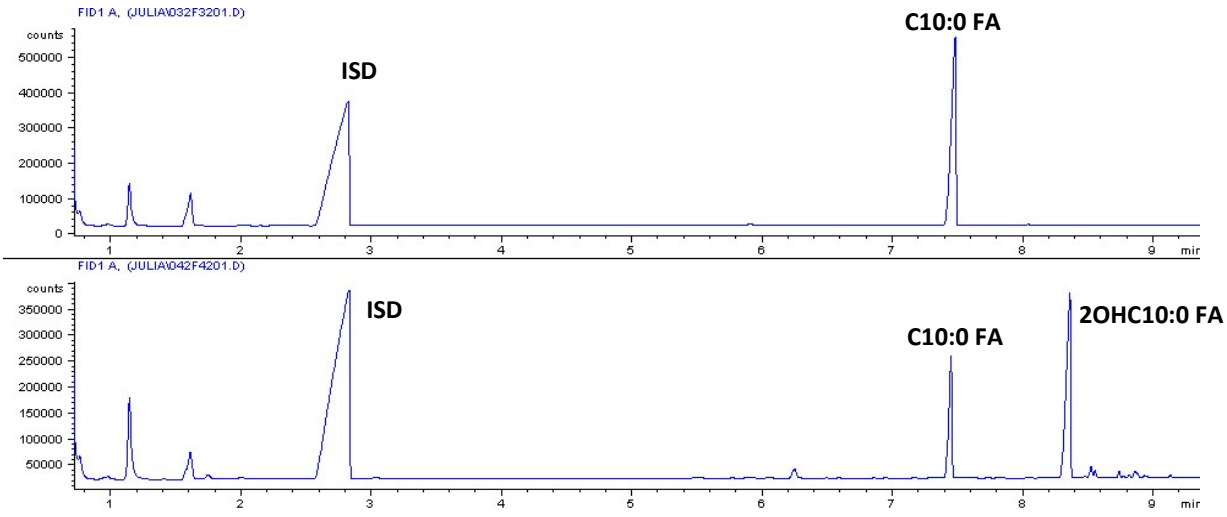

Figure 30 Preparative scale conversion of decanoic acid (5 mM) with P450$_{J\alpha}$ on 50 mL with automated peroxide supply. Samples were analyzed with GC-FID. Formed α-hydroxy acids were identified by mass fragmentation (GC-MS) and by comparison to analytical data generated by the α-hydroxylase P450$_{CLA}$ [36]. Top chromatogram is the control without catalyst. Lower chromatogram shows the ISD = internal standard 0.1% (v/v) 1-octanol.

Summary of both 50 mL reactions is given in Table 25 showing that dodecanoic acid is the preferred substrate for conversions with P450$_{J\alpha}$ reaching a total turnover number of 700. In contrast, Dennig et al (2019) reported a TTN conversions of C12:0 with P450$_{CLA}$ of up to 1666 [37]. Problems occurring during preparative scale reactions are the operational stability of the catalyst and the solubility issues of fatty acids in aqueous solutions. Therefore, the order of substrate addition was crucial to avoid extensive substrate precipitation. Otherwise, a decrease in conversion could occur due to the inaccessibility of the precipitated substrate for the P450$_{J\alpha}$.

Table 25 Summary of catalytic data obtained from prep-scale conversions of P450$_{J\alpha}$. Total turnover number TTN corresponds to the number of catalytic cycles performed until the catalyst is inactivated [108]. Samples were analyzed by GC-MS and GC-FID.

Substrate	Conversion [%]	α-OH [%]	β-OH [%]	1-alkene	TTN [-]
C12:0	83	>98	<2	no	700
C10:0	70	>98	<2	no	653

3.3.6. Verification of α-hydroxy acid formation by ^{1}H-NMR

^{1}H-NMR was used to confirm the formation of the respective α-hydroxy fatty acid by P450$_{J\alpha}$. For this, several milligrams of isolated product were required for this analysis. α-Hydroxy fatty acids were therefore isolated from the preparative scale conversions of dodecanoic and decanoic acid. After extraction with ethyl acetate and freeze drying the product was dissolved in deutereated MeOH followed ^{1}H-NMR analysis. Isolated yields of the corresponding hydroxyl fatty acids of C10:0 and C12:0

were 34% (16 mg isolated product and 50% (27 mg isolated product), respectively. The obtained spectrum for α-hydroxy dodecanoic acid is depicted in Figure 31. Integration and comparison with published data [37] confirmed the structure of the α-hydroxy fatty acid. Signal intensities are based on the amount of hydrogen atoms, for instance the tallest signal at 1.45-0.96 corresponds to 16 hydrogen atoms of CH_2-atoms from the α-hydroxy dodecanoic acid. Remaining substrate in the mixture is indicated by the shift ranging from 1.79-1.46 (2 H). The α-hydrogen of the α-hydroxy dodecanoic acid is represented by the signal at 4.02 (1 H). Conversion of dodecanoic acid with $P450_{J\alpha}$ was calculated in the sample indicated the presence of 30%, which is 10% higher than determined by GC-MS. Reason therefore could be the low solubility of C12:0 (<2 mM) in aqueous solutions resulting in heterogeneous material that might not have been transferred during sampling. Also the isolated product from the 50 mL conversion of C10:0 was analyzed by H-NMR (appendix section Figure 75). Here, the NMR revealed a conversion of more than 90% in comparison to 70% of the GC-FID analysis. Sublimation of decanoic acid during freeze-drying process could explain the gap in substrate conversion [109, 110]. This phase transition could appear due to the lower melting point of C10:0 as compared to C12:0.

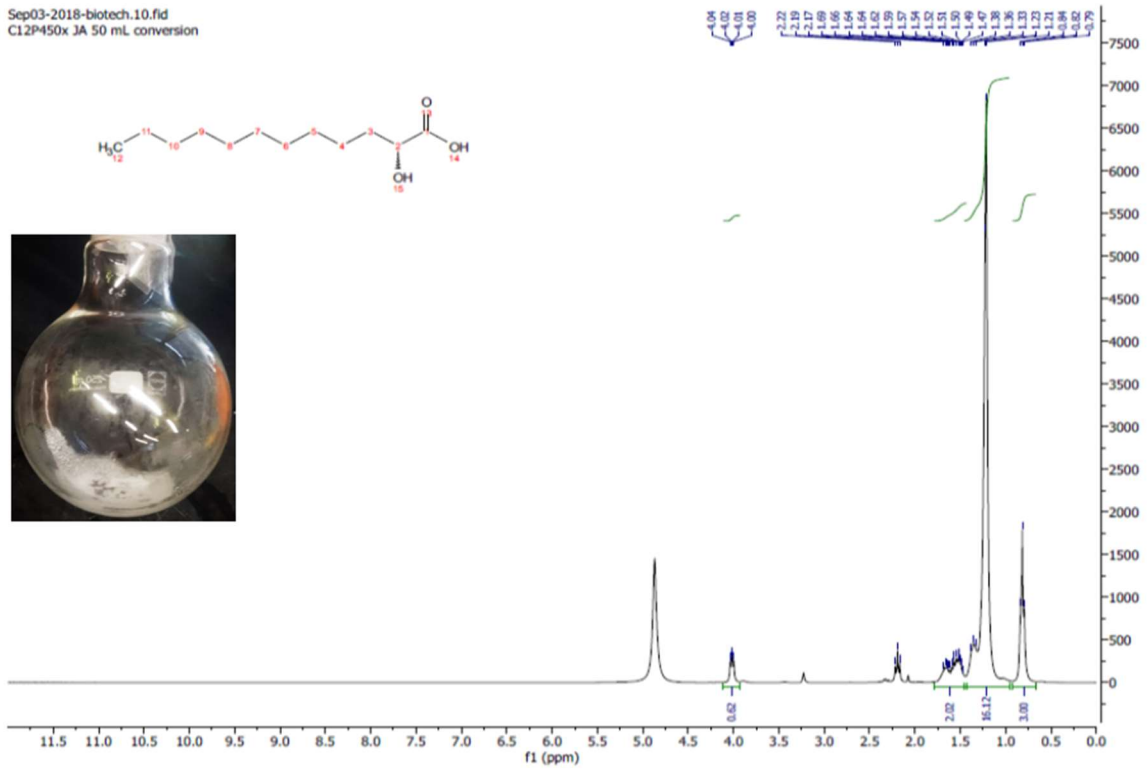

Figure 31 ^{1}H-NMR of isolated α-OH C12:0 (27 mg white solid; 55% isolated yield) from conversion of 5 mM C12:0 with $P450_{J\alpha}$ on 50 mL scale and supplementation of 16 mM H_2O_2. Impurities at ~2.21 ppm correspond to traces of recovered substrate (~30%).

3.3.7. Biocatalytic conversion of oleic acid with $P450_{J\alpha}$

An enhanced minimal substrate screening was carried out with P450Jα for conversions of oleic acid, adipic acid and 10-undecene acid. Conversion was only detected for oleic acid and it proved to be a remarkably good substrate for $P450_{J\alpha}$ with conversion exceeding 90%. GC-MS analysis revealed the formation of the corresponding α-hydroxy fatty acid. In the case of oleic acid, product identification is even more important as it has never been converted in a single enzyme application. Therefore a prep-scale set-up was carried out (initially with 50 mL) with a reaction volume of 100 mL. The peroxide supply was reduced to 0.5 mM per pulse. Due to the low solubility of oleic acid in aqueous solutions the substrate addition was critical. By slowly adding the reaction buffer C to the dissolved fatty acid (in EtOH), a white emulsion was prepared. To monitor catalyst stability, the active enzyme concentration of $P450_{J\alpha}$ was monitored by CO-titration during the whole time course. The resulting curves are show in Figure 32. Concerning the stability of the heme group against the H_2O_2, active enzyme could be determined until a peroxide concentration of 5.6 mM (<0.1 µM active $P450_{J\alpha}$). Until this point, the conversion reached 91% which was even higher compared to dodecanoic acid (83%), which was thought to be the so far best natural substrate. The minor substrate conversion after depletion of the active enzyme can be explained by analytical differences caused by the inhomogeneous emulsion. Based on the GC-MS mass fragment analysis of the only formed product, it is likely that $P450_{J\alpha}$ performs highly region-selective hydroxylation at the α-carbon of the oleic acid (note: only cis-oleic acid was used).

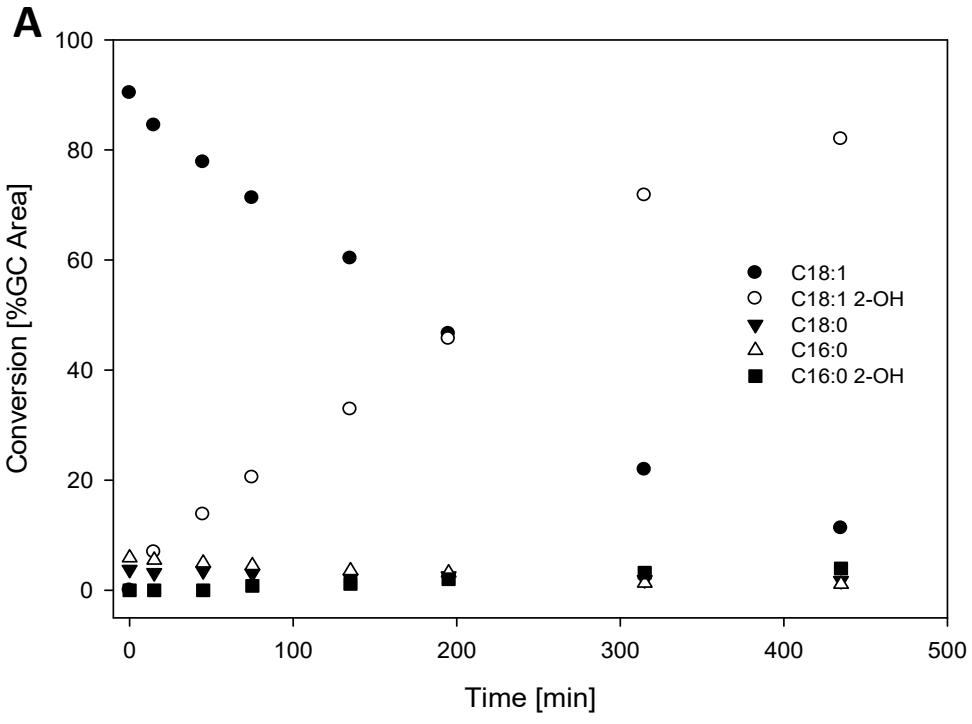

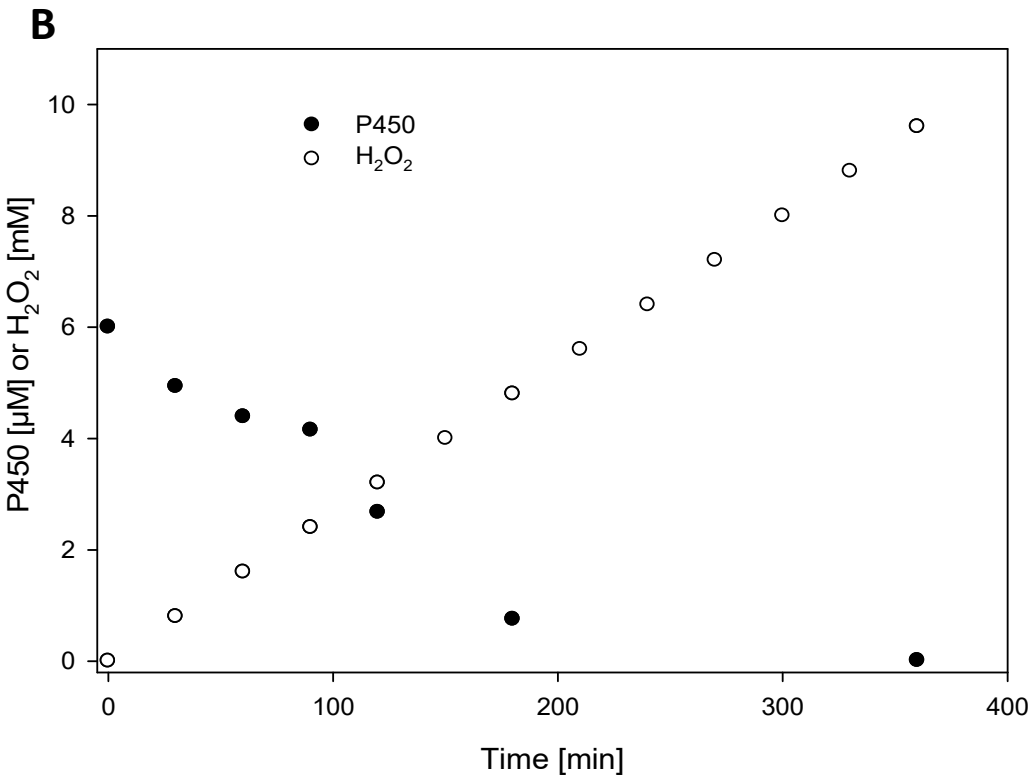

Figure 32 Time course for preparative conversion of 5 mM C18:1 (141 mg) with P450$_{J\alpha}$ on 100 mL scale. The substrate has a purity of 90% (determined by GC) and contained significant traces of methyl stearic acid and palmitic acid (C16:0). **A** = Conversion after 15 h and addition of 0.5 mM H_2O_2 per 30 min (in total 15 mM). **B** = Active protein concentration of P450$_{J\alpha}$ throughout the reaction.

Throughout the reaction the formation of several by-products could be detected despite at very low amount (<10%) (Figure 32B). Formed by-products were identified by GC-MS fragmentation pattern analysis and using the commercial compound library NIST [94].The distribution of the compounds in the prep-scale reaction with oleic acid is depicted in Figure 33. Hexadecanoic acid (C16:0) and methyl stearate were the major contaminants (<6%) of the oleic acid substrate. Over the time course of the reaction three addition peaks were formed. The formed products correspond to α-hydroxy oleic acid and the corresponding ketoacid as well as α-hydroxy hexadecanoic acid. At the end of the reaction higher H_2O_2 concentrations (10 mM) can lead to over-oxidation and formation of α-ketoacids and shorter chain fatty acids/hydroxy acids [97].

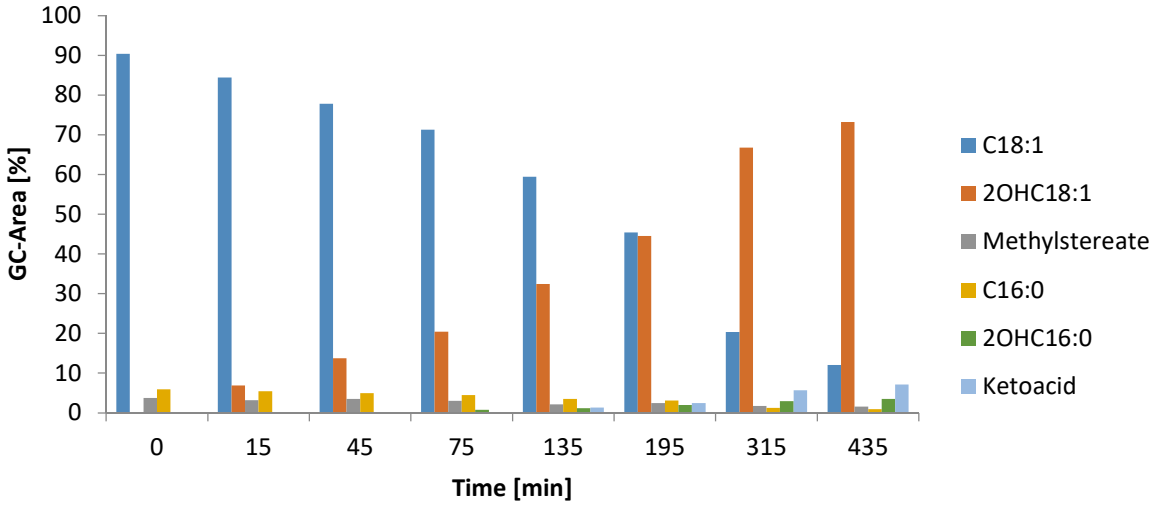

Figure 33 Evolution of substrate/product ratios during conversion of C18:1 with $P450_{J\alpha}$ on 100 mL scale. Substrate conversion/product formation was determined with GC-MS and products were identified by mass fragmentation and in comparison to the provided compound library NIST [94].

To confirm the formation of the respective α-hydroxy fatty acid during the conversion of oleic acid with $P450_{J\alpha}$ ^{1}H-NMR analysis of the isolated product was performed. The extraction yielded 79% and 118 mg of dried material. Figure 34 shows the resulting NMR spectrum of isolated material in DMSO-d6. The signal at 3.89 ppm (1H) is from the α-hydrogen whereas the signals at 1.58-1.45 ppm (2H) are derived from the hydrogens bound around the β-carbon of the substrate. Based on the integration results from the ^{1}H-NMR, the conversion of oleic acid was calculated to be 80%. 5 mM of oleic acid in 100 mL aqueous solution exceeded the solubility limit resulting in a turbid emulsion. Said inhomogeneity could have an influence on the sampling and the analysis. Concluded, the formation of α-hydroxy fatty acid during the conversion of oleic acid with $P450_{J\alpha}$ could be confirmed by ^{1}H-NMR.

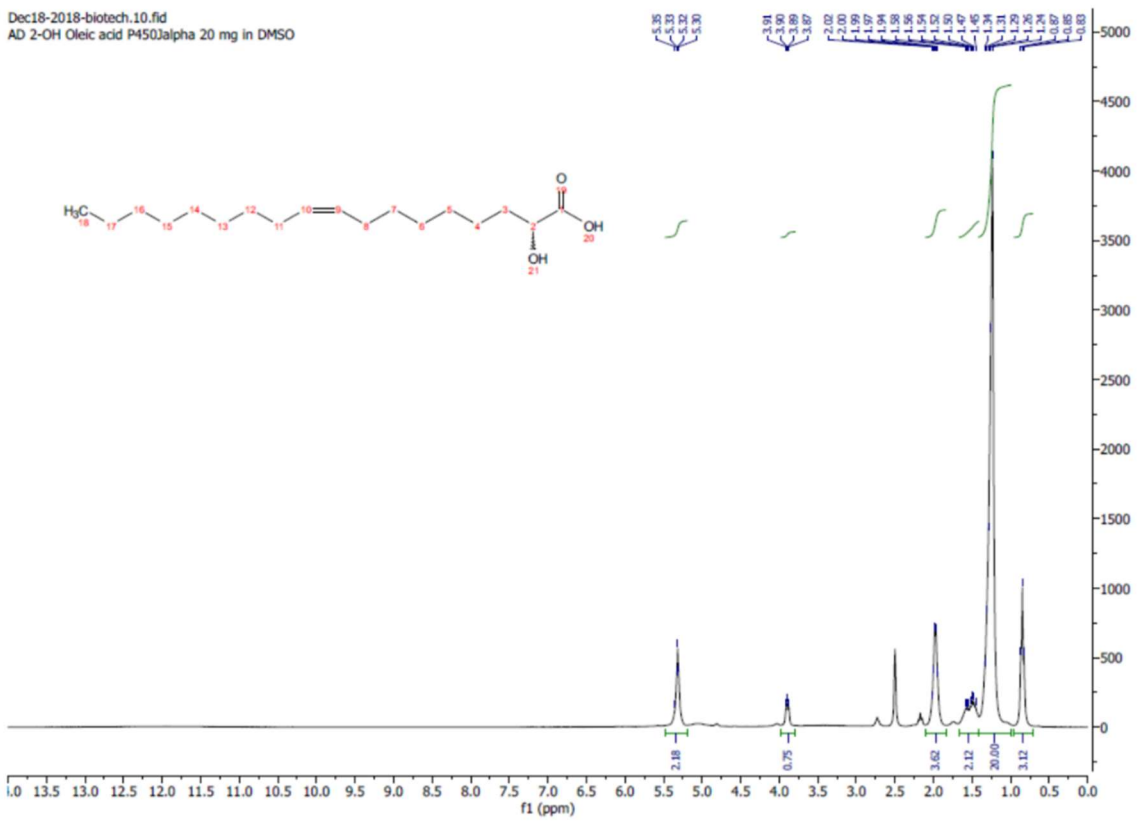

Figure 34 ^{1}H-NMR of isolated α-OH C18:1 (118 mg; transparent/clear oily liquid at RT). The product was obtained with 79% isolated yield from conversion of 5 mM C18:1 with $P450_{J\alpha}$ on 100 mL. Isolated yield [in %] was calculated based on measured mass [mg] of isolated and dried products and the maximum theoretical yields [mg] obtained after full conversion of C18:1 into the respective α-HA. Impurities at ~2.21 ppm correspond to traces of recovered substrate (~ 19%).

Based on promising results from prep-scale reactions and test conversions of oleic acid with $P450_{J\alpha}$, the corresponding key kinetic parameters were determined and summarized in Table 26. Overall, oleic acid outplayed dodecanoic acid as "ideal" substrate for $P450_{J\alpha}$. This is reasoned by higher specific activity (15.2 U mg^{-1}) as well as higher turnover numbers (731 min^{-1}). To benchmark $P450_{J\alpha}$ with known catalysts for conversions of oleic acid, reactions (optimized set-up from $P450_{J\alpha}$) were carried out with $P450_{CLA}$ and $P450_{BS\beta}$. Both catalysts reached lower conversion of oleic acid with 49% for $P450_{CLA}$ and 78% for $P450_{BS\beta}$ (Table 27). Main Products formed for $P450_{CLA}$ and $P450_{BS\beta}$ were α- or β-hydroxy oleic acids, respectively.

Table 26 Summary of determined kinetic parameters of $P450_{J\alpha}$ for conversion of oleic acid.

Catalytic numbers oleic acid	
specific activity [U mg^{-1}]	15.2
TON [min^{-1}]	731
TTN [-]	1497

Table 27 Conversion of oleic acid with $P450_{J\alpha}$ in comparison to $P450_{CLA}$ and $P450_{BS\beta}$. Reactions were done with the optimized reaction set-up. Samples were analyzed with GC-MS.

Oleic acid	Conversion [%]
$P450_{CLA}$	49
$P450_{J\alpha}$	88
$P450_{Bs\beta}$	78

3.3.8. Dissociation constant determination of $P450_{J\alpha}$ and oleic acid

Subsequently, the dissociation constant of $P450_{J\alpha}$ for oleic acid was determined as it proved to be the most suitable substrate. Due to the higher conversion of oleic acid, it was expected that the enzyme shows higher affinity for oleic acid than for C12:0/C10:0. Determination was carried out by titrating substrate to an enzyme solution followed by photometrical measurement. Saturation of P450Jα with oleic acid could not be achieved and therefore no k_D-value could be determined (Figure 35). Still $P450_{J\alpha}$ leaves the low spin to enter the high spin state at low concentrations of oleic acid. This also fits the high conversions of oleic acid with $P450_{J\alpha}$ and H_2O_2.

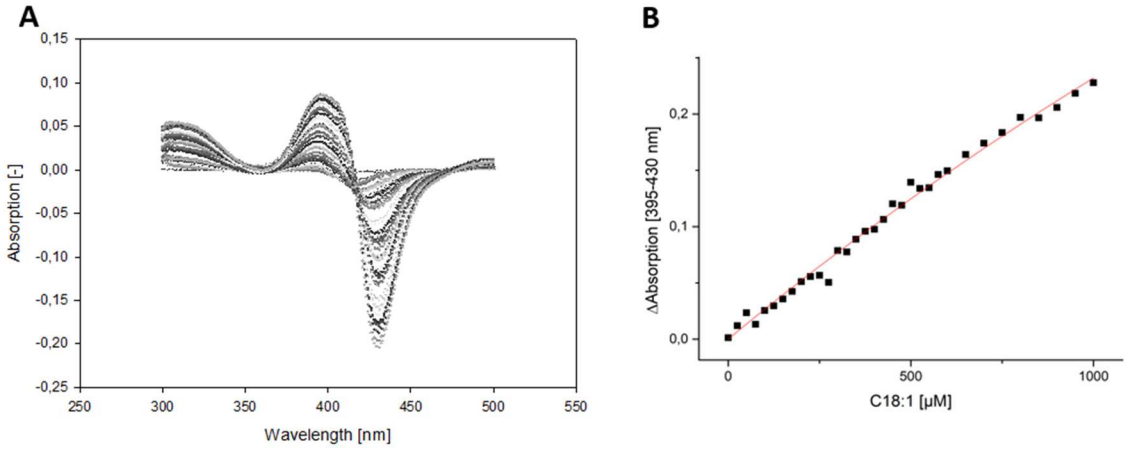

Figure 35 Ligand titration experiment for C18:1 and purified $P450_{J\alpha}$. A = Absorbance difference spectra recorded at varying ligand concentrations (0 to 2.2 mM). B = The absorbance changes at 420 and 395 nm were plotted against the corresponding FA concentration. Data was fitted with Michaelis-Menten equation using Origin 9.0 software.

Furthermore, the enzymatic conversion of oleic acid has not been reported before. Already existing systems to convert oleic acid mainly focus on whole cell applications. Organisms like yeast (*Saccharomyces ceravisiae*) or bacteria such as *E. coli* were applied to turn oleic acid into more valuable compounds [111–113].

3.4. "Smarter" H_2O_2 supply to improve catalyst stability

After characterization of the newly discovered α-hydroxylase $P450_{J\alpha}$ and the investigation of its potential for prep-scale application, still several challenges remain. The first problem to address is the oxidant H_2O_2. On the one hand it is required for efficient substrate conversion and on the other hand higher peroxide concentrations could lead to inactivation of the catalyst (Figure 32). Therefore a "smarter" H_2O_2 delivery system is necessary. A possible solution is the coupling of fatty acid conversions to H_2O_2 in-situ producing reactions such as the oxidation of glucose catalyzed by the glucose oxidase [114]. The second investigated option is the application of urea-H_2O_2, which can provide a slow release system for peroxide.

3.4.1. GOX-coupled conversion of fatty acids with $P450_{J\alpha}$

A "smarter" peroxide supply for peroxygenases could be ensured by coupling the fatty acid conversion with a slow release system peroxide. A good candidate therefore is the glucose oxidase GOX [114]. It catalyzes the oxidation of glucose to glucuronic acid while utilizing oxygen as electron acceptor to release peroxide. The reaction is depicted in Figure 36.

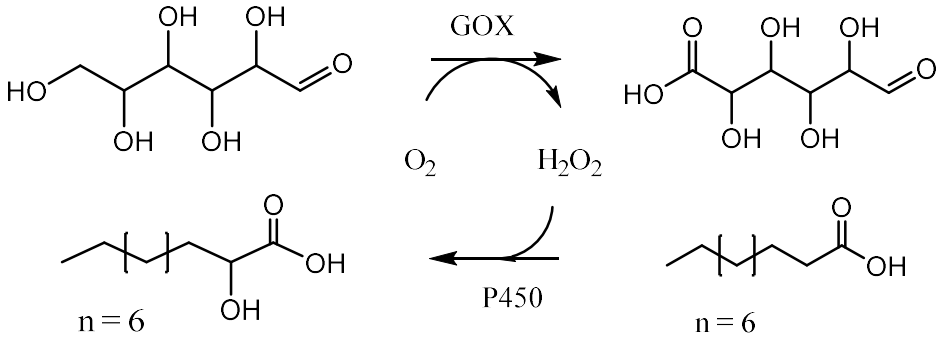

Figure 36 Slow peroxide release system by coupling fatty acid conversion to glucose oxidation (GOX).

Due to the high activity of GOX, the ideal catalyst concentration/activity has to be identified to couple both reactions to avoid poising of the P450 with H_2O_2. The specific activity of the GOX was calculated based on the oxygen consumption, which was measured with an oxygen sensor. The obtained value was 27 U mg^{-1} for the commercial GOX (*Aspergillus niger*) from Sigma Aldrich. Based on the determined activity of the GOX and in respect to the turnover numbers of $P450_{J\alpha}$ different oxidase concentrations were investigated (appendix section Figure 119). Finally, 0.002 mg mL^{-1} of GOX turned out to be the most suitable enzyme concentration reaching a conversion of 80% of 2 mM C12:0 with $P450_{J\alpha}$. Subsequently, various concentrations of glucose and dodecanoic acid (equimolar) were investigated for conversion of C12:0 with $P450_{J\alpha}$ (3 µM). The obtained results are presented in Table 28, showing that conversion decreases with the increase in substrate concentration. But the amount of converted

substrate was highest for the approach with 10 mM glucose and substrate as well as 6 µM $P450_{J\alpha}$. Although increased catalyst loading only had a minor effect on substrate conversion.

Table 28 Conversion of C12: 0 with $P450_{J\alpha}$ coupled to in-situ production of H_2O_2 with glucose oxidase. Substrate and glucose concentrations were equimolar and varied from 2 to 10 mM. 6 µM of $P450_{J\alpha}$ were applied (a).

Glucose/C12:0 [mM]	Conversion [%]
2	81
5	78
10	57
10[a]	65

Equimolar concentrations of glucose and substrate turned out to almost reach the conversion in reactions with direct H_2O_2 supply. Alternative substrate conversion was investigated at varying glucose concentrations (2 to 10 mM) and 2 mM C12:0. The obtained product distribution is shown in Figure 37. The product distribution revealed, that next to the formation of the α-hydroxy dodecanoic acid, $P450_{J\alpha}$ catalyzes over-oxidations which in turn lead to decarboxylation of products in excess of H_2O_2 [97]. This was mainly indicated by the formation of undecanoic acid and α-hydroxy undecanoic acid. Over-oxidation and decarboxylations were detectable in particular at 5 and 10 mM glucose that led to locally higher peroxide concentrations. Also traces of the respective α-ketoacid were formed during the set-up with 5 mM glucose. Full substrate conversion could be achieved for the reaction set-ups with 5 and 10 mM of glucose. Notably, this was not possible for reactions with direct peroxide supply. An explanation could be the uncoupling of the heme iron complex as the peroxide tends to dissociate which results in decreased conversion.

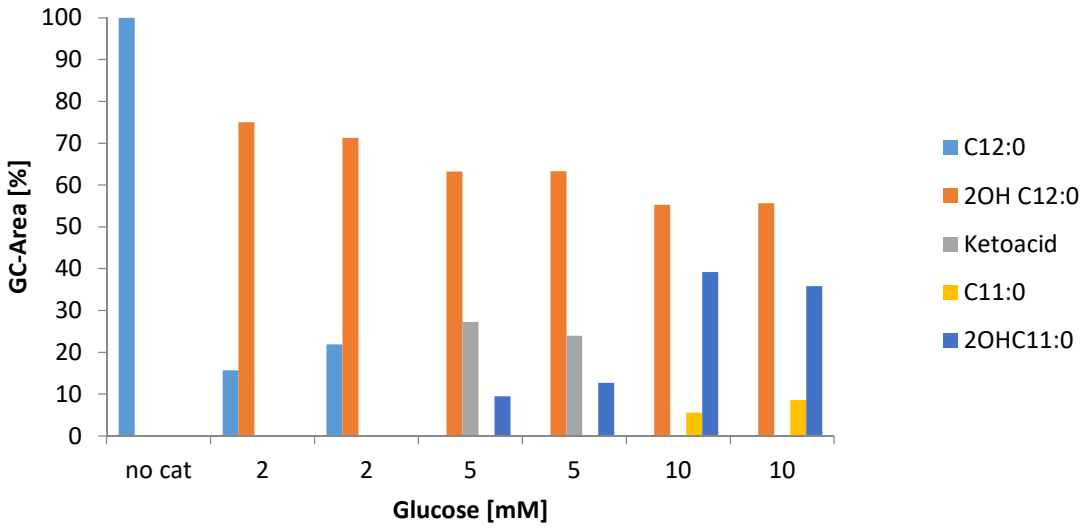

Figure 37 Conversion of C12:0 with $P450_{J\alpha}$ coupled with glucose oxidase for in-situ H_2O_2 generation. Substrate concentration stayed constant (2 mM C12:0) and glucose was varied from 2 to 10 mM. 3 µM $P450_{J\alpha}$ and 0.002 mg mL^{-1} GOX were applied.

3.4.2. Fatty acid conversion coupled with GOX and L-LOX

Besides GOX also L-LOX (α-hydroxy acid oxygenase) was added to the conversion of fatty acids with a CYP152 enzyme. $P450_{BSβ}$ was selected as catalyst as it displays low regioselectivity and therefore produces a mixture of α- and β-hydroxy fatty acids and 1-tridecene [40]. Since the removal of the *S*-enantiomer of the α-hydroxy fatty can be catalyzed by the L-LOX while forming further H_2O_2, the addition of L-LOX was expected to enhance substrate conversion (Figure 38).

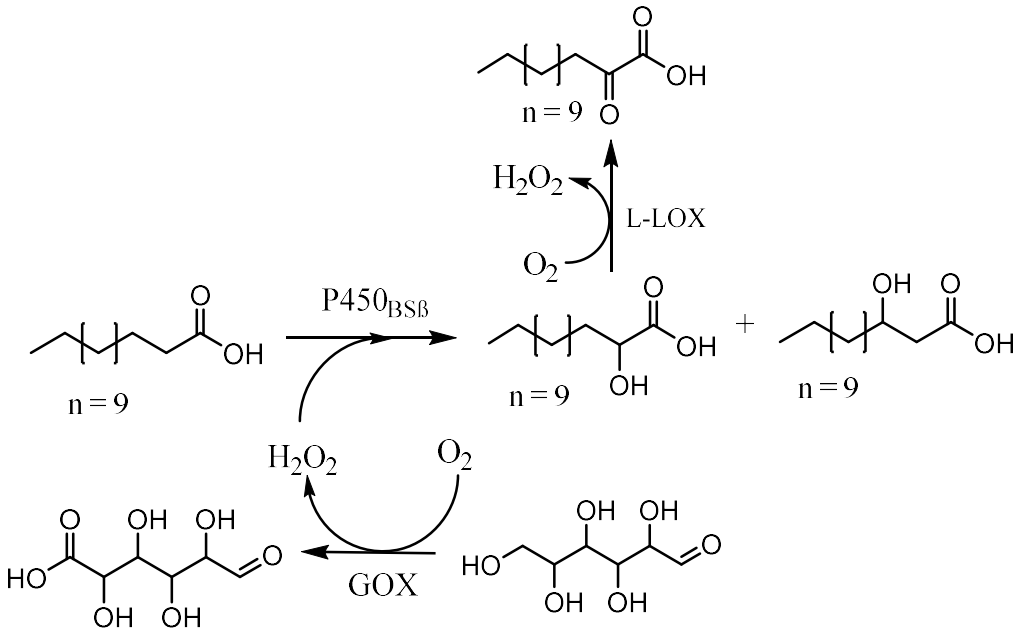

Figure 38 Slower peroxide release system (GOX) for fatty acid conversion (C14:0) with $P450_{BSβ}$ coupled to L-LOX for enhanced substrate conversion.

Tetradecanoic acid (C14:0) was selected as model due to high turnover numbers [38]. The obtained results of the fatty acid conversion with $P450_{BSβ}$ coupled to GOX and L-LOX are shown in Figure 39 and Figure 40. As expected, highest substrate conversion was reached with the GOX + L-LOX approach with 76% in respect to the GOX-coupled conversion with 56%. The ratio of the α- and β-hydroxy acids formed during the conversion of C14:0 was not influenced by the addition of L-LOX. Besides α- /β-hydroxy fatty acids and the α-ketoacid, the 1-alkene tridecene was formed. Detected products were identified by comparison to the compound library NIST and to reported analytical data from $P450_{BSβ}$ [38, 40, 94].

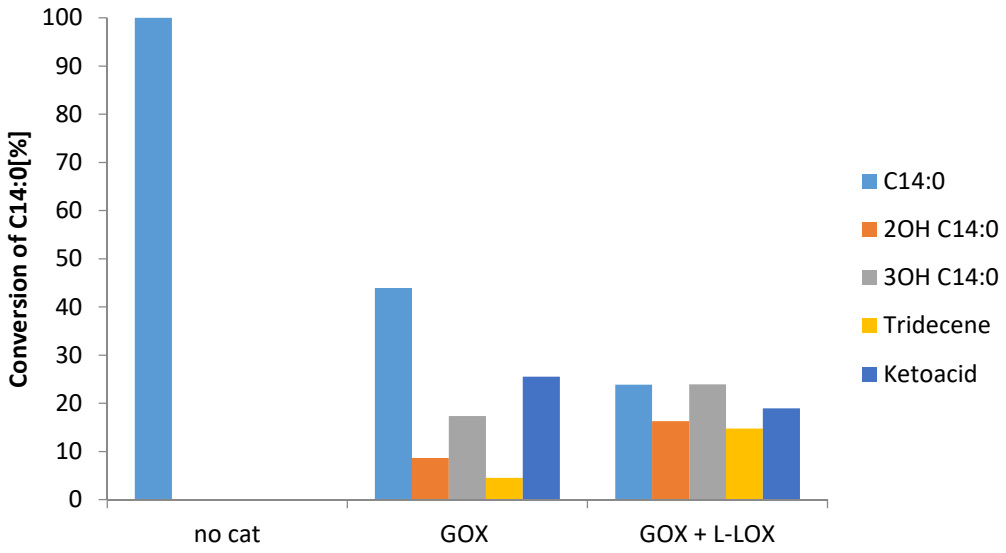

Figure 39 Conversion of C14:0 with $P450_{BS\beta}$ in presence of GOX and L-LOX to enhance substrate conversion. Formed products were identified by mass fragmentation and comparison to analytical data from $P450_{BS\beta}$ [38].Samples were analyzed with GC-MS.

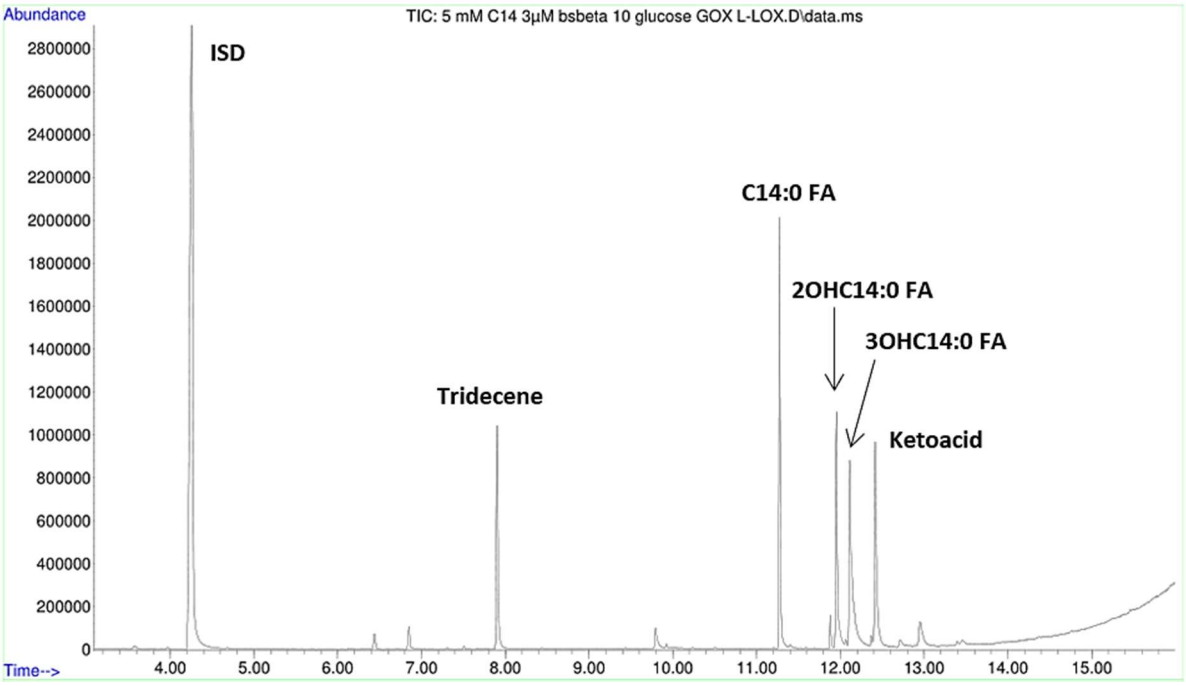

Figure 40 GC-MS trace from the conversion of C14:0 with $P450_{BS\beta}$ in presence of GOX and L-LOX. Reaction set-up contained 5 mM C14:0, 3 µM $P450_{BS\beta}$, 10 mM glucose, 0.005 mg mL^{-1} GOX and 2 mg mL^{-1} L-LOX. Formed products were identified by comparison to the NIST data bank and analytical data from $P450_{BS\beta}$ [38, 40, 94]. ISD = internal standard 0.1% (v/v) 1-octanol.

3.4.3. Urea-H_2O_2 as slow release system from hydrogen peroxide CYP152 reactions

Another possibility for a smarter peroxide delivery is the application of a slow release system such as H_2O_2 adducted to urea [115]. The difference in molecular mass is around 60 g mol^{-1} (94.07 g mol^{-1} Urea-H_2O_2, 34.01 g mol^{-1} H_2O_2, Sigma Aldrich). Therefore the urea-H_2O_2 is thought to slower release peroxide which could be beneficial for the catalyst lifetime [16]. To verify this hypothesis, the oxygen release during the catalytic conversion of peroxide with catalase was monitored using an O_2-sensor. Comparison of both oxidants revealed similar production of oxygen as determined by O_2 formation rates with 0.7 µM s^{-1} for Urea-H_2O_2 and H_2O_2 (Figure 41).

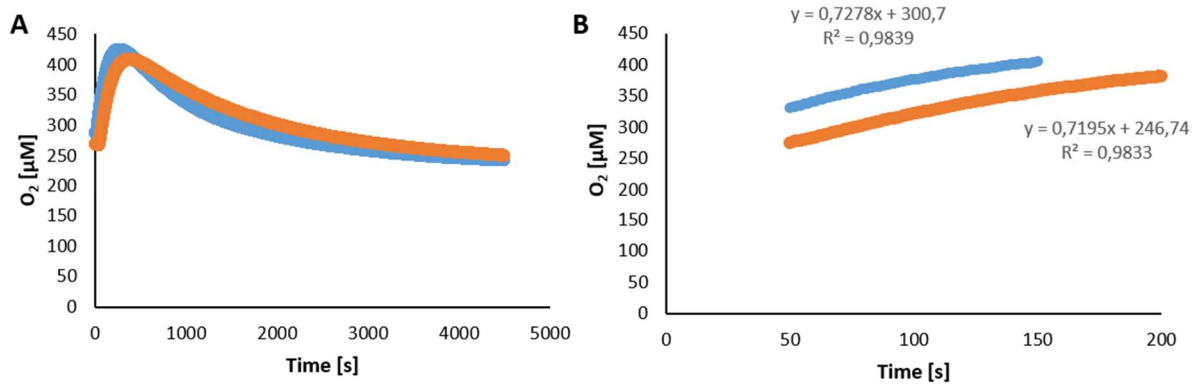

Figure 41 O_2 release from conversion of H_2O_2 (blue) and Urea-H_2O_2 (orange) with catalase measured with O_2 sensor. Slopes were used to calculate the O_2 [µM] released per second which is 0.7 µM s^{-1} for H_2O_2 and for Urea-H_2O_2

The effect of slower peroxide release was investigated for the conversion of fatty acids with $P450_{BS\beta}$. Different concentrations of decanoic acid ranging from 1 mM to 10 mM were applied, whereas urea-peroxide was added equimolar to the substrate concentration. In comparison the reactions under the same conditions were done using H_2O_2 as oxidant. But for the regular peroxide only reactions with substrate concentrations from 3 to 10 mM were carried out. No significant difference between urea-H_2O_2 and H_2O_2 in substrate conversion could be determined for higher decanoic acid/peroxide concentrations (Figure 42). Additional urea-peroxide is more expensive compared to regular peroxide (4-fold at identical supplier). Concluded, the urea-H_2O_2 did not qualify as candidate for a slower peroxide release system.

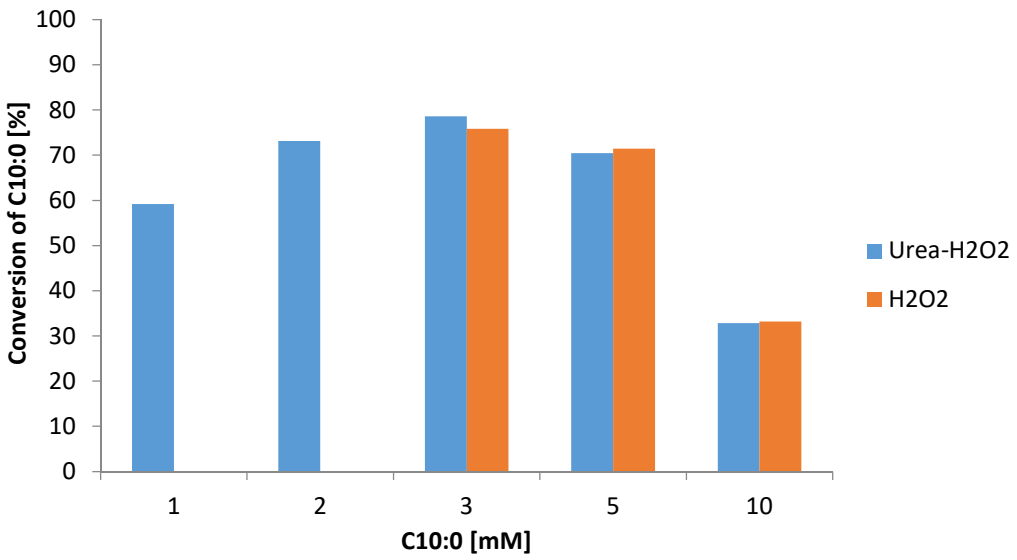

Figure 42 Conversion of decanoic acid with $P450_{BS\beta}$ [3 µM] using either H_2O_2 or Urea-H_2O_2 as oxidant. Substrate and peroxide were equimolar and varied from 1 to 10 mM. Samples were analyzed with GC-MS.

3.5. Immobilization of CYP152s

Stability improvement of enzymes against harsh reaction conditions can be achieved by immobilization of the catalyst on solid carrier material [55]. This strategy permits a continuous reaction set-up as well as reusability of the enzyme in ideal case. Disadvantages are a decrease in turnover numbers caused by the fixation of the enzyme on the carrier and mass transfer limitations of substrates and cofactors into particles. Successful immobilization has been reported for P450s but not in particular for the CYP152 family [50]. The following section covers the immobilization of CYP152s whereas a comparison of immobilization via ionic and affinity binding was carried out.

3.5.1. Immobilization of $P450_{BS\beta\_Z}$ via ionic binding

Ionic binding of CYP152s onto an ionic carrier material was achieved by cloning the positively charged Z_{basic2} protein tag at the N-terminus of the target enzymes. Immobilization was done directly from the cell free extract to avoid expensive and time consuming purification steps [74]. Valikhani et al (2018) already reported the successful immobilization of $P450_{BM3\_Z}$ on ReliSorb™ SP400 applying this direct and oriented immobilization method [50]. The peroxygenase and β-hydroxylase $P450_{BS\beta\_Z}$ was the catalyst of choice as an expression strain carrying the ready-made construct was available. Additional also $P450_{BM3\_Z}$ was immobilized to evaluate and compare the immobilization efficiency.

3.5.1.1. Immobilization directly from cell free extracts

The immobilization process directly from cell free extracts containing either $P450_{BS\beta\_Z}$ or $P450_{BM3\_Z}$ was monitored by determining the remaining active enzyme concentration in the supernatant with CO-titration after each immobilization step. SDS-PAGE was used to determine the selectivity of the ionic binding and purity of the protein on carriers. Immobilized proteins were dissolved from the carrier by sodium dodecyl sulfate and separated on the gel. Lane 1 and 2 in Figure 43 show a clear band at 125 kDa which matches the expected size of $P450_{BM3\_Z}$ [116]. $P450_{BS\beta\_Z}$ is depicted in lane 3 with 55 kDa [86]. Additional bands appear for both P450s especially for smaller protein sizes. Those bands correspond to minor impurities that are typically found during purification of proteins by ion exchange chromatography. Obtained results show that immobilization of $P450_{BS\beta\_Z}$ on ReliSorb™ SP400 works sufficiently. These impurities could have an impact on the immobilization efficiency as less binding sites are available (not detected here). Furthermore, they could also affect the catalyzed reaction and for instance lead to by-product formation [55].

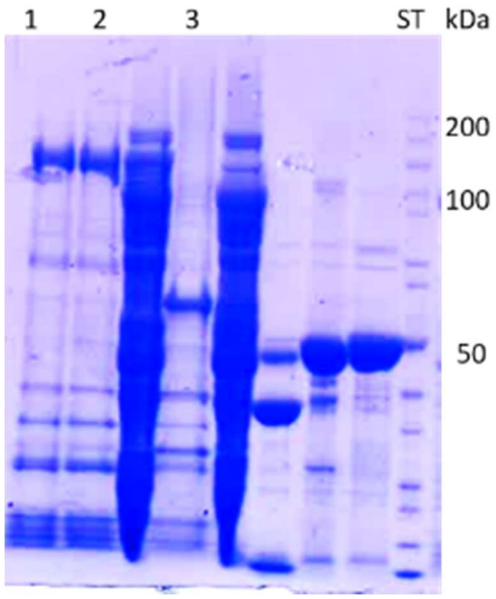

Figure 43 SDS-PAGE of immobilized $P450_{BM3\_Z}$ and $P450_{BS\beta\_Z}$ on ReliSorb™ SP400. After immobilization the bound protein was dissolved from the carrier with SDS. Lane 1+2 contain $P450_{BM3\_Z}$ (125 kDa) [116]. Lane 3 represents $P450_{BS\beta}$_Z (55 kDa) [86]. ST = unstained protein ladder (page ruler from Thermo Fisher Scientific).

Results from the CO-titrations were used to calculate the immobilization efficiencies of $P450_{BS\beta\_Z}$ and $P450_{BM3\_Z}$ on ReliSorb™ SP400. Figure 44 shows the obtained results for both P450s after each immobilization step. Highest efficiency was reached after the first step, where in the case of $P450_{BS\beta\_Z}$ >99% of the offered active enzyme was bound to the carrier. The obtained value for $P450_{BM3\_Z}$ was around 50% lower. This could be explained by the difference in initially offered enzyme which was 2 µM for $P450_{BS\beta\_Z}$ and 5 µM for $P450_{BM3\_Z}$. In general the immobilization efficiency was lower for the subsequent steps. The main reason therefore is the reduced number of available binding sites.

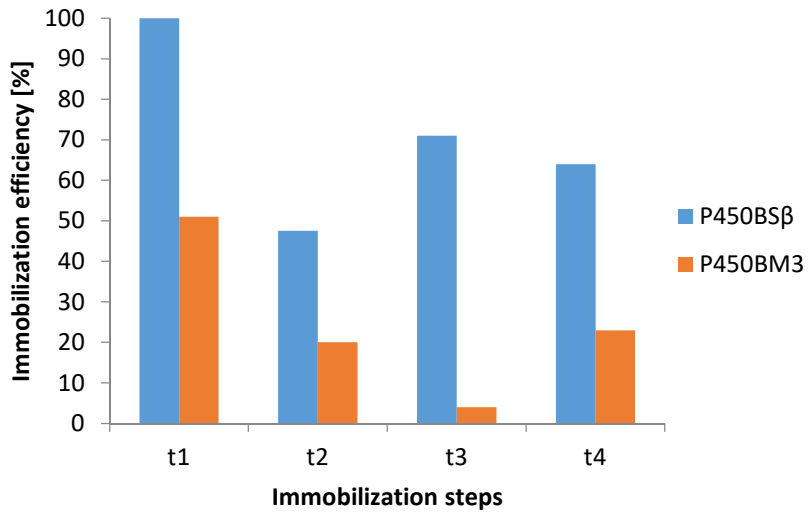

Figure 44 Comparison of immobilization efficiencies of $P450_{BS\beta\_Z}$ and $P450_{BM3\_Z}$ for immobilization on ReliSorb™ SP400. Starting active protein concentrations for $P450_{BS\beta\_Z}$ and for $P450_{BM3\_Z}$ were 2 µM and 5 µM, respectively. Immobilization efficiencies are based on remaining active enzyme concentration in the supernatant after the immobilization step.

Table 29 summarizes immobilization parameters for $P450_{BS\beta\_z}$ and $P450_{BM3\_z}$ on ReliSorb™ SP400. Besides immobilization efficiencies also the remaining active enzyme concentration after every immobilization step as well as the bound enzyme are shown. The total amount of bound enzyme was 5.7 µM and 5.1 µM for $P450_{BS\beta\_z}$ and $P450_{BM3\_z}$, respectively. Less $P450_{BM3\_z}$ was immobilized in total even when more enzyme was offered for every immobilization step. A possible explanation could be found in the protein size, where $P450_{BM3\_z}$ (125 kDa) occupies more space per mol than $P450_{BS\beta\_z}$ (55 kDa) which is 2.5 fold lighter. Larger molecules inside the particle could also lead to increased blocking of binding sites and mass transfer.

Table 29 Immobilization efficiencies obtained for binding of $P450_{BS\beta\_z}$ and $P450_{BM3\_z}$ on ReliSorb™ SP400 carrier. Start concentration was 2 µM for $P450_{BS\beta\_z}$ and 5 µM $P450_{BM3\_z}$ which were loaded every step. Efficiency was determined indirectly by measuring the remaining active enzyme concentration in the supernatant.

$P450_{BS\beta\_z}$	t_1	t_2	t_3	t_4
$P450_{BS\beta\_z}$ [µM]	0	1.05	0.58	0.72
Efficiency [%]	100	45.7	71	64
E_{bound} [µM]	2	0.95	1.42	1.28
$P450_{BM3\_z}$	t_1	t_2	t_3	t_4
$P450_{BM3\_z}$ [µM]	2.56	4.19	5.02	4.04
Efficiency [%]	51	20	4	23
E_{bound} [µM]	2.66	1.03	0.2	1.18

At next, conversions of dodecanoic acid (2 mM) were done with the immobilized $P450_{BS\beta\_z}$ (~5 mg) and adding H_2O_2 (0.5 mM per 30 min, in total 2 mM). Neither substrate depletion nor accumulation of a product could be detected by GC-MS analysis. Reasons therefore could be divers ranging from the immobilization process to substrate transfer into the active site of the catalyst. Another problem could be the co-immobilization of catalases, as several impurities were detected by the SDS-PAGE (Figure 43). Therefore a larger amount of H_2O_2 was added to the carrier material containing the immobilized $P450_{BS\beta\_z}$. Instant bubble formation likely caused by oxygen release confirmed the presence of catalases on the carrier. The ReliSorb™ SP400 carrier itself did not show any catalase activity. Catalases display extremely high turnover numbers by far exceeding activities of most CYP152s which require the peroxide for effective fatty acid conversion.

3.5.1.2. Immobilization of purified $P450_{BS\beta\_Z}$ via ionic binding

The removal of catalases in the cell free extract containing $P450_{BS\beta\_Z}$ proved to be necessary. Ion exchange chromatography was the method of choice based on the positively charged Z_{basic2}-tag. After binding of $P450_{BS\beta\_Z}$ increasing NaCl concentrations were applied for elution. Monitoring of the purification step was achieved by monitoring the UV-signal and conductivity of the flow by an Aekta prime pump system. Figure 45 shows the chromatogram obtained from the purification of $P450_{BS\beta\_Z}$. The UV-signal is depicted in blue, whereas the two signals in the beginning correspond to the unbound proteins from the cell free extract. Highlighted in red is the protein peak for $P450_{BS\beta\_Z}$, whereas the purified catalyst was collected in fractions 26 to 32. To confirm the production of $P450_{BS\beta\_Z}$ (protein size and purity) a SDS-PAGE of the collected fractions was carried out (Figure 46). The resulting gel separation showed a clear band at 55 kDa for $P450_{BS\beta\_Z}$ and still minor impurities of smaller proteins. Additionally, the active enzyme concentration of the collected fractions was determined by CO-titration (Figure 46). The highest value was determined for fraction 30 with 1 µM. After pooling of the fractions only 1.5 µM (in 5 mL) active and purified $P450_{BS\beta\_Z}$ could be detected. Valikhani et al (2018) reported an active enzyme concentration of 4 µM of $P450_{BM3\_Z}$ in the cell free extract [50]. For comparison, the expression of the His-tagged $P450_{BS\beta}$ yields 380 µM of active protein concentration from 1 L culture, which is more than 200 fold.

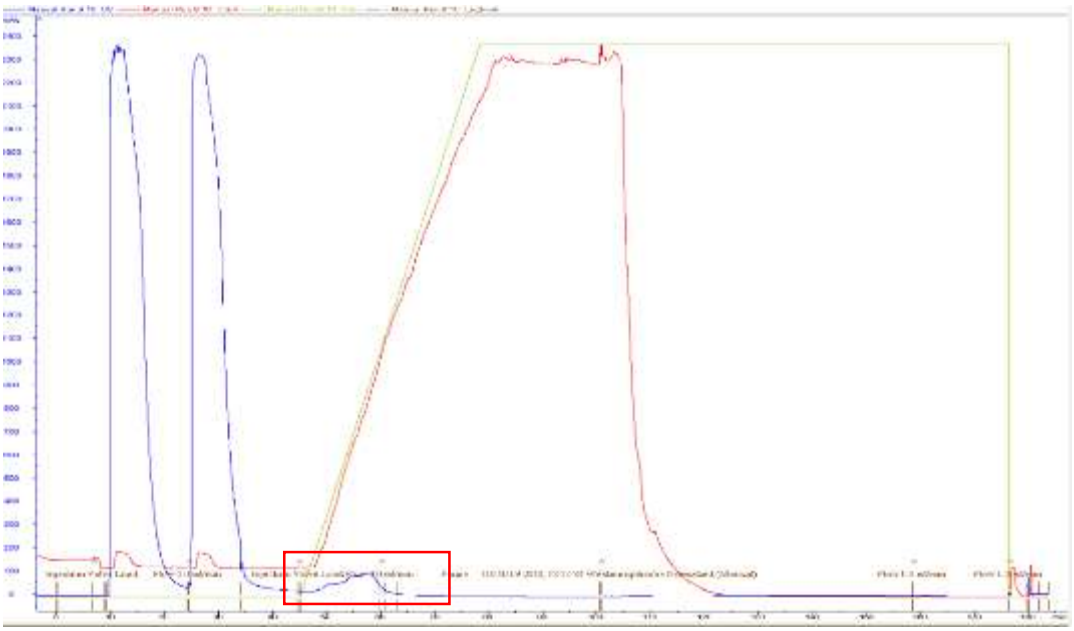

Figure 45 Purification of $P450_{BS\beta\_Z}$ with ion exchange chromatography. Purification was done with the Aekta prime system with an ion-exchange column. Peak corresponding to $P450_{BS\beta\_Z}$ is highlighted red. Blue is the UV-Signal and red the conductivity.

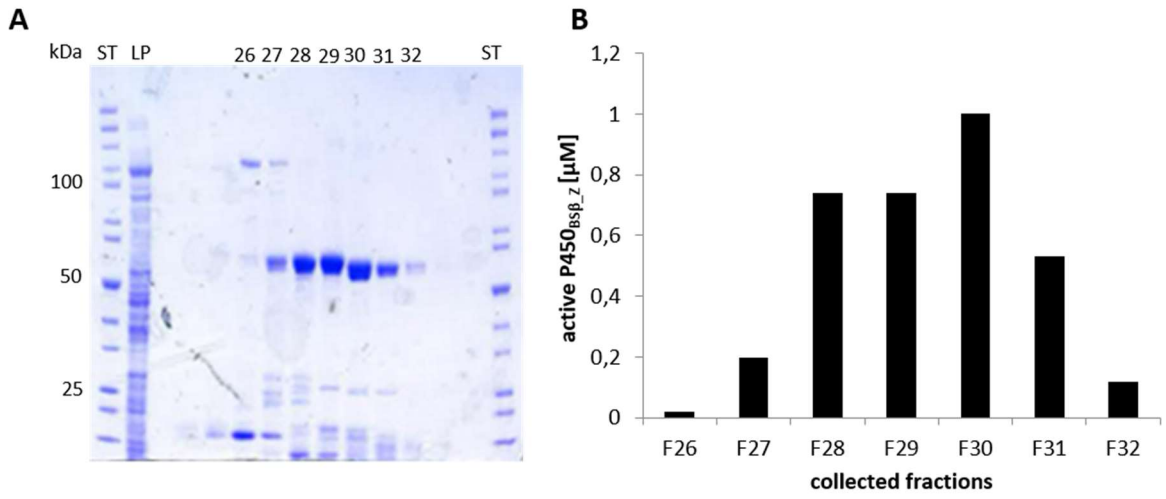

Figure 46 Evaluation of protein purification process from $P450_{BS\beta\_Z}$ with ion-exchange chromatography with a SDS-PAGE (A) and CO-titration (B) of collected fractions. ST is the unstained page-ruler form Thermo Fisher Scientific. LP is loading peak and the fractions 26-32 are the collected fractions from the purification of $P450_{BS\beta\_Z}$ (A). Determination of active protein concentration in the collected fractions was carried out with CO-titration (B).

Purified $P450_{BS\beta\_Z}$ was immobilized on ReliSorb SP400™. The immobilization process was monitored by determining the remaining active enzyme concentration (CO-titration) and the total protein concentration in the supernatant after each immobilizations step. Table 30 compares immobilization from the cell extracts containing $P450_{BS\beta\_Z}$ to the immobilization of purified $P450_{BS\beta\_Z}$. Protein concentrations decreased after every immobilization step in both samples. Especially the amount of bound protein differs whereas for the cell free extract around 10 mg mL^{-1} are immobilized compared to a maximum of 0.37 mg mL^{-1} using purified $P450_{BS\beta\_Z}$. Therefore several unspecific proteins were co-immobilized for the approach with cell free extracts. This could have an impact on the catalyst $P450_{BS\beta\_Z}$ as well as on the mass transfer in the particle and on the product formation (by-products).

Table 30 Immobilization efficiency using purified $P450_{BS\beta\_Z}$ in comparison to cell extracts containing $P450_{BS\beta\_Z}$. Immobilization was carried out in four consecutive steps (t1-t4). Protein concentration [mg mL^{-1}] was determined spectrophotometrically (280 nm) and active P450 concentration [µM] was determined with CO-titration from the supernatant after each immobilization step. Immobilization efficiency corresponds to $(c_0\text{-}c)/c_0$ x 100. Total immobilized catalyst concentration was 3.9 µM for the purified $P450_{BS\beta\_Z}$ approach and 5.5 µM for the cell extract approach. n.d. = not determined

purified	t_0	t_1	t_2	t_3	t_4
$P450_{BS\beta\_Z}$ [mg mL^{-1}]	0.4	0.1	0.2	0.3	0.2
$P450_{BS\beta\_Z}$[µM]	1.6	0.3	0.7	0.7	0.8
Efficiency [%]	-	79	58	57	51
E_{bound} [µM]	-	1.3	0.9	0.9	0.8
cell extract	t_0	t_1	t_2	t_3	t_4
$P450_{BS\beta\_Z}$ [mg mL^{-1}]	131	120	118	n.d.	n.d.
$P450_{BS\beta\_Z}$ [µM]	2	0.2	1.1	0.6	0.7
Efficiency [%]	-	93	48	71	64
E_{bound} [µM]	-	1.9	1	1.4	1.3

Immobilization efficiencies of purified $P450_{BS\beta\_Z}$ and the cell extract containing the respective P450 are depicted in Figure 47. Surprisingly immobilization was slightly more successful for the direct approach from the cell free extract with a total of 5.5 µM of bound enzyme compared to 3.9 µM of the purified catalyst approach. Obtained results are in contrast to already published data. Immobilization directly from the cell free extract containing the catalyst is thought to be less efficient as several of the available binding sites of the carrier could be occupied by the other proteins present in cell extracts (Figure 4) [55]. Although Bolivar and Nidetzky (2012) reported nearly complete selectivity (no binding of unspecific proteins) for the immobilization from a cell free extract containing an enzyme tagged with Z_{basic2} [74]. Obtained results indicate, that the effect of the other proteins present in the cell free extract on the immobilization efficiency could be neglected.

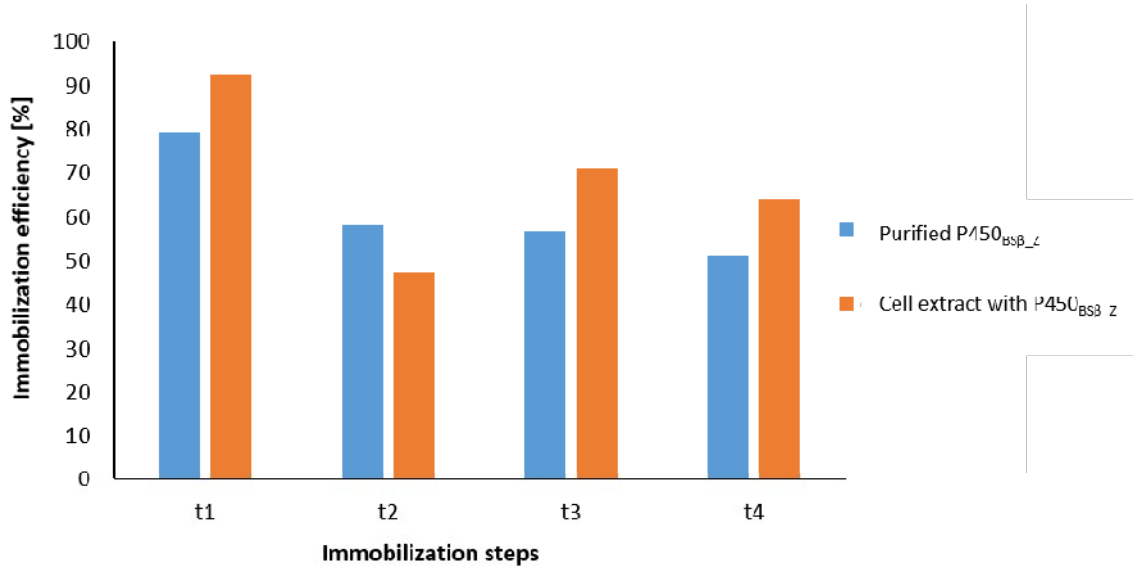

Figure 47 Immobilization efficiency of purified $P450_{BS\beta\_Z}$ in comparison to cell free extract containing $P450_{BS\beta\_Z}$. Active protein concentration was determined with CO-titration from the supernatant. From purified $P450_{BS\beta\_Z}$ was 1.7 µM were applied. For cell free extract 2 µM $P450_{BS\beta\_Z}$ were used for immobilization.

Subsequently, the presence of catalases on the carrier after the immobilization of the purified $P450_{BS\beta\_Z}$ was investigated. Highly concentrated peroxide was added to the carrier and only minor bubble formation appeared indicating little catalase activity. Reactions with the immobilized and purified $P450_{BS\beta\_Z}$ were carried out. Dodecanoic acid was used as model substrate together with H_2O_2 as oxidant. No substrate conversion could be detected during GC-MS analysis, although co-immobilized catalases were reduced by the additional chromatography step. Next, the activity of the free and purified $P450_{BS\beta\_Z}$ was investigated. Applied reaction set up contained 0.4 mM C10:0, 0.5 µM $P450_{BS\beta\_Z}$ and 0.4 mM H_2O_2. Obtained results revealed full substrate conversion and formation of the corresponding hydroxy fatty acids (Figure 48). This excludes the Z_{basic2}-tag as possible reason for the inactivity of the immobilized $P450_{BS\beta\_Z}$.

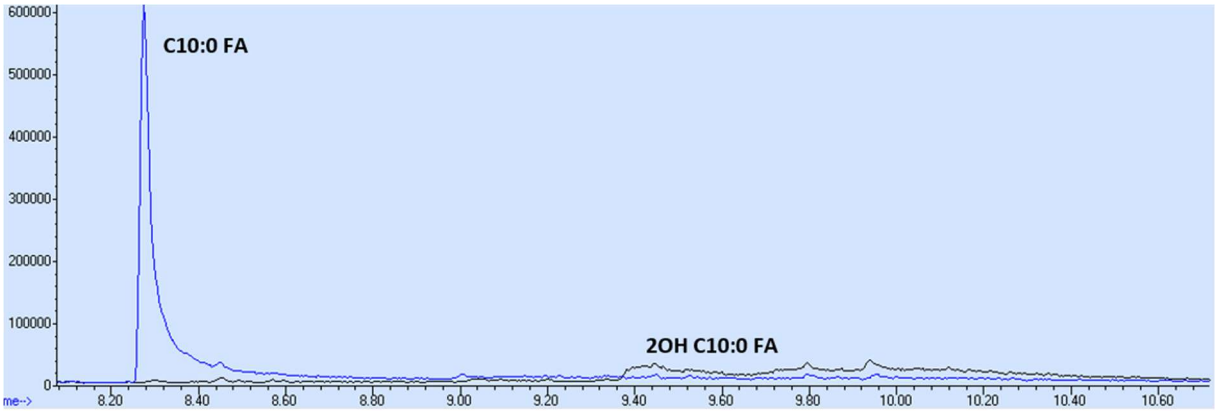

Figure 48 GC-MS trace from the conversion of C10:0 with free and purified $P450_{BS\beta\_Z}$. Blue is the no catalyst control and black corresponds to the enzymatic reaction.

Another possible explanation why the immobilization of $P450_{BS\beta\_Z}$ results in an inactive heterogeneous catalyst could be found in the protein structure. Compared to the successful immobilized $P450_{BM3}$, which is a homodimer (125 kDa), the monomeric $P450_{BS\beta}$ is rather light with 55 kDa [86, 116]. Furthermore, the position of the Z_{basic2}-tag (N-terminal for $P450_{BS\beta\_Z}$ and $P450_{BM3\_Z}$) could also affect the immobilization process. Although no influence of the Z_{basic2}-tag on enzyme immobilization has been reported before [73]. Still, a switch of the protein tag from the N- to the C-terminus could lead to an active heterogeneous catalyst for monomeric P450s.

3.5.2. Immobilization of P450s via affinity binding

Affinity binding between the metal activated carrier material and the His-tagged P450s leads to the formation of a metal chelate complex. This is the standard method for active enzyme purification. In contrast to the ion exchange chromatography ($P450_{BS\beta\_Z}$), no problems with catalase can occur [21]. Applied carrier materials from EnginZyme are based on controlled porosity glass. Carriers are activated with Fe^{3+} and show different properties concerning hydrophobicity. Immobilization was done as one-step approach due to rapid and efficient formation of the metal-chelate complex. Table 31 shows the immobilization of $P450_{BS\beta}$ on three different carriers (hydrophilic, hydrophobic, semi-hydrophobic). Highest immobilization efficiency was reached for the hydrophobic carrier with 92%, followed by the semi-hydrophilic with 32% and the hydrophilic with 27%. Colorization of the carrier caused by the immobilization of the red P450s is depicted in Figure 49. The shown control (C) is carrier EziG™ Fe1 in ddH_2O.

Table 31 Immobilization efficiencies determined from immobilization of purified $P450_{BS\beta}$ on three different EziG™ carriers in a one-step approach. EziG™ Fe1 is hydrophilic, EziG™ Fe2 is hydrophobic and EziG™ Fe3 is semi-hydrophilic. For the immobilization 5.3 µM $P450_{BS\beta}$ were used.

	EziG™ Fe1	EziG™ Fe2	EziG™ Fe3
$P450_{BS\beta}$ [µM]	3.9	0.4	3.6
E_{bound} [µM]	1.4	4.9	1.7
Efficiency [%]	27	92	32

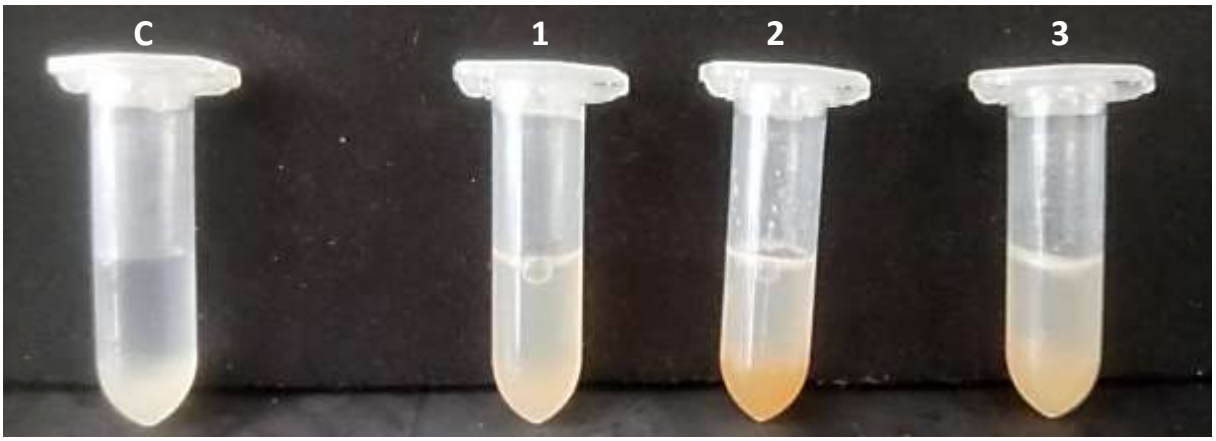

Figure 49 Colorization of EziG™ Fe1, Fe2 and Fe3 during the immobilization of $P450_{BS\beta}$. On the left a control (C) of the carrier EziG™ Fe1 in ddH_2O. 1 = EziG™ Fe1 is hydrophilic. 2 = EziG™ Fe2 is hydrophobic. 3 = EziG™ Fe3 is semi-hydrophilic.

Subsequent fatty acid conversion with the immobilized $P450_{BS\beta}$ on EziG™ and peroxide as oxidant was not successful. Obtained results showed that neither immobilization of $P450_{BS\beta}$ via ionic binding nor via affinity binding led to an active heterogeneous catalyst. As the His-tagged $P450_{CLA}$ and $P450_{J\alpha}$ were available, they were also used for immobilization. Furthermore, the influence of the position of the His-tag (N-terminal $P450_{CLA}$/C-terminal $P450_{J\alpha}$) on the immobilization could be investigated.

$P450_{CLA}$ and $P450_{J\alpha}$ were immobilized on EziG™ Fe2 (hydrophobic) and EziG™ Fe3 (semi-hydrophilic) each. This time highly concentrated enzyme solutions (20 µM) were applied and the production of the heterogeneous catalyst was carried out in one step.

Table 32 depictures the immobilization efficiencies where especially the amount of bound enzyme between 7.5 $mg/g_{carrier}$ and 8.9 $mg/g_{carrier}$ is impressive for one loading. This also indicates that Immobilization of the P450s worked extremely well on both carriers (hydrophobic, semi-hydrophilic).

	P450CLA		P450Jα	
Carrier	EziGTM Fe2	EziGTM Fe3	EziGTM Fe2	EziGTM Fe3
Catalyst [µM]	2	4.4	1.6	1.8
Efficiency [%]	90	78	92	91
Ebound [µM]	18	15.7	18.4	18.2

Due to the high concentration of bound P450s, the carriers turned red during the immobilization (Figure 50).

Table 32 Result of the immobilization of $P450_{Cla}$ and $P450_{J\alpha}$ on EziG™ Fe2 and Fe3. For the immobilization of both CYP152 20 µM were used. EziG™ Fe 2 is hydrophobic and EziG™ Fe3 is semi-hydrophilic. Active enzyme concentrations were determined from the supernatant after immobilization with CO-titration.

	$P450_{CLA}$		$P450_{J\alpha}$	
Carrier	EziG™ Fe2	EziG™ Fe3	EziG™ Fe2	EziG™ Fe3
Catalyst [µM]	2	4.4	1.6	1.8
Efficiency [%]	90	78	92	91
E_{bound} [µM]	18	15.7	18.4	18.2

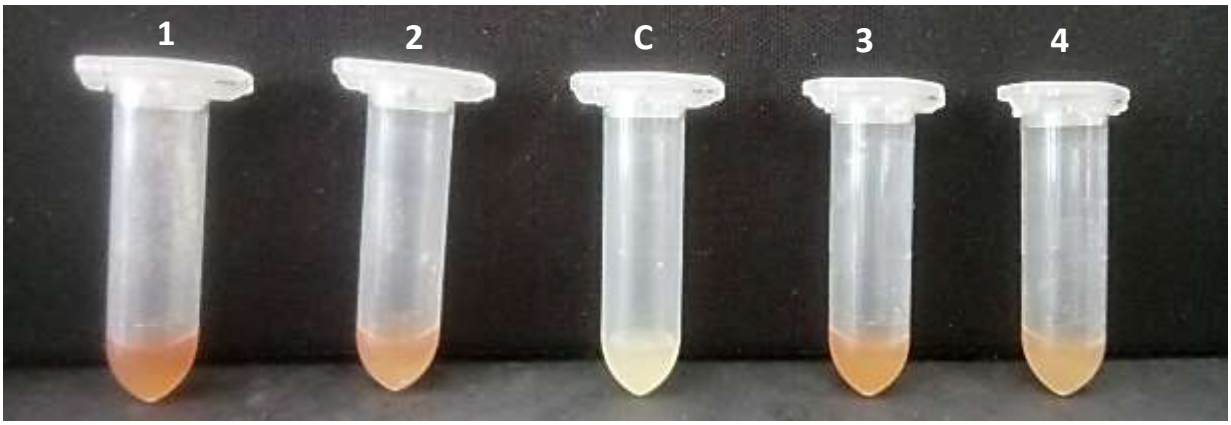

Figure 50 Colorization of EziG™ Fe1, Fe2 and Fe3 during immobilization of $P450_{CLA}$ and $P450_{J\alpha}$. 1 = $P450_{Cla}$ on EziG™ Fe2. 2 = $P450_{Cla}$ on EziG™ Fe3. 3 = $P450_{J\alpha}$ on EziG™ Fe2. 4 = $P450_{J\alpha}$ on EziG™ Fe3**.** 20 µM of active P450 were loaded in one step. C = negative control corresponds to EziG™ Fe3 in ddH_2O.

Although the amount of bound enzyme is high, no substrate depletion or product formation could be determined for conversions of C12:0 with the immobilized $P450_{CLA}$ and $P450_{J\alpha}$. The next step was the immobilization of $P450_{BM3}$ on all three EziG™ carriers. $P450_{BM3}$ proofed to be active as heterogeneous catalyst if immobilized on ReliSorb™ SP400. Therefore it was the perfect candidate to prove whether the EnginZyme carriers are suitable for immobilization of P450s in general and further application in fatty acid conversion.

The freeze-dried cell extract containing the His-tagged $P450_{BM3}$ was applied for the production of the heterogeneous catalyst using EziG™ materials as carrier. According to the supplier (EnginZyme) no purification is required beforehand because the EziG™ carriers could link the immobilization and the purification step. Immobilization of $P450_{BM3}$ via affinity binding was again a one-step approach where more than 90% of the offered enzyme was bound to all three of the applied EziG™ carriers (Table 32).

In total around 4.5 µM of $P450_{BM3}$ were immobilized on 100 mg carrier. For immobilization via ionic binding four steps were required to bind an equal concentration of $P450_{BM3}$.

	EziG™ Fe1	EziG™ Fe2	EziG™ Fe3
$P450_{BM3}$ [µM]	0.43	0.23	0.2
Efficiency [%]	91	95	96
E_{bound} [µM]	4.46	4.66	4.69

Table 33 Immobilization efficiency of $P450_{BM3}$ from cell extract on EziG™. For the immobilization 4.9 µM of $P450_{BM3}$ were used in one step. EziG™ Fe1 is hydrophilic, EziG™ Fe2 is hydrophobic and EziG™ Fe3 is semi-hydrophilic.

Conversion of dodecanoic acid with the immobilized $P450_{BM3}$ was done using NADPH as electron source. GC-MS analysis revealed substrate depletion as well as the formation of the ω-1, ω-2 and ω-3 hydroxydodecanoic acids (Figure 51). Highest conversion was reached with $P450_{BM3}$ immobilized on the hydrophobic carrier EziG™ Fe2 with 62%, followed by semi-hydrophilic EziG™ Fe3 with 56% and hydrophilic EziG™ with 23% (Table 34). In comparison, Thompson et al (2019) reported a conversion of 59% for decanoic acid with $P450_{BM3}$ immobilized on a semi-hydrophilic carrier from EnginZyme [117]. Obtained results indicated that the mass transfer of the substrate into the particle is not the general problem. Additionally, the EnginZyme carrier proved to be suitable for immobilization of P450s. Still the immobilization of the monomeric P450s ($P450_{BS\beta}$, $P450_{CLA}$ and $P450_{J\alpha}$) leads to inactivation of the catalyst. Reasons therefore cover a broad range from structural differences to particle architecture. The commercially available EziG™ carriers seemed to be perfect candidates for immobilization of CYP152s as the immobilization via affinity worked extremely fast (within minutes) and for high catalyst concentrations (up to 20 µM). Removal of the catalyst from the carrier using an excess of imidazole was not possible. The porous particle architecture of the EnginZyme carriers should provide a very efficient immobilization and enhance mass transfer. However, highly porous materials also increase the possibility of clogging. For instance, the immobilization of too much catalyst could lead to inaccessibility of substrate transport routes and active sites of P450s.

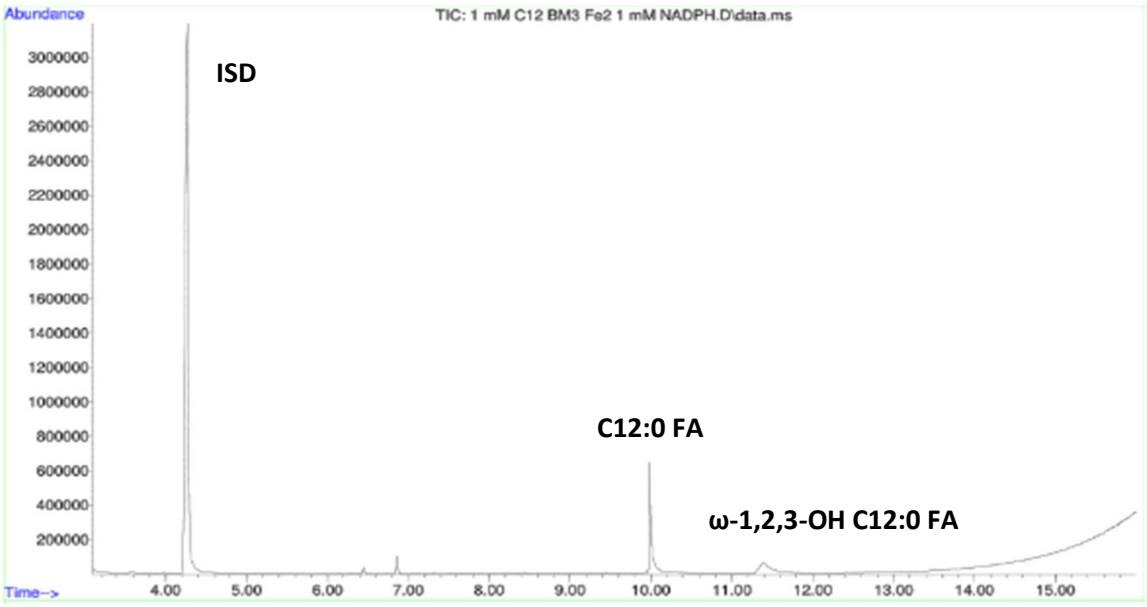

Figure 51 GC-MS trace of conversion of C12:0 (1 mM) with immobilized $P450_{BM3}$ (1.4 µM) on EziG™ Fe2 and NADPH (1 mM). Produced ω-hyroxyfatty acids were identified by mass fragmentation analysis and in comparison to analytical data from conversions with free $P450_{BM3}$. ISD = internal standard 0.1% (v/v) 1-octanol.

Table 34 Conversions of C12:0 with immobilized $P450_{BM3}$ on EziG™ carriers. Reaction set-up contained 1 mM C12:0, 1.4 µM immobilized $P450_{BM3\_Z}$ and 1 mM NADPH.

$P450_{BM3}$	Conversion [%]
no cat	0
EziG™ Fe1	23
EziG™ Fe2	62
EziG™ Fe3	56

Concluded, the heterogeneous catalyst from $P450_{BM3}$ is active if immobilized via ionic and affinity binding. Although, the approach with the ionic binding has a major drawback namely the extremely low expression yield caused by the Z_{basic2}-tag (200 fold less). Suitable carries for the production of the heterogeneous catalyst $P450_{BM3}$ are ReliSorb™ SP400 and EnginZyme (EziG™ Fe1, Fe2, Fe3). Additionally, also the immobilization of monomeric peroxygenases of the CYP152 family ($P450_{BSβ}$, $P450_{CLA}$, $P450_{Jα}$) on said carrier materials worked out very efficient especially for the affinity binding approach. Still no activity could be determined for the immobilized CYP152 members during the conversion of dodecanoic acid. The main difference in substrate conversion comparing $P450_{BM3}$ and the monomeric P450s are the oxidants O_2 and H_2O_2, respectively. Therefore, the inactivity of the immobilized monomeric P450s could be caused by the decomposition of peroxide by the Fe^{3+}- complex (TTN = 35 for hemin) of the EnginZyme carriers [118]. This is why a screening of different materials activated with either Ni^{2+} or Cu^{2+} was done subsequently.

3.5.3. Activated particle screening for an active heterogeneous catalyst

Immobilization of monomeric CYP152s via affinity binding on ready-made EziG™ carriers (activated with Fe^{3+}) led to inactive heterogeneous catalysts. As high protein concentrations could be immobilized, the inaccessibility of substrate transfer routes and the active sites of the CYP152s for fatty acids could be a general problem. Another point to consider is the chelated metal ion Fe^{3+}, which could degrade the peroxide require for successful fatty acid conversion [118]. This is why a screening of different materials activated either with Ni^{2+} or Cu^{2+} was carried out to produce an active heterogeneous catalyst from CYP152s. Selection of materials included ReliZyme™ (methacrylic polymer matrix) from Residion S.r.l., agarose and controlled porosity glass. Those carriers were freshly activated with the corresponding metal ions [82]. Catalysts of choice were $P450_{BM3}$ as it showed activity on all carriers as well as the monomeric $P450_{Jα}$. $P450_{BM3}$ was immobilized directly from cell free extracts whereas for $P450_{Ja}$ purified catalyst was used. Initial concentrations of the enzymatic solutions for immobilization were 4.3 µM for $P450_{BM3}$ and 15.9 µM for $P450_{Jα}$ which were incubated with 100 mg carrier. Overall immobilization was more efficient for $P450_{BM3}$ reaching up to 95% with Ni^{2+} activated ReliZyme™. The same carrier and metal combination also turned out to be most suitable for the immobilization of $P450_{Jα}$ with 89%. Table 35 summarizes the immobilization of $P450_{BM3}$ and $P450_{Jα}$ on different carrier materials.

Table 35 Screening of differently activated particles for immobilization efficiency of $P450_{BM3}$ and $P450_{Jα}$. Immobilization was done from the cell free extract containing $P450_{BM3}$ or with the purified $P450_{Jα}$. Offered concentrations were 4.3 µM and 15.9 µM for $P450_{BM3}$ and $P450_{Jα}$, respectively.

$P450_{BM3}$	Cation	Efficiency [%]	E_{bound} [µM]	$P450_{BM3}$ [µM/$g_{carrier}$]
ReliZyme™	Ni^{2+}	95	4.1	41
Agarose	Ni^{2+}	76	3.3	33
Agarose	Cu^{2+}	61	2.6	26
CPG	Ni^{2+}	78	3.4	34
CPG	Cu^{2+}	78	3.4	34
$P450_{Jα}$	Cation	Efficiency [%]	E_{bound} [µM]	$P450_{Jα}$ [µM/$g_{carrier}$]
ReliZyme™	Ni^{2+}	89	14.2	142
Agarose	Ni^{2+}	26	4.1	41
Agarose	Cu^{2+}	21	3.3	33
CPG	Ni^{2+}	16	2.6	26
CPG	Cu^{2+}	8	1.3	13

ReliZyme™ from Residion S.r.l. is based on a methacrylic polymer matrix.
CPG corresponds to controlled porosity glass.

Besides ReliZyme™ also agarose and CPG were investigated as carriers. Concerning $P450_{BM3}$ acceptable immobilization yields of 61 to 78% could be reached for both carrier materials. In contrast only <30% of immobilization efficiency were determined for $P450_{Jα}$ using the same carriers. Noteworthy, the carriers were freshly activated before immobilization in contrast to the already activated commercial

carriers EziG™. Concluded, ReliZyme™ turned out to be the best material for the immobilization of P450s. Concerning the metals, no significant difference could be detected between Ni^{2+} and Cu^{2+}. Although immobilization efficiency was always slightly decreased for carriers activated with Cu^{2+} (Figure 52). Subsequently, substrate conversion was carried out with all the heterogeneous catalysts produced from the different materials.

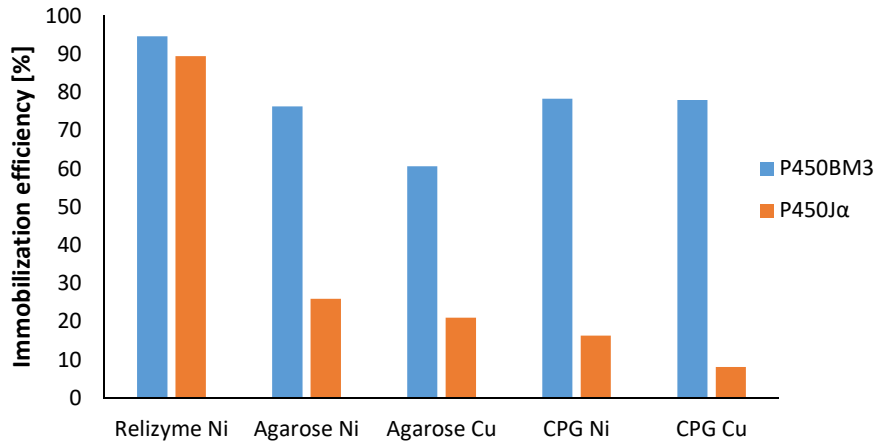

Figure 52 Immobilization efficiency of $P450_{Jα}$ and $P450_{BM3}$ on different materials. $P450_{BM3}$ was immobilized from cell free extract and for $P450_{Jα}$ the purified enzyme was immobilized.

GC-MS analysis of the reactions with immobilized $P450_{BM3}$ and $P450_{Ja}$ revealed formation of the corresponding hydroxy fatty acid for all carriers except for agarose Ni^{2+} and Cu^{2+}. Highest conversion for both enzymes were obtained for ReliZyme™ bound protein reaching 22% and 38% for $P450_{BM3}$ and $P450_{Jα}$, respectively (Table 36). The agarose carrier activated with Cu^{2+} turned out to be the least suitable carrier as nearly no conversion could be detected for both P450s. Finally the immobilization of the monomeric His-tagged $P450_{Jα}$ led to an active heterogeneous catalyst. Although conversion of C12:0 is lower in comparison to the free enzyme (80%). This can serve as good starting point to further investigate the system. Reasons therefore could be limitations in mass transfer of the substrate into the particle, blockage of available binding sites and well as decrease in activity caused by conformational changes due to the immobilization process. Additional further optimization of the carrier material and the reaction conditions should be considered.

Table 36 Conversion rates of $P450_{J\alpha}$ and $P450_{BM3}$ immobilized on different materials. Purified $P450_{J\alpha}$ was immobilized and $P450_{BM3}$ from cell free extract. Samples were analyzed with GC-MS.

Conversion [%]	$P450_{BM3}$	$P450_{J\alpha}$
Relizyme™ Ni	21.5	38
Agarose Ni	13	4
Agarose Cu	0.6	0
CPG Ni	15	0.6
CPG Cu	16	5

Reaction set-up for $P450_{BM3}$ contained 2 mM C12:0, 0.8 µM to 1.2 µM immobilized catalyst and 2 mM NADPH.
Reaction set-up for $P450_{J\alpha}$ contained 2 mM C12:0, 0.4 µM to 4.3 µM immobilized catalyst and 2 mM H_2O_2.

Concluded, the first functional heterogeneous CYP152 catalyst was successfully constructed. Additionally, also the immobilization of $P450_{BM3}$ via affinity binding resulted in an active catalyst. A major difference for the immobilization via Z_{basic2}/His-tag is the required time to bind proteins. The His-tag approach was carried out in one-step approach in contrast to four consecutive loadings for the immobilization with the Z_{basic2} tagged enzyme. Removal of the P450s (immobilized via affinity) using EnginZyme carriers was not possible indicating problems in accessing the bound protein in the nanoporous cavities, which is also supported by the loss in activity. Further protein yields of the Z_{basic2} tagged $P450_{BS\beta}$ were more than 200 fold lower in respect to the His-tagged version of the enzyme.

3.5.4. In-particle measurement with $P450_{BM3\_Z}$ immobilized on sepharose

A major limitation in the determination of the immobilization efficiencies are the analytics. The amount of bound catalyst is typically based on the decrease of active enzyme concentration in the supernatant. As the immobilization process often lasts for 1 h or longer under rotation and at room temperature it is very likely, that the active enzyme concentration is also decreased by denaturation of the enzyme and not only by immobilization . Therefore the implementation of in-particle measurements could play a key role as the immobilized and active protein concentration could be determined directly. The fastest way to determine the active enzyme concentration of P450s is via CO-titration. Using sepharose activated with ? is suitable for the in-particle measurement due to its transparent nature. Immobilization of $P450_{BM3\_Z}$ on sepharose was carried out directly from cell free extracts. An immobilization efficiency of 94% was reached after the first binding step (Table 37). This value was determined indirectly by measurement of the remaining supernatant. In total 0.03 µM/$mg_{carrier}$ of $P450_{BM3\_Z}$ were immobilized.

Table 37 Immobilization efficiency of $P450_{BM3\_Z}$ on sepharose. CO-titration was used to determine active enzyme concentration remaining in the supernatant after each step of the immobilization (t_1-t_4). Total enzyme bound to the carrier was 3.2 µM.

	t_0	t_1	t_2	t_3	t_4
$P450_{BM3\_Z}$ [mg mL^{-1}]	33	24.4	29	23	23.3
$P450_{BM3\_Z}$ [µM]	1	0.1	0.2	0.2	0.3
Efficiency [%]	-	94	85	75	71
E_{bound} [µM]	-	0.9	0.8	0.7	0.7

Subsequently, the in-particle measurement was carried out by adding <1 mg of carrier (0.03 µM $P450_{BM3\_Z}$) to the immobilization buffer in a microtiter plate. The sample was reduced and a spectral scan from course 400 to 600 nm was recorded. Samples were subsequently gassed with CO (1 min) and again measured over a wavelength course of 400 to 600 nm. The resulting absorbance spectra and difference curve from the CO-titration is shown in Figure 53. The typical peak at 450 nm indicates the presence of active $P450_{BM3\_Z}$. Calculations revealed an active protein concentration of 0.3 µM/$mg_{carrier}$ in contrast to the 0.03 µM/$mg_{carrier}$, which were determined from supernatants during the immobilization process. Concerning the calculations, the path length was decreased to 0.3 to 0.5 cm for the measurement in microtiter plates. The obtained 0.3 µM/$mg_{carrier}$ from the in-particle measurement would correspond to 30 µM bound catalyst during the immobilization on 100 mg carrier. This is not possible as in total only 4 µM of $P450_{BM3\_Z}$ were offered. Further required steps are the preparation of a calibration curve and the determination of the extinction coefficient for the carrier material with the bound $P450_{BM3\_Z}$. Concluded, in particle-measurements and also quantification for P450s might become feasible, although further investigations are required for implementation.

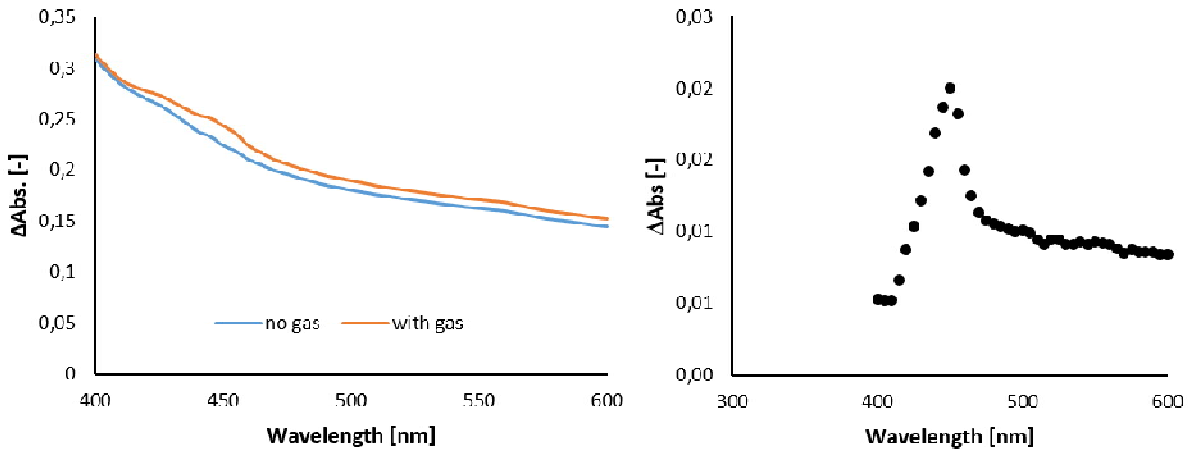

Figure 53 CO-titration of immobilized $P450_{BM3\_Z}$ on sepharose as in-particle measurement. Determined active protein concentration was 0.2 µM (CO-titration).

4. Summary and Conclusions

The newly discovered $P450_{J\alpha}$ derived from *Jeotgaliccocus sp.* ATCC 8456 was characterized from a biochemical and catalytical point of view to investigate its potential for synthetic applications up to preparative scales. Due to structural resemblances, sequence identities of up to 50% and catalytic activity, $P450_{J\alpha}$ can be assigned as member of the CYP152 family. Characterized members from this family like $P450_{CLA}$ and $P450_{BS\beta}$ were used as benchmarking systems to evaluate the performance of $P450_{J\alpha}$. Protein expression of the new α-hydroxylase reached acceptable yields with more than 40 mg per liter culture. Additional, $P450_{J\alpha}$ displayed high stability during long time storage in liquid (4 °C), which could also be observed for $P450_{CLA}$. The biochemical characterization was completed by the determination of the dissociation constants of $P450_{J\alpha}$ for fatty acids, which are the natural substrates of CYP152s [23]. Obtained k_D-values of $P450_{J\alpha}$ for C10:0 and C12:0 reached up to 184 µM which is in a similar range as reported data from $P450_{BS\beta}$ and $P450_{CLA}$ [36]. The determined dissociation constants indicate and acceptable affinity of $P450_{J\alpha}$ for the medium chain fatty acids (C10:0, C12:0).

Subsequently, the catalytical characterization of $P450_{J\alpha}$ was carried out by determining the kinetic parameters as well as the regio- and stereoselectivity. Substrate scope ranged from C6:0 to C16:0. Dodecanoic acid turned out to be the most suitable substrate for $P450_{J\alpha}$ with turnover numbers of 387 min^{-1}. Based on the high regio-selectivity of $P450_{J\alpha}$ for the hydroxylation at the α-carbon atom (>95%) it was classified as α-hydroxylase. Only traces of β-hydroxyfatty acids could be detected (<5%). Shorter chain fatty acids (<C10:0) yielded further 1-alkenes indicating that $P450_{J\alpha}$ is also able to catalyze oxidative decarboxylation. Concerning the stereoselectivity, $P450_{J\alpha}$ reached an e.e. value of 95% for the *S*-enantiomer of the α-hydroxy decanoic acid. Interestingly, oleic acid proved to be an even better substrate for the α-hydroxylase $P450_{J\alpha}$ during an enhanced substrate screening. Turnover numbers reached 731 min^{-1}, which is nearly two fold higher compared to the best saturated fatty acid (C12:0). Furthermore, the biocatalytic α-hydroxylation of oleic acid has never been reported before. In comparison to the CYP152s, $P450_{J\alpha}$ displays all the desired features for implementation in preparative scales. $P450_{J\alpha}$ outplays the other CYP152s by combining acceptable turnover numbers with high regio- and stereoselectivites completed with high storage stabilities [35, 37–39].

To investigate the potential of $P450_{J\alpha}$ for applications in industrial scale, preparative scale conversions were carried out in volumes of 50 to 100 mL and under automated peroxide supply. A present problem to face was the catalyst stability as after a maximum of 5.5 h no further conversion could be detected (prep-scale C10:0, C12:0). This could be explained by the high peroxide concentrations (>5 mM) which could lead to catalyst destruction. Another obstacle to overcome is the substrate solubility whereas especially the solubility of medium and long chain fatty acids in aqueous solutions is limited (2 mM >C12:0). Especially the order of the fatty acid addition turned out to be important as for instance only

the addition of buffer C to the dissolved C18:1 leads to the desired emulsion. Otherwise the inaccessibility of the substrate due to precipitation could lead to decreased conversion. Product isolation from preparative scales yielded up to 79% in particular for 100 mL set-ups (C18:1). Subsequently carried out ^{1}H-NMRs confirmed the formation of the corresponding α-hydroxy products classifying $P450_{J\alpha}$ as α-hydroxylase.

The catalyst stability against peroxide is a major challenge that needs to be addressed for fatty acid conversion with peroxygenases from the CYP152 family. To increase the catalyst robustness, two approaches were considered. First a "smarter" peroxide supply was investigated including the application of an alternative oxidant and the coupling to a peroxide producing reaction. Using urea-peroxide as oxidant for slower H_2O_2 release did not have an effect on the substrate conversion with $P450_{J\alpha}$. In contrast, the coupling of fatty acid conversions with $P450_{J\alpha}$ to a peroxide releasing reaction (GOX) led to an increase in substrate conversion of 14% (full conversion) in comparison to direct peroxide supply. This is why the coupling of the fatty acid conversions with CYP152s to the peroxide releasing GOX is a promising alternative to direct peroxide supply.

The second approach for improving catalyst stability was the immobilization of selected P450s from CYP102 and CYP152 on solid carrier material. Next to enhanced robustness of the catalyst, the production of a heterogeneous catalyst also facilitates the application in continuous systems and allows the reusability of the enzyme [55–57]. A comparison between two immobilization strategies namely ionic (Z_{basic2}-tag) and affinity (His-tag) binding was carried out. One of the major differences was the time required for immobilization. For the affinity binding approach a one-step immobilization was carried out whereas the ionic binding approach required four consecutive loading steps. Furthermore, the expression of the Z_{basic2}-tagged enzymes was around 200 fold lower compared to the His-tagged version. Subsequently, a selection of carriers was investigated, where especially the commercially available materials like EziG™ and ReliSorb™ SP400 were not suitable for the immobilization of CYP152 family members. The production of a heterogeneous $P450_{J\alpha}$ catalyst was successful using ReliZyme™ and controlled porosity glass. Possible reasons therefore could be found in the different particle architecture and in the activation with Ni^{2+} and Cu^{2+}. EziG™ carriers are highly porous leading to enhanced blockage of substrate transfer into the active sites of the immobilized CYP152s. Furthermore, EziG™ carriers contain chelated Fe^{3+} which could degrade the peroxide required for fatty acid conversion [118]. Still obtained conversion of dodecanoic acid with $P450_{J\alpha}$ immobilized on ReliZyme™ activated with Ni^{2+} did not exceed 38%. The potential of $P450_{J\alpha}$ as heterogeneous catalyst is supported by the high substrate conversion of the free enzyme (86%). However, further optimization of the immobilization process is required to allow the application of $P450_{J\alpha}$ as heterogeneous catalyst in continuous industrial processes.

Concluded, $P450_{J\alpha}$ is a robust fatty acid hydroxylase combines (other than most CYP152s) many of the desired properties for synthetic applications. The enzyme can be produced in sufficient quantity, has high storage stability, is regio- and enantioselective and can be operated at TTN ≥1000. For example, $P450_{SP\alpha}$ very high initial turnover numbers with 3000 min^{-1}, but in contrast the protein expression yield is very low [16, 35]. $P450_{J\alpha}$ could not reach such but it provides acceptable in-operando stability in preparative scale reactions (up to 100 mL). Smarter or slower peroxide delivery system based on the coupling to H_2O_2 releasing reactions (GOX) might be a successful strategy in the further to boost TTN values further. Immobilizing the catalyst on solid carrier material can further solve challenges related to stability against organic solvents and heterogeneous substrates. Still further improvement especially concerning the robustness of the $P450_{J\alpha}$ should be considered for the implementation in continuous industrial processes.

5. Appendix

5.1. Biochemical Characterization

5.1.1. Active enzyme concentration $P450_{CLA}$, $P450_{BS\beta}$ and $P450_{BS\beta\_Z}$

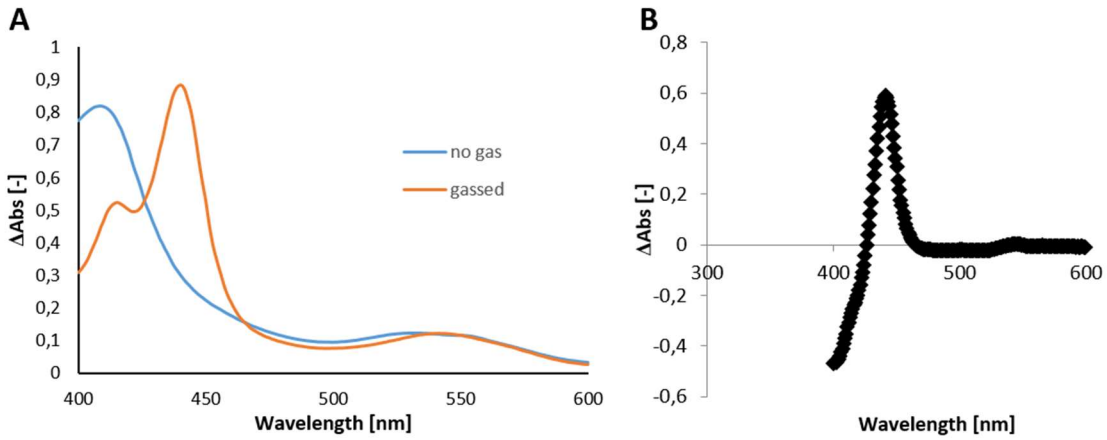

Figure 54 Absorbance spectra of $P450_{CLA}$ before and after CO gassing is depicted in A. In B the CO difference spectra from CO-titration with the purified $P450_{CLA}$ is shown in A. Determined active $P450_{CLA}$ concentration was 335 µM.

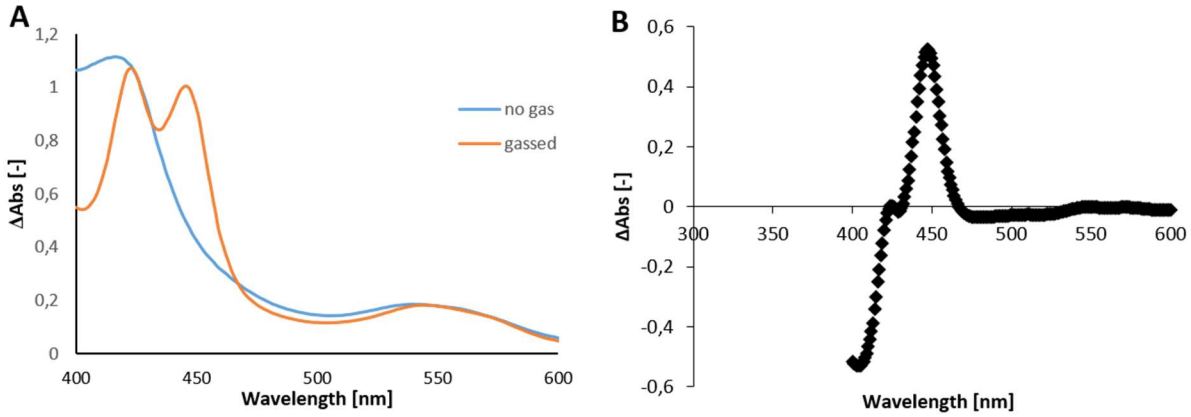

Figure 55 Absorbance spectra of $P450_{BS\beta}$ before and after CO gassing is shown in A. In B CO difference spectra from CO-titration with purified $P450_{BS\beta}$ is depicted. Determined active $P450_{BS\beta}$ concentration was 302 µM.

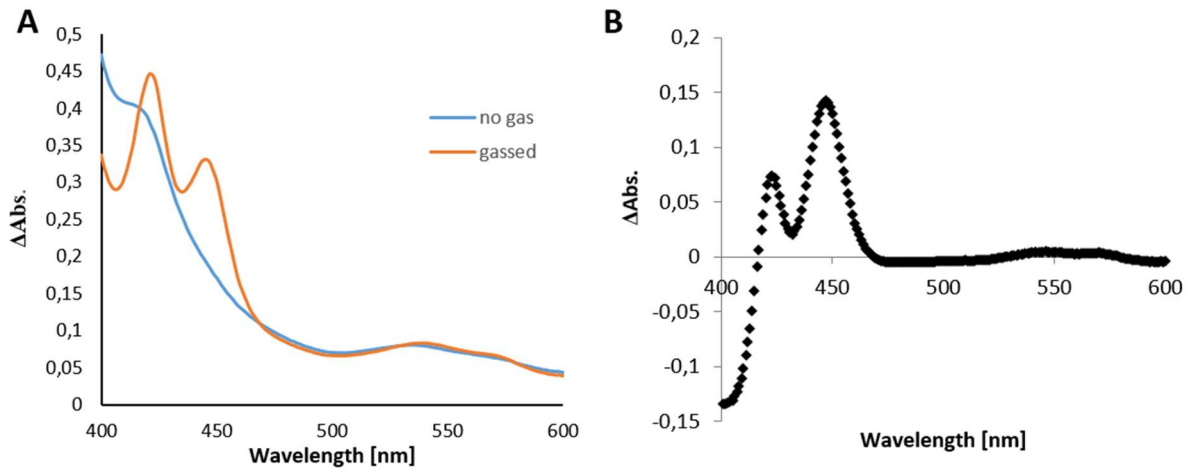

Figure 56 Absorbance spectra of $P450_{BS\beta\_z}$ before and after Co gassing is shown in A. In B the CO difference spectra from CO-titration with purified $P450_{BS\beta\_z}$ is depictured. Determined active $P450_{BS\beta\_z}$ concentration was 1.6 µM.

5.1.2. Homology model $P450_{CLA}$

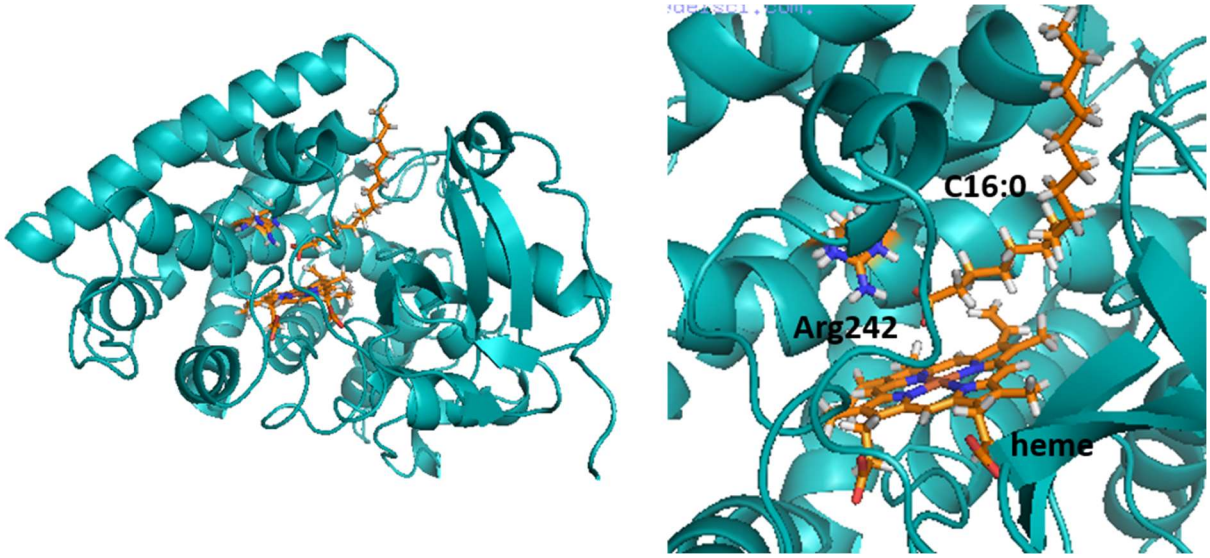

Figure 57 Homology model of P450CLA based on crystal structures of $P450_{SP\alpha}$ and $P450_{BS\beta}$ [38, 86]. Holoenzyme was generated with Swissmodel. Heme group and fatty acid (C16:0) were added with YASARA.

5.1.3. Storage stability of CYP152

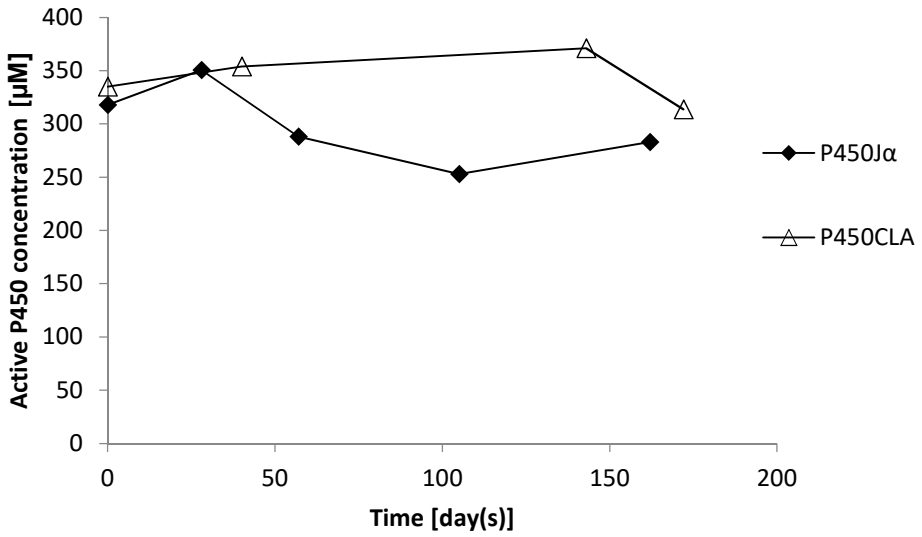

Figure 58 Storage stability of His-tag purified $P450_{J\alpha}$ and $P450_{CLA}$ in dialysis buffer (0.1 M KPi, 300 mM KCl, pH 7.5) and 4 °C (5 to 20 mL samples).

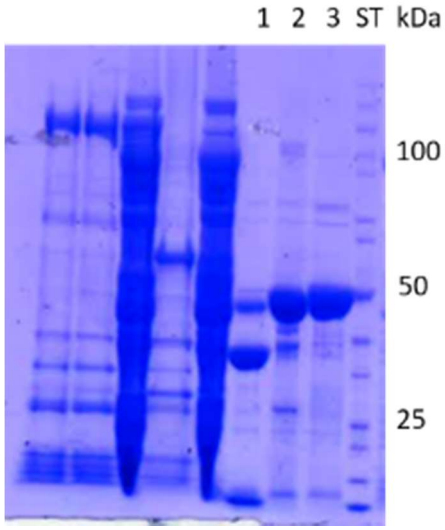

Figure 59 Size and purity determination of the expressed CYP152 family members $P450_{BS\beta}$ (1), $P450_{CLA}$ (2) and $P450_{J\alpha}$ (3). ST = unstained page ruler Thermo Fisher Scientific.

5.1.4. LigPlots from $P450_{BS\beta}$, $P450_{CLA}$, $P450_{SP\alpha}$ and OleT

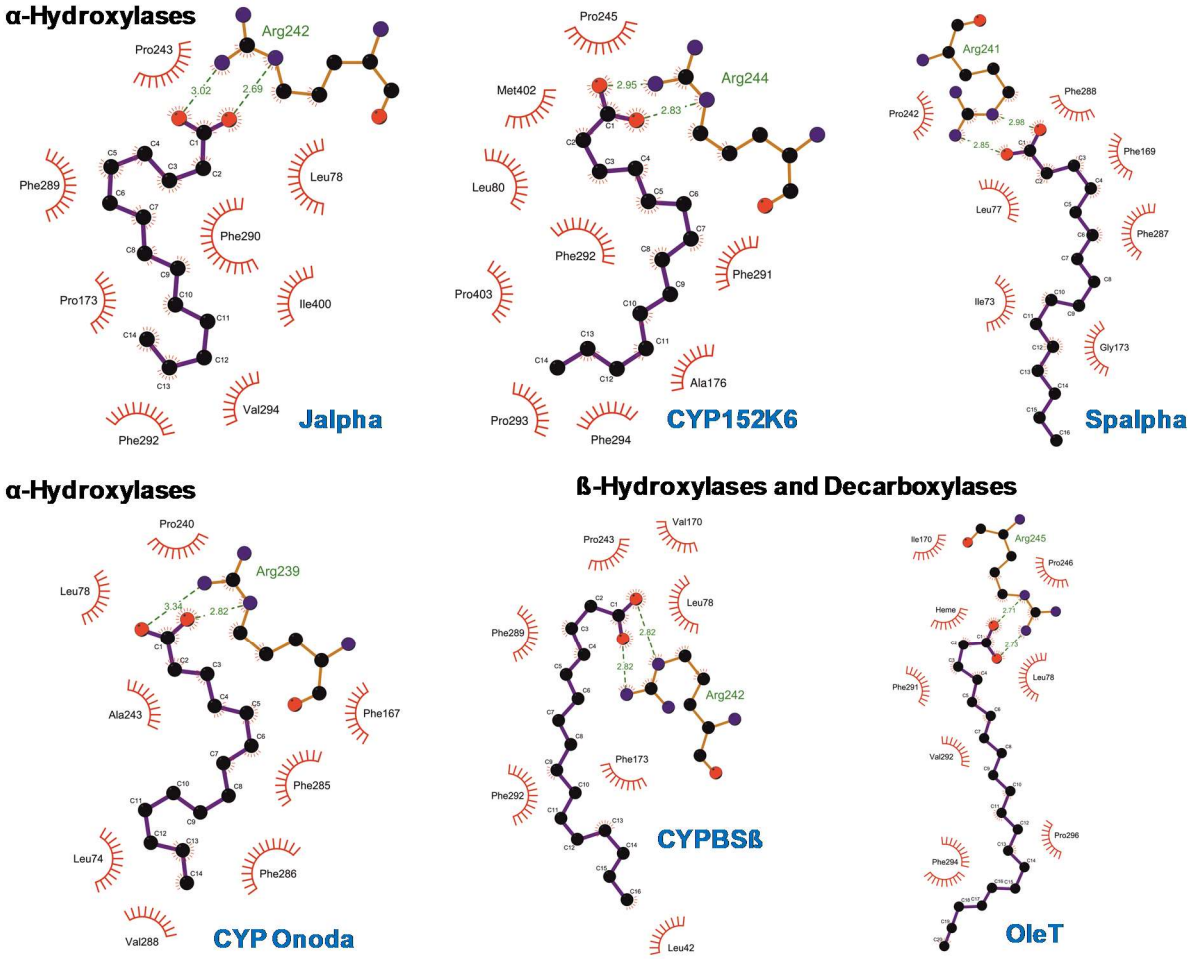

Figure 60 LigPlots of selected CYP152s with palmitic acid (C16:0) as ligand. LigPlots were generated with LigPlot [88] based on the protein models ($P450_{J\alpha}$, $P450_{CLA}$) or on the crystal structure ($P450_{BS\beta}$, OleT, $P450_{SP\alpha}$, $P450_{Ex\alpha}$) [38, 41, 86, 97].

5.1.5. Determination of the dissociation constant

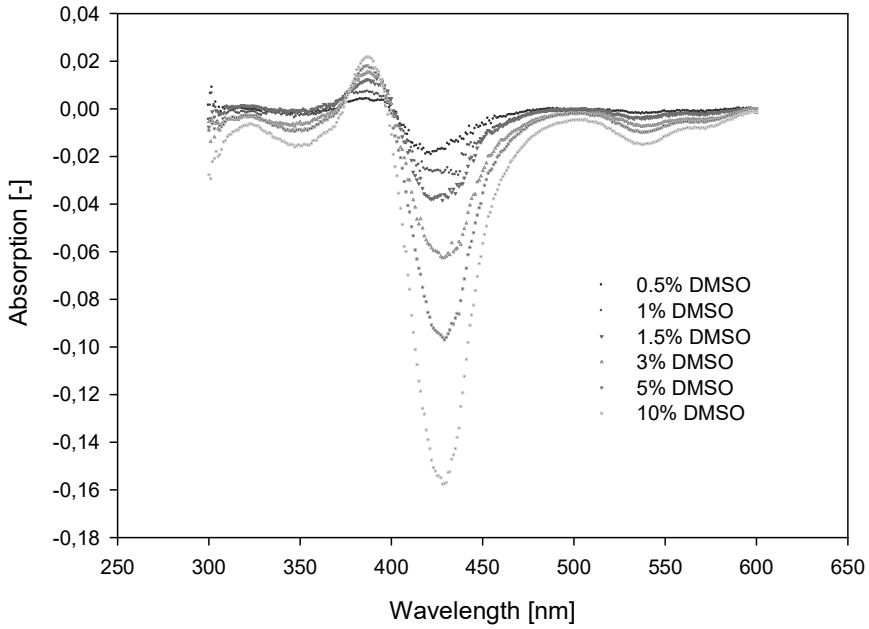

Figure 61 Investigation of the influence of DMSO on the shifts in spin states of P450$_{J\alpha}$. DMSO was titrated to a 1.5 µM enzyme solution in buffer C.

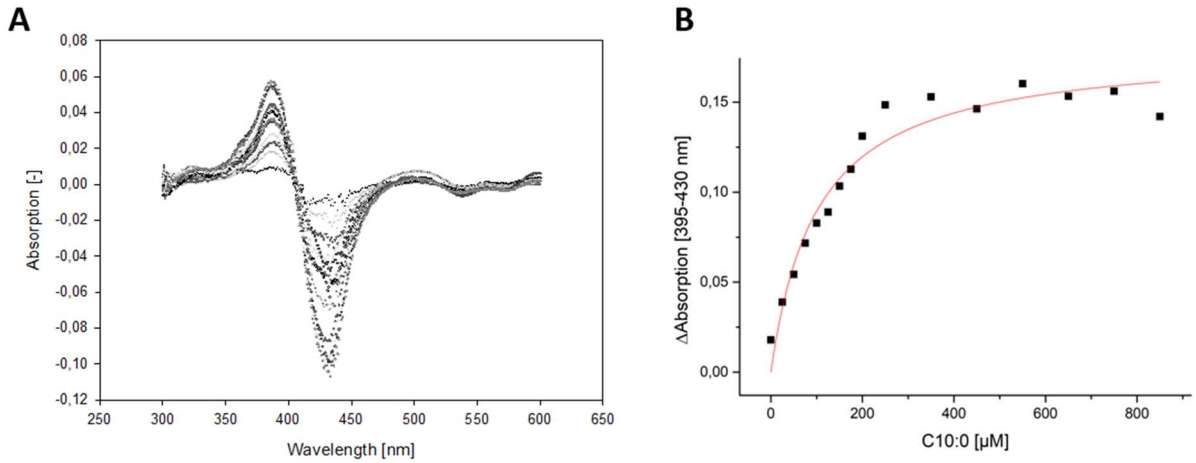

Figure 62 Ligand titration experiment for C10:0 and purified P450$_{J\alpha}$. A = Absorbance difference spectra recorded at varying ligand concentrations (0 to 2.6 mM). B = The absorbance changes at 420 and 395 nm were plotted against the corresponding FA concentration. Data fitting was done with Hill function (n = 4.01) using Origin 9.0 software.

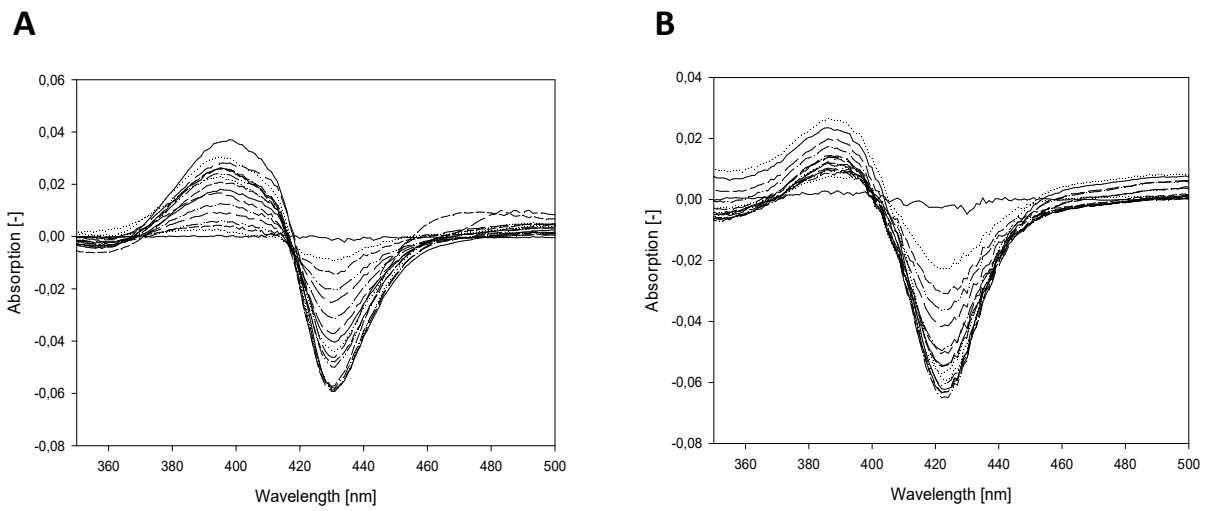

Figure 63 Ligand titration experiment for C12:0 and purified CYP152s. A = $P450_{CLA}$ (0 to 0.535 mM C12:0). B = $CYP_{BSß}$ (0 to 0.35 mM C12:0) [36]. In both cases saturation of the enzyme was achieved. Experiments were done to validate the applied method.

5.2. Analytical Data

5.2.1. Conversion of C6:0

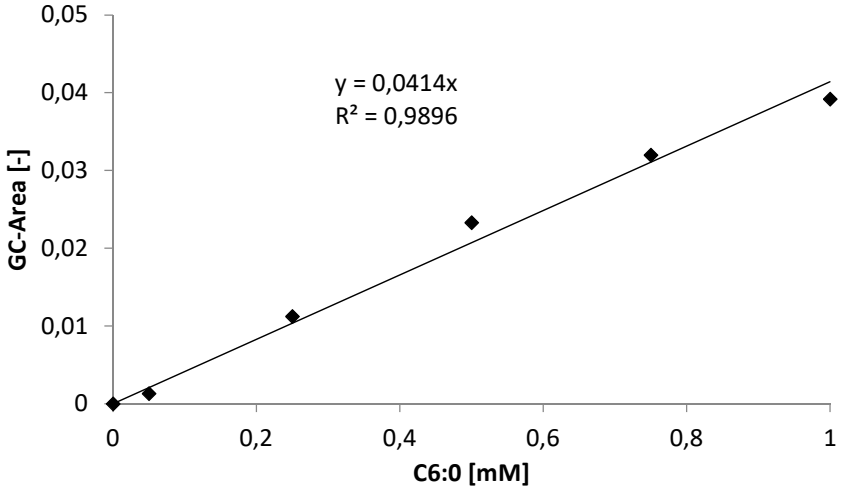

Figure 64 Calibration curve for quantification of C6:0 (hexanoic acid).

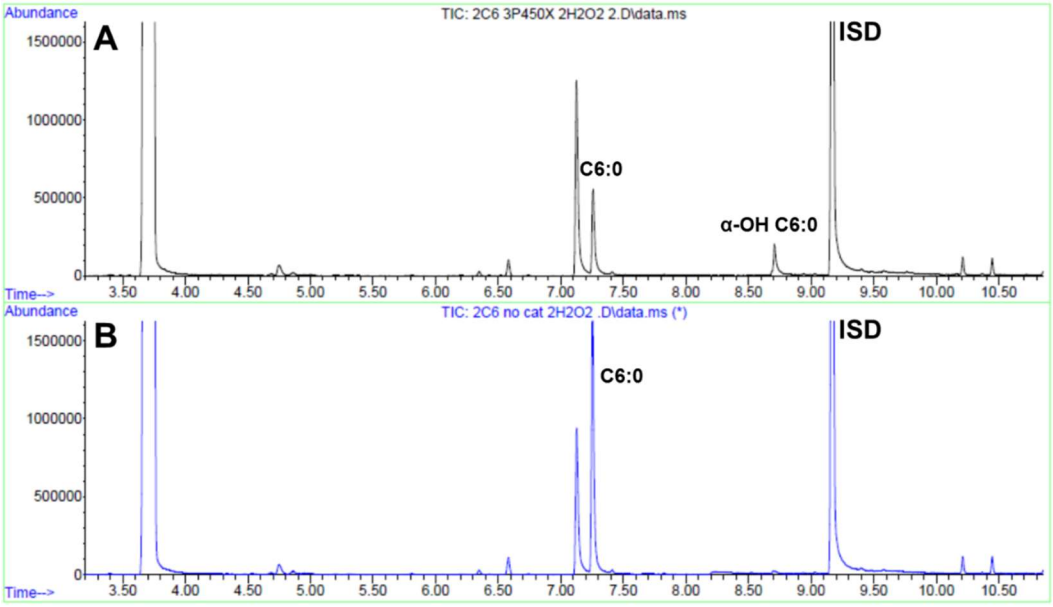

Figure 65 Conversion of C6:0 (2 mM) with P450$_{J\alpha}$. A = Conversion after 2 h and addition of 0.5 mM per 30 min H_2O_2 (in total 2 mM). B = Control reaction without catalyst. ISD = internal standard (1-octanol; 0.1% v/v).

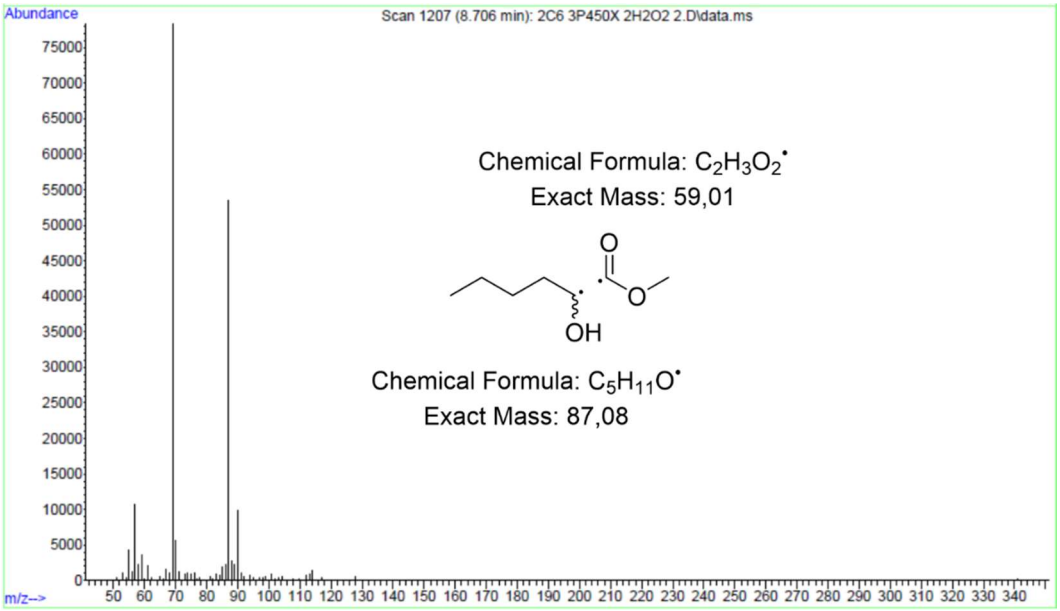

Figure 66 GC-MS spectrum of α-OH C6:0 (m/z = 146.09; methyl ester) produced from C6:0 by P450$_{J\alpha}$.

5.2.2. Conversion of C8:0

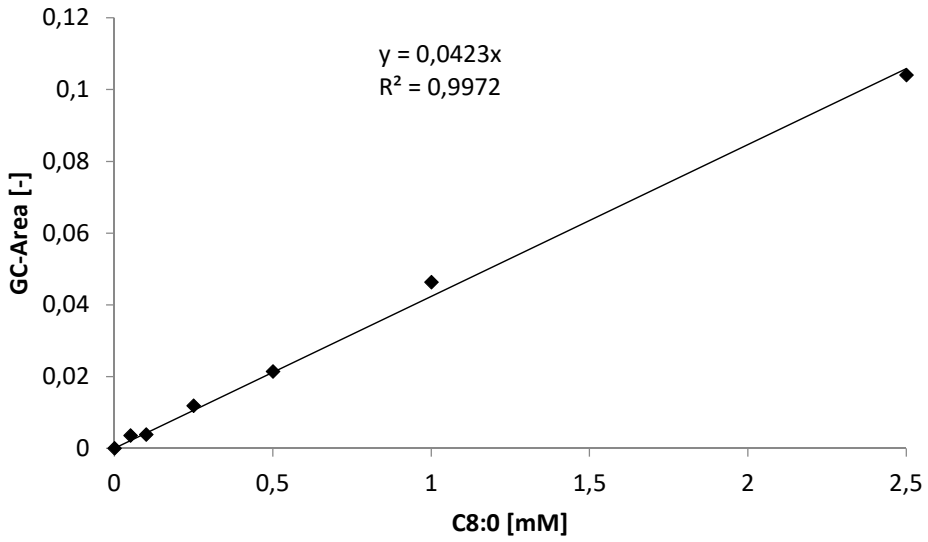

Figure 67 Calibration curve for quantification of C8:0 (octanoic acid).

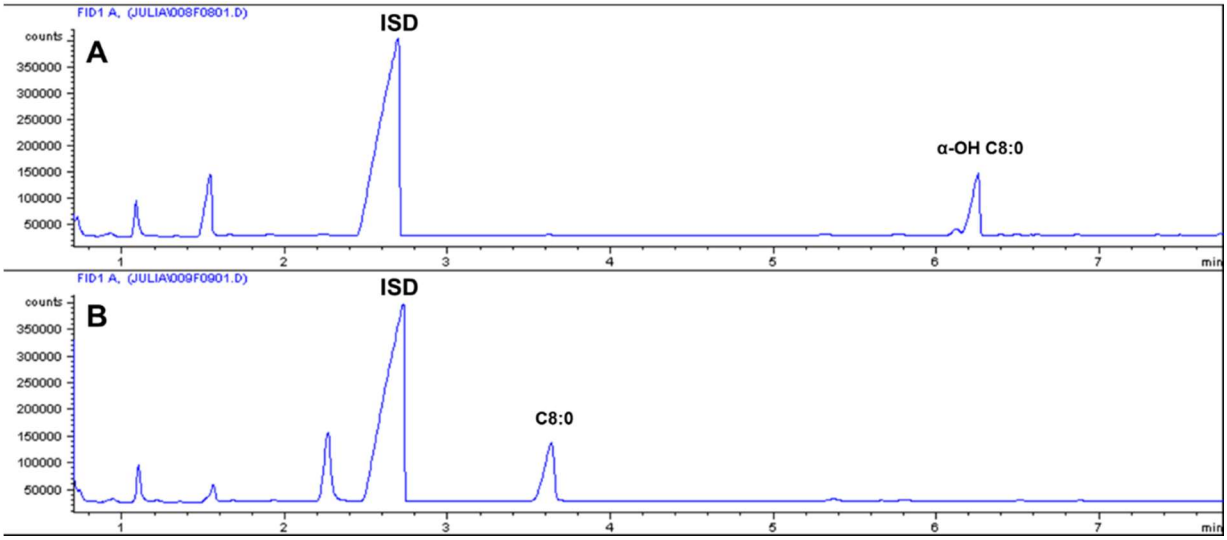

Figure 68 GC-FID traces for the conversion of C8:0 (2 mM) with $P450_{CLA}$. A = Conversion after addition of 2 mM H_2O_2. B = Control reaction without catalyst. ISD = internal standard (1-octanol; 0.1% v/v).

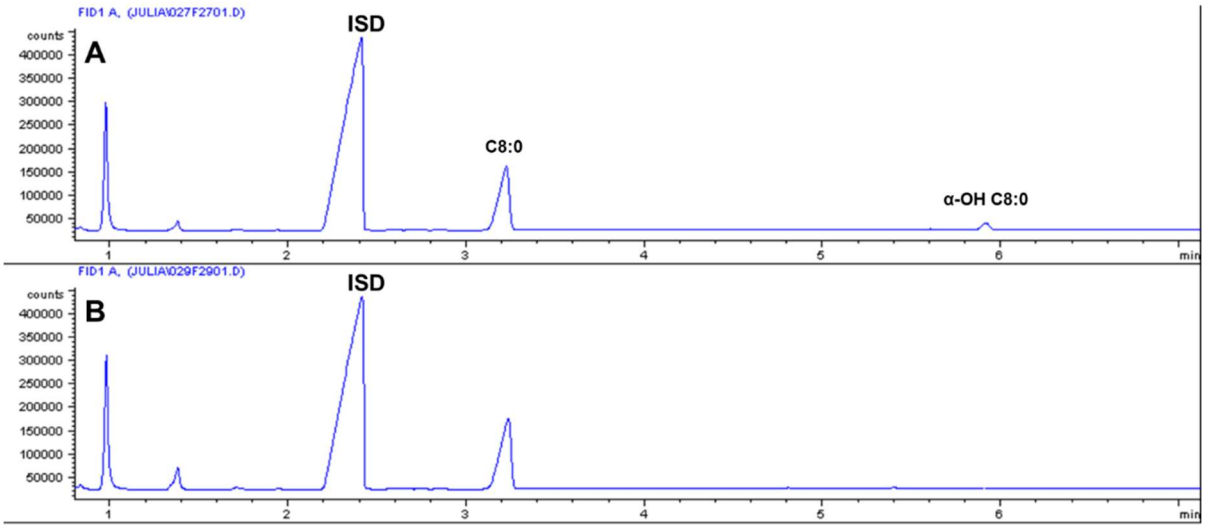

Figure 69 GC-FID traces for the conversion of C8:0 (2 mM) with P450$_{Jα}$. A = Conversion after addition of 2 mM H_2O_2. B = Control reaction without catalyst. Retention times are shifted compared to Figure S17 due to varying gas-pressure in GC-FID. ISD = internal standard (1-octanol; 0.1% v/v).

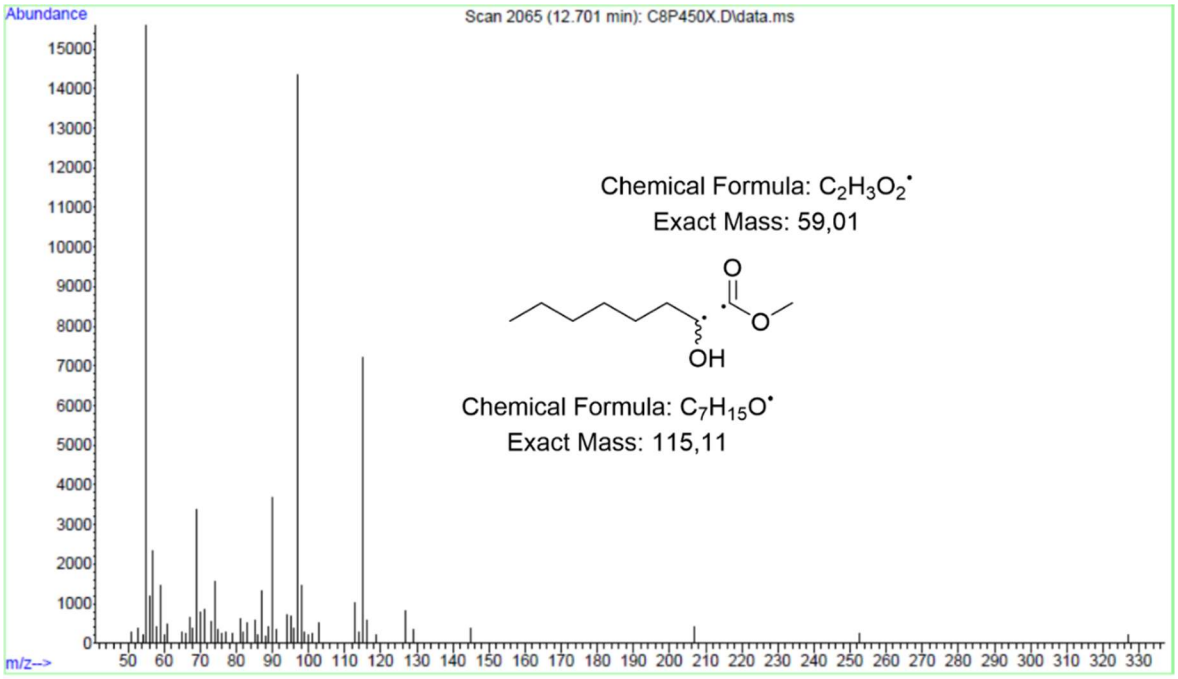

Figure 70 GC-MS spectrum of α-OH C8:0 (m/z = 174.13; methyl ester) produced from C8:0 by P450$_{Jα}$.

5.2.3. Conversion of C10:0

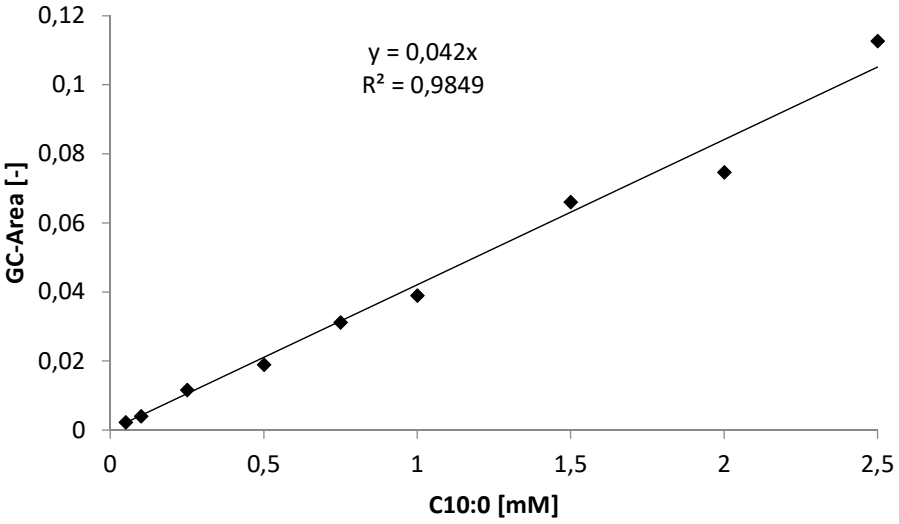

Figure 71 Calibration curve for quantification of C10:0 (decanoic acid).

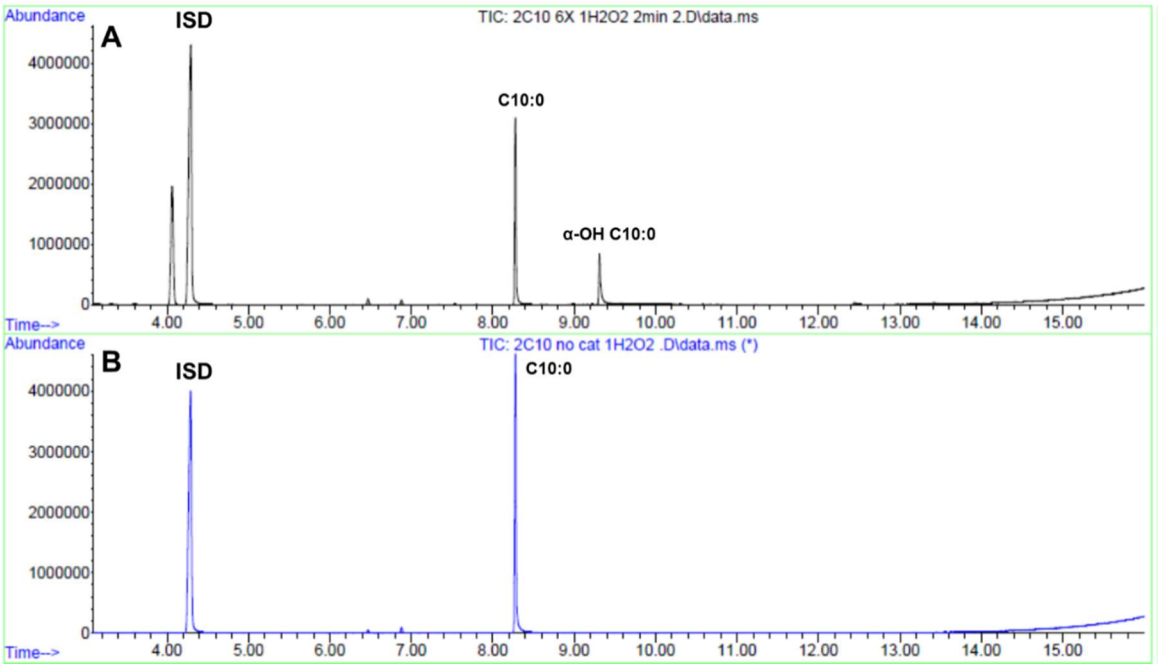

Figure 72 Conversion of C10:0 2 mM) with P450$_{Jα}$. A = Conversion after 2 min and addition of 1 mM H_2O_2 at once. B = Control reaction without catalyst. ISD = internal standard (1-octanol; 0.1% v/v).

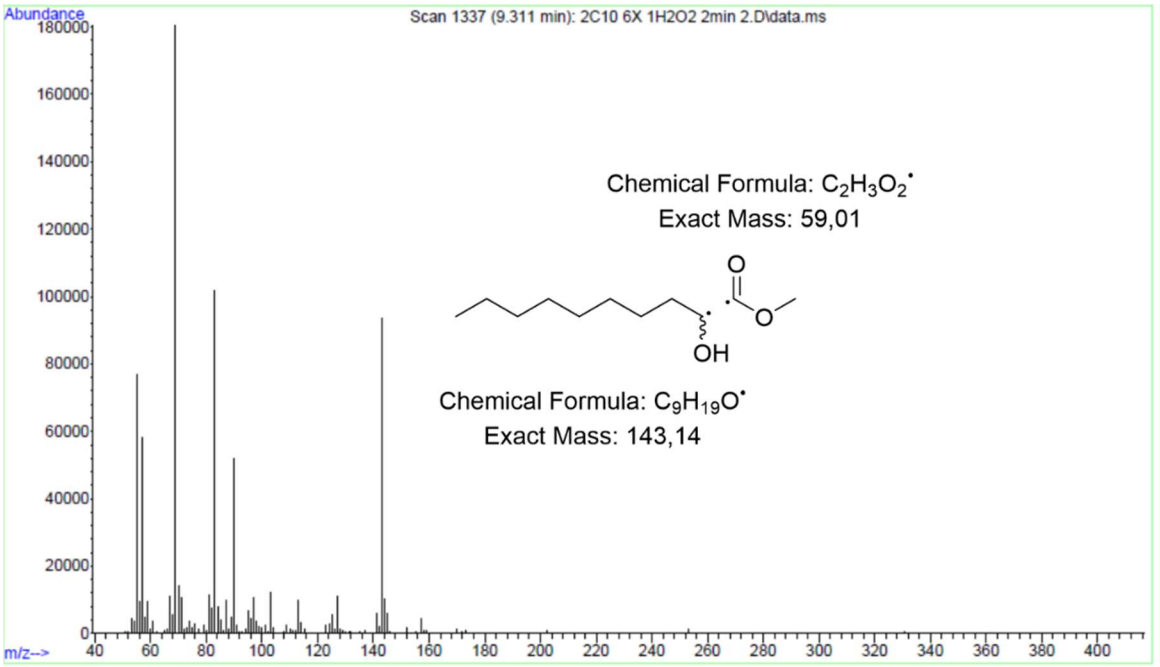

Figure 73 GC-MS spectrum of α-OH C10:0 (*m*/z = 202.16; methyl ester) produced from C10:0 by P450$_{J\alpha}$.

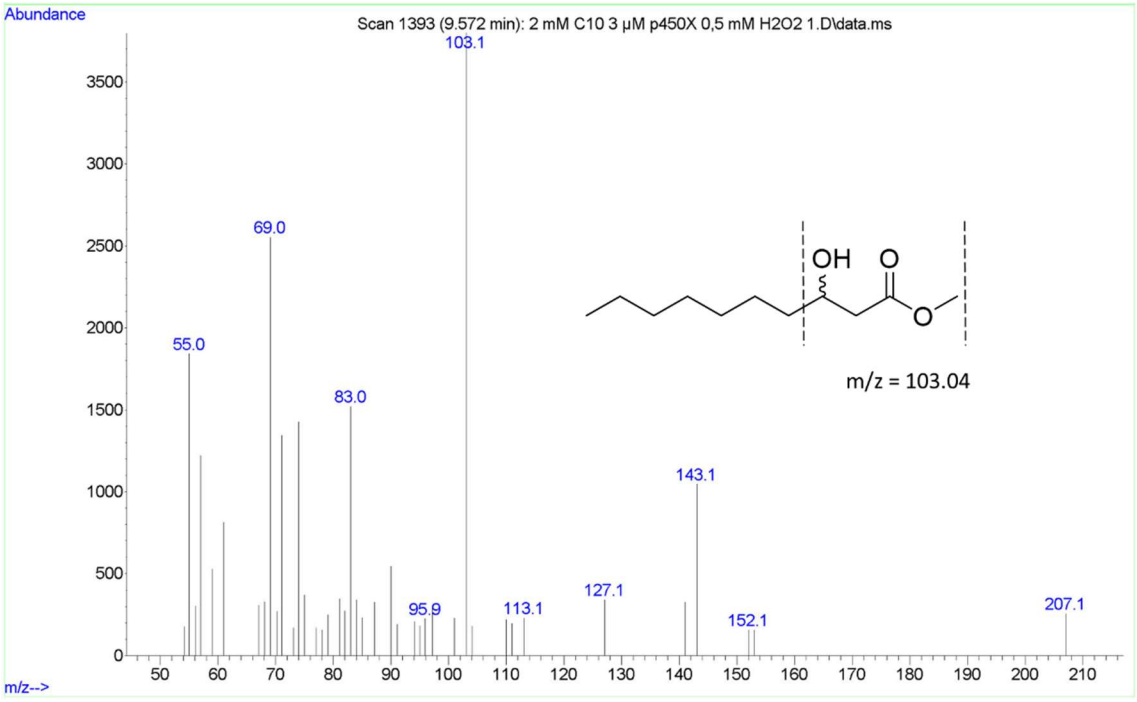

Figure 74 GC-MS spectrum of β-OH C10:0 produced from C10:0 by P450$_{J\alpha}$.

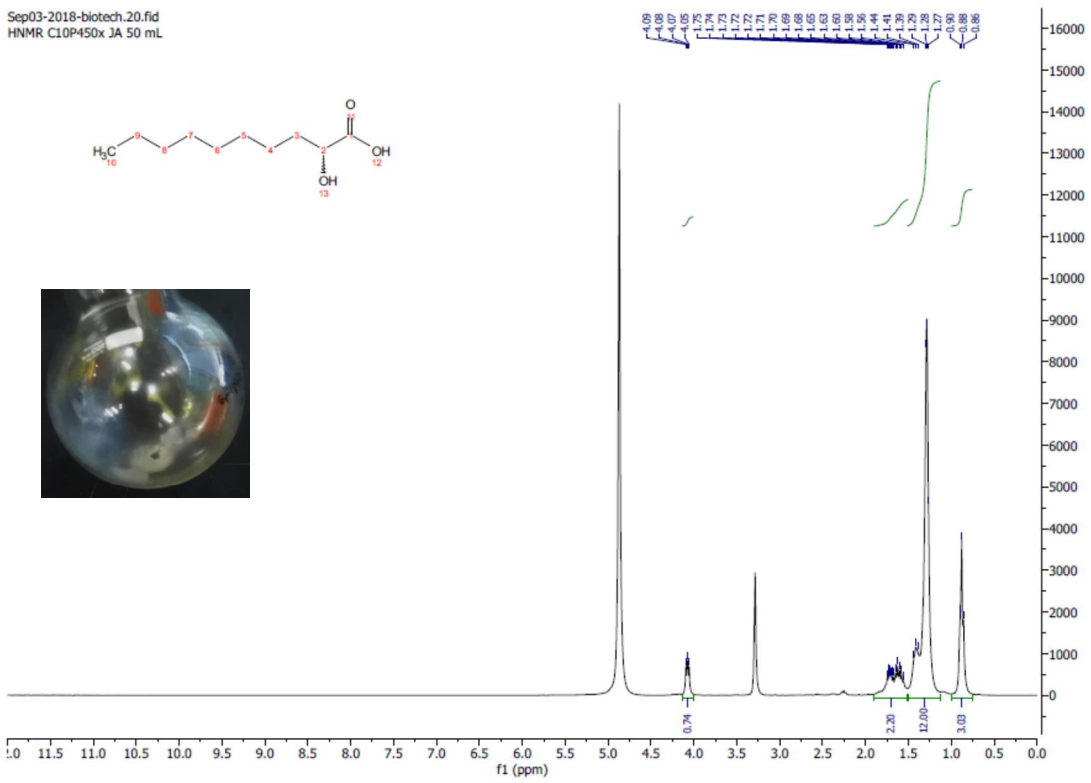

Figure 75 ^{1}H-NMR of isolated α-OH C10:0 (15.8 mg; white solid; >36% isolated yield) from conversion of 5 mM C10:0 with $P450_{Jα}$ on 50 mL scale and supplementation of 16 mM H_2O_2. Impurities at ~2.21 ppm correspond to traces of recovered substrate (~ 7% C10:0).

5.2.4. Conversion of C12:0

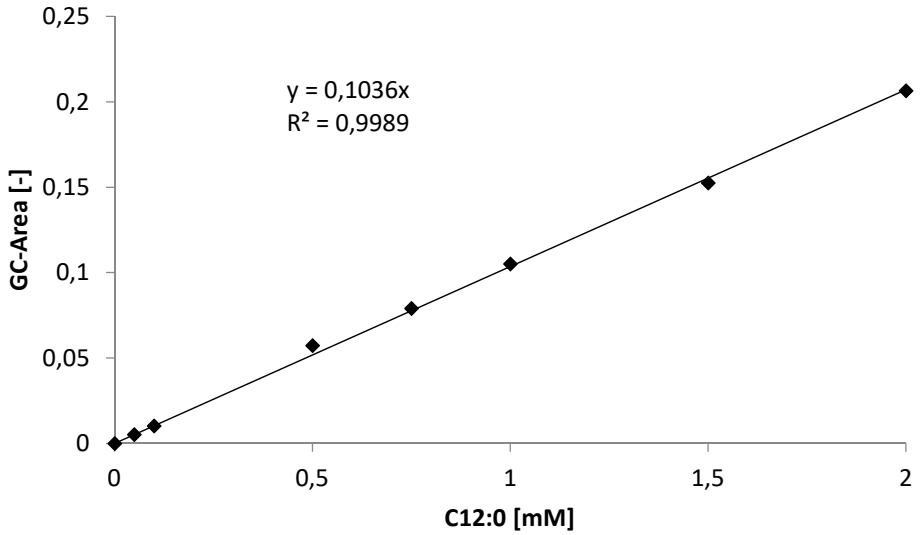

Figure 76 Calibration curve for quantification of C12:0 (dodecanoic acid).

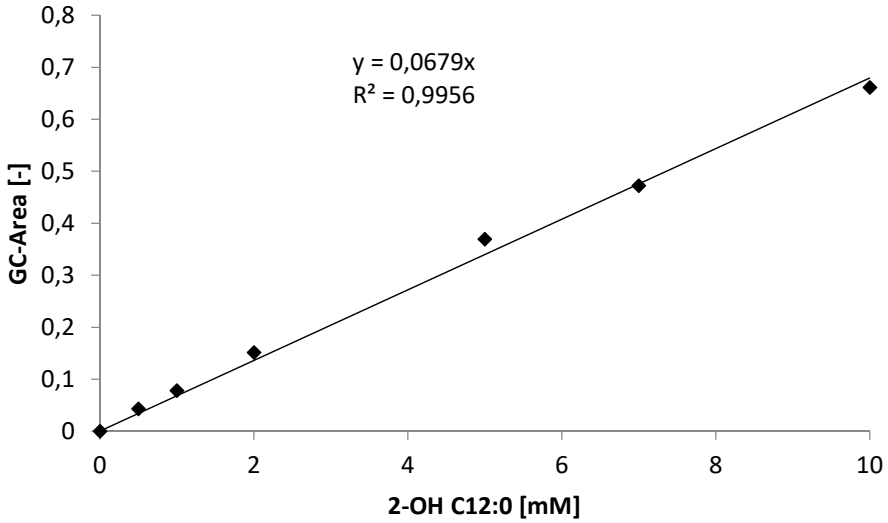

Figure 77 Calibration curve for quantification of 2-OH C12:0 (2-hydroxy dodecanoic acid).

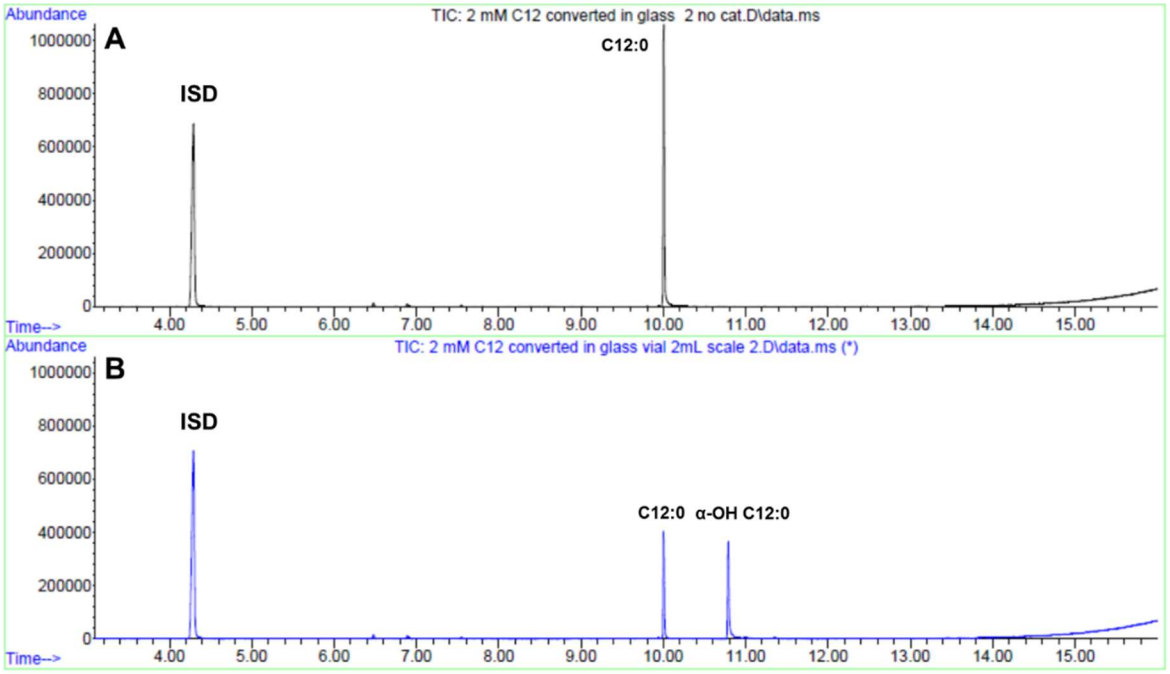

Figure 78 Conversion of C12:0 (2 mM) with P450$_{J\alpha}$. A = Control reaction without catalyst. B = Conversion after 2 h and addition of 0.5 mM H_2O_2 per 30 min (in total 2 mM). ISD = internal standard (1-octanol; 0.1% v/v).

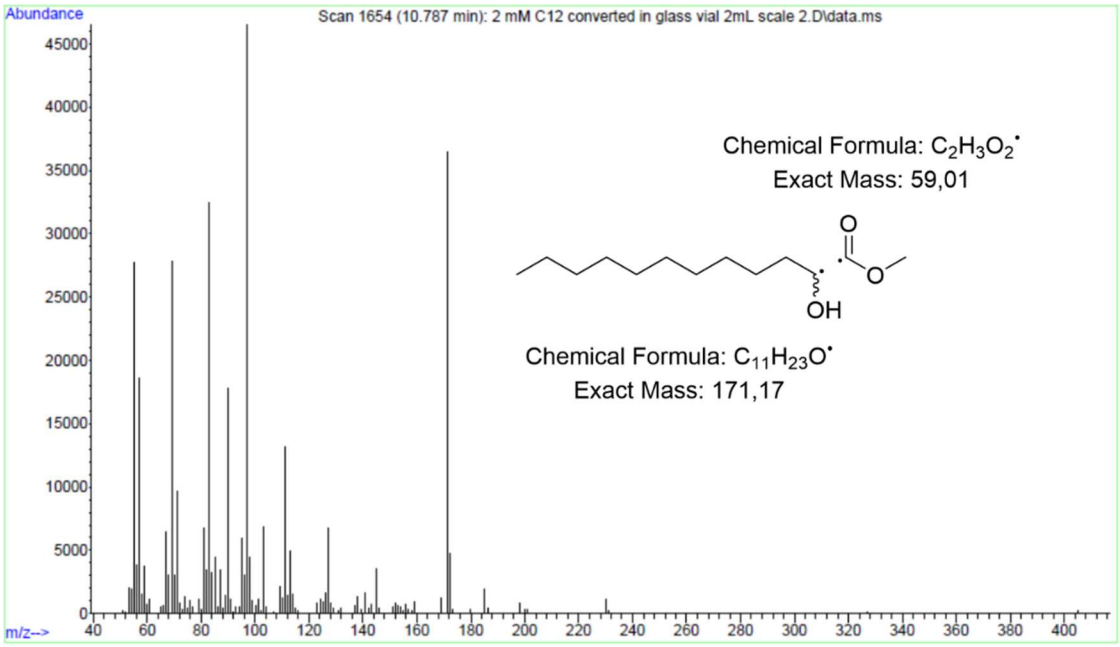

Figure 79 GC-MS spectrum of α-OH C12:0 (*m/z* = 230.19; methyl ester) produced from C12:0 by $P450_{J\alpha}$.

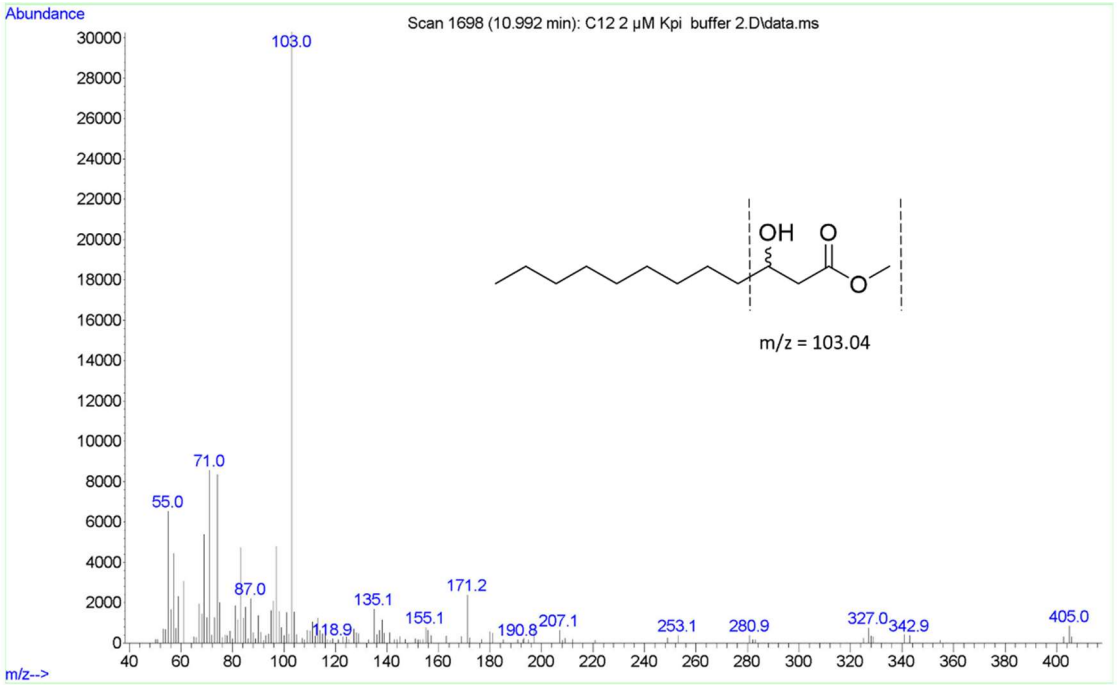

Figure 80 GC-MS spectrum of β-OH C12:0 produced from C12:0 by $P450_{J\alpha}$.

5.2.5. Conversion of C14:0

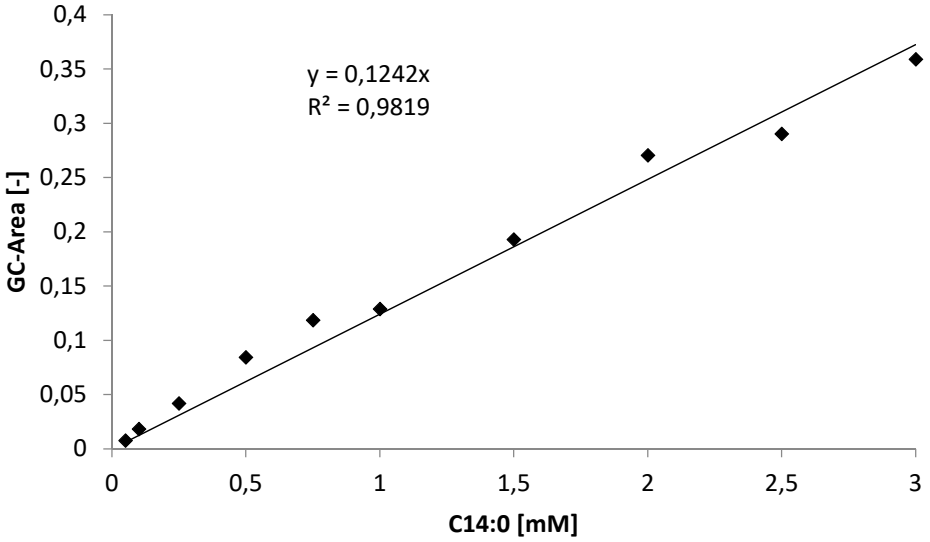

Figure 81 Calibration curve for quantification of C14:0 (tetradecanoic acid).

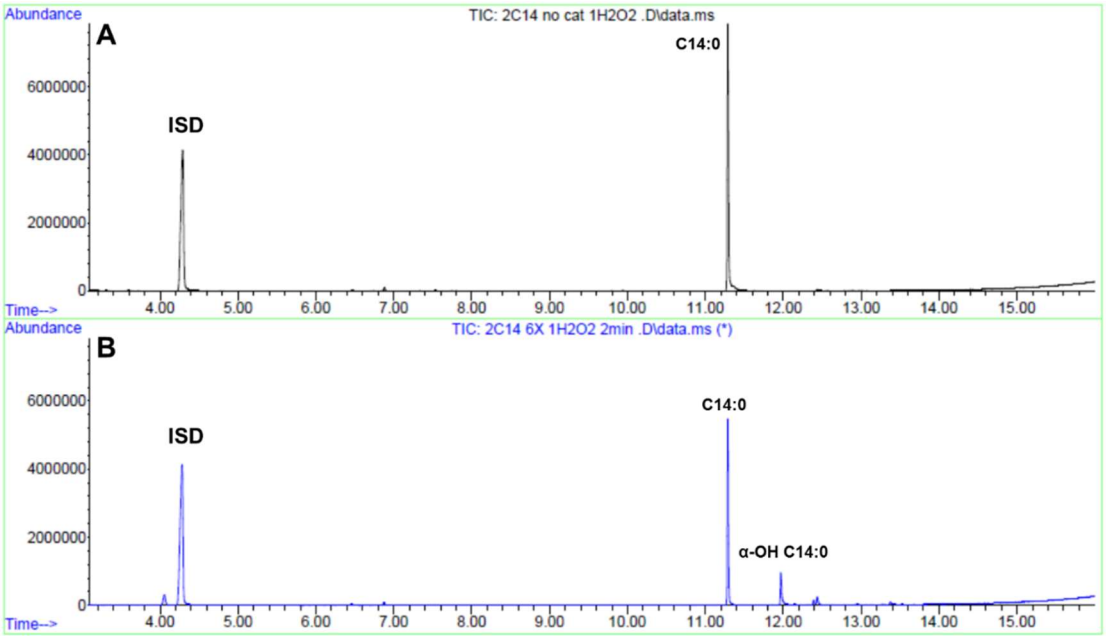

Figure 82 Conversion of C14:0 (2 mM) with $P450_{J\alpha}$. A = Control reaction without catalyst. **B** = Conversion after 2 min and addition of 1 mM H_2O_2 at once. ISD = internal standard (1-octanol; 0.1% v/v).

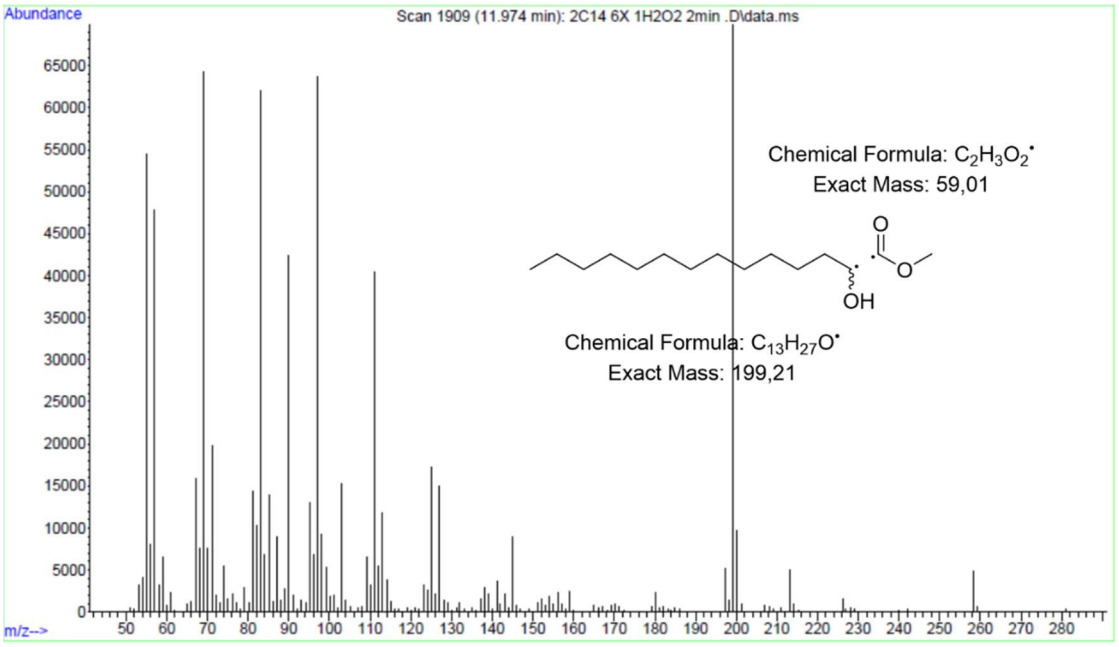

Figure 83 GC-MS spectrum of α-OH C14:0 (m/z = 258.22; methyl ester) produced from C14:0 by $P450_{J\alpha}$.

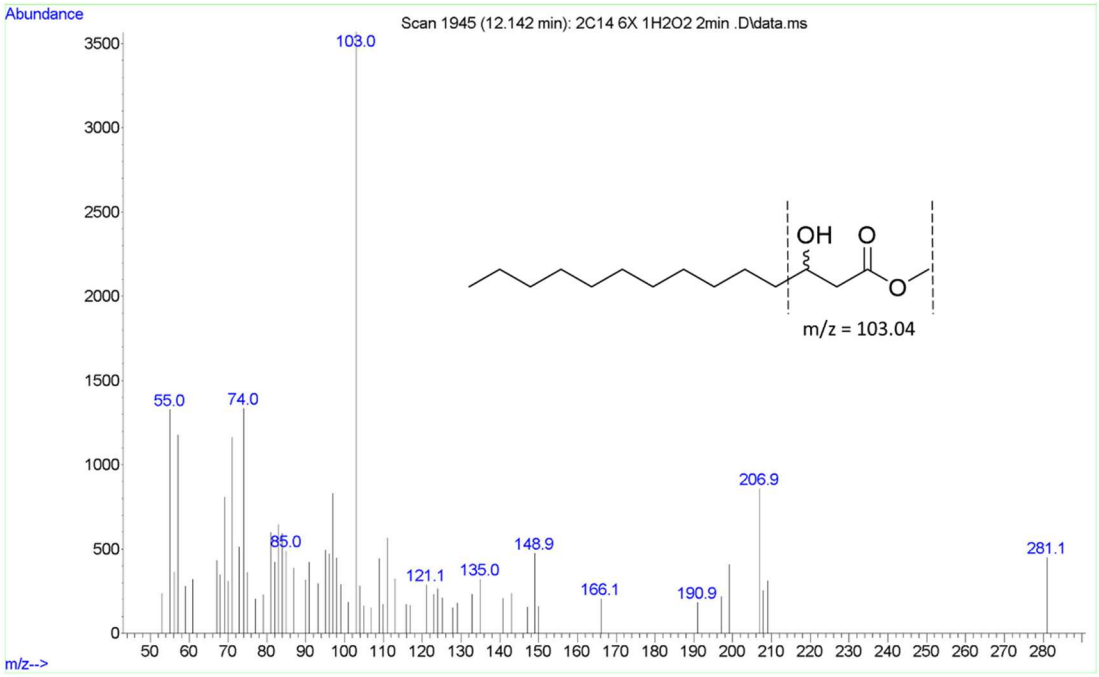

Figure 84 GC-MS spectrum of β-OH C14:0 (m/z = 258.22) produced from C14:0 by $P450_{J\alpha}$.

5.2.6. Conversion of C15:0

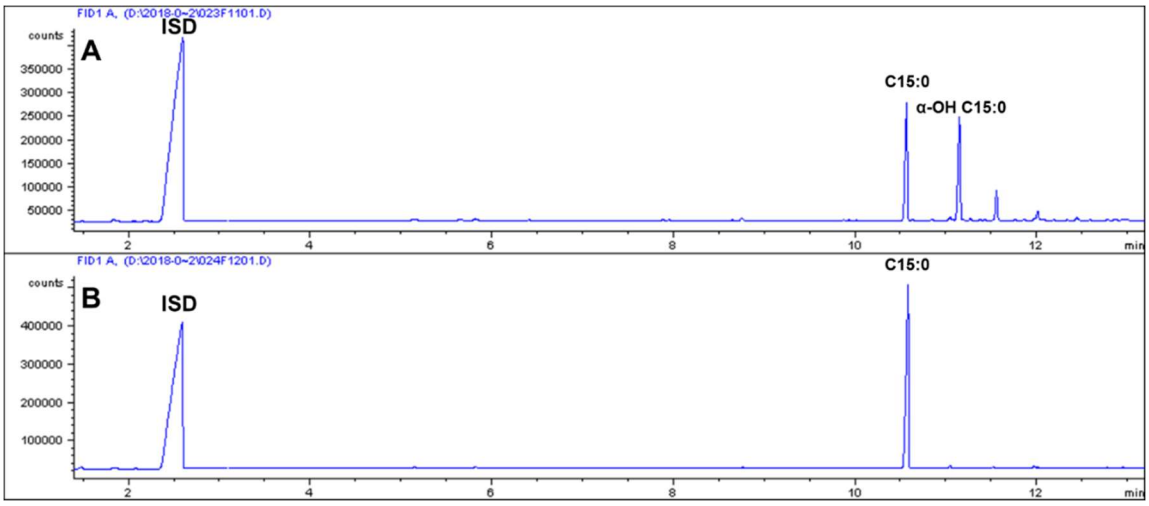

Figure 85 Conversion of C15:0 (2 mM) with P450$_{J\alpha}$. A = Conversion after 2 h and addition of 0.5 mM H_2O_2 per 30 min (in total 2 mM). B = Control reaction without catalyst. ISD = internal standard (1-octanol; 0.1% v/v).

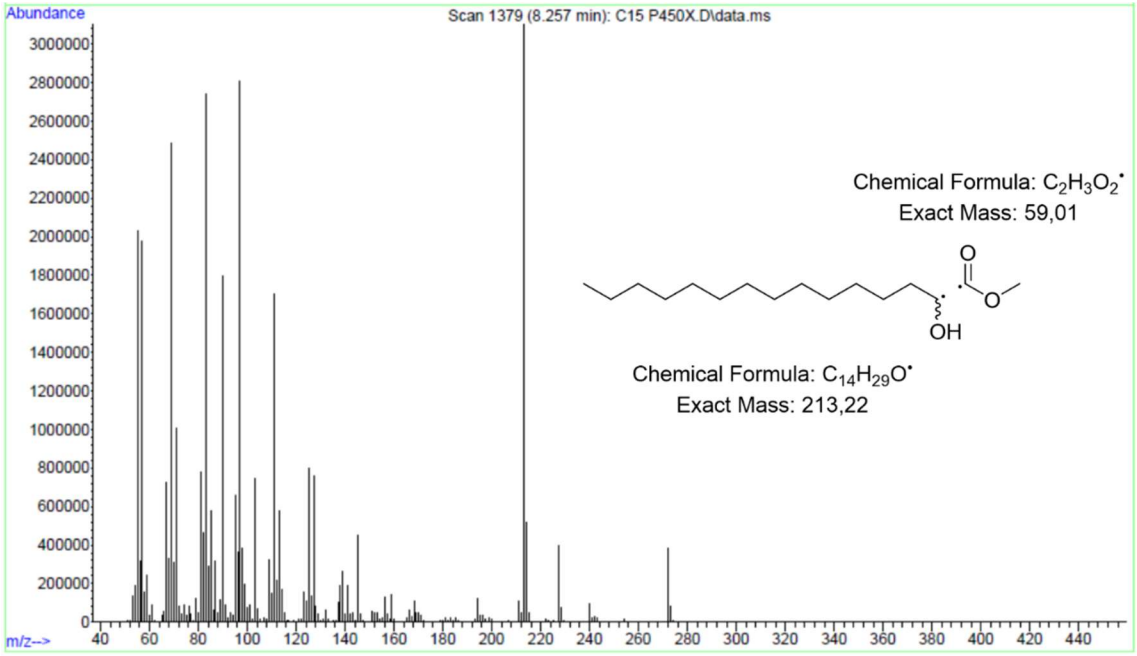

Figure 86 GC-MS spectrum of α-OH C15:0 (*m*/z = 272.24; methyl ester) produced from C15:0 by P450$_{J\alpha}$.

5.2.7. Conversion of C16:0

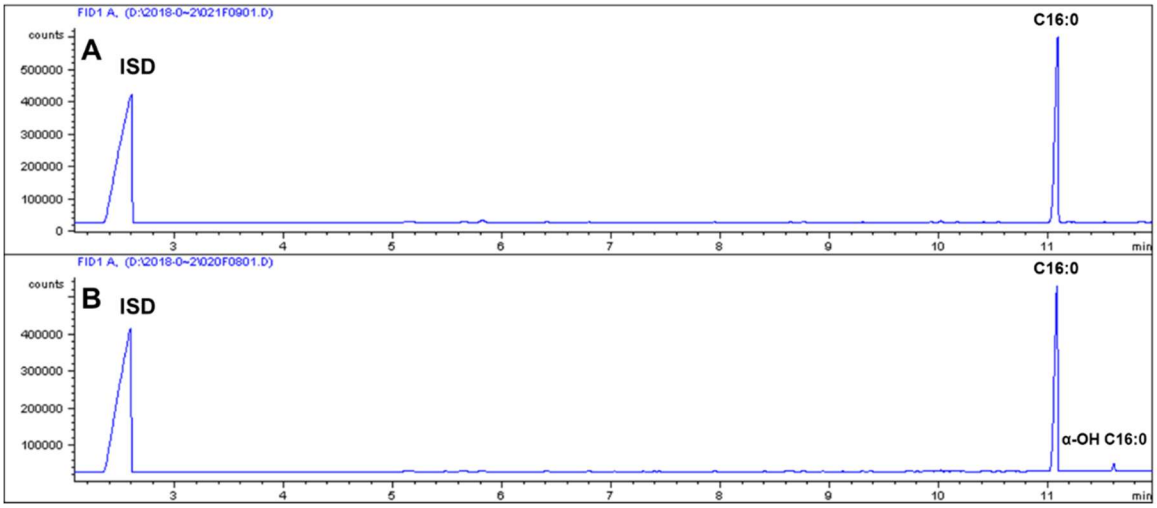

Figure 87 Conversion of C16:0 (2 mM) with P450$_{J\alpha}$. A = Control reaction without catalyst. B = Conversion after 2 h and addition of 0.5 mM H_2O_2 per 30 min (in total 2 mM). ISD = internal standard (1-octanol; 0.1% v/v).

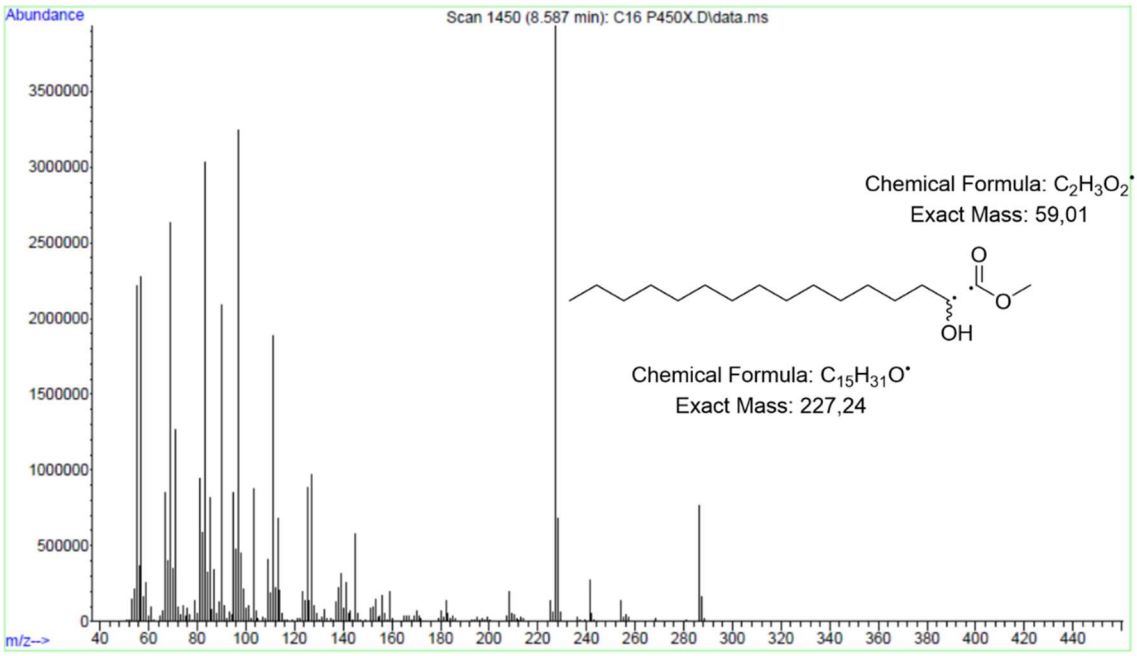

Figure 88 GC-MS spectrum of α-OH C16:0 (*m*/z = 286.25; methyl ester) produced from C16:0 by P450$_{J\alpha}$.

5.2.8. Conversion of C18:1

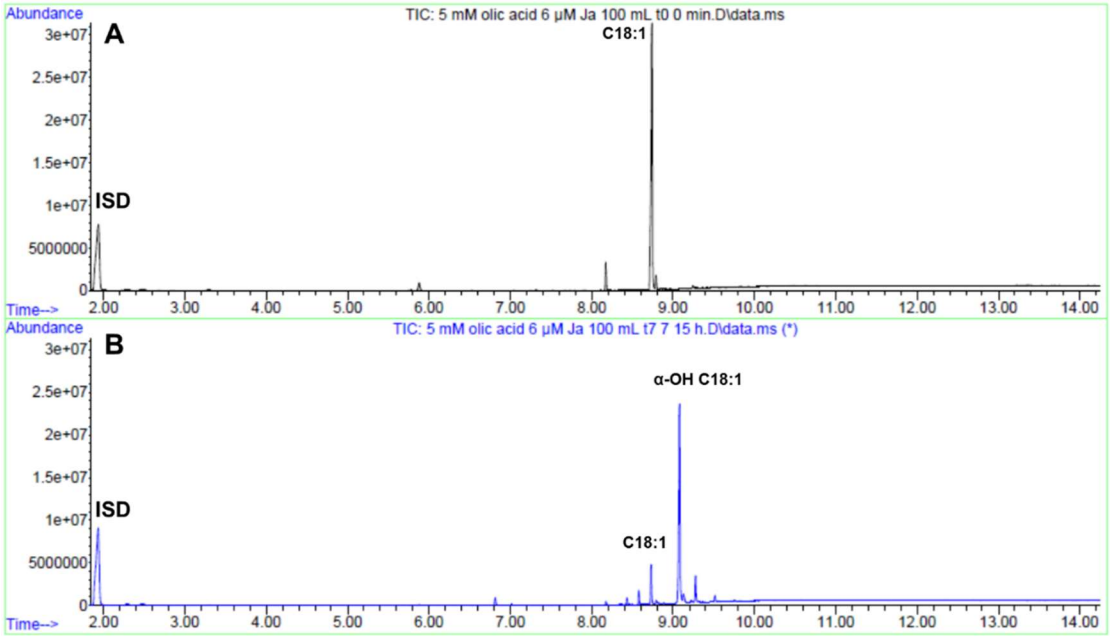

Figure 89 Conversion of C18:1 (5 mM) with P450$_{J\alpha}$ on 100 mL scale. A = Control reaction without catalyst. B = Conversion after 15 h and addition of 0.5 mM H_2O_2 per 30 min (in total 15 mM). ISD = internal standard (1-octanol; 0.1% v/v).

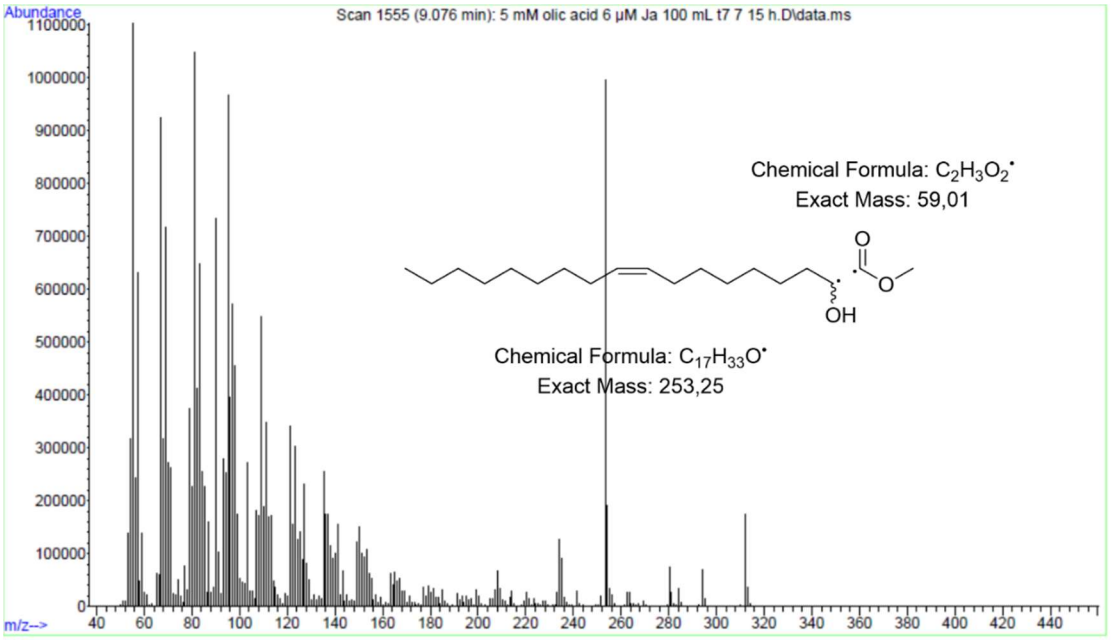

Figure 90 GC-MS spectrum of α-OH C18:1 (*m/z* = 312.27; methyl ester) produced from C18:1 by P450$_{J\alpha}$.

5.3. Catalytical characterization

5.3.1. Determination of the stereoselectivity of $P450_{J\alpha}$

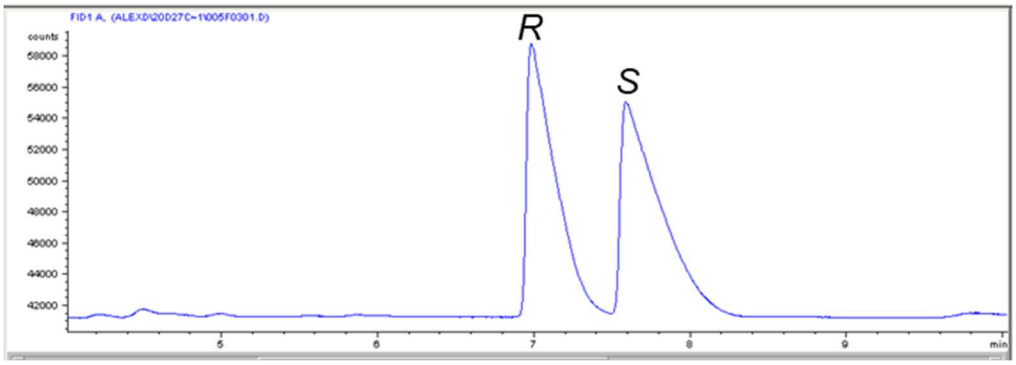

Figure 91 Chiral separation of a blend of enzymatically produced *R*- and *S*-2-OH C10:0. The blend was generated by spiking a P450Jα sample with material generated from a L-LOX oxidized sample that was asymmetrically reduced by D-HIC-DH.

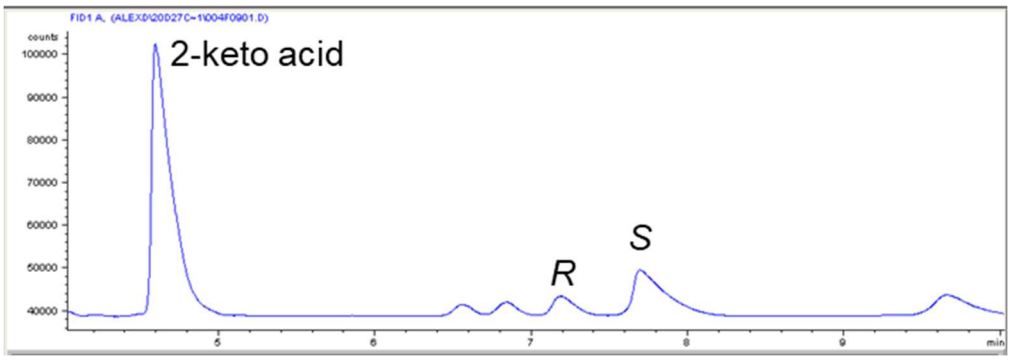

Figure 92 Chiral analysis of a L-LOX oxidized reaction sample containing *R*- and *S*-2OH C10:0 produced by $P450_{J\alpha}$.

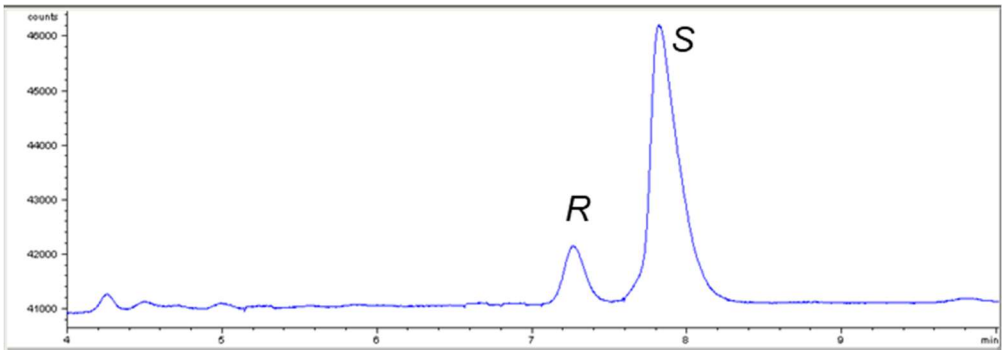

Figure 93 Chiral analysis of *R*- and *S*-2-OH C10:0 produced by $P450_{CLA}$.

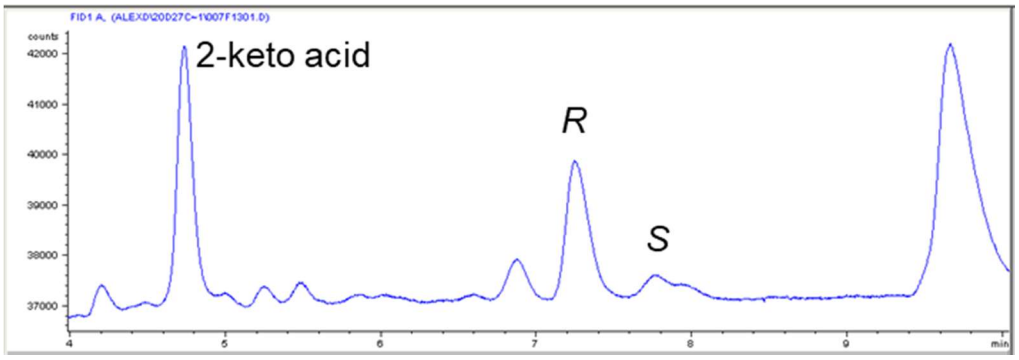

Figure 94 Chiral analysis of a L-LOX oxidized reaction sample containing *R*- and *S*-2-OH C10:0 produced by P450$_{CLA}$.

5.3.2. 1-alkene formation of α-selective P450s and P450$_{BS\beta}$

5.3.2.1. 1-pentene formation of C6:0

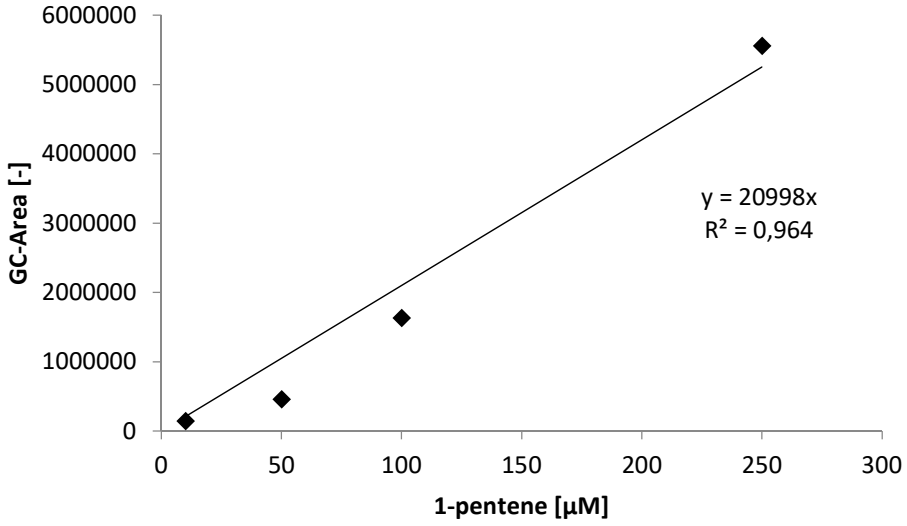

Figure 95 Calibration curve for quantification of 1-pentene. 1-pentene is highly volatile, therefore the deviations are higher.

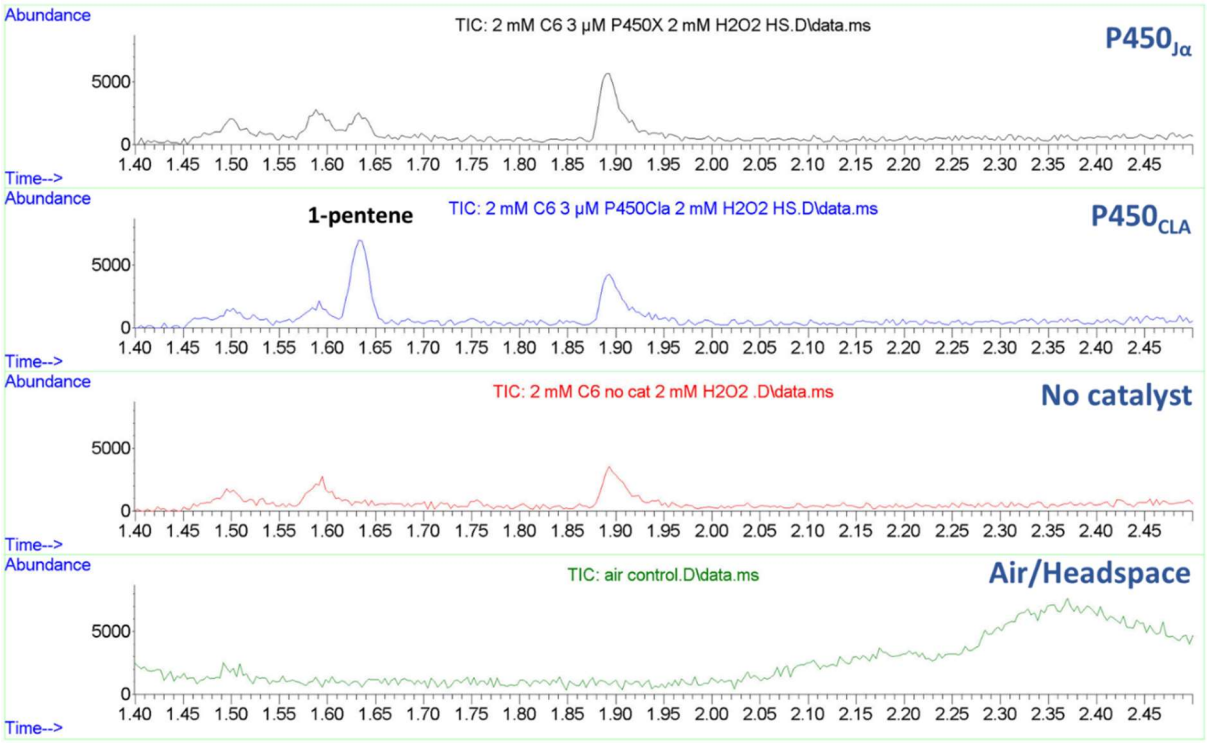

Figure 96 Headspace GC-MS analysis for the conversion of C6:0 (2 mM) with CYPs. Retention time for 1-pentene is 1.60 to 1.65 min.

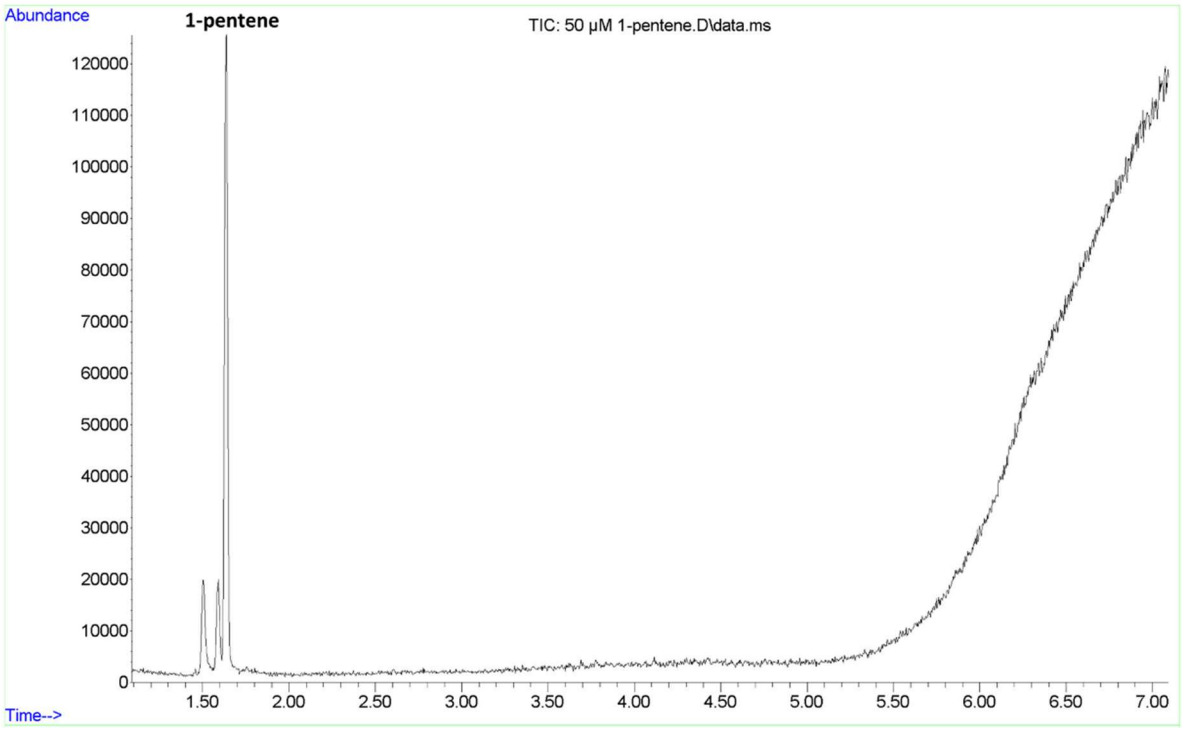

Figure 97 GC-MS headspace analysis of 1-pentene.

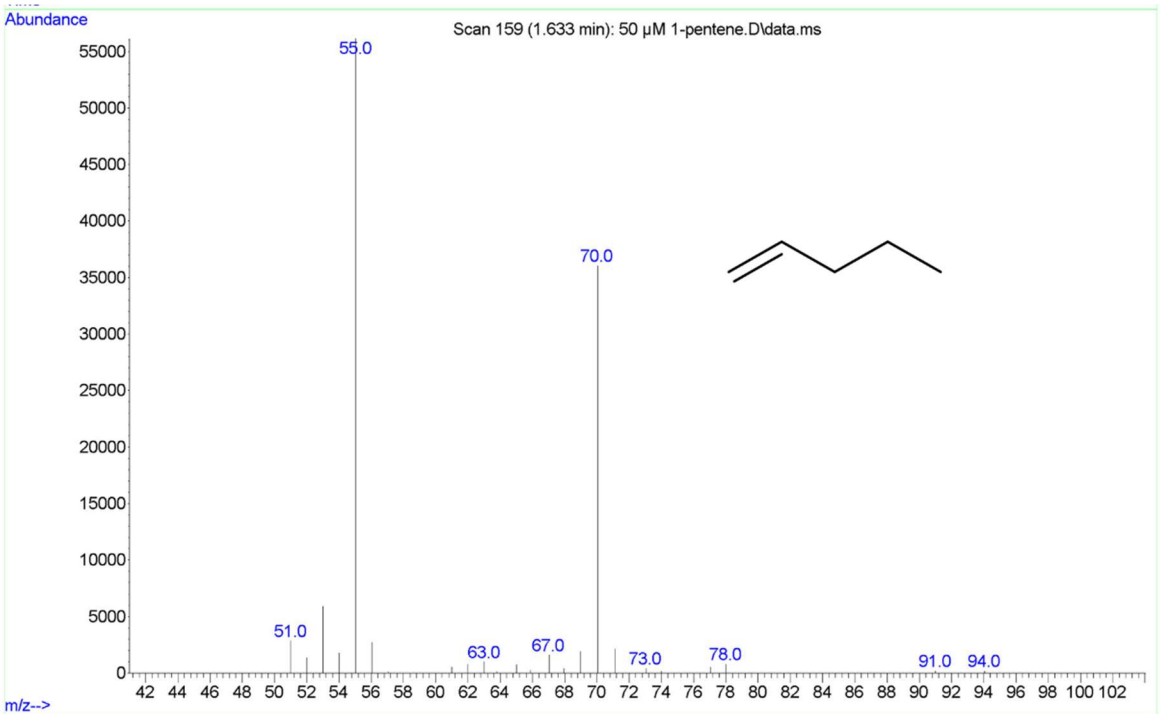

Figure 98 GC-MS spectrum of 1-pentene (m/z = 70.08, commercial reference).

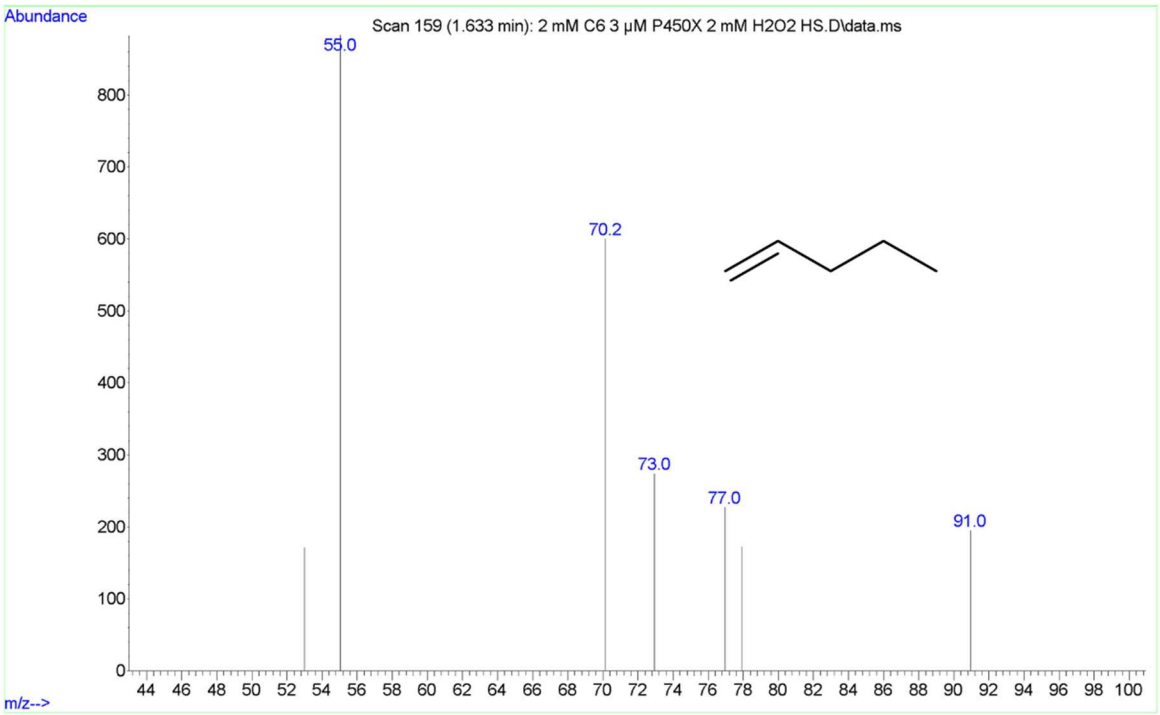

Figure 99 GC-MS spectrum of 1-pentene (m/z = 70.08) produced from C6:0 by $P450_{J\alpha}$.

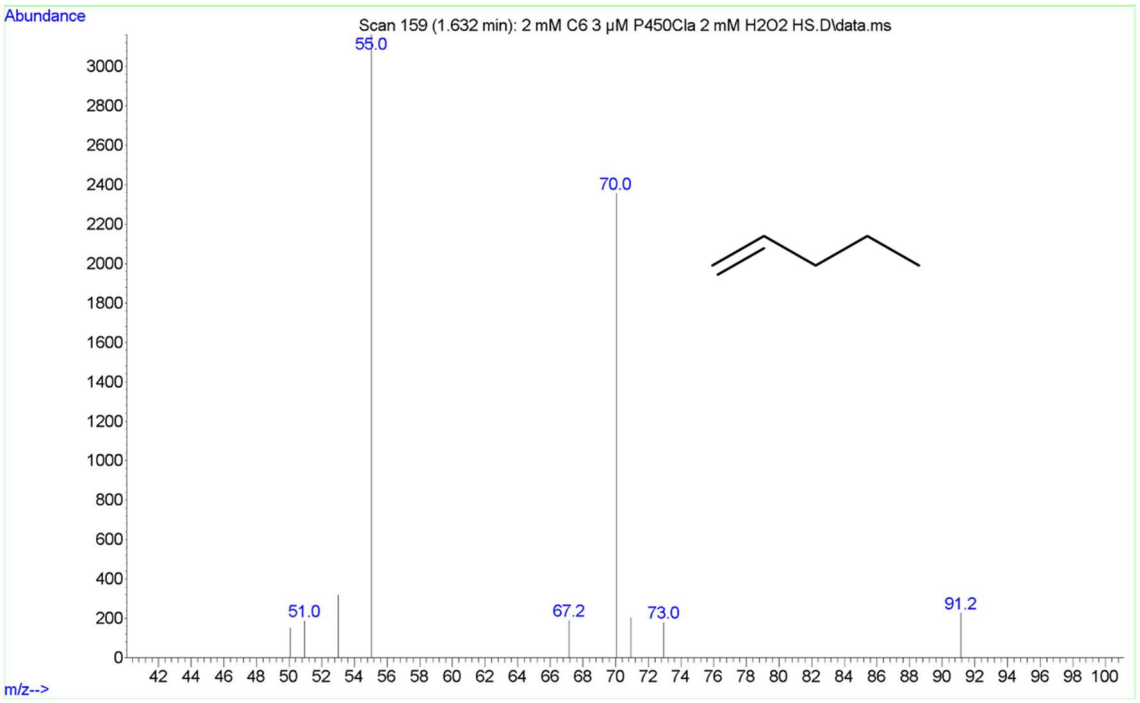

Figure 100 GC-MS spectrum of 1-pentene (m/z = 70.08) produced from C6:0 by $P450_{CLA}$.

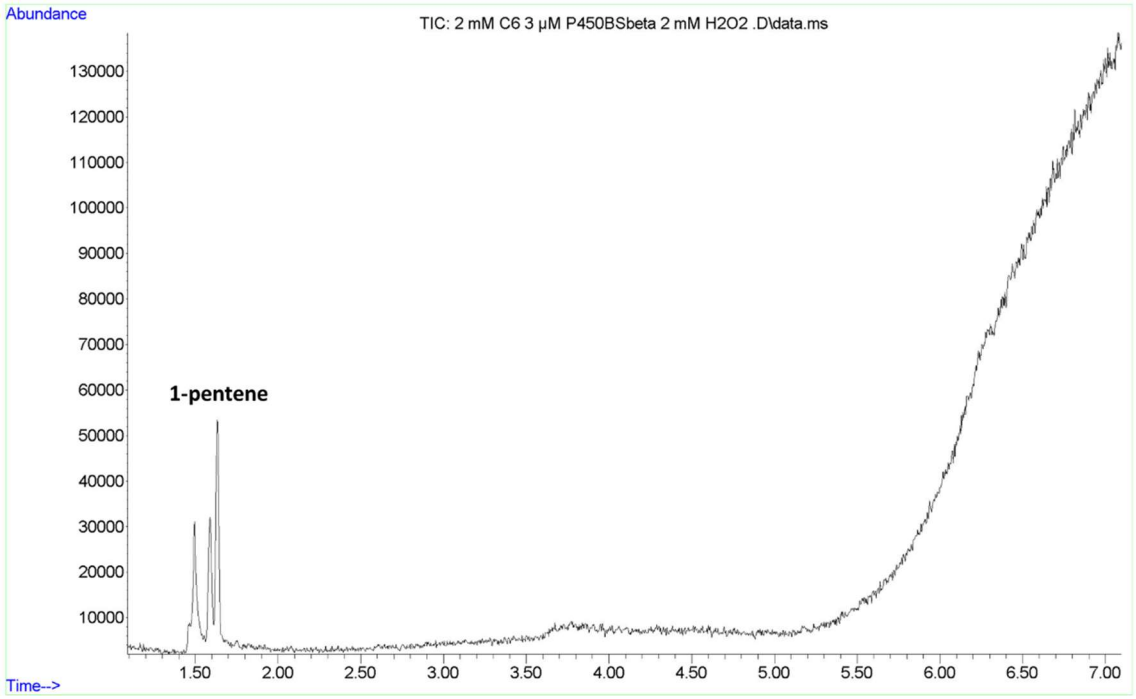

Figure 101 GC-MS headspace analysis for the conversion of C6:0 (2 mM) with $P450_{BS\beta}$. Retention time for 1-pentene is 1.60 to 1.65 min.

Figure 102 GC-MS spectrum of 1-pentene (m/z = 70.08) produced from C6:0 by $P450_{BS\beta}$.

5.3.2.2. 1-heptene formation from C8:0

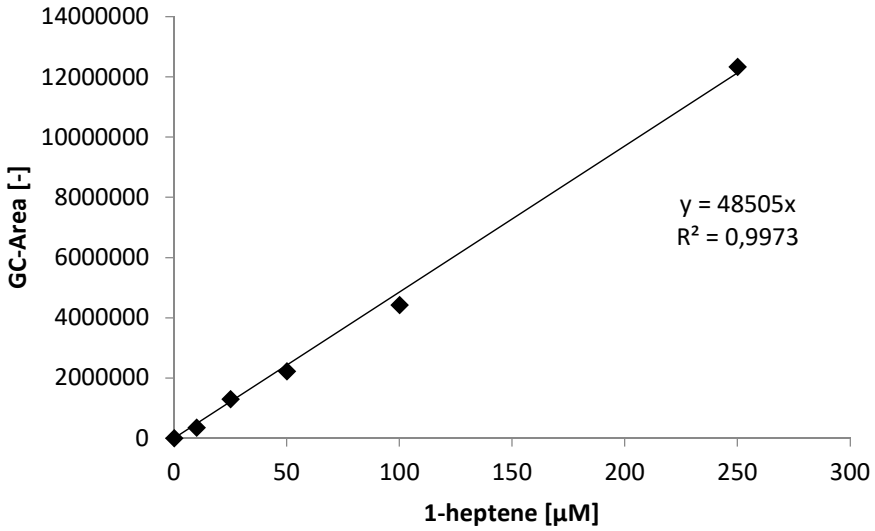

Figure 103 Calibration curve for quantification of 1-heptene.

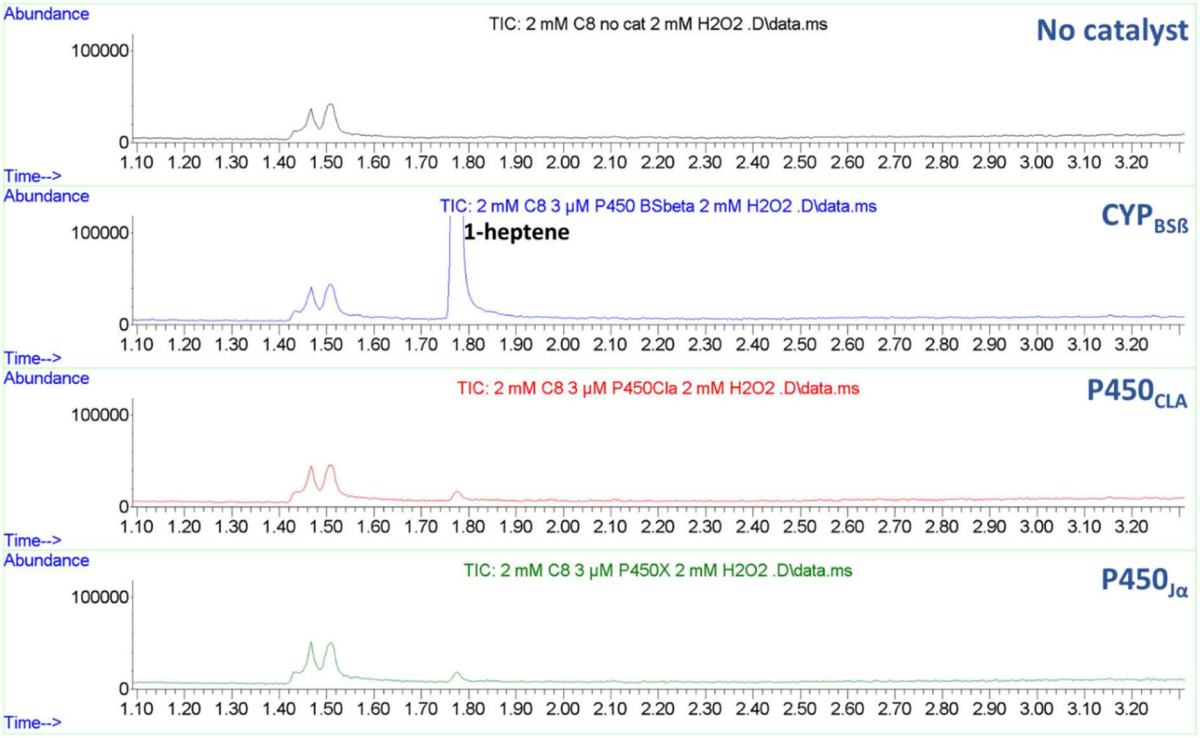

Figure 104 GC-MS headspace analysis for the conversion of C8:0 (2 mM) with CYP152s. Retention time for 1-heptene is 1.7 to 1.8 min.

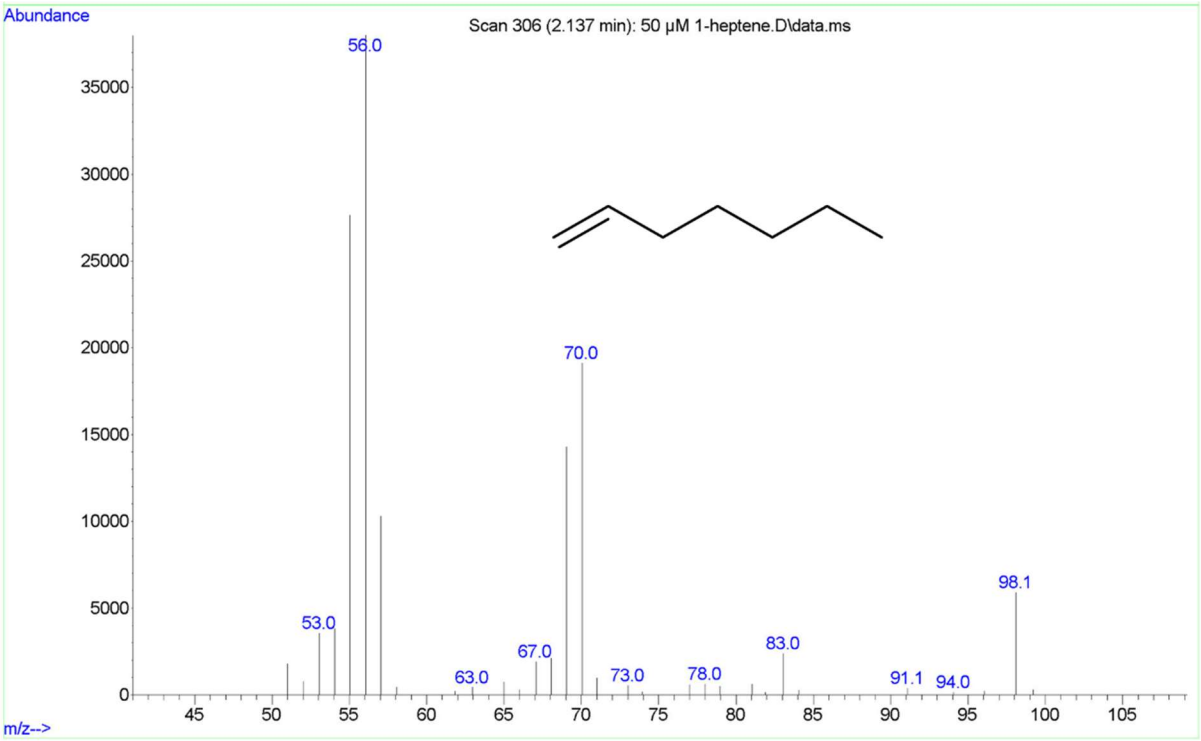

Figure 105 GC-MS spectrum of 1-heptene (m/z = 98.11, commercial reference).

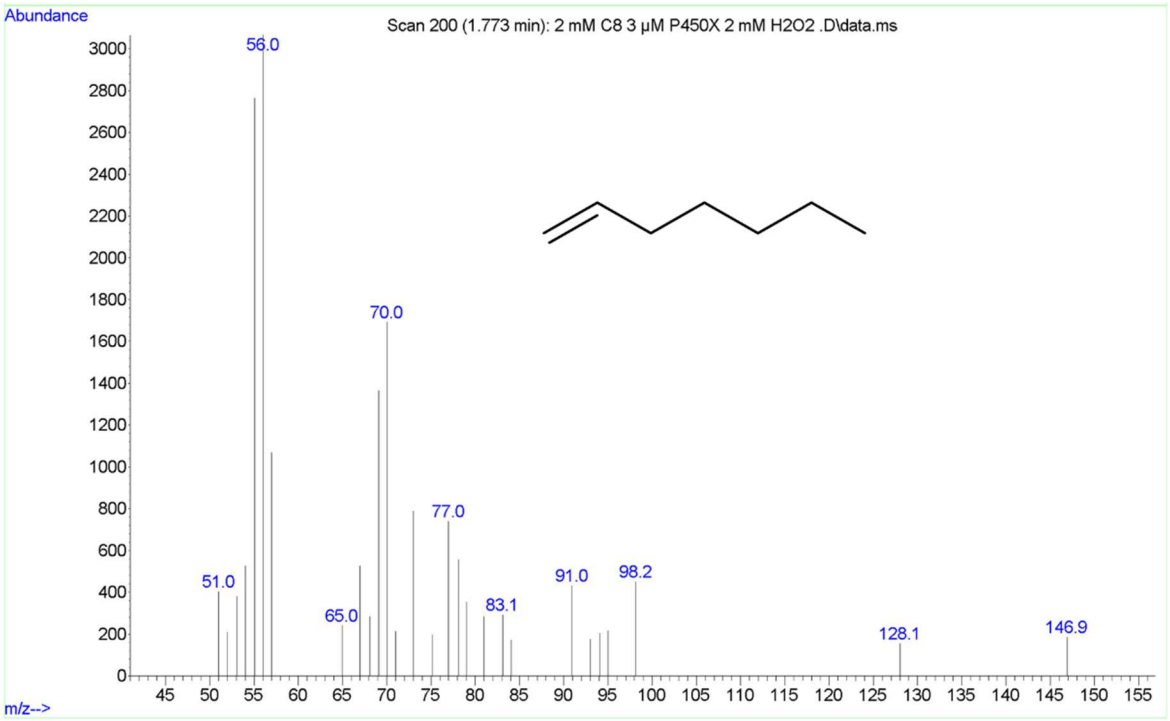

Figure 106 GC-MS spectrum of 1-heptene (m/z = 98.11) produced from C8:0 by $P450_{Jα}$.

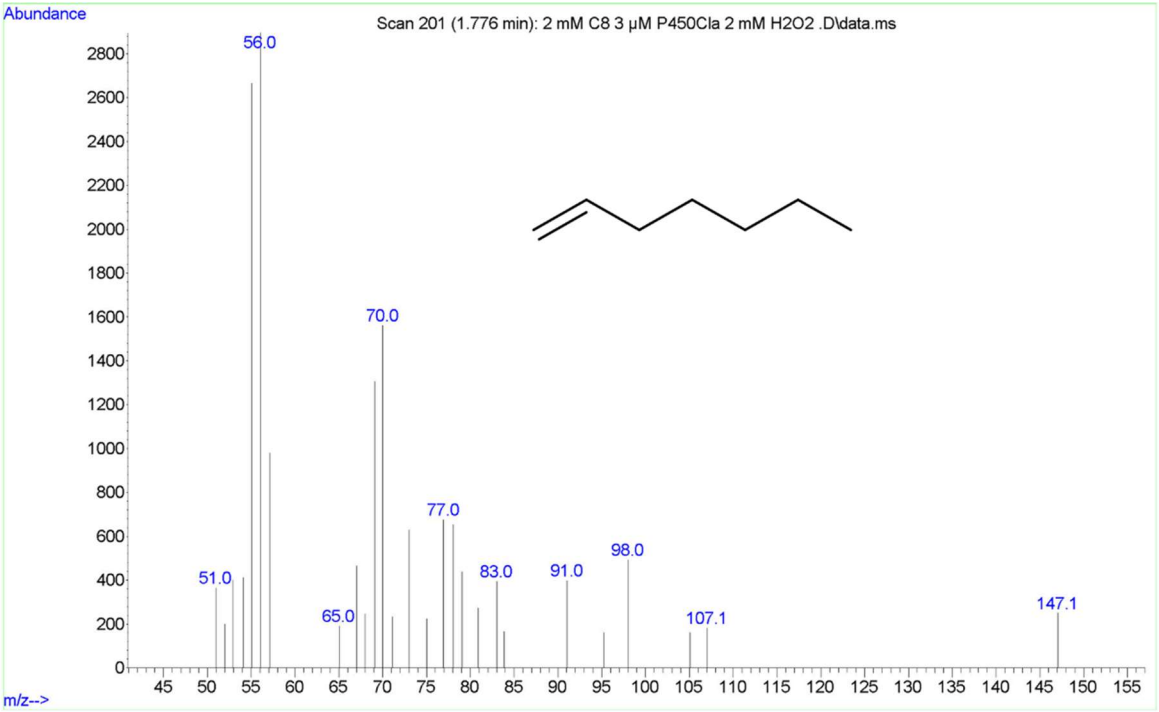

Figure 107 GC-MS spectrum of 1-heptene (m/z = 98.11) produced from C8:0 by $P450_{CLA}$.

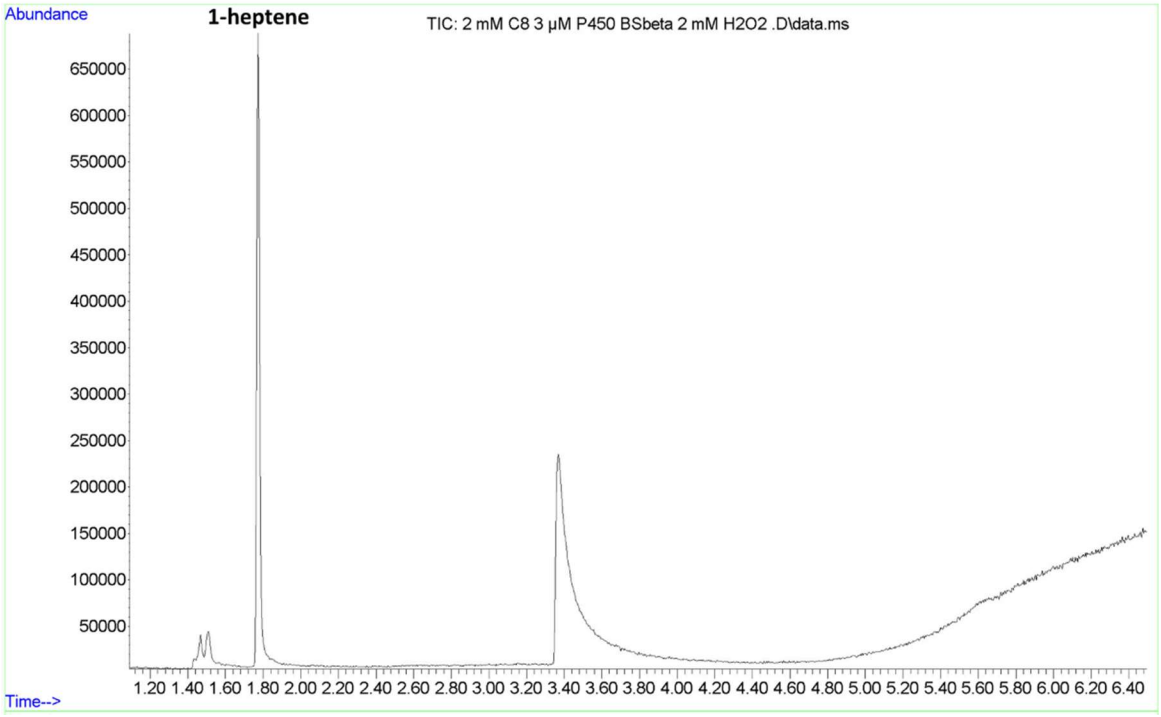

Figure 108 GC-MS headspace analysis for the conversion of C8:0 with P450$_{BS\beta}$. Retention time for 1-heptene is 1.7 to 1.8 min.

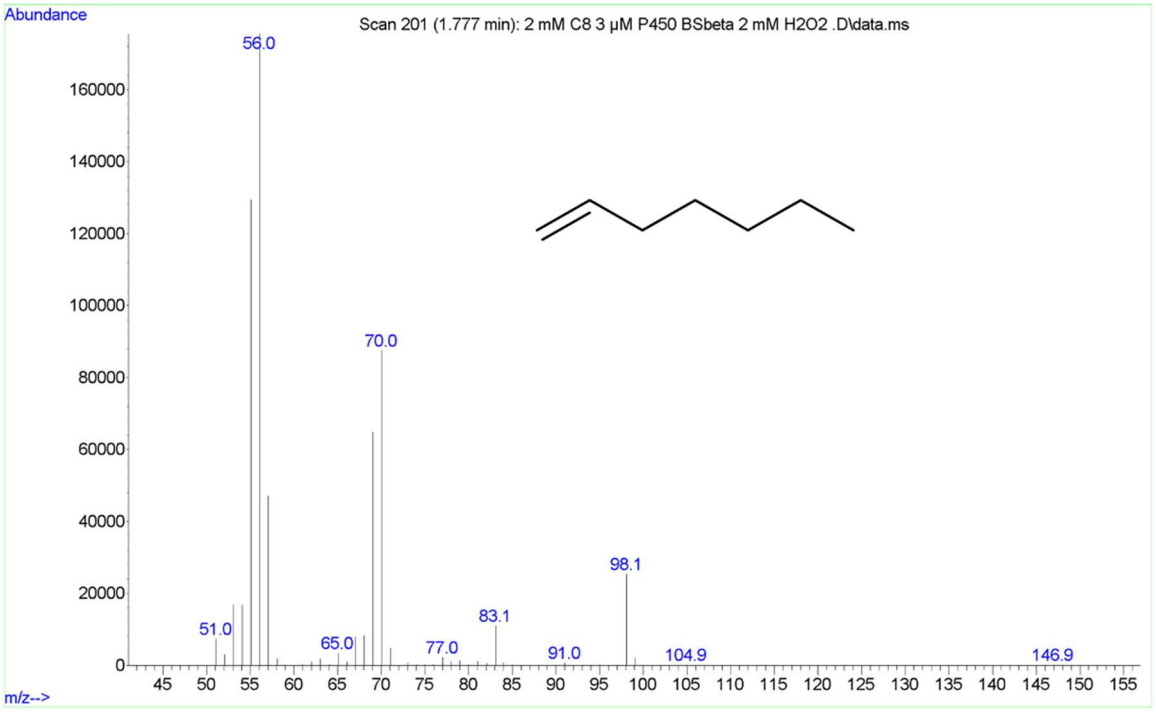

Figure 109 GC-MS spectrum of 1-heptene (m/z = 98.11) produced from C8:0 by P450$_{BS\beta}$.

5.3.3.1-nonene formation from C10:0

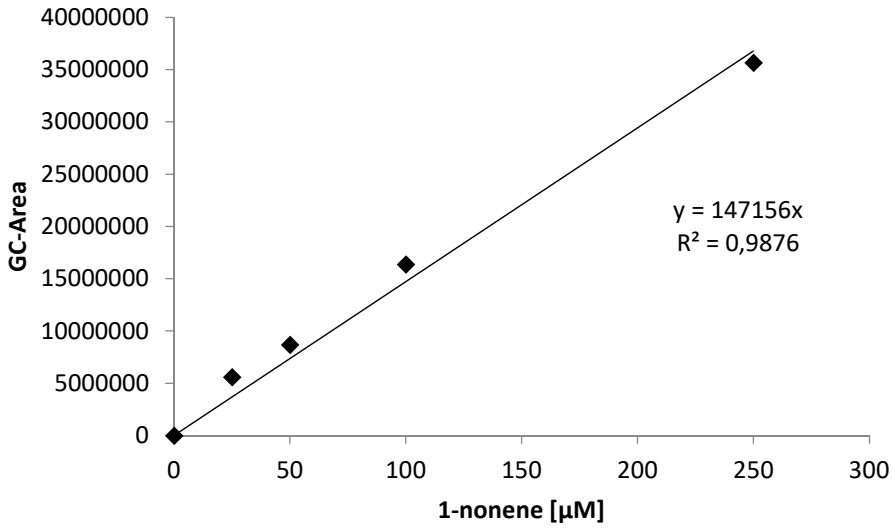

Figure 110 Calibration curve for quantification of 1-nonene.

Figure 111 GC-MS headspace analysis for the conversion of C10:0 (2 mM) with $P450_{BS\beta}$. Retention time for 1-nonene is 2.3 to 2.4 min.

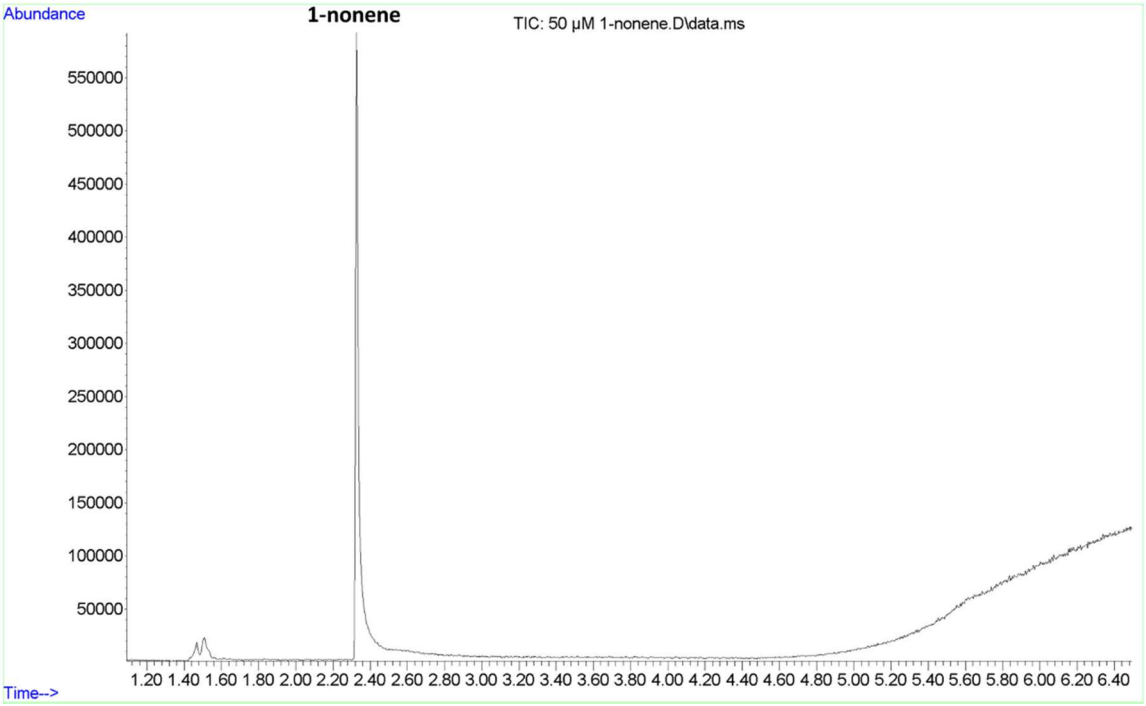

Figure 112 GC-MS headspace analysis of 1-nonene (commercial reference).

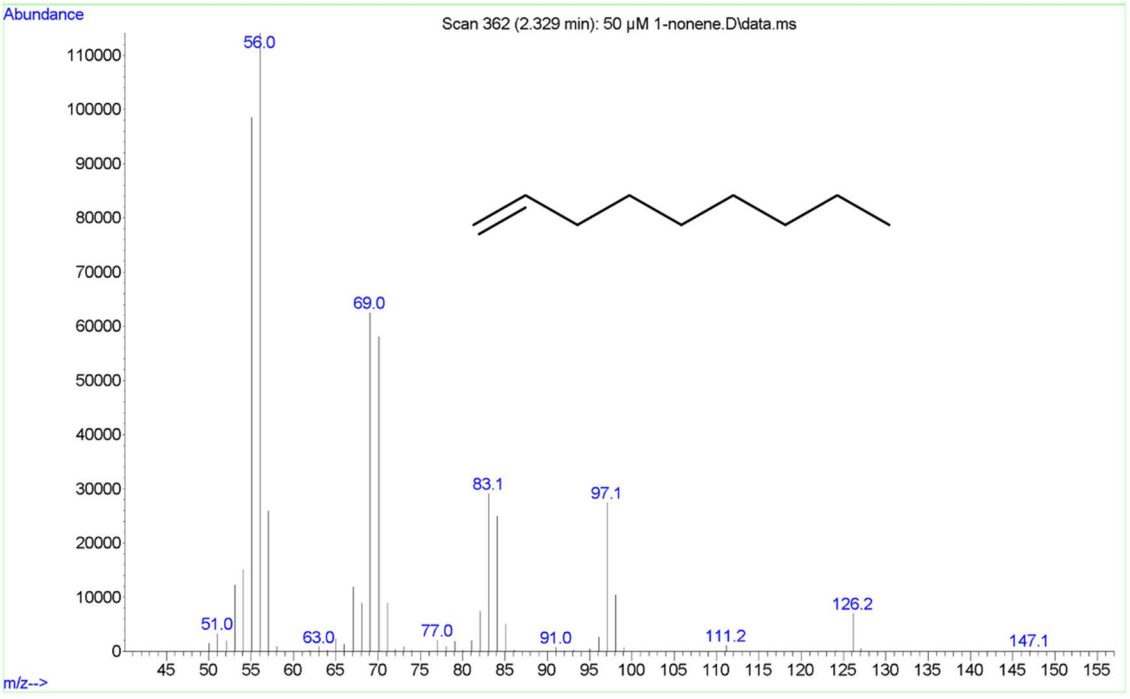

Figure 113 GC-MS spectrum of 1-nonene (m/z = 126.14, commercial reference).

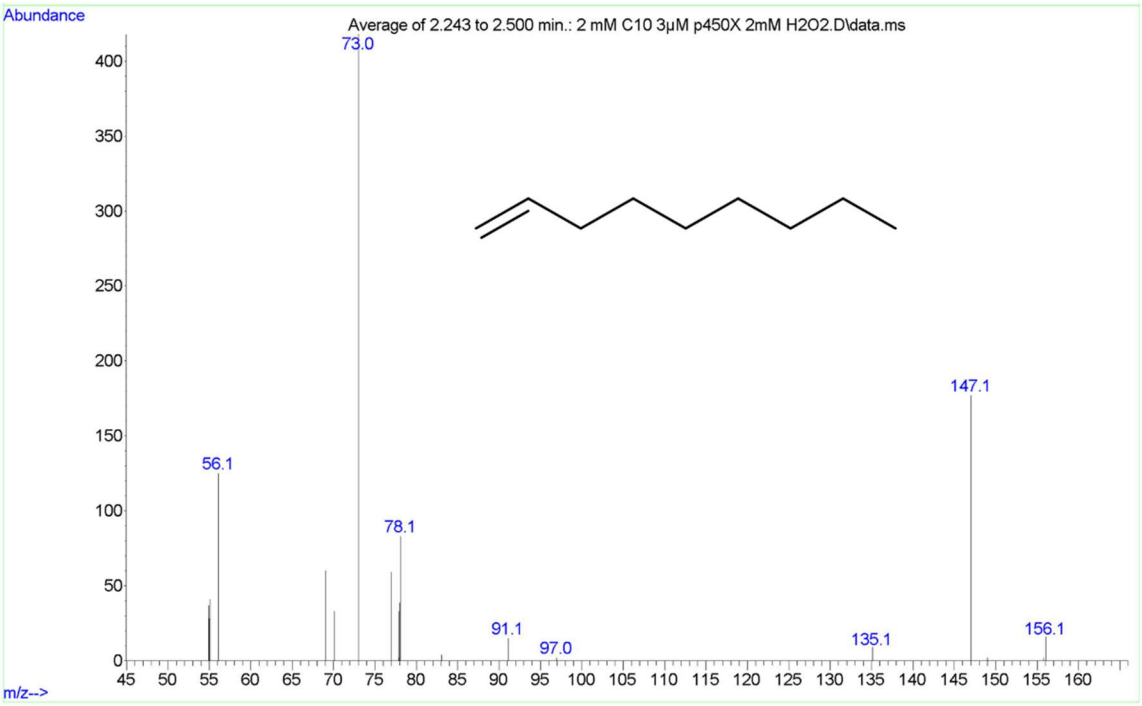

Figure 114 GC-MS spectrum of 1-nonene (m/z = 126.14) produced from C10:0 by $P450_{J\alpha}$.

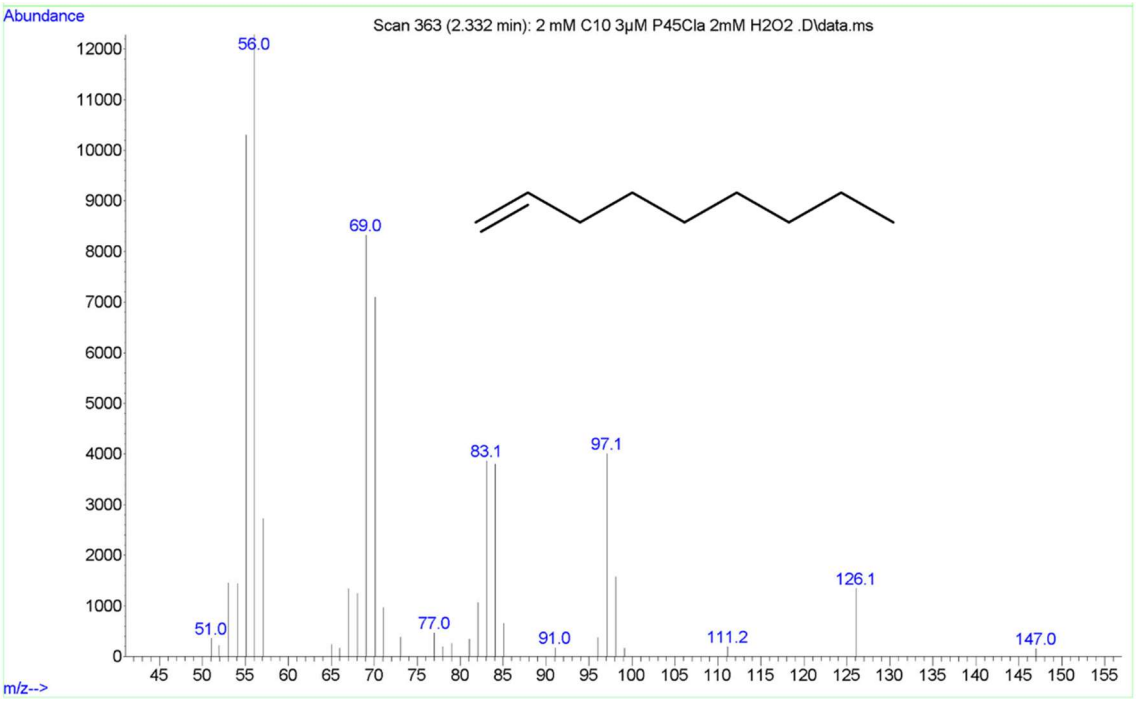

Figure 115 GC-MS spectrum of 1-nonene (m/z = 126.14) produced from C10:0 by $P450_{CLA}$.

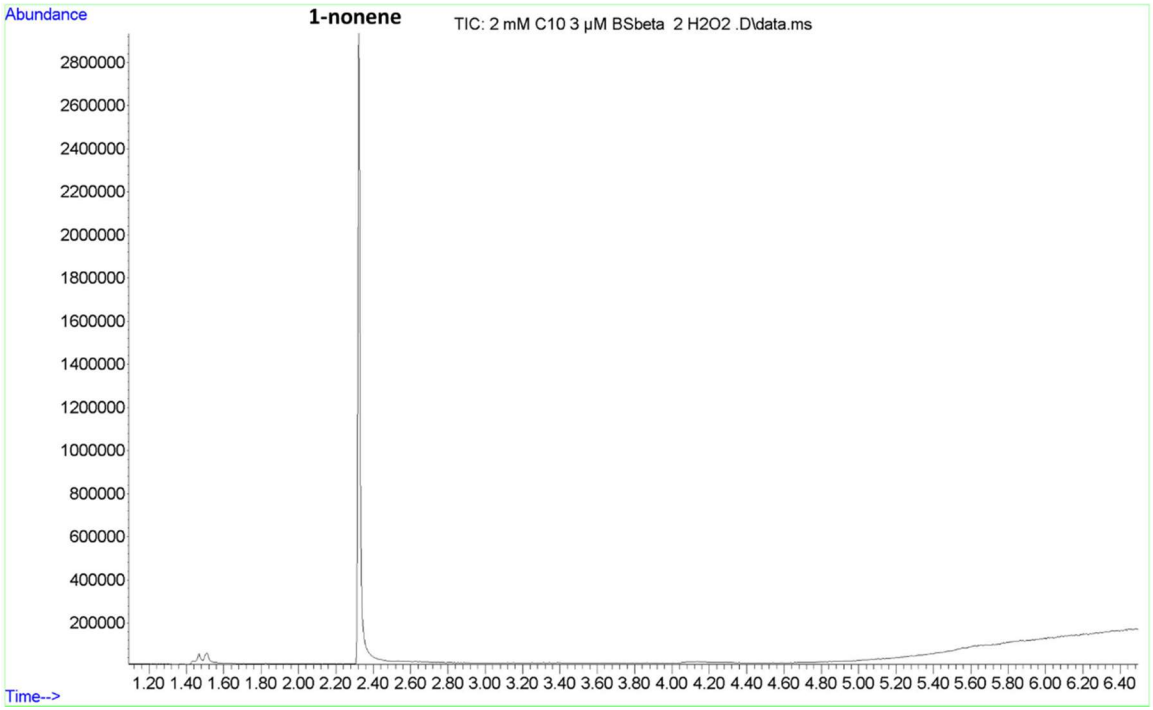

Figure 116 GC-MS headspace analysis for the conversion of C10:0 (2 mM) with P450$_{BS\beta}$. Retention time for 1-nonene is 2.3 to 2.4 min.

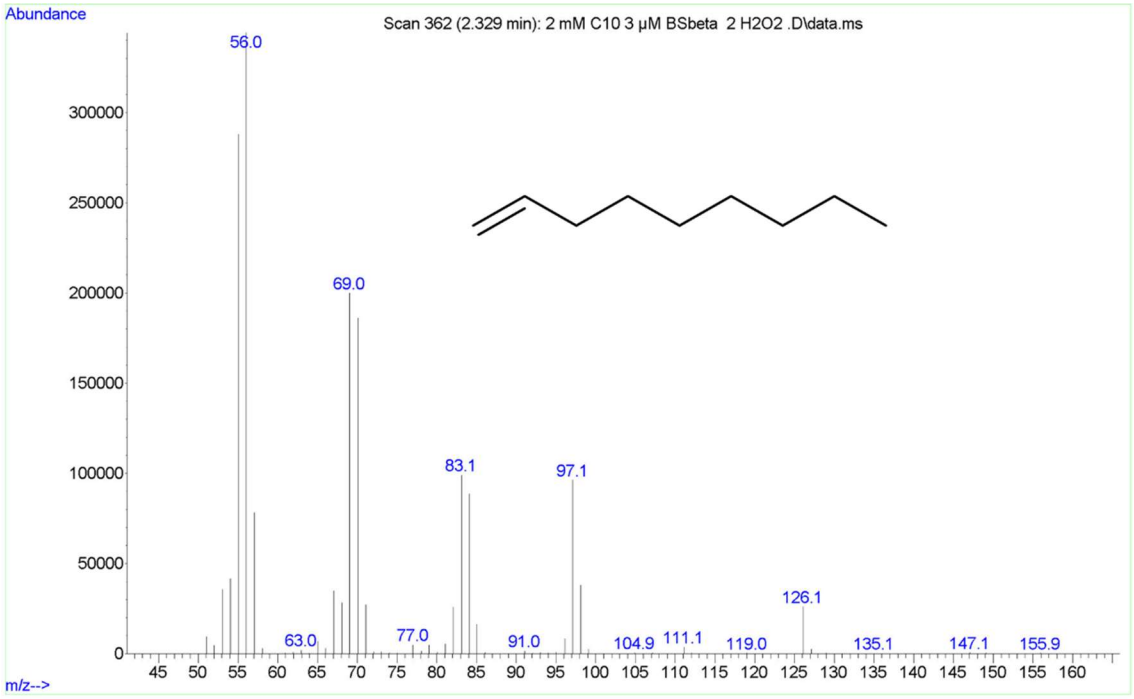

Figure 117 GC-MS spectrum of 1-nonene (m/z = 126.14) produced from C10:0 by P450$_{BS\beta}$.

5.4. Smarter H_2O_2 supply by coupling the fatty acid conversion to GOX and L-LOX

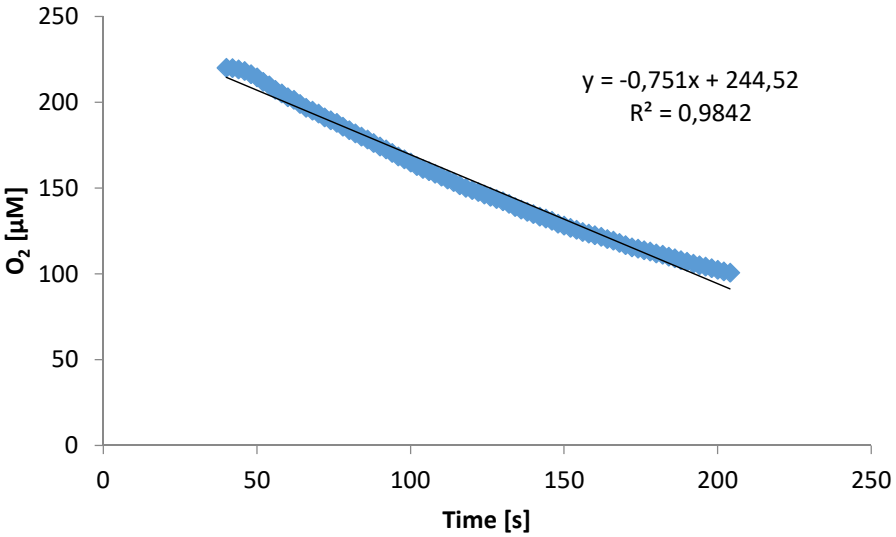

Figure 118 Determination of the specific activity [U mg^{-1}] of the commercial GOX. The oxygen consumption of the conversion of glucose with GOX was measured with an O_2-sensor.

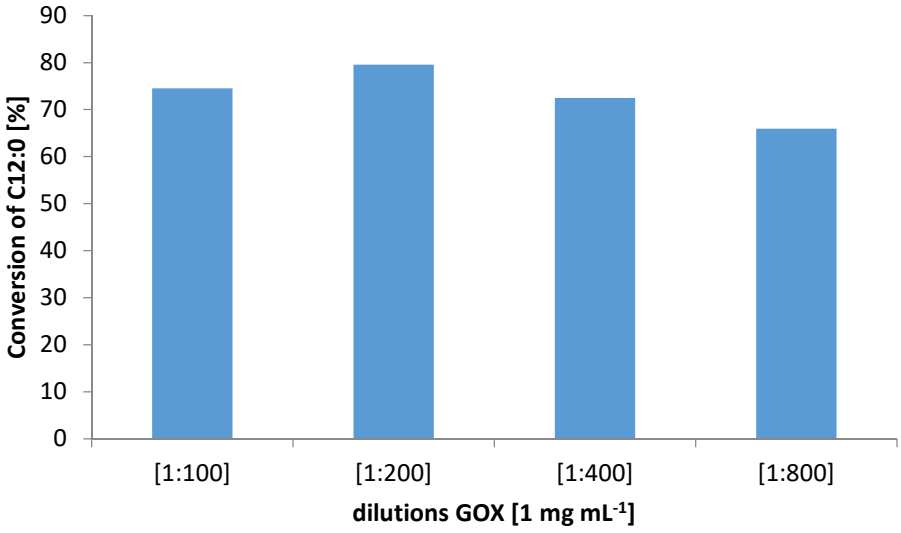

Figure 119 Screening for the ideal GOX concentration for coupling with fatty acid conversion by P450$_{J\alpha}$. Stock solution with 1 mg mL^{-1} GOX was diluted accordingly.

REFERENCES

[1] McCance, R.A.; Widdowson, E.M. *McCance and Widdowson's The composition of foods,* 7th ed.; Royal Society of Chemistry: Cambridge, **op. 2015**.

[2] McNaught, A.D.; Wilkinson, A. *IUPAC compendium of chemical terminology,* 2nd ed.; Blackwell Science: Oxford, **1997**.

[3] Pleissner, D.; Lam, W.C.; Sun, Z.; Lin, C.S.K. Food waste as nutrient source in heterotrophic microalgae cultivation. *Bioresource technology*, **2013**, *137,* 139–146.

[4] Ravindran, R.; Jaiswal, A.K. Exploitation of Food Industry Waste for High-Value Products. *Trends in Biotechnology*, **2016**, *34,* 58–69.

[5] Garnett, T. Where are the best opportunities for reducing greenhouse gas emissions in the food system (including the food chain)? *Food Policy*, **2011**, *36,* S23-S32.

[6] Garnett, T. Food sustainability: problems, perspectives and solutions. *The Proceedings of the Nutrition Society*, **2013**, *72,* 29–39.

[7] *Sustainable Food Systems from Agriculture to Industry;* Elsevier, **2018**.

[8] Metzger, J.O.; Bornscheuer, U. Lipids as renewable resources: current state of chemical and biotechnological conversion and diversification. *Applied microbiology and biotechnology*, **2006**, *71,* 13–22.

[9] Baumann, H.; Bühler, M.; Fochem, H.; Hirsinger, F.; Zoebelein, H.; Falbe, J. Natural Fats and Oils—Renewable Raw Materials for the Chemical Industry. *Angew. Chem. Int. Ed. Engl.*, **1988**, *27,* 41–62.

[10] Johnston, J.B.; Ouellet, H.; Podust, L.M.; Ortiz de Montellano, P.R. Structural control of cytochrome P450-catalyzed ω-hydroxylation. *Archives of biochemistry and biophysics*, **2011**, *507,* 86–94.

[11] Fatih Demirbas, M. Biorefineries for biofuel upgrading: A critical review. *Applied Energy*, **2009**, *86,* S151-S161.

[12] Lundemo, M.T.; Woodley, J.M. Guidelines for development and implementation of biocatalytic P450 processes. *Applied microbiology and biotechnology*, **2015**, *99,* 2465–2483.

[13] Sakaki, T. Practical Application of Cytochrome P450. *Biological ^|^ Pharmaceutical Bulletin*, **2012**, *35,* 844–849.

[14] Urlacher, V.B.; Girhard, M. Cytochrome P450 monooxygenases: an update on perspectives for synthetic application. *Trends in Biotechnology*, **2012**, *30,* 26–36.

[15] Arias, S.; Sandoval, A.; Arcos, M.; Cañedo, L.M.; Maestro, B.; Sanz, J.M.; Naharro, G.; Luengo, J.M. Poly-3-hydroxyalkanoate synthases from Pseudomonas putida U: substrate specificity and ultrastructural studies. *Microbial biotechnology*, **2008**, *1,* 170–176.

[16] Gandomkar, S.; Dennig, A.; Dordic, A.; Hammerer, L.; Pickl, M.; Haas, T.; Hall, M.; Faber, K. Biocatalytic Oxidative Cascade for the Conversion of Fatty Acids into α-Ketoacids via Internal H2O2Recycling. *Angewandte Chemie (International ed. in English)*, **2018**, *57,* 427–430.

[17] D'Este, M.; Alvarado-Morales, M.; Angelidaki, I. Amino acids production focusing on fermentation technologies - A review. *Biotechnology advances*, **2018**, *36,* 14–25.

[18] Kim, S.; Cheong, S.; Chou, A.; Gonzalez, R. Engineered fatty acid catabolism for fuel and chemical production. *Current opinion in biotechnology*, **2016**, *42,* 206–215.

[19] Sun, Y.; Zeng, W.; Benabbas, A.; Ye, X.; Denisov, I.; Sligar, S.G.; Du, J.; Dawson, J.H.; Champion, P.M. Investigations of heme ligation and ligand switching in cytochromes p450 and p420. *Biochemistry*, **2013**, *52,* 5941–5951.

[20] Whitehouse, C.J.C.; Bell, S.G.; Wong, L.-L. P450(BM3) (CYP102A1): connecting the dots. *Chemical Society reviews*, **2012**, *41,* 1218–1260.

[21] Dennig, A.; Kuhn, M.; Tassoti, S.; Thiessenhusen, A.; Gilch, S.; Bülter, T.; Haas, T.; Hall, M.; Faber, K. Oxidative Decarboxylation of Short-Chain Fatty Acids to 1-Alkenes. *Angewandte Chemie (International ed. in English)*, **2015**, *54,* 8819–8822.

[22] Oliw, E.H.; Bylund, J.; Herman, C. Bisallylic hydroxylation and epoxidation of polyunsaturated fatty acids by cytochrome P450. *Lipids*, **1996**, *31,* 1003–1021.

[23] Kim, K.-R.; Oh, D.-K. Production of hydroxy fatty acids by microbial fatty acid-hydroxylation enzymes. *Biotechnology advances*, **2013**, *31,* 1473–1485.

[24] Salaün, J.-P.; Helvig, C. Cytochrome P450-Dependent Oxidation of Fatty Acids. *Drug Metabolism and Drug Interactions*, **1995**, *12,* 353.

[25] van Bogaert, I.N.A.; Groeneboer, S.; Saerens, K.; Soetaert, W. The role of cytochrome P450 monooxygenases in microbial fatty acid metabolism. *The FEBS journal*, **2011**, *278,* 206–221.

[26] Nelson, D.R.; Koymans, L.; Kamataki, T.; Stegeman, J.J.; Feyereisen, R.; Waxman, D.J.; Waterman, M.R.; Gotoh, O.; Coon, M.J.; Estabrook, R.W.; Gunsalus, I.C.; Nebert, D.W. P450 superfamily: update on new sequences, gene mapping, accession numbers and nomenclature. *Pharmacogenetics*, **1996**, *6,* 1–42.

[27] Ciaramella, A.; Minerdi, D.; Gilardi, G. Catalytically self-sufficient cytochromes P450 for green production of fine chemicals. *Rend. Fis. Acc. Lincei*, **2017**, *28,* 169–181.

[28] Haines, D.C.; Tomchick, D.R.; Machius, M.; Peterson, J.A. Pivotal Role of Water in the Mechanism of P450BM-3 †. *Biochemistry*, **2001**, *40,* 13456–13465.

[29] Conner, K.P.; Woods, C.M.; Atkins, W.M. Interactions of cytochrome P450s with their ligands. *Archives of biochemistry and biophysics*, **2011**, *507,* 56–65.

[30] Denisov, I.G.; Makris, T.M.; Sligar, S.G.; Schlichting, I. Structure and chemistry of cytochrome P450. *Chemical reviews*, **2005**, *105,* 2253–2277.

[31] Meunier, B.; Visser, S.P. de; Shaik, S. Mechanism of oxidation reactions catalyzed by cytochrome p450 enzymes. *Chemical reviews*, **2004**, *104,* 3947–3980.

[32] *Reviews of Physiology Biochemistry and Pharmacology, Volume 127;* Springer-Verlag: Berlin/Heidelberg, **1996**.

[33] Hammerer, L.; Winkler, C.K.; Kroutil, W. Regioselective Biocatalytic Hydroxylation of Fatty Acids by Cytochrome P450s. *Catal Lett*, **2018**, *148,* 787–812.

[34] Hsieh, C.H.; Huang, X.; Amaya, J.A.; Rutland, C.D.; Keys, C.L.; Groves, J.T.; Austin, R.N.; Makris, T.M. The Enigmatic P450 Decarboxylase OleT Is Capable of, but Evolved To Frustrate, Oxygen Rebound Chemistry. *Biochemistry*, **2017**, *56,* 3347–3357.

[35] Matsunaga, I.; Sumimoto, T.; Ueda, A.; Kusunose, E.; Ichihara, K. Fatty acid-specific, regiospecific, and stereospecific hydroxylation by cytochrome P450 (CYP152B1) from Sphingomonas paucimobilis: substrate structure required for alpha-hydroxylation. *Lipids*, **2000**, *35,* 365–371.

[36] Girhard, M.; Schuster, S.; Dietrich, M.; Dürre, P.; Urlacher, V.B. Cytochrome P450 monooxygenase from Clostridium acetobutylicum: a new alpha-fatty acid hydroxylase. *Biochemical and biophysical research communications*, **2007**, *362,* 114–119.

[37] Dennig, A.; Blaschke, F.; Gandomkar, S.; Tassano, E.; Nidetzky, B. Preparative Asymmetric Synthesis of Canonical and Non-canonical α-amino Acids Through Formal Enantioselective Biocatalytic Amination of Carboxylic Acids. *Adv. Synth. Catal.*, **2019**, *54,* 8819.

[38] Fujishiro, T.; Shoji, O.; Nagano, S.; Sugimoto, H.; Shiro, Y.; Watanabe, Y. Crystal structure of H2O2-dependent cytochrome P450SPalpha with its bound fatty acid substrate: insight into the regioselective hydroxylation of fatty acids at the alpha position. *J. Biol. Chem.*, **2011**, *286,* 29941–29950.

[39] Liu, Y.; Wang, C.; Yan, J.; Zhang, W.; Guan, W.; Lu, X.; Li, S. Hydrogen peroxide-independent production of α-alkenes by OleTJE P450 fatty acid decarboxylase. *Biotechnology for biofuels*, **2014**, *7,* 28.

[40] Rude, M.A.; Baron, T.S.; Brubaker, S.; Alibhai, M.; Del Cardayre, S.B.; Schirmer, A. Terminal olefin (1-alkene) biosynthesis by a novel p450 fatty acid decarboxylase from Jeotgalicoccus species. *Applied and environmental microbiology*, **2011**, *77,* 1718–1727.

[41] Belcher, J.; McLean, K.J.; Matthews, S.; Woodward, L.S.; Fisher, K.; Rigby, S.E.J.; Nelson, D.R.; Potts, D.; Baynham, M.T.; Parker, D.A.; Leys, D.; Munro, A.W. Structure and biochemical properties of the alkene producing cytochrome P450 OleTJE (CYP152L1) from the Jeotgalicoccus sp. 8456 bacterium. *J. Biol. Chem.*, **2014**, *289,* 6535–6550.

[42] Matthews, S.; Belcher, J.D.; Tee, K.L.; Girvan, H.M.; McLean, K.J.; Rigby, S.E.J.; Levy, C.W.; Leys, D.; Parker, D.A.; Blankley, R.T.; Munro, A.W. Catalytic Determinants of Alkene Production by the Cytochrome P450 Peroxygenase OleTJE. *J. Biol. Chem.*, **2017**, *292,* 5128–5143.

[43] Moore, R.L.; Cook, C.O.; Williams, R.; Goodwin, D.C. Substitution of strictly conserved Y111 in catalase-peroxidases: Impact of remote interdomain contacts on active site structure and catalytic performance. *Journal of inorganic biochemistry*, **2008**, *102,* 1819–1824.

[44] Clark, J.P.; Miles, C.S.; Mowat, C.G.; Walkinshaw, M.D.; Reid, G.A.; Daff, S.N.; Chapman, S.K. The role of Thr268 and Phe393 in cytochrome P450 BM3. *Journal of inorganic biochemistry*, **2006**, *100,* 1075–1090.

[45] Tanaka, A.; Hoshino, E. Secondary calcium-binding parameter of Bacillus amyloliquefaciens α-amylase obtained from inhibition kinetics. *Journal of Bioscience and Bioengineering*, **2003**, *96,* 262–267.

[46] Jung, S.T.; Lauchli, R.; Arnold, F.H. Cytochrome P450: taming a wild type enzyme. *Current opinion in biotechnology*, **2011**, *22,* 809–817.

[47] Hlavica, P. Assembly of non-natural electron transfer conduits in the cytochrome P450 system: a critical assessment and update of artificial redox constructs amenable to exploitation in biotechnological areas. *Biotechnology advances*, **2009**, *27,* 103–121.

[48] Hrycay, E.G.; Bandiera, S.M. The monooxygenase, peroxidase, and peroxygenase properties of cytochrome P450. *Archives of biochemistry and biophysics*, **2012**, *522,* 71–89.

[49] Shoji, O.; Watanabe, Y. Peroxygenase reactions catalyzed by cytochromes P450. *Journal of biological inorganic chemistry : JBIC : a publication of the Society of Biological Inorganic Chemistry*, **2014**, *19,* 529–539.

[50] Valikhani, D.; Bolivar, J.M.; Dennig, A.; Nidetzky, B. A tailor-made, self-sufficient and recyclable monooxygenase catalyst based on coimmobilized cytochrome P450 BM3 and glucose dehydrogenase. *Biotechnology and bioengineering*, **2018**, *115,* 2416–2425.

[51] Bernhardt, R.; Urlacher, V.B. Cytochromes P450 as promising catalysts for biotechnological application: chances and limitations. *Applied microbiology and biotechnology*, **2014**, *98,* 6185–6203.

[52] Girhard, M.; Machida, K.; Itoh, M.; Schmid, R.D.; Arisawa, A.; Urlacher, V.B. Regioselective biooxidation of (+)-valencene by recombinant E. coli expressing CYP109B1 from Bacillus subtilis in a two-liquid-phase system. *Microbial cell factories*, **2009**, *8,* 36.

[53] Donova, M.V.; Nikolayeva, V.M.; Dovbnya, D.V.; Gulevskaya, S.A.; Suzina, N.E. Methyl-beta-cyclodextrin alters growth, activity and cell envelope features of sterol-transforming mycobacteria. *Microbiology (Reading, England)*, **2007**, *153,* 1981–1992.

[54] Kühnel, K.; Maurer, S.C.; Galeyeva, Y.; Frey, W.; Laschat, S.; Urlacher, V.B. Hydroxylation of Dodecanoic Acid and (2R,4R,6R,8R)-Tetramethyldecanol on a Preparative Scale using an NADH- Dependent CYP102A1 Mutant. *Adv. Synth. Catal.*, **2007**, *349,* 1451–1461.

[55] Garcia-Galan, C.; Berenguer-Murcia, Á.; Fernandez-Lafuente, R.; Rodrigues, R.C. Potential of Different Enzyme Immobilization Strategies to Improve Enzyme Performance. *Adv. Synth. Catal.*, **2011**, *353,* 2885–2904.

[56] Rodrigues, R.C.; Ortiz, C.; Berenguer-Murcia, Á.; Torres, R.; Fernández-Lafuente, R. Modifying enzyme activity and selectivity by immobilization. *Chemical Society reviews*, **2013**, *42,* 6290–6307.

[57] Bornscheuer, U.T. Immobilizing enzymes: how to create more suitable biocatalysts. *Angewandte Chemie (International ed. in English)*, **2003**, *42,* 3336–3337.

[58] Iyer, P.V.; Ananthanarayan, L. Enzyme stability and stabilization—Aqueous and non-aqueous environment. *Process Biochemistry*, **2008**, *43,* 1019–1032.

[59] Homaei, A.A.; Sariri, R.; Vianello, F.; Stevanato, R. Enzyme immobilization: an update. *Journal of chemical biology*, **2013**, *6,* 185–205.

[60] Velasco-Lozano, S.; Benítez-Mateos, A.I.; López-Gallego, F. Co-immobilized Phosphorylated Cofactors and Enzymes as Self-Sufficient Heterogeneous Biocatalysts for Chemical Processes. *Angewandte Chemie (International ed. in English)*, **2017**, *56,* 771–775.

[61] HARTMEIER, W. Immobilized biocatalysts ? From simple to complex systems. *Trends in Biotechnology*, **1985**, *3,* 149–153.

[62] Mateo, C.; Palomo, J.M.; Fernandez-Lorente, G.; Guisan, J.M.; Fernandez-Lafuente, R. Improvement of enzyme activity, stability and selectivity via immobilization techniques. *Enzyme and Microbial Technology*, **2007**, *40,* 1451–1463.

[63] Clark, D.S. Can immobilization be exploited to modify enzyme activity? *Trends in Biotechnology*, **1994**, *12,* 439–443.

[64] Sheldon, R.A. Enzyme Immobilization: The Quest for Optimum Performance. *Adv. Synth. Catal.*, **2007**, *349,* 1289–1307.

[65] Cao, L.; van Langen, L.; Sheldon, R.A. Immobilised enzymes: carrier-bound or carrier-free? *Current opinion in biotechnology*, **2003**, *14,* 387–394.

[66] Ducharme, J.; Auclair, K. Use of bioconjugation with cytochrome P450 enzymes. *Biochimica et biophysica acta. Proteins and proteomics*, **2018**, *1866,* 32–51.

[67] Baess, D.; Jänig, G.R.; Ruckpaul, K. Wechselwirkungen der Komponenten des Zytochrom P-450 Monooxygenasesystems aus Lebermikrosomen. I. Immobilisierung der solubilisierten und partiell gereinigten Proteinkomponenten. *Acta biologica et medica Germanica*, **1975**, *34,* 1745–1754.

[68] Axarli, I.; Prigipaki, A.; Labrou, N.E. Engineering the substrate specificity of cytochrome P450 CYP102A2 by directed evolution: production of an efficient enzyme for bioconversion of fine chemicals. *Biomolecular engineering*, **2005**, *22,* 81–88.

[69] Bolivar, J.M.; Nidetzky, B. Positively charged mini-protein Zbasic2 as a highly efficient silica binding module: opportunities for enzyme immobilization on unmodified silica supports. *Langmuir : the ACS journal of surfaces and colloids*, **2012**, *28,* 10040–10049.

[70] Hedhammar, M.; Hober, S. Z(basic)--a novel purification tag for efficient protein recovery. *Journal of chromatography. A*, **2007**, *1161,* 22–28.

[71] Gräslund, T.; Ehn, M.; Lundin, G.; Hedhammar, M.; Uhlén, M.; Nygren, P.-Å.; Hober, S. Strategy for highly selective ion-exchange capture using a charge-polarizing fusion partner. *Journal of chromatography. A*, **2002**, *942,* 157–166.

[72] Gräslund, T.; Lundin, G.; Uhlén, M.; Nygren, P.-Å.; Hober, S. Charge engineering of a protein domain to allow efficient ion-exchange recovery. *Protein Eng Des Sel*, **2000**, *13,* 703–709.

[73] Wiesbauer, J.; Bolivar, J.M.; Mueller, M.; Schiller, M.; Nidetzky, B. Inside Cover: Oriented Immobilization of Enzymes Made Fit for Applied Biocatalysis: Non-Covalent Attachment to Anionic Supports using Zbasic2 Module (ChemCatChem 8/2011). *ChemCatChem*, **2011**, *3,* 1218.

[74] Bolivar, J.M.; Nidetzky, B. Oriented and selective enzyme immobilization on functionalized silica carrier using the cationic binding module Z basic2: design of a heterogeneous D-amino acid oxidase catalyst on porous glass. *Biotechnology and bioengineering*, **2012**, *109,* 1490–1498.

[75] Dennig, A.; Lülsdorf, N.; Liu, H.; Schwaneberg, U. Regioselective o-hydroxylation of monosubstituted benzenes by P450 BM3. *Angew. Chem. Int. Ed. Engl.*, **2013**, *52,* 8459–8462.

[76] Solé, J.; Caminal, G.; Schürmann, M.; Álvaro, G.; Guillén, M. Co-immobilization of P450 BM3 and glucose dehydrogenase on different supports for application as a self-sufficient oxidative biocatalyst. *J. Chem. Technol. Biotechnol.*, **2019**, *94,* 244–255.

[77] Crowe, J.; Döbeli, H.; Gentz, R.; Hochuli, E.; Stüber, D.; Henco, K. 6xHis-Ni-NTA chromatography as a superior technique in recombinant protein expression/purification. *Methods in molecular biology (Clifton, N.J.)*, **1994**, *31,* 371–387.

[78] Piesecki, S.; Teng, W.Y.; Hochuli, E. Immobilization of beta-galactosidase for application in organic chemistry using a chelating peptide. *Biotechnology and bioengineering*, **1993**, *42,* 178–184.

[79] Tomme, P.; Boraston, A.; McLean, B.; Kormos, J.; Creagh, A.L.; Sturch, K.; Gilkes, N.R.; Haynes, C.A.; Warren, R.A.J.; Kilburn, D.G. Characterization and affinity applications of cellulose-binding domains. *Journal of Chromatography B: Biomedical Sciences and Applications*, **1998**, *715,* 283–296.

[80] Engelmark Cassimjee, K.; Kadow, M.; Wikmark, Y.; Svedendahl Humble, M.; Rothstein, M.L.; Rothstein, D.M.; Bäckvall, J.-E. A general protein purification and immobilization method on controlled porosity glass: biocatalytic applications. *Chemical communications (Cambridge, England)*, **2014**, *50,* 9134–9137.

[81] *chromatography 6th edition - fundamentals and applications of chromatography and related differential migration methods;* Elsevier, **2004**.

[82] Armisén, P.; Mateo, C.; Cortés, E.; Barredo, J.L.; Salto, F.; Diez, B.; Rodés, L.; García, J.L.; Fernández-Lafuente, R.; Guisán, J.M. Selective adsorption of poly-His tagged glutaryl acylase on tailor-made metal chelate supports. *Journal of chromatography. A*, **1999**, *848,* 61–70.

[83] Matsunaga, I.; Ueda, A.; Fujiwara, N.; Sumimoto, T.; Ichihara, K. Characterization of the ybdT gene product of Bacillus subtilis: Novel fatty acid β-hydroxylating cytochrome P450. *Lipids*, **1999**, *34,* 841–846.

[84] OMURA, T.; SATO, R. THE CARBON MONOXIDE-BINDING PIGMENT OF LIVER MICROSOMES. II. SOLUBILIZATION, PURIFICATION, AND PROPERTIES. *J. Biol. Chem.*, **1964**, *239,* 2379–2385.

[85] Waterhouse, A.M.; Procter, J.B.; Martin, D.M.A.; Clamp, M.; Barton, G.J. Jalview Version 2--a multiple sequence alignment editor and analysis workbench. *Bioinformatics (Oxford, England)*, **2009**, *25,* 1189–1191.

[86] Lee, D.-S.; Yamada, A.; Sugimoto, H.; Matsunaga, I.; Ogura, H.; Ichihara, K.; Adachi, S.-I.; Park, S.-Y.; Shiro, Y. Substrate recognition and molecular mechanism of fatty acid hydroxylation by cytochrome P450 from Bacillus subtilis. Crystallographic, spectroscopic, and mutational studies. *J. Biol. Chem.*, **2003**, *278,* 9761–9767.

[87] Waterhouse, A.; Bertoni, M.; Bienert, S.; Studer, G.; Tauriello, G.; Gumienny, R.; Heer, F.T.; Beer, T.A.P. de; Rempfer, C.; Bordoli, L.; Lepore, R.; Schwede, T. SWISS-MODEL: homology modelling of protein structures and complexes. *Nucleic acids research*, **2018**, *46,* W296-W303.

[88] Wallace, A.C.; Laskowski, R.A.; Thornton, J.M. LIGPLOT: a program to generate schematic diagrams of protein-ligand interactions. *Protein Eng Des Sel*, **1995**, *8,* 127–134.

[89] Oliver, C.F.; Modi, S.; Sutcliffe, M.J.; Primrose, W.U.; Lian, L.Y.; Roberts, G.C. A single mutation in cytochrome P450 BM3 changes substrate orientation in a catalytic intermediate and the regiospecificity of hydroxylation. *Biochemistry*, **1997**, *36,* 1567–1572.

[90] Modi, S.; Primrose, W.U.; Boyle, J.M.B.; Gibson, C.F.; Lian, L.-Y.; Roberts, G.C.K. NMR Studies of Substrate Binding to Cytochrome P450 BM3: Comparisons to Cytochrome P450 cam. *Biochemistry*, **1995**, *34,* 8982–8988.

[91] Li, Q.-S.; Ogawa, J.; Schmid, R.D.; Shimizu, S. Residue size at position 87 of cytochrome P450 BM-3 determines its stereoselectivity in propylbenzene and 3-chlorostyrene oxidation. *FEBS Letters*, **2001**, *508,* 249–252.

[92] Michaelis, L.; Menten, M.L.; Johnson, K.A.; Goody, R.S. The original Michaelis constant: translation of the 1913 Michaelis-Menten paper. *Biochemistry*, **2011**, *50,* 8264–8269.

[93] Lim, J.B.; Barker, K.A.; Eller, K.A.; Jiang, L.; Molina, V.; Saifee, J.F.; Sikes, H.D. Insights into electron leakage in the reaction cycle of cytochrome P450 BM3 revealed by kinetic modeling and mutagenesis. *Protein science : a publication of the Protein Society*, **2015**, *24,* 1874–1883.

[94] Stein, S.E. *NIST/EPA/NIH Mass Spectral Library-PC Version, NIST Standard Reference Database 1A*.

[95] Busto, E.; Simon, R.C.; Richter, N.; Kroutil, W. One-Pot, Two-Module Three-Step Cascade To Transform Phenol Derivatives to Enantiomerically Pure (R)- or (S)- p -Hydroxyphenyl Lactic Acids. *ACS Catal.*, **2016**, *6,* 2393–2397.

[96] Frederick, K.R.; Tung, J.; Emerick, R.S.; Masiarz, F.R.; Chamberlain, S.H.; Vasavada, A.; Rosenberg, S.; Chakraborty, S.; Schopfer, L.M.; Schopter, L.M. Glucose oxidase from Aspergillus niger. Cloning, gene sequence, secretion from Saccharomyces cerevisiae and kinetic analysis of a yeast-derived enzyme. *J. Biol. Chem.*, **1990**, *265,* 3793–3802.

[97] Onoda, H.; Shoji, O.; Suzuki, K.; Sugimoto, H.; Shiro, Y.; Watanabe, Y. α-Oxidative decarboxylation of fatty acids catalysed by cytochrome P450 peroxygenases yielding shorter-alkyl-chain fatty acids. *Catal. Sci. Technol.*, **2018**, *8,* 434–442.

[98] Xu, H.; Ning, L.; Yang, W.; Fang, B.; Wang, C.; Wang, Y.; Xu, J.; Collin, S.; Laeuffer, F.; Fourage, L.; Li, S. In vitro oxidative decarboxylation of free fatty acids to terminal alkenes by two new P450 peroxygenases. *Biotechnology for biofuels*, **2017**, *10,* 208.

[99] Matsunaga, I.; Yokotani, N.; Gotoh, O.; Kusunose, E.; Yamada, M.; Ichihara, K. Molecular Cloning and Expression of Fatty Acid α-Hydroxylase from Sphingomonas paucimobilis. *J. Biol. Chem.*, **1997**, *272,* 23592–23596.

[100] Girvan, H.M.; Poddar, H.; McLean, K.J.; Nelson, D.R.; Hollywood, K.A.; Levy, C.W.; Leys, D.; Munro, A.W. Structural and catalytic properties of the peroxygenase P450 enzyme CYP152K6 from Bacillus methanolicus. *Journal of inorganic biochemistry*, **2018**, *188,* 18–28.

[101] Amaya, J.A.; Rutland, C.D.; Makris, T.M. Mixed regiospecificity compromises alkene synthesis by a cytochrome P450 peroxygenase from Methylobacterium populi. *Journal of inorganic biochemistry*, **2016**, *158,* 11–16.

[102] Hasemann, C.A.; Kurumbail, R.G.; Boddupalli, S.S.; Peterson, J.A.; Deisenhofer, J. Structure and function of cytochromes P450:a comparative analysis of three crystal structures. *Structure*, **1995**, *3,* 41–62.

[103] Dawson, J.H.; Holm, R.H.; Trudell, J.R.; Barth, G.; Linder, R.E.; Bunnenberg, E.; Djerassi, C.; Tang, S.C. Letter: Oxidized cytochrome P-450. Magnetic circular dichroism evidence for thiolate ligation in the substrate-bound form. Implications for the catalytic mechanism. *Journal of the American Chemical Society*, **1976**, *98,* 3707–3708.

[104] Yoon, J.-H.; Lee, K.-C.; Weiss, N.; Kang, K.H.; Park, Y.-H. Jeotgalicoccus halotolerans gen. nov., sp. nov. and Jeotgalicoccus psychrophilus sp. nov., isolated from the traditional Korean fermented seafood jeotgal. *International journal of systematic and evolutionary microbiology*, **2003**, *53,* 595–602.

[105] Liu, W.-Y.; Jiang, L.-L.; Guo, C.-J.; Yang, S.S. Jeotgalicoccus halophilus sp. nov., isolated from salt lakes. *International journal of systematic and evolutionary microbiology*, **2011**, *61,* 1720–1724.

[106] Hoyles, L.; Collins, M.D.; Foster, G.; Falsen, E.; Schumann, P. Jeotgalicoccus pinnipedialis sp. nov., from a southern elephant seal (Mirounga leonina). *International journal of systematic and evolutionary microbiology*, **2004**, *54,* 745–748.

[107] Leiros, I.; Wang, E.; Rasmussen, T.; Oksanen, E.; Repo, H.; Petersen, S.B.; Heikinheimo, P.; Hough, E. The 2.1 A structure of Aerococcus viridans L-lactate oxidase (LOX). *Acta crystallographica. Section F, Structural biology and crystallization communications*, **2006**, *62,* 1185–1190.

[108] Fromm, H.J.; Hargrove, M. *Essentials of Biochemistry;* Springer Berlin Heidelberg: Berlin, Heidelberg, **2012**.

[109] Pikal, M.J.; Shah, S.; Senior, D.; Lang, J.E. Physical Chemistry of Freeze-drying: Measurement of Sublimation Rates for Frozen Aqueous Solutions by a Microbalance Technique. *Journal of Pharmaceutical Sciences*, **1983**, *72,* 635–650.

[110] Xiang, J.; Hey, J.M.; Liedtke, V.; Wang, D.Q. Investigation of freeze-drying sublimation rates using a freeze-drying microbalance technique. *International journal of pharmaceutics*, **2004**, *279,* 95–105.

[111] YUAN, C.; BLOCH, K. Conversion of oleic acid to linoleic acid. *J. Biol. Chem.*, **1961**, *236,* 1277–1279.

[112] Phukan, M.M.; Bora, P.; Gogoi, K.; Konwar, B.K. Biodiesel from Saccharomyces cerevisiae: fuel property analysis and comparative economics. *SN Appl. Sci.*, **2019**, *1,* 266.

[113] Lee, D.-S.; Song, J.-W.; Voß, m.; Schuiten, E.; A, R.K.; Kwon, Y.-U.; Bornscheuer, U.; Park, J.-B. Enzyme Cascade Reactions for the Biosynthesis of Long Chain Aliphatic Amines from Renewable Fatty Acids. *Adv. Synth. Catal.*, **2019**.

[114] Wilson, R.; Turner, A.P.F. Glucose oxidase: an ideal enzyme. *Biosensors and Bioelectronics*, **1992**, *7,* 165–185.

[115] Kureshy, R.I.; Khan, N.-u.H.; Abdi, S.H.R.; Patel, S.T.; Jasra, R.V. Enantioselective epoxidation of non-functionalised alkenes using a urea–hydrogen peroxide oxidant and a dimeric homochiral Mn(III)-Schiff base complex catalyst. *Tetrahedron: Asymmetry*, **2001**, *12,* 433–437.

[116] Sevrioukova, I.F.; Li, H.; Zhang, H.; Peterson, J.A.; Poulos, T.L. Structure of a cytochrome P450-redox partner electron-transfer complex. *Proceedings of the National Academy of Sciences of the United States of America*, **1999**, *96,* 1863–1868.

[117] Thompson, M.P.; Derrington, S.R.; Heath, R.S.; Porter, J.L.; Mangas-Sanchez, J.; Devine, P.N.; Truppo, M.D.; Turner, N.J. A generic platform for the immobilisation of engineered biocatalysts. *Tetrahedron*, **2019**, *75,* 327–334.

[118] Waldmeier, P.; Sigel, H. Metal ions and hydrogen peroxide. XXIV. On the kinetics and mechanism of the catalase-like activity of the Fe3+ complex of 4,4′,4″,4‴-tetrasulfophthalocyanine. *Inorganica Chimica Acta*, **1971**, *5,* 659–665.